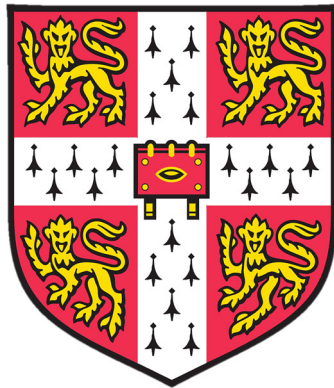


Water flow beneath past ice sheets



James David Kirkham

British Antarctic Survey

&

Scott Polar Research Institute

University of Cambridge

This dissertation is submitted for the degree of

Doctor of Philosophy

Corpus Christi College

November 2022

For my grandparents

“Land really is the best art”

— Andy Warhol

Declaration

I hereby declare that except where specific reference is made to the work of others, the contents of this dissertation are original and have not been submitted in whole or in part for consideration for any other degree or qualification in this, or any other university. This dissertation is my own work and contains nothing which is the outcome of work done in collaboration with others, except as specified in the text and Acknowledgments. This dissertation does not exceed the length limits prescribed by the Degree Committee for the Faculty of Earth Sciences and Geography.

James David Kirkham

November 2022

Abstract

Water flow beneath past ice sheets

James David Kirkham

The movement of water beneath ice sheets exerts an important, yet poorly understood, control on how ice masses respond to climatic warming. However, the subglacial realm of ice sheets is one of the most inaccessible environments on Earth. Consequently, little is known about the processes that operate beneath today's ice masses — and how these will evolve in the future. Subglacial landforms present in formerly-glaciated regions provide comparatively accessible records of glacial erosion, deposition, and sediment transport beneath ice sheets that have undergone deglaciation. This thesis investigates the potential of these landforms to reconstruct the flow of water beneath past ice sheets as analogues for how contemporary ice masses will evolve in a warming climate. A combination of geophysical approaches, including multibeam-bathymetric surveys, high-resolution 3D seismic-reflection data, conventional 3D seismic-reflection data, and geotechnical information from boreholes, is used to investigate the flow of water beneath ice sheets which covered western Europe and more expansive regions of the Antarctic continental shelf in the past. These data are first used to constrain the routing and fluxes of subglacial water beneath the retreating West Antarctic Ice Sheet. The impact of subglacial water flow on ice-sheet dynamics during deglaciation is then examined by imaging the internal structures of ancient channels incised by meltwater — tunnel valleys — in the North Sea. The unprecedented detail provided by the high-resolution 3D seismic-reflection data provides links between ice-sheet dynamics and subglacial meltwater flow during deglaciation. A numerical modelling approach constrains these linkages further by estimating the time that the meltwater channels take to form beneath deglaciating ice sheets. Finally, the sedimentation patterns resulting from subglacial water flow and other glacially-influenced processes during deglaciation are examined. Greater coverage of geophysical data on formerly glaciated continental margins, combined with chronological constraints from shallow drilling, will improve understanding of the hydrological systems and dynamics of former and contemporary ice sheets.

Acknowledgements

Arguably the most important section of this thesis is located right at the beginning: the acknowledgments. That's because none of the discoveries, insights and findings detailed in the subsequent pages would have been possible without the guidance of a number of fantastic mentors, colleagues, and friends who have helped to make the last 4 years such an incredible journey. This section provides a short flavour of my gratitude.

The first, and one of the largest, thank yous goes to Kelly Hogan, who has been a truly outstanding supervisor and friend over the last 6 years. From patiently scouring text for my recurrently incorrect use of hyphens to navigating through an oil refinery in Punta Arenas to shop for emergency clothes, Kelly has provided endless support throughout this process and has just been a top-notch supervisor in every aspect. Rob Larter has been equally amazing. Alongside his encyclopaedic knowledge of the Antarctic continental shelf and his thought-provoking insights into glacial processes, Rob helped me to realise a lifelong dream of conducting fieldwork in Antarctica — an experience that will stay with me for a lifetime. I am extremely grateful to Julian Dowdeswell who first brought me into the fold of palaeo-glaciologists through the Scott Polar Research Institute's Debenham Scholarship programme — funded by a bequest from the late Barbara Debenham in memory of Frank Debenham, one of the members of Scott's 1910–1913 (Terra Nova) Expedition to Antarctica. I have benefitted greatly from Julian's ability to envisage how to answer 'big picture' science questions and his excellent guidance over the last 6 years. I have also benefitted immensely from Neil Arnold's perspectives and assistance, particularly in growing the numerical modelling side of this project. Neil's ability to ask searching glaciological questions in simple ways has sharpened the angle of much of the work presented in this thesis. Overall, I could not have wished for a better team of supervisors — thank you all for helping me to grow so much throughout this experience.

Next on the list of thank yous is Ed Self, who has been one of the sparks to ignite this project. Ed's excitement, dedication and belief in this work has been infectious from day

one. He has tirelessly lobbied for greater access to data, spotted potential opportunities to bridge academic questions with industry datasets, and has put up with my endless questions about seismic interpretation over the last four years! I have also enjoyed our long, and sometimes nonsensical, email threads. Similarly, Ken Games provided essential contributions to set up the project and ultimately make it so successful. Thank you. As well as my colleagues from Gardline Limited, many of the discoveries in this thesis would not have been possible without the generous provision of data from bp, Harbour Energy, Equinor Energy AS, Lundin Energy Norway AS, Petoro AS, Aker BP ASA, TotalEnergies EP Norge AS and CNOOC. I would like to specifically thank Andy Hill, Gareth Wood, Gavin Eardley, George Moise and Inger Helene Gram Reese for their assistance in securing the data, and their interest and belief in the project throughout. Sarah Beadle, Hayley Mackenzie, David Allan Feller, Clody Howlett and the rest of the Cambridge and BAS legal contracts teams are gratefully thanked for their efforts in securing confidentiality agreements to allow me to access many of the datasets used in this thesis remotely due to the COVID-19 pandemic. S&P Global and Schlumberger are also thanked for providing academic seismic interpretation software licenses.

This project has benefitted immensely from the collaboration and guidance of a number of external advisors. I am grateful to Dag Ottesen, from the Geological Survey of Norway, for his insightful perspectives from the Norwegian margin and the North Sea, as well as his provision of otherwise inaccessible marine geophysical data from Svalbard at the start of the project. Margaret Stewart, from the British Geological Survey, has been extremely helpful in sharing her insights about tunnel valleys. I have benefitted greatly from inspiring discussions with Mads Huuse from the University of Manchester, who has brought over two decades of knowledge about tunnel valleys and the North Sea to bear on this project. A nod of thanks is also given to Kofi Owusu for speedily fixing any VPN issues preventing me from remotely accessing data from the University of Manchester. I am also very grateful to Chris Clark, Jeremy Ely, and the rest of the PalGlac group at the University of Sheffield for providing brilliant guidance, amazing model data, and several opportunities to present work to their group. I have always found these discussions to be highly thought provoking and they have opened my mind to ample possibilities to expand this work further in the future. I would also like to thank Calvin Shackleton, Stephen Livingstone, Chris Stokes, Sean Gulick, Benjamin Bellwald and Brian Todd for their help in sharpening the arguments made in some of these chapters through the peer-review process.

This PhD project simply would not have been the same if I were not able to undertake it at the British Antarctic Survey — one of the most inspiring organisations I've ever

had the pleasure of working at. It's hard not to fall in love with BAS' mission, but it's the people at BAS who make it the brilliant organisation it is. I want to thank all of the staff and fellow students that have made my years at BAS so special. I am very grateful to Dom Hodgson, Claus Dieter Hillenbrand, Jo Johnson, James Smith and the rest of the PICC team for supporting me throughout this journey, and to my officemates, fellow students and friends who have accompanied me along the way. These are far too numerous to list exclusively here but I wish to mention Julien Bodart, Bryony Freer, Dorothea Moser, Rob Law, Craig Walton, Jon Adams, Will Scott, Becky Dell, Ella Gilbert, Max Lowe, Morgan Seag, Richard Clements, Georgia Tindale, Scott Remer, and Alex Bradley by name. Thank you all for making this such a fantastic experience. I would also like to thank Inka Koch, who encouraged me to first apply to this position, and Andrew Williamson for his continued friendship and support throughout this experience, especially through the 'completely wild' times.

The Natural Environment Research Council is thanked for funding this research under grant NE/L002507/1. Ali Teague also deserves special recognition for expertly dealing with any organisational matter related to PhD funding or administration over the last four years. Eric Wolff and the administrators of the Cambridge ESS DTP are also gratefully thanked for their support in handling the fallout of the COVID-19 pandemic, and for making funds available to ensure that this research was not cut short by the disruption of the pandemic.

This PhD has had many special moments, but being one of the first people in the World to work on Thwaites Glacier up close is definitely a highlight that I will never forget. My fieldwork in West Antarctica was supported by a grant from the Scott Polar Research Institute's B.B. Roberts Fund and a research support grant issued by Corpus Christi College. I am grateful to the International Thwaites Glacier Collaboration and the THOR team, especially those that I sailed with on cruise NBP1902, for involving me in such a collaborative and exciting community. I would also like to mention David Vaughan whose words of leadership and his desire to integrate early-career researchers so fundamentally into the Thwaites project still inspires me to this day.

Meaningful science requires effective communication. My own abilities to communicate scientific findings have grown immensely thanks to the tireless efforts of the BAS Communications Team, in particular Athena Dinar. This team has brought a previously obscure glacial landform to the attention of international media twice in just two years — generating media coverage that I never would have dreamed of at the outset of this PhD! I am immensely grateful. I am also extremely thankful for the insights into the

science-policy world that I have gained through undertaking a UKRI policy internship at the UK Government Office for Science. I would like to thank the entire GO-Science team for the warm welcome that I received there, for the trust and opportunities to pursue topics that I thought were deserving of policy attention, and the UKRI interns for establishing such a rewarding and fun environment to work in. Within the GIO team, particular mentions go to James Gingell, Oliver Johnson and Owen Jackson for their leadership and guidance during this time. I grew a lot through this experience. I would also like to thank Pam Pearson and the International Cryosphere Climate Initiative for the opportunity to attend COP27 and for the trust that they emplaced in me to give multiple talks, panel discussions and media interviews during this conference. I hope that we were able to play some small role in ensuring that these negotiations progressed in the right direction.

Finally, and most significantly, I thank my family for their continued love and support (even if they still don't really understand what it is I actually do), and Alice, who continues to be my rock throughout this experience and life more broadly. This thesis is dedicated to my grandparents, who fostered in me a love of discovery and science from an early age. Much of this work was conducted in the darkest depths of the COVID-19 pandemic, and we were devastated to lose my grandfather, Michael Kirkham, to this terrible disease early last year. The love of science that my grandparents nurtured kept this project going through those dark times. The discoveries that follow are dedicated to them.

Table of contents

Declaration	vii
Abstract	ix
Acknowledgements	xi
Table of contents	xv
List of figures	xix
List of tables	xxii
Nomenclature	xxiii
Preface	xxvi
1 Introduction	1
1.1 Thesis motivation	1
1.1.1 The short record of modern glaciological observations	5
1.2 Research aim and objectives	6
1.3 Thesis structure	7
2 Literature Review	8
2.1 Chapter overview	8
2.2 Subglacial hydrological theory	8
2.2.1 Water routing and impacts on ice flow	8
2.2.2 Inefficient (distributed) subglacial drainage systems	10
2.2.3 Efficient (channelised) subglacial drainage systems	13
2.3 Subglacial water storage	14
2.3.1 Subglacial lakes	14
2.3.2 Groundwater	18
2.4 Observations of water flow beneath ice sheets	19
2.4.1 The contemporary Antarctic ice sheets	19
2.4.2 Records of past water flow beneath the Antarctic ice sheets	23
2.4.3 The contemporary Greenland Ice Sheet	26
2.4.4 Records of past water flow beneath the Greenland Ice Sheet	30
2.5 Tunnel valleys	31
2.5.1 General character and the formation of tunnel valleys	31

2.5.2	Tunnel valleys in the North Sea	33
2.5.3	Tunnel valley infill	36
2.5.3.1	General infill patterns	36
2.5.3.2	The infill of tunnel valleys in the North Sea	39
2.6	Summary	42
3	Methodology and datasets	44
3.1	Background: Marine acoustic methods and glaciology	44
3.2	Multibeam swath bathymetry	45
3.2.1	Introduction	45
3.2.2	Multibeam bathymetric data used in this thesis	47
3.3	Seismic-reflection methods	48
3.3.1	Introduction	48
3.3.2	3D seismic data	51
3.3.3	High-resolution 3D seismic data	53
3.4	Seismic methods employed in this thesis	55
3.4.1	GSeis ³ high-resolution 3D seismic data	56
3.4.2	Regional scale 3D seismic data	57
4	Past water flow beneath Pine Island and Thwaites glaciers, West Antarctica	59
4.1	Introduction	60
4.2	Methods	63
4.2.1	Bathymetric and terrestrial data	63
4.2.2	Derivation of channel metrics	64
4.2.3	Modelling past subglacial water flow	66
4.2.3.1	Palaeo ice-sheet reconstruction	66
4.2.3.2	Flow routing	67
4.3	Results	69
4.3.1	Morphology of channels in Pine Island Bay	69
4.3.2	Comparison with the Labyrinth	71
4.3.3	Modelled subglacial hydrology	72
4.4	Discussion	78
4.4.1	Channel formation	78
4.4.2	Channel water sources	80
4.5	Conclusions	88
5	Tunnel valley infill and genesis revealed by high-resolution 3D seismic data	89
5.1	Introduction	90
5.2	Data and methods	90
5.3	Buried landforms within tunnel valleys	91
5.4	Discussion	98
5.5	Conclusions	100

6	Tunnel valley formation beneath deglaciating mid-latitude ice sheets:	102
	Observations and modelling	
6.1	Introduction	103
6.2	Methods	108
6.2.1	Detailed channel morphology from high-resolution 3D seismic data	108
6.2.2	Modelling subglacial water flux and routing	110
6.2.2.1	BRITICE-CHRONO ice sheet modelling data	110
6.2.2.2	Subglacial water routing	112
6.2.2.3	Tunnel valley carrying capacity	113
6.2.3	Modelling tunnel valley erosion	113
6.2.3.1	Erosion model	113
6.2.3.2	Testing scenarios of tunnel valley formation: outburst floods versus steady seasonal melt supply	115
6.3	Results	119
6.3.1	Tunnel valley morphology and discharge	119
6.3.2	Modelled water routing	124
6.3.3	Tunnel valley erosion	128
6.3.3.1	Erosion from seasonal surface drainage	128
6.3.3.2	Erosion from outburst floods	129
6.4	Discussion	131
6.4.1	Morphological insights into tunnel valley incision processes	131
6.4.1.2	The origin of glacial curvilineations	133
6.4.2	Mechanisms and rates of tunnel valley erosion	134
6.4.3	Implications for tunnel valley genesis and ice-sheet dynamics	138
6.5	Conclusions	140
7	The infill of buried tunnel valleys in the central North Sea:	141
	Implications for sedimentary processes and ice-sheet dynamics	
7.1	Introduction	142
7.2	Regional setting	144
7.3	Datasets and methods	147
7.3.1	High-resolution 3D seismic data	147
7.3.2	Regional scale 3D seismic data	148
7.3.3	Geotechnical information from industry-acquired boreholes	149
7.3.4	Mapping of buried tunnel valleys	149
7.3.5	Examination of tunnel valley infill	150
7.4	Results and interpretation	150
7.4.1	Mapped tunnel valleys	150
7.4.2	Types of tunnel valley infill	154
7.4.2.1	Geotechnical borehole information	154
7.4.2.2	Infill character observed in 3D seismic data	157
7.4.2.3	Study Area 1	161
7.4.2.4	Study Area 2	164

7.5	Discussion	166
7.5.1	Implications for North Sea glacial history	166
7.5.2	Patterns of tunnel valley sedimentation	168
7.6	Conclusions	176
8	Synthesis and conclusions	177
8.1	Purpose of this chapter	177
8.2	Flux and routing of water beneath deglaciating ice sheets	177
8.2.1	Advances made in this thesis	177
8.2.2	Directions for future work	180
8.3	The impact of subglacial water flow on ice-sheet dynamics during deglaciation	184
8.3.1	Advances made in this thesis	184
8.3.2	Directions for future work	187
8.4	Sedimentation patterns resulting from subglacial water flow and other processes during deglaciation	189
8.4.1	Advances made in this thesis	189
8.4.2	Directions for future work	192
8.5	Thesis summary and conclusions	194
	Bibliography	195

List of figures

1.1	Projections of selected climate change indicators under the Intergovernmental Panel on Climate Change’s five ‘Shared Socioeconomic Pathways’ (SSPs).	3
1.2	Mass change of the Greenland and Antarctic ice sheets, and their contribution to global mean sea-level change.	4
2.1	Idealised routing of subglacial water beneath an ice mass.	10
2.2	The variety of subglacial drainage systems observed and theorised to exist beneath glaciers and ice sheets.	11
2.3	Inventory of subglacial lakes in the northern hemisphere and beneath the Antarctic Ice Sheet.	16
2.4	Relationship between discharge rate and lake drainage volume for active subglacial lakes and ice-marginal lakes.	18
2.5	Subglacial hydrology of the Antarctic Ice Sheet.	20
2.6	Early examples and interpretations of meltwater-derived morphology on the Antarctic continental shelf.	24
2.7	Distribution of bedrock meltwater channels on Antarctic inner continental shelves.	25
2.8	Hydrology of the Greenland Ice Sheet.	28
2.9	Distribution of tunnel valleys and meltwater channels in the North Sea and Northwest Europe.	35
2.10	Examples of buried and infilled tunnel valleys exposed in outcrops from Germany and Denmark.	37
2.11	Examples of tunnel valley cross sections and infill structures.	38
2.12	Example of the northward-dipping clinoforms found to infill tunnel valleys in the southern and southeastern sectors of the North Sea.	41
3.1	Acoustic methods used to image submarine glacial landforms in marine settings.	46
3.2	Example of a modern marine setup for large-scale 3D seismic data collection.	51
3.3	A 3D seismic volume displayed within seismic interpretation software.	52
3.4	Differences between high-resolution 3D seismic reflection data and conventional 3D seismic reflection data.	55
3.5	Comparison between seafloor iceberg scours mapped using multibeam bathymetric data and buried iceberg ploughmarks mapped using high-resolution 3D seismic data.	56
3.6	The GSeis ³ acquisition system.	58

4.1	Overview map displaying the location of features and regions referred to in Chapter 4.	62
4.2	Methods of quantifying channel morphometry.	65
4.3	Channelised bathymetry of the region offshore of Pine Island and Thwaites glaciers.	70
4.4	Comparison between the results of Kirkham (2017) and Kirkham et al. (2019).	71
4.5	Size-frequency distributions of the morphometric characteristics of the channels comprising the Labyrinth and those present offshore of Pine Island and Thwaites glaciers.	72
4.6	Modelled water flow beneath Pine Island and Thwaites glaciers at the LGM.	73
4.7	Spatial variation of channel size within Pine Island Bay.	75
4.8	Relationship between modelled water flux and channel size through a channel basin system.	76
4.9	Schematic of channel formation over multiple glacial interglacial cycles.	81
5.1	Distribution of buried tunnel valleys in the central North Sea.	91
5.2	Seismic character of buried tunnel valleys in the central North Sea.	92
5.3	Comparison of conventional 3D seismic-reflection data and high-resolution 3D seismic-reflection data.	93
5.4	Glacial landforms buried inside tunnel valleys.	94
5.5	Comparison between the morphology of eskers buried within tunnel valleys in the North Sea and those in other locations.	95
5.6	Comparison between ridges found buried within North Sea tunnel valleys and rhombohedral crevasse squeeze ridges in Svalbard.	97
5.7	Ice-sheet regimes implied by landform assemblages and stratigraphic relationships inside tunnel valleys.	101
6.1	Previously proposed mechanisms of tunnel valley formation.	105
6.2	Study area.	110
6.3	Distribution of grain sizes from boreholes drilled into the infill of tunnel valleys in the central-northern North Sea, the southern North Sea, and southern Sweden.	114
6.4	Tunnel valley morphology imaged using high-resolution 3D seismic data.	121
6.5	Buried glacial curvilineations (GCLs) imaged within tunnel valleys.	122
6.6	Smaller channel systems comprising the base of some tunnel valleys.	123
6.7	Elongate bedforms present adjacent to a tunnel valley.	124
6.8	Modelled water flow paths and fluxes beneath the British-Irish and Fennoscandian ice sheets.	126
6.9	Example of a detailed subglacial water routing model run and resulting tunnel valley properties.	127

6.10	Tunnel valley erosion rates into a sedimentary substrate as a proportion of modelled tunnel valley length for the seasonal drainage mechanism (migrating 100 m wide channels).	130
6.11	Tunnel valley formation beneath a deglaciating mid-latitude ice sheet.	136
7.1	Study area.	146
7.2	Comparison between high-resolution 3D seismic data and the conventional 3D seismic data previously used to investigate tunnel valley infill in the central North Sea.	151
7.3	Distribution and infill character of tunnel valleys in Study Area 1.	152
7.4	Distribution and infill character of tunnel valleys in Study Area 2.	153
7.5	Study Area 3.	154
7.6	Geotechnical boreholes in Study Area 3.	156
7.7	Seismic facies identified within the infill of central North Sea tunnel valleys.	158
7.8	Potential clinoform structures imaged within a tunnel valley.	159
7.9	Dimensions and infill character of tunnel valleys in the central North Sea.	163
7.10	High-amplitude reflections associated with subglacial landforms and shallow gas buried within the central North Sea tunnel valleys.	164
7.11	Gas-charged eskers buried within tunnel valleys.	171
7.12	Comparison of amplitude anomaly extractions between depths where tunnel valleys are present and the underlying gas-charged Crenulate Reflector.	174
8.1	Comparison between the size of a conventional 3D seismic acquisition system and the considerably more compact high-resolution 3D seismic P-Cable setup.	183
8.2	Likelihood of sedimentary basins beneath the Antarctic Ice Sheet and the formerly glaciated Antarctic continental shelf.	184
8.3	Examples of borehole samples recovered from the North Sea by the hydrocarbon industry after triaxial geotechnical testing.	193

List of tables

4.1	Details of the geophysical cruise data used in Chapter 4.	63
4.2	Volume, filling time, local steady state discharge, and potential mean flood discharge of lakes displayed in Fig. 4.6.	78
6.1	Definitions, values and sources of parameters used in Chapter 6.	118

Nomenclature

Abbreviations

2D	Two dimensional
3D	Three dimensional
CNS	Central North Sea
DEM	Digital elevation model
DTM	Digital terrain model
ELA	Equilibrium line altitude
EMODnet	European Marine Observation and Data Network
GCL	Glacial curvilineations
GEBCO	General Bathymetric Chart of the Oceans
GHF	Geothermal heat flux
GNSS	Global Navigation Satellite System
GPL	General Power Law
GPS	Global positioning system
HR3D	High-resolution 3D
IBCSO	International Bathymetric Chart of the Southern Ocean
IMBIE	Ice Sheet Mass Balance Inter-comparison Exercise
LGM	Last Glacial Maximum
LIMA	Landsat Image Mosaic of Antarctica
MIC	Mýrdalsjökull Ice Cap
MIS	Marine Isotope Stage
MPhil	Master of Philosophy
MSGLs	Megascale glacial lineations
MV	Motor vessel
N-channel	Nye channel
NED	National Elevation Dataset of the USA
PDB	Palmer Deep Basin
PDOS	Palmer Deep Outlet Sill
PGS	Petroleum Geo-Services
PIG	Pine Island Glacier
PISM	Parallel Ice Sheet Model
PMIP	Paleoclimate Modeling intercomparison Project
R-channel	Röthlisberger channel
RRS	Royal Research Ship
RV	Research Vessel
RVIB	Research Vessel/Ice Breaker
SGL	Subglacial lake
SRME	Surface Related Multiple Elimination
SSP	Shared Socioeconomic Pathway
TAM	Transantarctic Mountains

TFD	Time-frequency domain
TG	Thwaites Glacier
TV	Tunnel valley
TWT	Two-way travel time
UHR2D	Ultra-high-resolution 2D
UK	United Kingdom
VE	Vertical exaggeration
VIC	Vatnajökull Ice Cap
WAIS	West Antarctic Ice Sheet
w.e.	Water Equivalent
WCRP	World Climate Research Program

Roman symbols

a	Power law equation constant
b	Channel shape parameter
\bar{c}	Sediment concentration in water
D	Depth
\dot{D}	Deposition rate
D_{15}	15 th percentile grain size
\dot{E}	Erosion rate
F	Frequency
f_{cc}	Channel roughness parameter
g	Acceleration due to gravity
h	Bed elevation
k	Uniform floatation factor
K_1	Erosion constant
K_2	Deposition constant
m	Manning coefficient
Q_{max}	Maximum discharge capable of being carried by a channel
R	Vertical resolution
S	Channel cross sectional area
v	Velocity of sound through water
V	Velocity of sound through rock
$W1$	Horizontal distance from the deepest point of a channel to its left side
$W2$	Horizontal distance from the deepest point of a channel to its right side
Z	Ice thickness

Greek symbols

α_{cc}	Channel geometry factor
λ	Wavelength
ϕ	Subglacial hydraulic potential
ϕ'	Subglacial hydraulic potential gradient
ρ_w	Density of water

ρ_s	Density of sediment
ρ_i	Density of ice
τ_{cc}	Channel bed shear stress
τ_k	Critical shear stress
u_c	Channel flow velocity
μ_w	Viscosity of water
v_s	Mean sediment settling velocity

Preface

The research conducted in this thesis was carried out by the author, James Kirkham. The material in Chapters 4, 5, and 6 is published (Kirkham et al., 2019, 2021, 2022), and the material in Chapter 7 will shortly be submitted for peer-review. The co-authors of these publications provided research oversight, methodological guidance, raw primary data (e.g., 3D seismic-reflection data), and processed supporting data (e.g., ice-sheet model reconstructions). All of the analysis and manuscript writing was undertaken by the thesis author, with the co-authors providing feedback. Named co-authors, and their contributions to the research, are identified in the author-contribution statements within the published papers.

Chapter 4 was published in *The Cryosphere* in July 2019:

Kirkham, J. D., Hogan, K. A., Larter, R. D., Arnold, N. S., Nitsche, F. O., Golledge, N. R., and Dowdeswell, J. A. (2019). Past water flow beneath Pine Island and Thwaites glaciers, West Antarctica. *The Cryosphere*, 13, 1959–1981, <https://doi.org/10.5194/tc-13-1959-2019>.

The concepts underpinning Chapter 4 were developed from an MPhil project (Kirkham, 2017) with a number of advancements. These are outlined below and in Sections 4.3.1 and 4.3.3 of Chapter 4. Recently acquired multibeam bathymetric data were used to expand the study area to Thwaites Glacier and further regions offshore from Pine Island Glacier. Over 40 % more bedrock channels were mapped and the boundaries of bedrock basins were redrawn utilising the new bathymetric data (Figures 4.4A, 4.4B). The modelling component of Chapter 4 was also substantially revised to incorporate the entire last glacial catchments of Pine Island and Thwaites glaciers, compared to only a restricted area offshore previously (see Figures 4.4C, 4.4D, 4.6B). This had a significant impact on the magnitude of the steady-state water discharges calculated by the model (see Figure 4.4E), increasing them by up to three orders of magnitude. The geothermal heat flux (Maule et al., 2005) and the basal topography (Fretwell et al., 2013) previously used to force the water routing model were also updated to higher resolution datasets (Martos et al., 2017 and Morlighem et al., 2019, respectively). Further numerical analyses, such as comparing channel dimensions to the proximity of basins and to the magnitude of the predicted water fluxes, were also undertaken.

A shorter version of Chapter 5 was published in *Geology* in September 2021, and is based solely on work undertaken for this PhD thesis:

Kirkham, J. D., Hogan, K. A., Larter, R. D., Self, E., Games, K., Huuse, M., Stewart, M. A., Ottesen, D., Arnold, N. S., and Dowdeswell, J. A. (2021). Tunnel valley infill and genesis revealed by high-resolution 3-D seismic data. *Geology*, 49(12), 1516-1520, <https://doi.org/10.1130/g49048.1>.

Chapter 6 was published in *Quaternary Science Reviews* in October 2022, and is based solely on work undertaken for this PhD thesis:

Kirkham, J. D., Hogan, K., Larter, R. D., Arnold, N., Ely, J. C., Self, E., Games, K., Huuse, M., Stewart, M., Ottesen, D., and Dowdeswell, J. A. (2022). Tunnel valley formation beneath deglaciating mid-latitude ice sheets: Observations and modelling. *Quaternary Science Reviews*, <https://doi.org/10.1016/j.quascirev.2022.107680>

Chapter 7 will be submitted to *Marine Geology*, and is based solely on work undertaken for this PhD thesis:

Kirkham, J. D., Hogan, K.A., Larter, R. D., Self, E., Games, K., Huuse, M., Le Heron, D.P., Stewart, M. A., Ottesen, D., Arnold, N. S. and Dowdeswell, J. A. The infill of buried Quaternary tunnel valleys in the central North Sea. *Marine Geology*.

Chapter 1

Introduction

1.1 Thesis motivation

The Earth is currently undergoing a period of anthropogenic global warming that is unparalleled in terms of absolute temperatures and unprecedented in its spatial uniformity over last two millennia (Neukom et al., 2019). Ice sheets and glaciers are sensitive indicators of climate change; their shrinkage visibly reflects the warming of the Earth's climate through time (Oerlemans, 1994). Currently, the Earth's cryosphere (including glaciers and ice sheets, seasonal snow cover and permafrost) covers up to 55 % of the global land surface and contains enough frozen water to raise global mean sea level by ~ 66 m (Vaughan et al., 2013). The majority of this sea-level equivalent is contained within the Antarctic Ice Sheet (57.9 m; Morlighem et al., 2019) whilst smaller, yet still significant, portions are contained within the Greenland Ice Sheet (7.42 m; Morlighem et al., 2017) and in smaller glaciers and ice caps situated across the globe (0.257 m; Millan et al., 2022).

Tide gauge and satellite altimetry observations show that the rate of global mean sea-level rise increased from 1.4 mm year^{-1} between 1901–1990 to 3.6 mm year^{-1} between 2006–2015 (Oppenheimer et al., 2019). More recently, the rate of global mean sea-level change has risen to 4.5 mm year^{-1} over the period 2013–2021, mostly driven by accelerated losses from ice sheets (World Meteorological Organization, 2022). Mass losses from glaciers, Greenland, and Antarctica contributed 21 %, 15 %, and 8 % to global mean sea-level changes between 1993 and 2018, respectively, with the remainder comprised of ocean thermal expansion and changes to land water storage (WCRP Global Sea Level Budget Group, 2018). More than 600 million people (~ 10 % of the global population) live within 10 m of sea level worldwide (Neumann et al., 2015). Consequently, the

accelerating contributions of glaciers and ice sheets to sea-level rise threaten to inundate significant parts of low-lying nation states, displace tens of millions of people in the developing world (Dasgupta et al., 2009; Bhattachan et al., 2018), increase the magnitude and likelihood of storm surges (Nicholls et al., 1999; Shepard et al., 2012), and damage coastal ecosystems (e.g., Ellison and Stoddart, 1991; Maschinski et al., 2011; Lendemer and Allen, 2014).

Currently, glaciers alone contribute 25–30 % to sea-level rise; this ice loss is now roughly comparable to the contributions from the Greenland Ice Sheet, and exceeds that from Antarctica (Zemp et al., 2019). However, it is widely acknowledged that within the twenty-first century, contributions from the Greenland and Antarctic ice sheets will begin to dominate the cryospheric portion of sea-level rise (e.g., Raper and Braithwaite, 2006; Church et al., 2013; Bamber et al., 2019). Furthermore, substantial multi-metre increases in future sea level cannot be ruled out under high-emission scenarios due to ice sheet instabilities, such as the collapse of a large West Antarctic drainage basin, that are currently poorly constrained (Figure 1.1; Lenton et al., 2019; Arias et al., 2021).

Although the mass change of the Greenland Ice Sheet was near negligible in the 1990s, annual mass losses have risen since then, with Greenland losing $3,902 \pm 342$ billion tonnes of ice between 1992 and 2018 — causing the mean sea level to rise by 10.8 ± 0.9 mm (Figure 1.2A; Shepherd et al., 2020). For Greenland, a trend of increasing mass loss is driven primarily by increasing meltwater runoff due to atmospheric warming since the late twentieth century (van den Broeke et al., 2016; Noël et al., 2019), and ocean warming (Wood et al., 2018).

In comparison, Antarctica lost $2,720 \pm 1,390$ billion tonnes of ice between 1992 and 2017, raising mean sea level by 7.6 ± 3.9 mm (Figure 1.2B; IMBIE, 2018). In recent decades, most Antarctic mass loss has been driven by trends in ocean warming. Particularly in West Antarctica, an eastward wind trend over the continental shelf break that is at least partially linked to anthropogenic forcing has driven intrusions of warm Circumpolar Deep Water across the inner continental shelf and up to the ice sheet grounding zone (e.g., Thoma et al., 2008; Cook and Vaughan, 2010; Dutrieux et al., 2014; Cook et al., 2016; Holland et al., 2019; Naughten et al., 2022). These intrusions, combined with atmospheric warming of several degrees on the western Antarctic Peninsula (e.g., Vaughan and Doake, 1996; Scambos et al., 2000), have caused the floating ice shelves present in these regions to thin and retreat, reducing their buttressing effect on the inland ice sheet. This process has triggered grounding-zone retreat (Rignot et al., 2014; Konrad et al., 2018; Gudmundsson et al., 2019), and the acceleration (Rignot et al., 2004) and

drawdown (Scambos et al., 2004) of a number of marine-terminating ice streams. These recent climatic and oceanic changes across Antarctica mean that its sea-level contribution could soon outpace all other sources (Pritchard et al., 2012; Rignot et al., 2014; Paolo et al., 2015). Moreover, a much more dramatic increase in ice discharge is possible in the coming decades due to the vulnerability of its marine-based sectors to instabilities that could facilitate ice-sheet collapse (Weertman, 1974; Mercer, 1978; Joughin et al., 2014; DeConto and Pollard, 2016; DeConto et al., 2021).

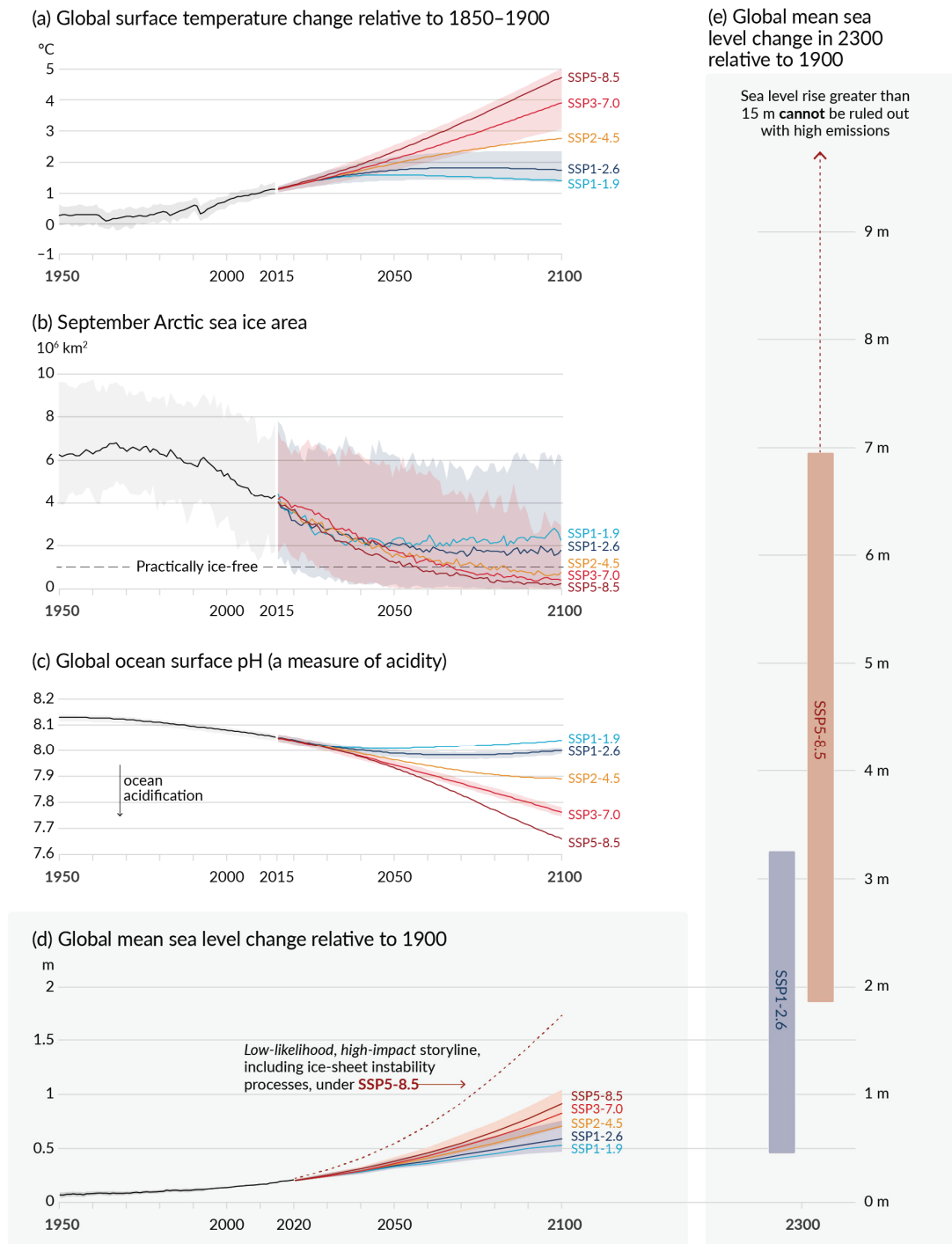


Figure 1.1. (Overleaf). Projections of selected climate change indicators under the Intergovernmental Panel on Climate Change’s five ‘Shared Socioeconomic Pathways’ (SSPs). Projections up to the year 2100 are shown in coloured lines for: (A) global surface temperature, (B) Arctic sea ice, (C) global ocean surface acidity, and (D) global mean sea-level change. A projection up to the year 2300 is shown for global mean sea-level change in (E), including a low-likelihood, high-impact storyline for a multi-metre increase in sea level that currently cannot be ruled out due to ice-sheet instabilities. The shading around each line represents projection uncertainty. Black curves represent historical simulations in panels A, B, and C, and historical observations in the case of Panel D. Figure is taken from the Intergovernmental Panel on Climate Change (2021).

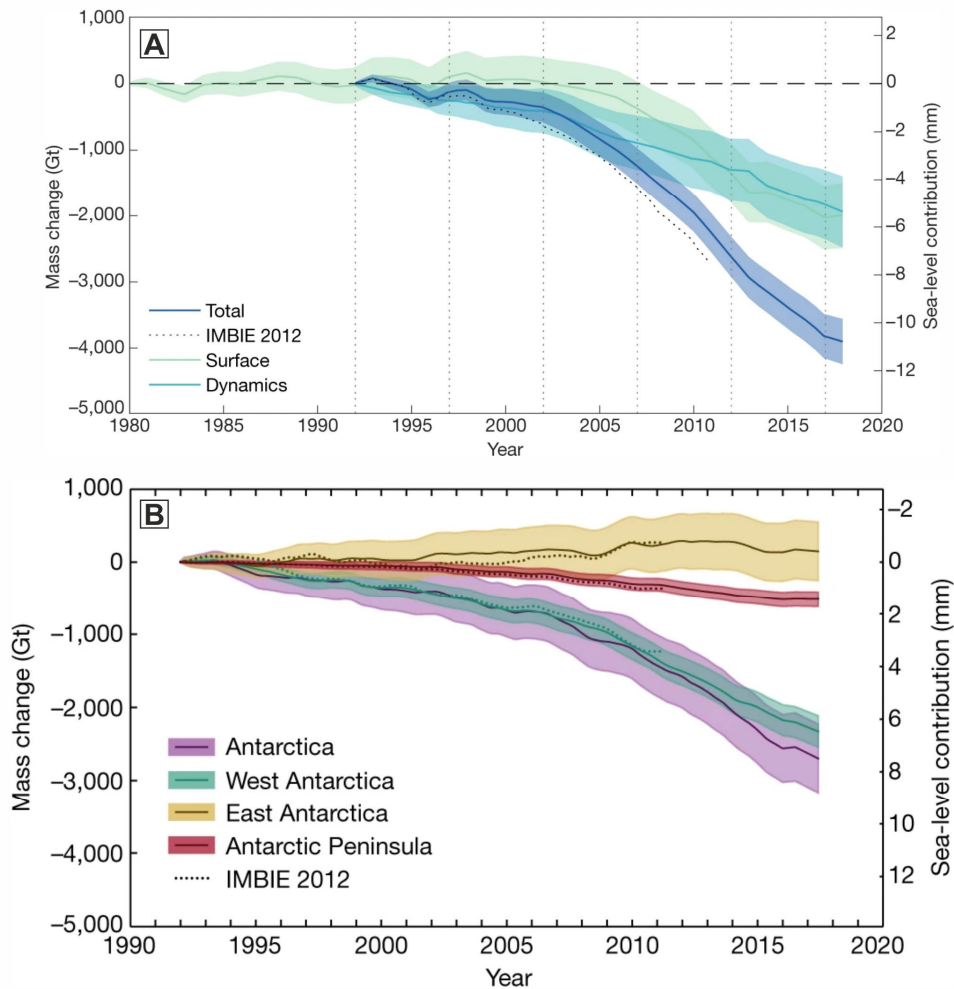


Figure 1.2. Mass change of the (A) Greenland and (B) Antarctic ice sheets, and their contribution to global mean sea-level change. The estimated 1σ uncertainties of the cumulative mass change is shaded. Figure (A) is reproduced from Shepherd et al. (2020) and shows both the total mass change from the entire Greenland Ice Sheet as well as mass change partitioned into surface and dynamic components. Figure (B) is reproduced from IMBIE (2018) and displays both the total mass change from Antarctica as well as the mass change from West Antarctica, East Antarctica, and the Antarctic Peninsula.

Substantial and rapid collapse of large ice sheets has occurred in the past (Scherer et al., 1998; Reyes et al., 2014; Dutton et al., 2015), possibly as recently as 125,000 years ago during the last interglacial period (e.g., O’Leary et al., 2013). Even more recently, during the last deglaciation (~18,000 years ago), melting of ice sheets in Antarctica, Europe and North America caused global sea level to rise by 18 m in 500 years (Cronin, 1982; Fairbanks, 1989; Deschamps et al., 2012; Lin et al., 2021). If changes of this scale were to happen in the present day, they would severely limit the effectiveness of humankind’s attempts to adapt to climate change, leading to economic damage and widespread threats to life and wellbeing (Climate Change Committee, 2021). The resulting acceleration in sea-level rise would require a large increase in adaptation or infrastructure replacement in coastal areas worldwide (Scambos et al., 2017), particularly when considering the impact of storm surges, which can raise sea levels locally by several metres during an event (Biasutti et al., 2012). These examples highlight the threat that ice sheets pose to populated coastlines around the world under high-end future climate warming scenarios.

1.1.1 The short record of modern glaciological observations

Over the past four decades, spaceborne measurements have allowed significant events in Earth’s recent climate history to be charted in remarkable detail (Shepherd et al., 2018). These satellite observations have documented the collapse of ice shelves along the Antarctic Peninsula (Rott et al., 1996; Scambos et al., 2004) and the acceleration of mass loss from glaciers in West Antarctica (IMBIE, 2018; Konrad et al., 2018; Rignot et al., 2019). However, the observational record of ice-sheet change is short in comparison to the timescales over which ice sheets respond to variations in climate, and a consensus is being built that ice sheets have the potential to act more dynamically than observed in the satellite era. For example, delicate landforms preserved in the seafloor record have been used to infer grounding-line retreat rates up to an order of magnitude higher than was previously thought possible based on satellite observations (Dowdeswell et al., 2020; Graham et al., 2022). Consequently, in order to fully incorporate the entire range of processes that occur in ice-sheet systems into models of ice-sheet evolution and sea-level rise, it is crucial to understand the range of processes that occur beneath ice sheets — including high-magnitude, low-frequency events and processes that might occur on geological timescales not covered by the satellite era of glaciology.

The storage, transfer, and expulsion of water beneath ice sheets is particularly poorly understood at present. Small transfers of water have been mapped beneath the Greenland and Antarctic ice sheets using satellite altimetry (Gray et al., 2005; Wingham et al., 2006; Fricker et al., 2007; Bowling et al., 2019; Livingstone et al., 2022), yet their flux is

several orders of magnitude smaller than other water transfers inferred from the geological record (Denton and Sugden, 2005; Domack et al., 2006; Lewis et al., 2006; Hogan et al., 2022). The transfer of subglacial water has a variable effect on ice-sheet flow and mass loss, with some studies observing a corresponding increase in ice velocity (Zwally et al., 2002; Stearns et al., 2008; Siegfried et al., 2016), and others reporting no distinguishable change at all (Smith et al., 2017). These discrepancies, combined with the fact that it is difficult to observe the processes operating at the base of contemporary ice sheets directly, has meant that the effect of subglacial water as a lubricant at the basal ice-sheet boundary is still insufficiently understood to be accurately incorporated into the current generation of ice-sheet models. Accordingly, subglacial water flow is absent from current assessments of future ice-sheet behaviour and is not considered in high-end projections of future sea-level rise (Fricker and Scambos, 2009; Flowers, 2015; Fricker et al., 2016; Goelzer et al., 2020). Consequently, there is great value in examining how water was transferred beneath former ice sheets as they underwent deglaciation, as these can be used as analogues for how contemporary ice sheets may evolve under future climate warming scenarios. This approach, used in the following chapters, can provide insights into important ice-sheet processes that may begin to operate in the future.

1.2 Research aim and objectives

Recent advances in surveying technology have driven an expansion of geophysical data coverage in formerly ice-covered regions. Unparalleled areal data coverage, and the improved resolution of the geophysical data available, mean that there has never been a better time to examine the former beds of ice sheets to investigate inaccessible glacial processes that are difficult to observe beneath their modern counterparts. The new geophysical data thus provide an opportunity to examine signatures of water flow beneath ancient ice sheets as they underwent deglaciation, providing analogues for how modern ice sheet drainage systems will evolve in a future warmer world. Consequently, this thesis aims to understand how the subglacial drainage systems of contemporary ice sheets may evolve under future climate warming scenarios using palaeo records of past ice sheet water drainage. Three primary objectives are outlined following this aim:

1. To constrain the routing and fluxes of subglacial water beneath past ice sheets. This work is presented in Chapters 4 and 6.
2. To examine the impact of subglacial water flow on ice-sheet dynamics during deglaciation. This work is presented in Chapter 5.

3. To investigate the sedimentation patterns resulting from subglacial water flow and other glacier-influenced processes during deglaciation. This work is presented in Chapter 7.

1.3 Thesis structure

This thesis consists of eight chapters. The current chapter has introduced the rationale for studying past ice-sheet dynamics and processes. In Chapter 2, a review of the literature on subglacial hydrology and water transport beneath contemporary and ancient ice sheets is undertaken. In Chapter 3, the data and methods used to investigate the water flow beneath past ice sheets are summarised. The production and transport of subglacial water beneath two major outlets of the West Antarctic Ice Sheet, ~20,000 years ago, is reconstructed in Chapter 4, using an approach that combines geophysical observations and numerical modelling. The thesis then pivots in Chapter 5 to the Northern Hemisphere, and utilises state-of-the-art 3D seismic reflection data to deliver new insights into how meltwater channels (tunnel valleys) were formed during the deglaciation of the European Ice Sheet complex and how these features influenced ice-sheet dynamics in the North Sea. In Chapter 6, a numerical model is applied to constrain how rapidly tunnel valleys can be incised beneath deglaciating ice sheets. The infill of buried tunnel valleys in the North Sea on a regional scale is used to examine large-scale ice-sheet sedimentation patterns in Chapter 7. Finally, in Chapter 8 a synthesis of the thesis and suggested directions for future research is provided.

Chapter 2

Literature Review

2.1 Chapter overview

The purpose of this chapter is to provide a review of previous research with which to contextualise the thesis. It is divided into three main sections: the first describes the history of subglacial hydrological theory; the second summarises recent evidence for dynamic and widespread water transport and storage beneath the contemporary Antarctic and Greenland ice sheets; the third describes the state of knowledge regarding tunnel valleys — large subglacial channels that act as records of water flow beneath past ice sheets.

2.2 Subglacial hydrological theory

2.2.1 Water routing and impacts on ice flow

A causal link between subglacial water flow and glacial dynamics has been postulated for over half a century, initially stemming from observations of seasonal changes in glacier velocities linked to meltwater availability (e.g., Weertman, 1972; Walder, 1982; Kamb, 1987). From the decades of research that followed, it has been demonstrated that subglacial water imparts a fundamental control on glacier and ice-sheet dynamics, and thus mass loss, through the manner in which water is stored beneath the ice and is evacuated to the glacier or ice-sheet margin. Subglacial water can be derived from several sources: surface meltwater that drains to the bed (Zwally et al., 2002; Das et al., 2008; Bartholomew et al., 2011a), basal melting of ice raised to the pressure melting point by geothermal or frictional strain heating (Dowdeswell et al., 2016a), and/or water influx from underlying aquifers (Bell, 2008; Christoffersen et al., 2014; Gustafson et al., 2022).

Excess subglacial water must drain to the ice-sheet margin otherwise the accumulated basal meltwater will elevate fluid pressures to above the overburden pressure exerted by the overlying ice. This would result in the widespread decoupling of the ice sheet from its bed, a condition that would lead to catastrophic surges and ice-sheet collapse if sustained over long timescales (Marczinek and Piotrowski, 2006; Piotrowski et al., 2009; Kehew et al., 2012).

Subglacial water can be evacuated to the ice-sheet margins by a variety of processes that can be divided into either efficient (channelised) or inefficient (distributed) drainage configurations. Theory initially developed from mountain glacier environments (e.g., Sharp et al., 1993; Hubbard et al., 1995; Willis et al., 1996) shows that these two drainage configurations typically have opposing effects on ice-flow dynamics by altering the effective pressure (ice overburden pressure minus basal water pressure) at the ice-bed interface. The presence of an efficient drainage structure allows water to be swiftly evacuated from the subglacial environment. This increases the coupling between the ice and the bed, thus increasing basal shear stresses, effective pressures, and reducing ice-flow velocities (Schoof, 2010; Hewitt, 2013). Conversely, elevated pore-water pressures resulting from the inefficient evacuation of subglacial meltwater from the base of an ice sheet can reduce the area of ice in contact with the bed, decrease effective basal pressures, and increase subglacial sediment deformation, thereby facilitating fast ice flow (Iken, 1981; Bindshadler, 1983; Tulaczyk et al., 2000a; Peters et al., 2006). Understanding the manner in which subglacial water flows beneath ice sheets, and its implications for ice-sheet dynamics, is thus critical to achieving accurate predictions of future ice-sheet behaviour (Flowers, 2015; Fricker et al., 2016). An understanding of subglacial water flow is also necessary in order to interpret geomorphological evidence of former ice-flow patterns in order to make the best use of these observations to inform numerical ice-sheet models.

The routing of subglacial water beneath an ice mass is dictated by gradients of hydraulic potential, determined as a function of the overburden pressure exerted by the weight of the overlying ice, the dimensions of the drainage system, and basal water pressure (Shreve, 1972; Hooke, 1989; Hooke et al., 1990; Schoof, 2010). Theoretical calculations suggest that in the subglacial hydrological system, planes of constant hydraulic potential will rise down-glacier with a gradient approximately eleven times that of the ice-surface slope (Figure 2.1) (Shreve, 1985). Accordingly, conduits should form normal to equipotential surfaces along lines of the steepest hydraulic potential. This means that the routing of water beneath an ice mass is predominantly determined by the ice-surface slope and is only weakly influenced by basal topography (Hooke, 1989). Consequently,

pressurised subglacial water does not need to follow the slope of the bed, and instead can flow across slopes or even uphill (Shreve, 1985). This is an important distinction between subglacial channels and surface streams, the direction of the latter being governed purely by differences in surface elevation along flow.

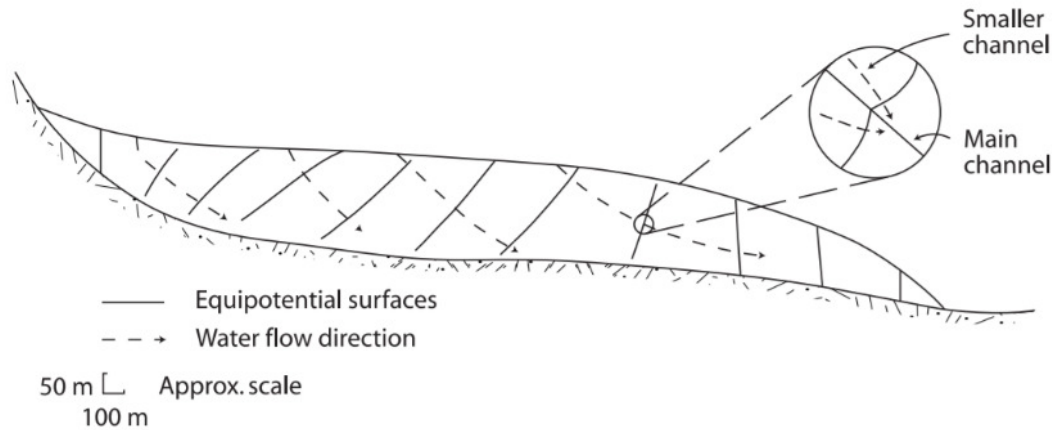


Figure 2.1. Idealised routing of subglacial water beneath an ice mass (dashed arrows), determined by planes of equipotential (solid lines) which rise down-glacier with a gradient of approximately eleven times the surface slope (Shreve, 1985). Figure is from Hooke (1989).

2.2.2 Inefficient (distributed) subglacial drainage systems

Although many methods of evacuating subglacial water to ice-sheet margins have been envisioned (Figure 2.2), subglacial water drainage mechanisms are rarely distinct and are likely to be well hydraulically connected between different regions of the bed (Davison et al., 2019; Lewington et al., 2020). Inefficient drainage systems distribute water over a broad spatial area. Where ice masses are underlain by permeable and porous sedimentary substrates, subglacial water transport can occur through Darcian flow driven out towards the ice margin by a comparatively high water head beneath the ice mass (Figure 2.2A; Boulton and Jones, 1979; Clarke et al., 1984; Boulton and Hindmarsh, 1987). Porous flow systems have a limited transport capacity and consequently they are favoured in areas characterised by low basal melt rates and in regions where ice is underlain by thick, highly permeable, aquifers (Alley, 1989). If porous water transfer cannot evacuate all of the water from beneath the ice, a dedicated drainage system must form.

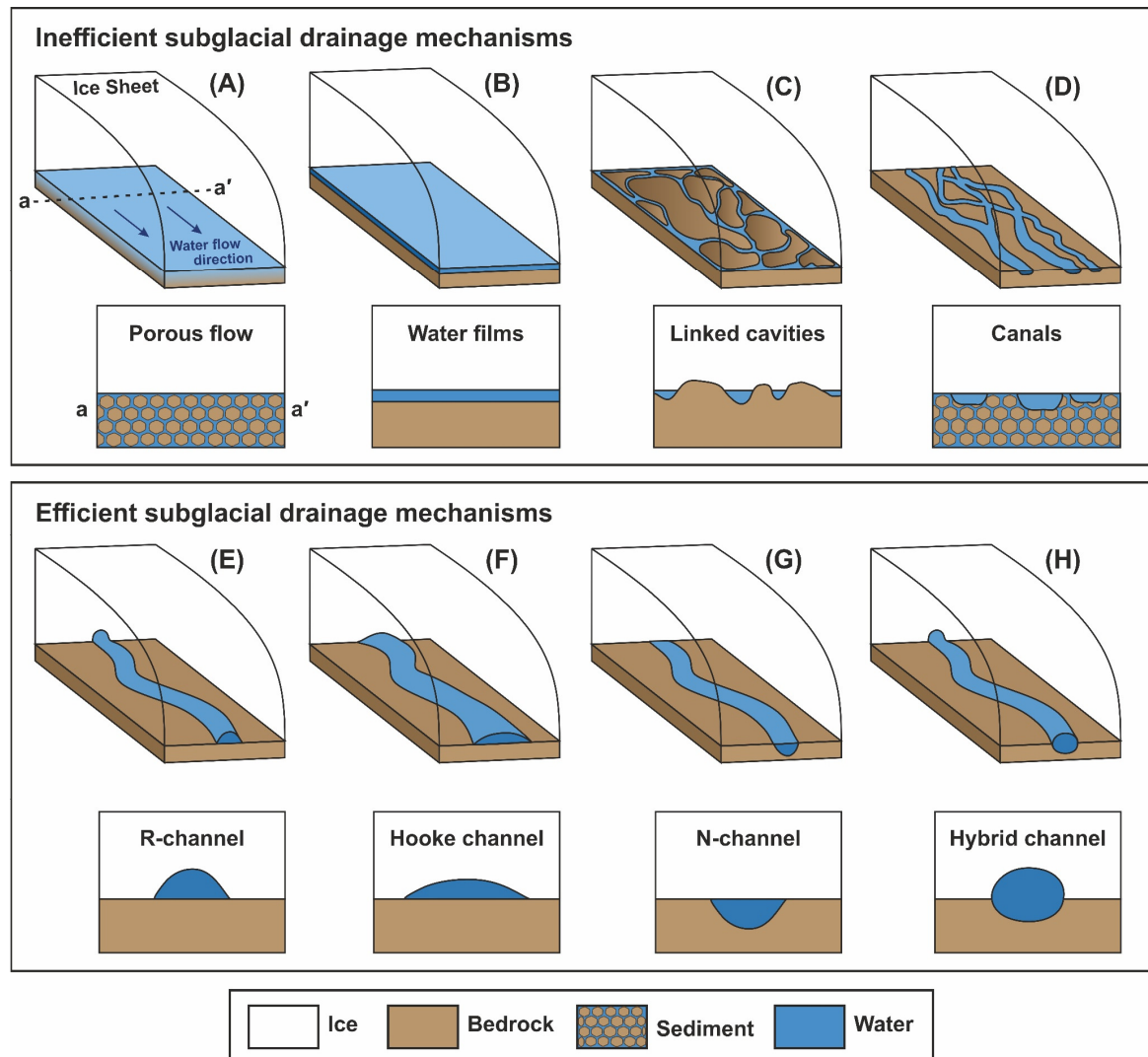


Figure 2.2. The variety of subglacial drainage systems observed and theorised to exist beneath glaciers and ice sheets. The different mechanisms envisioned to drain subglacial water from beneath glaciers and ice sheets are divided into inefficient (top panel) and efficient (lower panel) drainage systems. Inefficient drainage systems can consist of: **(A)** flows through porous sedimentary aquifers (Boulton and Jones, 1979; Clarke et al., 1984; Boulton and Hindmarsh, 1987), **(B)** water films (Weertman, 1972), **(C)** linked cavity systems (Lliboutry, 1968; Walder and Hallet, 1979; Walder, 1986; Kamb, 1987), and **(D)** shallow canals incised into sediment (Walder and Fowler, 1994; Ng, 2000). Efficient drainage systems can consist of: **(E)** Röthlisberger channels (Röthlisberger, 1972), **(F)** Hooke channels (Hooke et al., 1990), **(G)** Nye channels (Nye, 1976), or **(H)** a hybrid form of other efficient mechanisms. Note that some efficient subglacial drainage systems can also be arranged in a branching structure but only a single channel is shown here for visual simplicity. The location of profile a–a' applies to all figures. Figure is reproduced after Flowers (2015) and Davison et al. (2019).

One of the earliest conceptual models of inefficient subglacial drainage was proposed by Weertman (1957, 1972) who suggested that subglacial water transport occurs as a continuous film of water, several millimetres thick, flowing at the ice-bed interface (Figure 2.2B). The effective pressure of a water film is inversely proportional to the fraction of the bed occupied (Alley, 1989). Weertman (1972) argued that these water films could export the bulk of water generated by pressure melting as well as that derived from the surface. These films of water would then fill the spaces between basal irregularities, reduce friction with the overriding ice, and facilitate glacier sliding. However, the suitability of this theory was challenged by Walder (1982), who showed that films greater than a few millimetres thick are unstable due to preferential heat dissipation in areas of local water-sheet thickening, producing a feedback in which channelisation will eventually occur. Consequently, water films are unlikely to contribute significantly to subglacial water transport, although thicker water sheets may occur in areas where bed protrusions bridge the ice-bed interface and enhance the stability of the film (Creyts and Schoof, 2009; Davison et al., 2019).

The most commonly described inefficient subglacial drainage mechanism, which is used in most numerical models of subglacial water flow, consists of a distributed system of linked cavities produced by ice sliding over small bedrock perturbations (e.g., Hewitt, 2013; Werder et al., 2013; Figure 2.2C). The movement of ice over these bed perturbations produces lee-side cavities connected by narrow orifices that throttle water flow and alter the basal water pressure, regulating the rate of basal sliding (Lliboutry, 1968; Walder and Hallet, 1979; Walder, 1986; Kamb, 1987). Water flux through a linked cavity system is a function of water pressure and cavity size, which is in turn regulated by ice sliding speed, ice viscosity, subglacial discharge, and effective pressure. Increased water supply into the drainage system reduces effective pressure, forces cavity expansion, and increases the throughput of water. Variations in water input into linked cavity systems have been suggested as a possible explanation for glacier surges. Kamb (1987) proposed a glacier surge mechanism in which influxes of water delivered to the bed temporarily overwhelm the capacity of the linked cavity system, resulting in low effective pressures and enhanced basal sliding. The dimensions of the orifices eventually respond by expanding to accommodate the greater water fluxes, leading to the formation of a more efficient channelised system of drainage, which reduces effective pressures and terminates the surge.

On glacier beds composed of soft sediments, subglacial water can also be transported through wide, decimetre-deep, shallow canals (Figure 2.2D; Shoemaker, 1986; Walder and Fowler, 1994; Ng, 2000). The canals remain open due to the relatively high shear

strength and viscosity of the till (Alley, 1992). Although typically classified as an inefficient drainage system, sedimentary canals can also transport water efficiently at times if sediment and water fluxes through the canals are sufficiently high (Ng, 2000). Unlike other channelised systems of drainage, canals form distributed, non-arborescent systems characterised by low effective pressures. The low effective pressures predicted by this theory of subglacial drainage are consistent with those measured beneath Whillans Ice Stream in West Antarctica (Blankenship et al., 1986, 1987; Engelhardt et al., 1990), and with radar-echo specularity content analyses of the ice-bed interface of the upstream region of Thwaites Glacier (Schroeder et al., 2013; Hager et al., 2022). The association between subglacial canals and fast-flowing outlet glaciers and ice streams implies that this form of subglacial drainage may be a significant enabler of fast ice flow.

2.2.3 Efficient (channelised) subglacial drainage systems

Conduits formed upwards into the ice or downwards into the basal substrate comprise ‘efficient’ subglacial drainage systems (Figures 2.2E–H). The physical basis for efficient subglacial drainage systems was first described in a landmark theory by Röthlisberger (1972) that still forms the basis of even the most sophisticated subglacial drainage models today (Flowers, 2015). The theory described what have become known as Röthlisberger, or R, channels — hydraulically efficient semi-circular conduits incised upwards into the ice at the ice-bed interface (Figure 2.2E).

The dimensions of R-channels are governed by a balance between viscous heat dissipation from turbulent water flow and the creep closure of the channel walls by the overburden pressure exerted by the overlying ice. Consequently, R-channel formation is suppressed by low water discharges, high effective pressures, and weak hydropotential gradients from shallow ice-surface slopes. An inverse relationship exists between conduit diameter and internal water pressure, as melting of the channel walls at higher discharges decreases the water pressure within conduits as they enlarge (Schoof, 2010). Consequently, larger, lower pressure channels will tend to capture water from smaller high-pressure conduits — producing an arborescent channel configuration as the hydrological system evolves (Fountain and Walder, 1998; Bell, 2008). Due to being located beneath extant ice masses, the dimensions and arrangement of R-channels are difficult to monitor comprehensively. However, comparisons between modelled subglacial water fluxes and dye tracing experiments have inferred that R-channels beneath glaciers such as Midtdalsbreen, Norway, are typically ~15–20 m wide and are less than 0.1 m high (Willis et al., 2012).

Hooke et al. (1990) suggested that rather than exhibiting a semi-circular cross section, the channels formed by this drainage mechanism are more likely to have broader, lower

profiles because melting will be concentrated on the channel walls during times when the channels are only partially occupied with water. These broad, low-profile channels incised upwards into the ice are sometimes termed ‘Hooke’ channels (Figure 2.2F).

Persistent subglacial water flow along the ice-bed interface may also incise Nye, or N-channels, into the basal substrate, producing a signature of meltwater flow that is preserved on the ice-sheet bed (Figure 2.2G; Nye, 1976; Piotrowski, 1994, 1997b; Dowdeswell et al., 2016a). Such consistency in water routing is likely to occur where bedrock topography exerts a strong control on the hydraulic potential gradient, such as in steep-sided valleys or rough glacier beds (Benn and Evans, 2010). Most N-channels extend for a few tens to a few thousands of metres and can be up to tens of metres wide. The largest features, however, form huge meltwater channels up to kilometres wide and hundreds of kilometres long that are termed tunnel valleys (Section 2.5). Systems of N-channels may be arranged in dendritic networks which record subglacial water flow along discrete conduits, or anastomosing systems in which multiple channels split and re-join. Care must be taken when interpreting the geomorphology of former channel systems as anastomosing channels can reflect both distributed drainage in linked cavity networks or the time-transgressive switching of a single channel over time (Benn and Evans, 2010).

Subglacial water may also be transported through channels eroded both upwards into the ice and downwards into the substrate in a hybrid fashion (Figure 2.2H). Evidence for this subglacial water drainage mechanism is offered by the association between bedrock channels and eskers in palaeo-subglacial environments (e.g., Clark and Walder, 1994); this implies that R- and N-channels are end members of the same formative process (Davison et al., 2019).

2.3 Subglacial water storage

2.3.1 Subglacial lakes

Water that pools into lakes in the subglacial environment represents one of the most captivating frontiers of current glaciological research. Subglacial lakes can act as repositories for sediments that record ancient climatic conditions (Smith et al., 2018), provide habitats for extreme life (Christner et al., 2014), and modulate the flow, basal hydrology, biogeochemical fluxes, and geomorphological activity of ice sheets (Siegert, 2000; Fricker and Scambos, 2009; Fricker et al., 2016; Siegert et al., 2016; Livingstone et al., 2022). Globally, 773 subglacial lakes have currently been identified: 675 from Antarctica, 64 from Greenland, 2 beneath the Devon Ice Cap, 6 beneath Iceland’s ice caps and 26 from valley glaciers (Figure 2.3; Livingstone et al., 2022).

The first observations of subglacial lake activity were made in Iceland where outburst floods from these trapped water bodies — jökulhlaups — have been reported since the Middle Ages (Livingstone et al., 2022). In Antarctica, subglacial lakes were first detected in the 1970s when unusually strong, smooth and sharp basal reflections were observed beneath the ice in radio-echo sounding surveys at MHz frequencies (Robin et al., 1970; Oswald and Robin, 1973). In more recent decades, subglacial lakes have also been discovered beneath other ice masses, such as the Greenland Ice Sheet (Ekholm et al., 1998; Palmer et al., 2013; Bowling et al., 2019) and beneath ice caps in the Canadian Arctic (Rutishauser et al., 2018).

Subglacial lakes form when basal water collects in localised hydraulic potential minima. These regions of hydraulic potential minima can be caused by depressions in basal topography or the glacial surface (Shreve, 1972), ice flow over ‘sticky spots’ in the bed (Sergienko and Hulbe, 2011), or the impoundment of basal water behind frozen toes of ice (Gilbert et al., 2012; Livingstone et al., 2022). The dominant source of water for subglacial lakes varies geographically. Most Antarctic subglacial lakes exist in locations where basal temperatures are at the pressure-melting point due to a combination of geothermal and/or frictional heating, and the thermal insulation provided by thick ice cover (Wright and Siegert, 2012). In contrast, many subglacial lakes in Greenland receive considerable surface meltwater input, providing heat that prevents the subglacial water bodies from freezing even at temperatures below the pressure-melting point (Willis et al., 2015; Young et al., 2022). The water contained within Icelandic subglacial lakes is derived from both basal and surface melting because of the prominent influence of volcanism in this location (Björnsson, 2002).

Developments in technology have been key to identifying greater numbers of subglacial lakes over time. Radio-echo sounding can be used to measure the extent of subglacial lakes situated in bedrock basins, whilst seismic-reflection surveys can reveal water column thicknesses and the structure of lake sediments (Robin et al., 1970; Oswald and Robin, 1973; Palmer et al., 2013; Siegert et al., 2016; Smith et al., 2018). Recently, satellite observations of ice-surface displacements derived from satellite radar and laser altimeters have proved crucial in detecting subglacial lake activity indirectly and for estimating changes in lake volume (e.g., Gray et al., 2005; Wingham et al., 2006; Fricker et al., 2007; Smith et al., 2009a; McMillan et al., 2013; Siegfried et al., 2016). These instruments have helped to classify a new type of ‘active’ subglacial lake which periodically experience changes in volume (Figure 2.3).

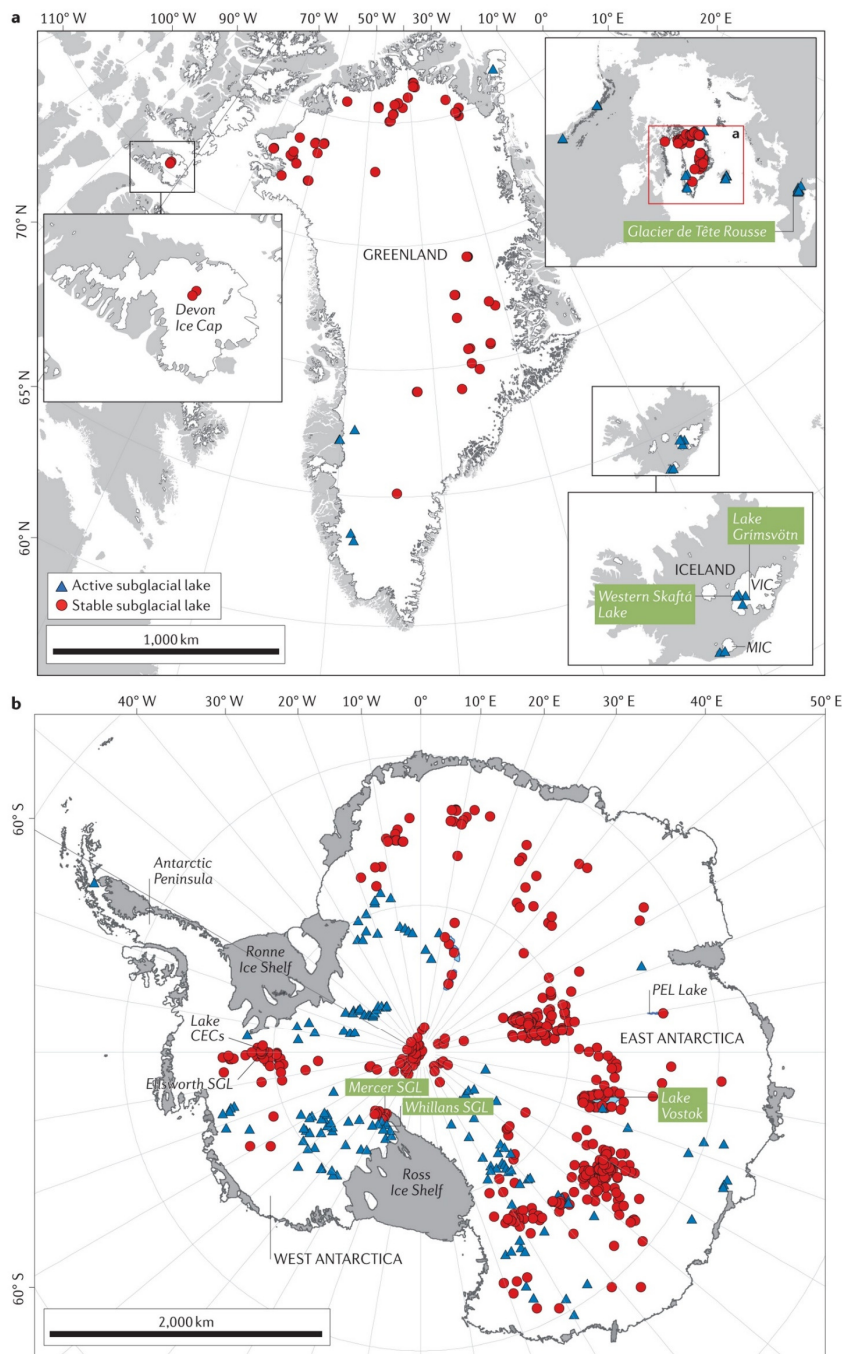


Figure 2.3. Inventory of subglacial lakes in (A) the northern hemisphere and (B) beneath the Antarctic Ice Sheet compiled by Livingstone et al. (2022). Red circles represent stable lakes identified from radio-echo sounding, and blue triangles represent active subglacial lakes that have been observed to drain at least once. Lakes labelled in green have been accessed and cleanly sampled with the exception of Glacier de Tête Rousse and Lake Vostok. The extents of larger lakes (such as PEL Lake and Lake Vostok) are displayed as blue polygons. MIC — Mýrdalsjökull Ice Cap; VIC — Vatnajökull Ice Cap. Figure is from Livingstone et al. (2022).

Over 80 % of the subglacial lakes reported in the most recent inventory are classified as ‘stable’ lakes that do not periodically drain (Livingstone et al., 2022). This implies that they are either closed systems or that the rate of subglacial water inflow and outflow is approximately equal. In contrast, a smaller percentage of subglacial lakes are classified as ‘active’ as their volumes change over timescales that can range from hours to months (e.g., Björnsson, 2002; Wingham et al., 2006; Fricker et al., 2016; Siegert et al., 2016). These active lakes tend to exist closer to the ice margin than stable lakes, have large upstream hydrological catchments, or form in areas where surface meltwater is abundant (excluding Antarctica where surface meltwater production is limited).

Generally, the active subglacial lakes observed to drain beneath Antarctic ice streams in a cascading manner over months are several orders of magnitude smaller (median volume = 0.12 km^3) than the stable lakes present beneath the Devon Ice Cap and the interiors of Antarctic and Greenland ice sheets ($<1 \text{ km}^3$ to $\sim 5400 \text{ km}^3$). Smaller lakes (median volume = 0.013 km^3), that drain with higher discharges over days to weeks, have been observed beneath Icelandic ice caps and the ablation zone of the Greenland Ice Sheet. Even smaller lakes ($\sim 0.0001 \text{ km}^3$) have been observed to drain rapidly (<1 hour to days) beneath valley glaciers, but events of this small magnitude occur so rapidly that they may be difficult to monitor beneath large ice sheets at present (Livingstone et al., 2022). Despite differences in the volume and timescale of drainage, active subglacial lakes across Iceland, Greenland, and Antarctica consistently exhibit quasi-linear relationships between mean discharge and lake volume (Figure 2.4). This quasi-linear relationship is consistent with Nye’s theory of lake drainage via subglacial channels (Nye, 1976), and suggests that drainage of active lakes in Greenland and Antarctica occurs predominantly through subglacial channels (Carter et al., 2017; Livingstone et al., 2022).

There is increasing evidence that subglacial lakes may harbour unique microbial life, particularly within their deeper waters and associated sediments (Karl et al., 1999; Siegert et al., 2001; Mikucki and Priscu, 2007). Subglacial lakes are subject to high pressures (~ 350 atmospheres), low temperatures (about $-3 \text{ }^\circ\text{C}$) and permanent darkness (Siegert et al., 2001; Siegert et al., 2003). Any microbes present must therefore use chemical sources to power biological processes rather than using solar radiation through photosynthesis; their source of energy will therefore be different from the majority of organisms on Earth (Siegert et al., 2001). In 2013, direct sampling of Subglacial Lake Whillans beneath the Whillans Ice Stream in West Antarctica recovered metabolically active microorganisms within the water column for the first time (Christner et al., 2014). These findings established that aquatic environments beneath the Antarctic Ice Sheet can support viable microbial ecosystems, confirming more than a decade of

circumstantial evidence regarding the presence of life beneath the Antarctic Ice Sheet (Karl et al., 1999; Priscu et al., 1999; Siegert et al., 2001; Lanoil et al., 2009).

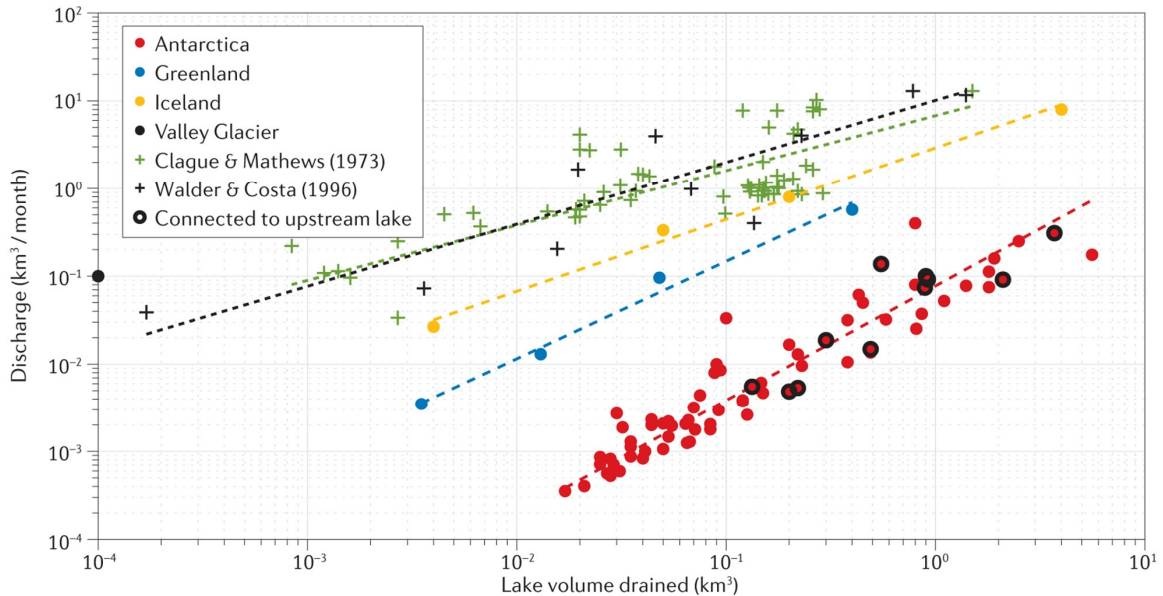


Figure 2.4. Relationship between discharge rate and lake drainage volume for active subglacial lakes and ice-marginal lakes draining through subglacial channels observed in Antarctica, Greenland and Iceland. Crosses denote peak discharges, whilst circles denote average discharges. Figure is reproduced from Livingstone et al. (2022), and includes data from Clague and Mathews (1973) and Walder and Costa (1996).

2.3.2 Groundwater

In addition to the ponding of water in lakes beneath ice sheets, groundwater — the infiltration and retention of water within underground aquifers — also makes up an important component of the subglacial hydrological system (Piotrowski, 1997a, b). Many contemporary glaciers and ice streams in Antarctica and Greenland are expected to be underlain by thick (100s–1000s m) sedimentary basins that have the capacity to host substantial groundwater in a subglacial hydrological system that is considerably deeper than the films, channels, lakes, and tills that occur near the ice-bed interface (Gustafson et al., 2022). Recent studies have indicated that significant quantities of meltwater can infiltrate into the subsurface under the ambient pressure exerted by the overlying ice sheet, becoming stored within the subglacial groundwater system (e.g., Clark et al., 2000; Grasby et al., 2000; Person et al., 2007; Siegert et al., 2018; Li et al., 2022). The basal substrate composition, as well as the location of impermeable permafrost layers, the

pressure exerted by the overlying ice, and the abundance of basal meltwater, regulates the location and rate of groundwater interchange (McEwen and Marsily, 1991).

On the timescale of the glacial-interglacial cycles (tens of thousands of years) of the Quaternary Period (2.58 Ma–present), numerical experiments demonstrate that high pressures at the ice-sheet bed force meltwater to infiltrate downwards into the subsurface during the ice sheet advance phase, with as much as 15–70 % of the basal meltwater infiltrating into the subsurface as recharge (Lemieux et al., 2008). In contrast, exfiltration of groundwater on the surface mainly occurs during ice-sheet recession as the remnant pressure in the subsurface is higher than the basal meltwater pressure. Consequently, ice-sheet advance and retreat has a prominent influence on the organisation of modern groundwater systems of formerly glaciated regions such as Canada and elsewhere (Person et al., 2007). By implication, the interaction between ice sheets and groundwater systems must be considered to ensure the safe long-term disposal of radioactive waste in deep geological repositories (Talbot, 1999; Lemieux et al., 2008; Iverson and Person, 2012).

2.4 Observations of water flow beneath ice sheets

2.4.1 The contemporary Antarctic ice sheets

The Antarctic cryosphere is typically divided into three ice sheets: the West Antarctic Ice Sheet (WAIS), the East Antarctic Ice Sheet and the Antarctic Peninsula Ice Sheet. Extremely low surface temperatures largely confine the influence of surface melting to the Antarctic Peninsula and the ice shelves fringing the continent (e.g., Tedesco, 2009; Tedesco and Monaghan, 2009; Tedesco et al., 2013; Bell et al., 2017; Kingslake et al., 2017; Bell et al., 2018). Although surface meltwater has been observed to transfer into the englacial system and be stored as lakes in some ice shelves (Lenaerts et al., 2016), and Antarctic surface melting is predicted to become increasingly prominent with continued climatic warming (Bell et al., 2018), the absence of surface melting for the majority of Antarctic’s ice sheets results in subglacial water being sourced from processes that operate almost exclusively at the ice-sheet bed (Rose et al., 2014; Noble et al., 2020). The expulsion of fresh subglacial meltwater into the more saline ocean waters causes buoyancy-related turbulence near the ice-sheet grounding zone — a mechanism that has been linked to enhanced ice melt and ice-shelf basal channel formation (Figure 2.5)(Le Brocq et al., 2013; Wei et al., 2020; Nakayama et al., 2021).

Low hydraulic-potential gradients facilitate extensive water ponding at the base of the Antarctic ice sheets, producing subglacial lakes in regions of hydraulic potential minima (Figures 2.3B, 2.5)(Robin et al., 1970; Oswald and Robin, 1973; Siegert et al., 1996;

Siegert et al., 2005; Siegert et al., 2016; Willis et al., 2016). Subglacial lakes have been detected beneath the ice using ice-penetrating radio-echo sounding surveys and satellite altimetry since the early 1970s (e.g., Robin et al., 1970; Oswald and Robin, 1973; Siegert et al., 1996; Siegert et al., 2005). To date, 675 subglacial lakes have been documented beneath Antarctica (Figure 2.3B; Livingstone et al., 2022). Radio echo sounding-detected subglacial lakes mostly occur beneath the warm-based interior of the ice sheet and are typically 1–5 km long (Livingstone et al., 2022). However, many larger tectonically controlled lakes also exist, including the 250-km-long Lake Vostok which contains $5400 \pm 1600 \text{ km}^3$ of water (Studinger et al., 2004). If all of the water stored in Antarctic subglacial lakes were to be released, it would raise mean sea levels by more than 35 mm (Dowdeswell and Siegert, 1999).

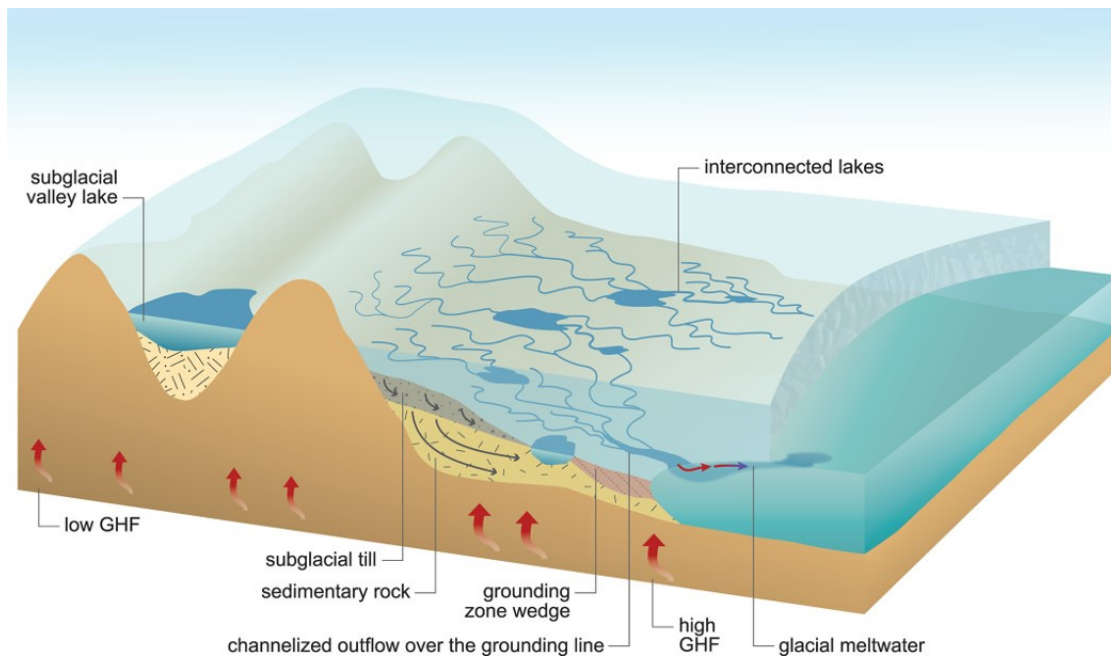


Figure 2.5. Subglacial hydrology of the Antarctic Ice Sheet. The schematic shows a channelized subglacial drainage network beneath a major ice stream composed of interconnected subglacial lakes. Larger, topographically constrained, subglacial lakes are present towards the interior of the ice sheet. Water is also transported through the subglacial till and can exchange with groundwater stored in deep sedimentary basins located beneath the ice sheet. Glacial meltwater is expelled at the ice-sheet grounding zone where it impacts sub-ice-shelf melt rates. GHF — geothermal heat flux. Figure is reproduced from Noble et al. (2020).

Subglacial lakes predominantly affect Antarctic ice dynamics in two ways. Firstly, as an ice sheet encounters a subglacial lake, the basal shear stress of the ice flowing over the lake drops to zero, resulting in a rapid acceleration of ice velocities (Pattyn, 2008). The

freezing of lake water onto the base of the ice sheet increases the basal thermal gradient and warms the basal ice. If the basal ice is warmed sufficiently to preserve this flattened thermal gradient downstream, it will prevent refreezing of the ice sheet onto the bed, distributing streaming flow over a broad spatial area (Bell et al., 2007). Subglacial lakes are commonly documented upstream of ice-stream onset zones, suggesting that this could be a mechanism that initiates the high flow velocities associated with streaming ice (Siegert and Bamber, 2000).

Secondly, about 40 % of Antarctic subglacial lakes have been observed to fill and drain over sub-decadal timescales (Gray et al., 2005; Wingham et al., 2006; Fricker et al., 2007; Smith et al., 2009a; Siegert et al., 2016; Smith et al., 2017). The routing of the water released from these active subglacial lakes can be traced for hundreds of kilometres, often triggering a cascade of further subglacial lake drainage downstream (Figure 2.5)(Wingham et al., 2006; Fricker et al., 2007; Flament et al., 2014; Fricker et al., 2014). Active lake drainage has been associated with a temporary (over several months) 10 % acceleration in the discharge of Byrd Glacier (Stearns et al., 2008), although this behaviour does not appear to be case for all subglacial lake drainage events (e.g., Smith et al., 2017). These differences may be related to the proportion of the bed inundated by subglacial lake water.

The rapid velocities associated with ice streams are commonly facilitated by the mechanical deformation of a weak and relatively thin layer of basal till (Blankenship et al., 1986; Engelhardt et al., 1990; Kamb, 2001). The low slope angles and metre(s)-thick tills present under many contemporary Antarctic ice streams may be conducive to a canalised drainage mechanism where shallow conduits are incised into the deforming substrate rather than forming discrete R- or N-channels (Figure 2.5)(Walder and Fowler, 1994; Ng, 2000). Seismic and radar surveys of the bed of the Rutford Ice Stream, West Antarctica, have revealed the presence of three channels ~50 m wide and <0.2 m deep, extending 5–10 km along the deforming bed of the ice stream, which may be interpreted as a canalised form of drainage (Murray et al., 2008).

The incidence of a canalised drainage mechanism beneath many contemporary Antarctic ice streams is also supported by borehole observations of low effective pressures (<0.2 MPa) beneath the Siple Coast ice streams in the Ross Sea Embayment (see Figure 2.3B for location) compared to the higher effective pressures expected for channels incised into bedrock, or upwards into the ice (Röthlisberger, 1972; Bindshadler, 1983; Engelhardt and Kamb, 1997; Kamb, 2001). Changes in the routing of subglacial meltwater beneath these ice streams have been associated with dynamic ice-flow behaviour including the

acceleration, deceleration, and on-off switching of the Whillans, Kamb and Bindschadler ice streams on the Siple Coast (Alley et al., 1994; Anandakrishnan et al., 1998; Jacobel et al., 2000; Joughin et al., 2002).

The Siple Coast ice streams have also been a focal point for the study of Antarctic groundwater flow and its impact on ice-sheet dynamics. Using numerical model simulations and ice-velocity inversions, Christoffersen et al. (2014) demonstrated that groundwater inflow constitutes 45 % of the hydrological budget of the ice streams — a value that is over five times the proportion contributed by localised basal melting. Their model results demonstrated that pore water can remain in the basal till layer for 1000–10,000 years; this length of time would provide ample opportunities for biogeochemical weathering to result in solute enrichment of the porewater that could serve as nutrients for microbial life (Christoffersen et al., 2014). Furthermore, Gustafson et al. (2022) noted that these estimates may only provide minimum values as the modelling only included shallow water volumes and fluxes within the till due to a lack of observations of any deep groundwater to constrain their modelling.

Recently, Gustafson et al. (2022) applied magnetotelluric and passive seismic methods to provide the first in-situ measurements of a deep groundwater system within a >1-km-thick sedimentary basin beneath Whillans Ice Stream on the Siple Coast. This basin was found to contain more than an order of magnitude more water than the shallow hydrologic systems typically considered in subglacial water models (e.g., Flowers et al. [2015] and references therein). The salinity of the groundwater contained within this sedimentary basin increased with depth, indicating that basal meltwater derived from the overlying ice streams can infiltrate hundreds of metres into the basal sediments and demonstrating that the deep and shallow elements of ice stream hydrological systems are physically connected (Figure 2.5)(Gustafson et al., 2022). Hydro-mechanical modelling conducted by Li et al. (2022) demonstrated that groundwater discharge rates from sedimentary basins scale with the rate of ice unloading during glacial retreat. Groundwater flow has been shown to increase geothermal heat fluxes under the East Antarctic Ice Sheet with implications for basal melting and thus ice-sheet flow (Gooch et al., 2016). Consequently, accelerated groundwater discharge triggered by rapid ice retreat is likely to amplify basal sliding, increasing the vulnerability of Antarctica’s most dynamic ice streams to enhanced mass loss (Gustafson et al., 2022; Li et al., 2022). The upward flux of deep groundwater into the shallow subglacial hydrological system may also transport nutrients produced by microbial communities (e.g., dissolved organic or inorganic carbon) towards the ice–bed interface, where it could help to nurture subglacial ecosystems (Gustafson et al., 2022).

Overall, contemporary observations show that subglacial water plays a major role in modulating the dynamics of the Antarctic ice sheets. However, many of the physical mechanisms responsible for regulating this behaviour remain unresolved. The impact of subglacial water on ice flow has also only been documented over relatively short (<decadal) timescales. Consequently, comparatively little is known about the effect of subglacial hydrology on ice-sheet dynamics over glacial-interglacial timescales.

2.4.2 Records of past water flow beneath the Antarctic ice sheets

Despite recent advances in Earth System Models, projections of the Antarctica's contribution to future global sea level still have a high degree of uncertainty due to difficulties in accurately parameterising the basal boundary conditions and sub-kilometre scale processes that operate at the ice-sheet bed (Joughin et al., 2009; Ritz et al., 2015; Bingham et al., 2017; Intergovernmental Panel on Climate Change, 2021; Hoffman et al., 2022). These uncertainties stem from the difficulty associated with obtaining observations of contemporary subglacial conditions. Consequently, the exact nature of the Antarctic subglacial hydrological system is still not fully resolved, leading to an inability for contemporary observations (e.g., Fricker et al., 2007; Schroeder et al., 2013; Fricker et al., 2014; Carter et al., 2017; Smith et al., 2017) to explain many features associated with the subglacial hydrological system preserved in the palaeo record (Lowe and Anderson, 2003; Ashmore and Bingham, 2014). Accordingly, uniting geomorphological evidence of past ice-sheet processes and contemporary glaciological observations has been identified as a 'grand challenge' for future research (Ashmore and Bingham, 2014).

One of the more striking discrepancies is the difference between the fluxes of water invoked for contemporary subglacial lake drainage and water transfer and the much larger fluxes of water in the past implied by palaeo-flow features. Lowe and Anderson (2002) first identified channelised features associated with subglacial meltwater on the Antarctic continental shelf (Figure 2.6). Over time, these channels have been revealed to be abundant on the largely bedrock-dominated inner continental shelves of the western Antarctic Peninsula (e.g., Ó Cofaigh et al., 2002; Ó Cofaigh et al., 2005; Domack et al., 2006; Anderson and Fretwell, 2008; Larter et al., 2019), West Antarctica (Figure 2.7) (e.g., Lowe and Anderson, 2003; Larter et al., 2009; Nitsche et al., 2013; Hogan et al., 2020; Kirkham et al., 2020; Hogan et al., 2022) and in East Antarctica (e.g., Fernandez et al., 2018; Nitsche and Correia, 2019). The bedrock channels are typically kilometres in width, several hundred metres deep and possess undulating thalwegs that indicate erosion by pressurised subglacial meltwater (Lowe and Anderson, 2002; Nitsche et al.,

2013; Hogan et al., 2022). Rarer instances of comparatively smaller channels (4–36 m deep and 200–2000 m wide) have also been observed incised into softer sediments in the Ross Sea (Simkins et al., 2017; Simkins et al., 2021).

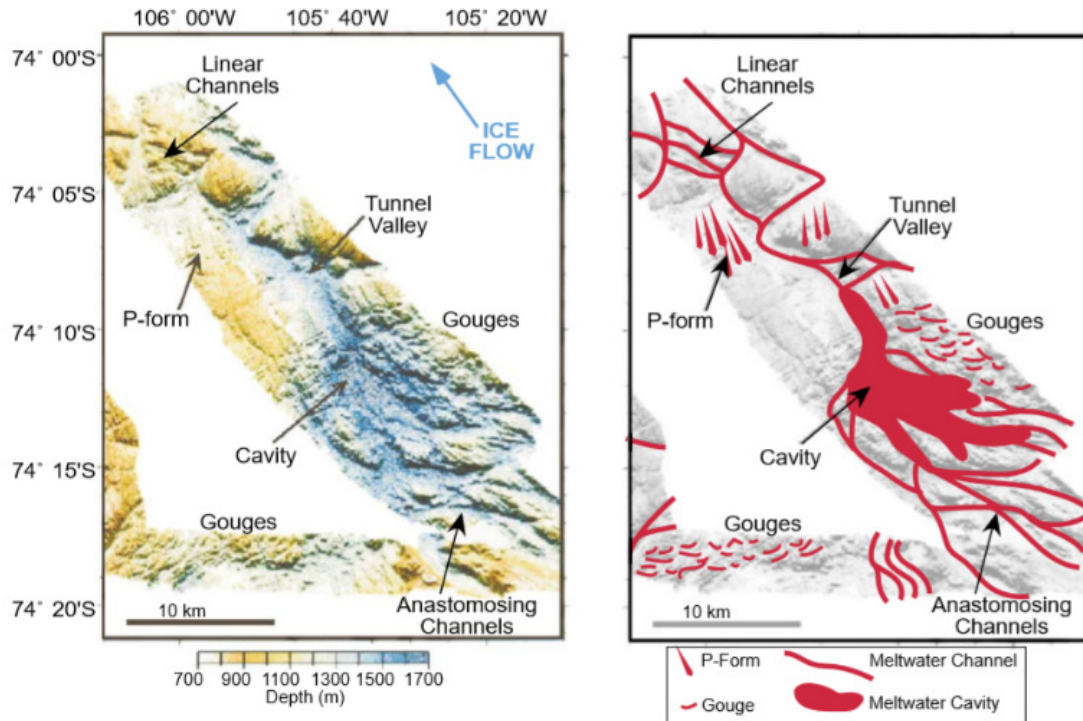


Figure 2.6. Early examples (left panel) and interpretations (right panel) of meltwater-derived morphology on the Antarctic continental shelf. Images are derived from multibeam-bathymetric data collected in Pine Island Bay, West Antarctica. Figure is reproduced from Lowe and Anderson (2002).

A fine-grained sediment drape frequently covers the bedrock channels and other regions of the West Antarctic continental shelf; this drape has been interpreted to reflect sediments released from meltwater plumes at the ice-sheet margin (Kirshner et al., 2012; Witus et al., 2014; Prothro et al., 2018; Lepp et al., 2022). Radiocarbon dating suggests that these plume deposits were formed offshore from the margin of the WAIS as it retreated over the last ~8000 years, indicating that past ice-sheet retreat coincided with abundant meltwater expulsion from the ice sheet (Kirshner et al., 2012; Witus et al., 2014).

High-resolution autonomous underwater vehicle imagery demonstrates that some channel sidewalls exhibit a stepped profile that probably indicates multi-stage incision with ice relaxing into the upper portion of the channel cross sections (Hogan et al., 2022). Nonetheless, the bedrock channels have been estimated to accommodate water discharges

four to five orders of magnitude greater than the peak discharges associated with contemporary subglacial lake drainage, even if partially filled with ice (Wingham et al., 2006; Fricker et al., 2007; Nitsche et al., 2013). The process responsible for the channel systems on the Antarctic continental shelf thus remains unresolved, limiting our understanding of Antarctic subglacial hydrology.

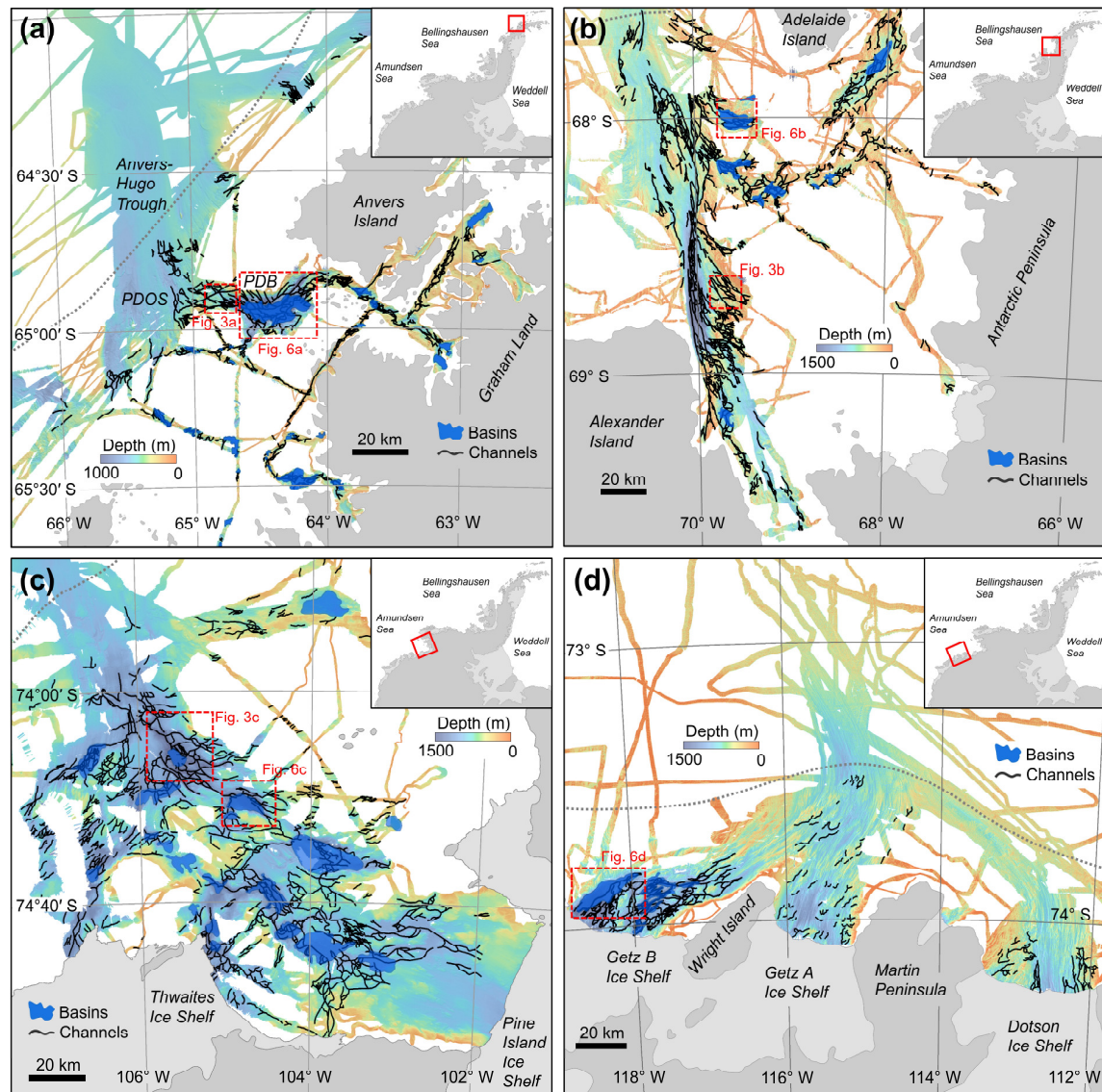


Figure 2.7. Distribution of bedrock meltwater channels on Antarctic inner continental shelves. Detailed multibeam-bathymetric data of: (A) Anvers Trough, (B) Marguerite Bay, (C) Pine Island Bay, and (D) offshore from the Dotson-Getz ice shelves. Channels are displayed as black lines and basins are shown as blue polygons. Note that the channels commonly terminate at the boundary between the inner-shelf bedrock and the outer shelf sedimentary strata (displayed as a stippled grey line). PDB — Palmer Deep Basin. PDOS — Palmer Deep Outlet Sill. Figure is reproduced from Kirkham et al. (2020).

In contrast to their widespread physical expression in the crystalline bedrock on the Antarctic inner continental shelf, geomorphological evidence of water transport is generally absent from the softer sediments present on the outer Antarctic continental shelf (Lowe and Anderson, 2003; Nitsche et al., 2013; Larter et al., 2019; Kirkham et al., 2020)(Figure 2.7). At the resolution of the multibeam-bathymetric data currently available in this region, no sedimentary fans are visible at the transition between inner shelf crystalline bedrock and outer shelf sedimentary strata (Ó Cofaigh et al., 2002; Livingstone et al., 2013a; Nitsche et al., 2013; Kirkham et al., 2020). The absence of sedimentary fans implies that the water transported through the bedrock channel network did not terminate abruptly at the inner-outer shelf boundary, and was instead transported across the shelf through a different mechanism (Dowdeswell et al., 2016a).

The interpretation that subglacial water crossed the entire continental shelf is supported by the abundance of gullies present beyond the Antarctic shelf break (e.g., Noormets et al., 2009; Gales et al., 2013). The near-symmetrical cross sections and relatively high average slopes of these gullies has been used to suggest that they were formed by a high-energy, gravity-driven erosional process consisting of flows of sediment and meltwater sourced from the grounded ice-sheet margin, operating in conjunction with retrogressive slope failures (Noormets et al., 2009). Consequently, it is likely that the meltwater transported through the inner-shelf channels reached the continental-shelf break, but little evidence of this was retained in the outer shelf sedimentary record (Dowdeswell et al., 2016a).

The absence of meltwater signatures imprinted on the outer-shelf sediments may reflect either: (i) drainage that occurred prior to the last phase of Last Glacial Maximum ice streaming, which then obliterated any meltwater signatures; (ii) that drainage at the outer shelf occurred through widely distributed channels or Darcian pore-water flow relative to the mineral skeleton (Kamb, 2001); or (iii) that any channels present are beyond the resolution of current multibeam echo-sounders (Dowdeswell et al., 2016b). Currently, the exact nature of this water flow mechanism remains poorly understood and has implications for understanding of subglacial hydrology and its interaction with ice dynamics.

2.4.3 The contemporary Greenland Ice Sheet

Unlike Antarctica, the hydrological system of the Greenland Ice Sheet is characterised by abundant surface melting and a strong seasonal element to meltwater production that has consequences for ice-sheet dynamics (e.g., Abdalati and Steffen, 2001; Zwally et al., 2002; Hanna et al., 2008; Bartholomew et al., 2011a; Chu, 2013; Banwell et al., 2016;

Stevens et al., 2016; Davison et al., 2019). Meltwater can be transported across the ice-sheet surface in supraglacial streams in the ablation season, or stored in lakes (Selmes et al., 2011; Smith et al., 2015), before draining through moulins, crevasses, or through hydrofracturing to provide an influx of meltwater into englacial and subglacial environments (Figure 2.8) (e.g., Das et al., 2008; Chu, 2013; Chudley et al., 2019; Davison et al., 2019). Meltwater transported through the Greenland Ice Sheet is ultimately expelled in the form of proglacial rivers in terrestrial environments, or in submarine meltwater plumes in marine or lacustrine settings (Figure 2.8; Chu, 2013); the transport of this meltwater into the ocean ultimately accounts for more than half of the mass lost from the Greenland Ice Sheet (Sasgen et al., 2012; Sasgen et al., 2020; Shepherd et al., 2020).

Supraglacial lakes that form on the surface of the Greenland Ice Sheet are some of the most spectacular features of the hydrological system and have gained widespread scientific interest due to their propensity to drain rapidly and impact ice-sheet dynamics (Das et al., 2008; Dow et al., 2015; Leeson et al., 2015; Bowling et al., 2019; Chudley et al., 2019). Das et al. (2008) provided the first observation of a supraglacial lake draining through thick, cold ice, through hydrofracturing. The lake emptied with a peak drainage rate of $8700 \text{ m}^3 \text{ s}^{-1}$ and resulted in ice-surface displacement and an increase in ice velocity within 24 hours of lake drainage. The gravitational potential energy of falling surface meltwater can elevate basal melt rates by up to two orders of magnitude when converted to heat in the basal drainage system (Young et al., 2022); this represents a significant source of heat beneath the Greenland Ice Sheet. However, although lake drainage is spectacular, the majority of supraglacial lakes in Greenland do not drain rapidly. Using a Greenland-wide survey of supraglacial lakes between 2005 and 2009, Selmes et al. (2011) demonstrated that only ~13 % of lakes drained rapidly, with the remainder losing water through overtopping into meltwater streams (Smith et al., 2015).

Lakes also exist in Greenland's subglacial environment (Figure 2.3A), but are less common than the examples identified in Antarctica (Palmer et al., 2013; Bowling et al., 2019; Livingstone et al., 2022). Currently, 64 subglacial lakes have been observed beneath the Greenland Ice Sheet (Livingstone et al., 2022). Three types of lakes have been identified: (i) stable lakes in northern and eastern regions above the equilibrium line position but away from the interior; (ii) hydrologically-active lakes near the equilibrium line position recharged by surface meltwater and; (iii) small, seasonally-active lakes below the equilibrium line position which form over winter and drain during the melt season (Bowling et al., 2019). On average, Greenland's subglacial lakes are nearly eight times shorter than their Antarctic counterparts (1.4 km compared to 11 km); this difference

reflects steeper average ice-surface gradients over Greenland and different bed topographic settings controlling the locations of the subglacial lakes (Livingstone et al., 2022). In contrast to Antarctic subglacial lakes, which typically occur in close proximity to ice divides under thick (>4000 m) warm-based ice, Greenland's subglacial lakes are typically absent beneath the isostatically depressed, largely frozen interior basin (MacGregor et al., 2016; Karlsson et al., 2021). Instead, Greenland's subglacial lakes are concentrated toward the ice margin where ice-surface speeds are higher and surface-to-bed hydraulic connectivity is more likely (Bowling et al., 2019).

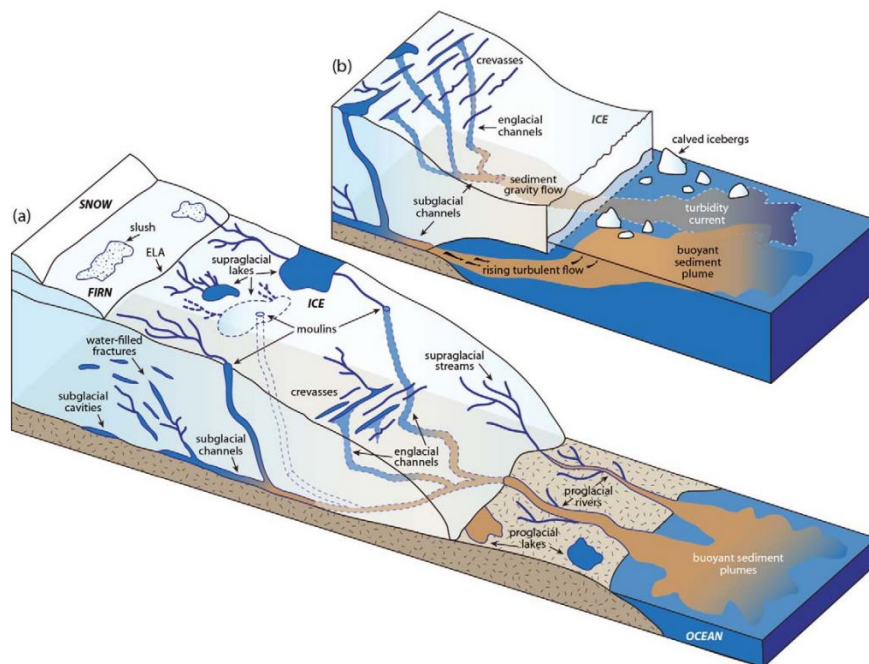


Figure 2.8. Hydrology of the Greenland Ice Sheet. (A) Schematic of a land-terminating outlet glacier. In the ablation zone, meltwater collects in supraglacial lakes and flows through supraglacial streams into crevasses and moulins to enter the englacial and subglacial hydrological systems. Water transported through englacial and subglacial conduits eventually exits the ice sheet through proglacial rivers and lakes which transport the meltwater into the ocean, producing a buoyant sediment plume. (B) Marine-terminating outlet glaciers exhibit the same supraglacial, englacial and subglacial meltwater transport mechanisms, but differences lie in their outlet mechanisms. Here, sediment-rich subglacial discharge is released tens to hundreds of meters below the water surface, and either rises to form a buoyant meltwater plume or may form a turbidity current beneath the water surface. Figure is reproduced from Chu (2013). ELA — equilibrium line altitude.

The input of meltwater into the englacial and subglacial environment has been widely observed to impact ice-sheet dynamics. Ice speeds in Greenland are largely set by basal motion, which is modulated by meltwater delivery to the ice-sheet base. Short-term accelerations in ice velocity have been observed following increased meltwater production, as well as the rapid drainage of supraglacial lakes (Das et al., 2008; Chudley et al., 2019), for both land-terminating (Zwally et al., 2002; Bartholomew et al., 2010; Palmer et al., 2011) and fast-moving marine terminating portions of the ice sheet (Joughin et al., 2008; Shepherd et al., 2009). The observed ice velocity changes have been attributed to the response of the subglacial hydrological system to increased seasonal meltwater input.

Rapid increases in meltwater from the ice-sheet surface result in periods in which the subglacial drainage system (predominantly arranged in a system of linked cavities early in the melt season) becomes highly pressurized, leading to periods when subglacial water pressures exceed the pressure exerted by the overlying ice, resulting in enhanced basal sliding (Schoof, 2010; Bartholomew et al., 2011b; Chandler et al., 2013; Mejía et al., 2021). However, the capacity of the subglacial drainage system then increases in response to increased meltwater input by switching from a distributed configuration to a more efficient channel-dominated system (Röthlisberger, 1972; Schoof, 2010; Sundal et al., 2011). This seasonal switch introduces a negative feedback that lowers the water pressure, increases bed friction, and reduces basal sliding (Cowton et al., 2013; Hoffman and Price, 2014; Hoffman et al., 2016; Stevens et al., 2016).

Although rapid meltwater influxes to the ice-sheet bed may increase short-term basal sliding, englacial and subglacial drainage systems may adjust to efficiently drain increased meltwater without significant changes to ice dynamics over seasonal and annual timescales (Chu, 2013; Andrews et al., 2014). Over longer (decadal to centennial) timescales, these observations suggest that increasing melt may help to buffer the Greenland Ice Sheet against rising ice losses in a warming climate. For example, Tedstone et al. (2015) reported a 12 % slowdown in ice velocity between the period 1985–1994 compared to 2007–2014 owing to the evolving efficiency of the subglacial drainage system in response to enhanced surface melting. As summers get hotter and longer, the increased occurrence and extent of channels will draw additional water out of the weakly connected drainage system, strengthening ice–bed coupling and decreasing ice velocities (Maier et al., 2022). This may produce a negative feedback in which the magnitude of ice discharge into the ocean is reduced, resulting in dynamic thickening that raises the ice sheet surface to cooler altitudes — decreasing surface melting (Pattyn et al., 2018).

However, the dynamic thickening feedback may be countered by an ice-sheet wide trend towards shallower ice-surface slopes as the ice sheet retreats inland. An observed 20–40 % contrast in basal slipperiness between steeper marine-terminating glaciers in north Greenland and the shallower surface slopes of glacier catchments in the south has been attributed to the steeper hydraulic potential gradients in the north Greenland examples which allow basal water to be rapidly evacuated from the subglacial hydrological system — increasing basal friction (Maier et al., 2022). As the ice sheet retreats further inland, surface slopes are expected to become shallower; this feedback will therefore result in more extensive basal water storage, increased slipperiness, and accelerated ice flow and ice losses (Maier et al., 2022).

Long-term projections of Greenland Ice Sheet change must also consider the impact of groundwater within the ice-sheet system. In-situ observations have shown that the groundwater system beneath the Greenland Ice Sheet responds to multi-annual, seasonal and even daily perturbations from the overlying ice sheet as a response to fluid pressure forcing at the ice/bed interface associated with changes in overlying ice loading and ice sheet hydrology (Liljedahl et al., 2021). Future ice losses are predicted to reduce groundwater discharge rates, with potential impacts to submarine freshwater discharge, freshwater delivery to fjords and biogeochemical fluxes in the Arctic (Liljedahl et al., 2021).

2.4.4 Records of past water flow beneath the Greenland Ice Sheet

Records of past water flow beneath the Greenland Ice Sheet are more sparse than their Antarctic counterparts. Channels incised into bedrock are present on the Greenland continental shelf (Ó Cofaigh et al., 2004; Dowdeswell et al., 2010), in addition to beneath the contemporary Greenland Ice Sheet (Bamber et al., 2013; Cooper et al., 2016; Keisling et al., 2020). However, these channels are not nearly as common as those offshore from Antarctica (e.g., Kirkham et al., 2020), and the formation of many has been attributed to turbidity currents or fluvial activity inherited from a preglacial landscape (Cooper et al., 2016; Batchelor et al., 2018). Despite the variety of mechanisms postulated to have formed bedrock channels offshore of the contemporary Greenland Ice Sheet, a system of roughly linear channels beneath Humboldt Glacier in northern Greenland appears similar to other large meltwater channels (tunnel valleys) found on the beds of former ice sheets (Livingstone et al., 2017). Radar bed-reflectivity anomalies suggest that basal meltwater continues to be actively routed down these subglacial meltwater channels to the coast beneath the extant ice sheet, potentially influencing basal traction and modern ice-sheet dynamics (Livingstone et al., 2017).

2.5 Tunnel valleys

2.5.1 General character and the formation of tunnel valleys

Unlike the majority of unconsolidated sediments present on the outer Antarctic continental shelf (Section 2.4.2), many other formerly glaciated regions contain abundant evidence of channelised subglacial water flow over soft sedimentary beds. Channels that are several kilometres wide and hundreds of metres deep, known as tunnel valleys, have been observed widely in sedimentary sequences both onshore and offshore in northwest Europe (e.g., Woodland, 1970; Ehlers et al., 1984; Jørgensen and Sandersen, 2006; Sandersen et al., 2009; Stackebrandt, 2009; Lang et al., 2012), North America (Boyd et al., 1988; Kehew and Kozłowski, 2007; Atkinson et al., 2013; MacRae and Christians, 2013; Pugin et al., 2014) and, perhaps most prominently, in the North Sea Basin (e.g., Huuse and Lykke-Andersen, 2000b; Praeg, 2003; Lonergan et al., 2006; Kristensen et al., 2007; Kristensen et al., 2008; Hepp et al., 2012; Janszen et al., 2012b; Stewart et al., 2013; Lohrberg et al., 2020; Ottesen et al., 2020). Tunnel valleys are also present, albeit less commonly, in Australia (Eyles and de Broekert, 2001), northwest Africa (Ghienne and Deynoux, 1998; Le Heron et al., 2004; Denis et al., 2007; Girard et al., 2012; Hirst et al., 2012; Ravier et al., 2015), South America (Vesely et al., 2021), and in the Arctic (Bjarnadóttir et al., 2017; Montelli et al., 2020), whilst some buried, and seemingly rare, examples exist on the Antarctic continental shelf within Late-Miocene and Pliocene-Pleistocene sedimentary strata (Alonso et al., 1992; Montelli et al., 2019).

Tunnel valleys are typically hundreds to thousands of metres wide, have steep-sided U- to V-shaped cross sections, and can extend for tens to hundreds of kilometres before terminating abruptly (Ehlers et al., 1984; Huuse and Lykke-Andersen, 2000b; Ottesen et al., 2020). Their planform geometry ranges from almost linear to complex anastomosing systems (Praeg, 2003; Moreau and Huuse, 2014). Undulating thalwegs distinguish tunnel valleys from other fluvial features (Ó Cofaigh, 1996) and suggest that they were incised in the subglacial environment where over-pressurised subglacial water can be driven uphill by the hydrostatic pressure exerted by the overlying ice mass (Shreve, 1972; Kristensen et al., 2008). Consequently, tunnel valleys are considered to be erosional features associated with subglacial drainage beneath large continental ice sheets.

Tunnel valleys are of interest for their ability to delineate former ice margins (e.g., Ehlers et al., 1984; Ehlers, 1990; Ehlers and Wingfield, 1991; Huuse and Lykke-Andersen, 2000b; Huuse and Lykke-Andersen, 2000a), whilst their sedimentary infill provides an analogy through which the processes of water flow and sediment transport beneath contemporary ice sheets can be inferred (Kehew et al., 2012; Stewart et al., 2012; van der Vegt et al.,

2012; Benvenuti et al., 2018). In many formerly glaciated regions, tunnel valleys are also important reservoirs of water, ore minerals and hydrocarbons; their variable infill can also produce difficulties when interpreting seismic profiles of the subsurface (Kristensen and Huuse, 2012; Frahm et al., 2020). They often contain shallow gas accumulations which represent drilling hazards and may create difficulties when installing seabed infrastructure (Lohrberg et al., 2020; Ottesen et al., 2020).

Despite being discovered over a century ago, (e.g., Jentzsch, 1884; Ussing, 1903, 1907), the mechanism by which tunnel valleys form remains controversial due to a lack of a single unifying mechanism that can explain the features (Ó Cofaigh, 1996; Kehew et al., 2012; Stewart et al., 2013). Comprehensive reviews of the various mechanisms proposed to explain tunnel valley formation are provided by Ó Cofaigh (1996), Kehew et al. (2012), and van der Vegt et al. (2012). Overall, the different hypotheses can be grouped into four categories:

- (i) Gradual formation by the deformation and removal of soft sediments, weakened by high fluid pressures, in subglacial drainage channels (e.g., Clayton et al., 1999; Boulton et al., 2009);
- (ii) Time-transgressive formation close to a retreating ice-sheet margin, with water supplied from either the ice-sheet surface or released episodically from permafrost-confined subglacial lakes (e.g., Jørgensen and Sandersen, 2006; Kristensen et al., 2008; Sandersen et al., 2009; van der Vegt et al., 2012);
- (iii) Simultaneous erosion of entire networks of tunnel valleys by enormous sheet floods sourced from catastrophic releases of water far from the ice-sheet margin (e.g., Wright, 1973; Kor et al., 1991; Brennand and Shaw, 1994);
- (iv) A polygenetic origin, resulting from reoccupation of an area by grounded ice and meltwater erosion over several glacial cycles (e.g., Huuse and Lykke-Andersen, 2000b; Moreau and Huuse, 2014).

Pervasive slumping of tunnel valley sides following their initial incision likely also plays an important role in shaping the morphology and determining the width of the valleys (Woodland, 1970; Ehlers and Linke, 1989; Prins et al., 2020). Recent technical improvements in mapping the full extent of tunnel valleys has highlighted their extreme size and length (>150 km long), lending support to theories in which tunnel valleys form gradually rather than via a catastrophic mechanism, as this would require an unreasonably large volume of water to be stored and released, often in the presence of no apparent reservoir (Ottesen et al., 2020).

Numerical simulations by Beaud et al. (2018b) have demonstrated that seasonal meltwater flows with relatively low discharges would be capable of incising channels with similar dimensions to tunnel valleys within the timescale of one glaciation. These findings support a time-transgressive model of tunnel valley formation mostly driven by ice-sheet retreat (Beaud et al., 2016; Beaud et al., 2018a; Beaud et al., 2018b). Such rapid erosion rates are supported by lithological and biostratigraphical data from northern Denmark which constrain the formation of a series of ~1 km wide, 5–10 km long, and up to 180 m deep tunnel valleys to within a period of just several hundred years (Sandersen et al., 2009). Similar results have also been reported by Giglio et al. (2021) in the Celtic Sea; the authors inferred that the maximum time available to carve an extensive system of tunnel valleys into lithified bedrock during the last glacial period was ~1000–2000 years.

The formation of tunnel valleys within just hundreds of years has implications for ice-sheet dynamics. Laboratory experiments have hinted that tunnel valley formation may help to stabilise ice sheets during deglaciation by draining away basal meltwater that might otherwise reduce basal friction and increase sliding, thus preventing catastrophic ice-sheet collapse (Lelandais et al., 2018). Similar inferences have been made by examining geomorphological records of past ice-sheet decay. In the case of the Laurentide Ice Sheet in North America, the development of tunnel valleys has been suggested to have led to stagnation of ice flow at the termini of ice streams (Patterson, 1997). This indicates that tunnel valley development could favour ice-sheet stability by preventing ice-stream destabilisation (Marczinek and Piotrowski, 2006). However, detailed numerical analyses of how tunnel valley formation interacts with, and influences ice-sheet dynamics remains lacking.

2.5.2 Tunnel valleys in the North Sea

The wealth of seismic-reflection data gathered in recent decades in the North Sea, combined with its location at the margin of the former Scandinavian and the British-Irish ice sheets, makes this region one of the most comprehensive stratigraphical records of glacial history in the Northern Hemisphere (Praeg, 2003; Lamb et al., 2018; Rea et al., 2018; Ottesen et al., 2020). The North Sea Basin has been glacially influenced discontinuously throughout most of the Quaternary (2.6 Ma onwards) and contains an over 1000-m thick sequence of sediments deposited during this time (Lamb et al., 2018; Ottesen et al., 2018; Rea et al., 2018). The earliest evidence of glacial influence in the North Sea is recorded in the form of ice-rafted debris recovered from the northern North Sea that has been present since ~2.7 Ma (Eidvin and Rundberg, 2001; Ottesen et al., 2009). Icebergs were present in the central and southern part of the basin by ~2 Ma (Rea

et al., 2018), and landforms produced by grounded ice have been observed on buried surfaces dating back to 1.87 Ma using 3D seismic-reflection data (Graham et al., 2010; Buckley, 2012; Rea et al., 2018).

Glacial influence in the North Sea intensified around the time of the Middle Pleistocene Transition (~ 1 Ma), culminating in three major glaciations that covered the majority of northern Europe and the North Sea (Figure 2.9). The majority of tunnel valleys in Europe are understood to have formed during these three major Pleistocene glaciations (Huuse and Lykke-Andersen, 2000b; Kehew et al., 2012; Stewart, 2016). By the time of the Elsterian glaciation (Marine Isotope Stage 12 [MIS12]; 430–450 ka), the North Sea Basin was largely infilled and the Fennoscandian and British-Irish ice sheets had coalesced to cover most of northern Europe, extending across the North Sea to reach a position close to the present-day coastlines of the Netherlands and East Anglia (Figure 2.9) (Hepp et al., 2012; Hughes et al., 2016; Patton et al., 2016; Batchelor et al., 2019; Gowan et al., 2021; Clark et al., 2022a,b). A similar maximum ice position was attained during the Saalian glaciation (MIS 10–6; ~ 300 –130 ka). The Fennoscandian Ice Sheet did not extend as far southwards during the Weichselian glaciation (~ 115 –11.7 ka), with ice covering northern Denmark and probably joining the British Irish Ice Sheet in the central North Sea but excluding western Germany and the southeast North Sea (Ehlers, 1990; Ehlers and Wingfield, 1991; Svendsen et al., 2004; Batchelor et al., 2019).

Water flowing beneath these ice sheets generated vast networks of tunnel valleys stretching across northwest Europe (Figure 2.9). For example, the central and southern North Sea contains thousands of tunnel valleys, both buried beneath and incised into the seabed. The open seafloor tunnel valleys were formed during the Weichselian glaciation (Stewart et al., 2012; Stewart et al., 2013; Stewart, 2016; Dove et al., 2017). These Weichselian valleys are underlain by a belt of larger buried tunnel valleys, correlated to the Elsterian glaciation, that extend from East Anglia towards the northern Netherlands, Germany, and Poland, deepening eastwards from ~ 100 m in England to over 400 m deep in Germany (Huuse and Lykke-Andersen, 2000b; Praeg, 2003; van der Vegt et al., 2012).

The largest, deepest, and most widespread tunnel valleys in the North Sea are generally associated with the Elsterian glaciation (Lee et al., 2012), especially in the southern North Sea and adjacent land areas due to their infilling with late Elsterian Lauenburg Clay and Holsteinian interglacial deposits (Huuse and Lykke-Andersen, 2000b). Elsterian tunnel valleys are commonly over 500 m deep, up to 6 km wide and are up to 155 km long (Praeg, 2003; Stackebrandt, 2009; Ottesen et al., 2020). The large dimensions of the

valleys have been attributed to their formation during the first period of ice sheet overriding in this region, meaning that the ice did not override any stiff till which would potentially limit the efficacy of meltwater erosion (Passchier et al., 2010). Comparatively less meltwater incision appears to have occurred during the Saalian glaciation, producing shallower tunnel valleys in the Danish Central Graben area and the UK and Dutch North Sea sectors (Hepp et al., 2012). Both surficial and buried tunnel valleys are widespread in all soft-bedded areas of northern Europe that were covered by the Weichselian ice sheet. At several kilometres wide and up to 300 m deep, Weichselian tunnel valleys tend to be intermediate in size when compared to those formed in the Saalian and Elsterian glaciations (Jørgensen and Sandersen, 2006; Sandersen et al., 2009).

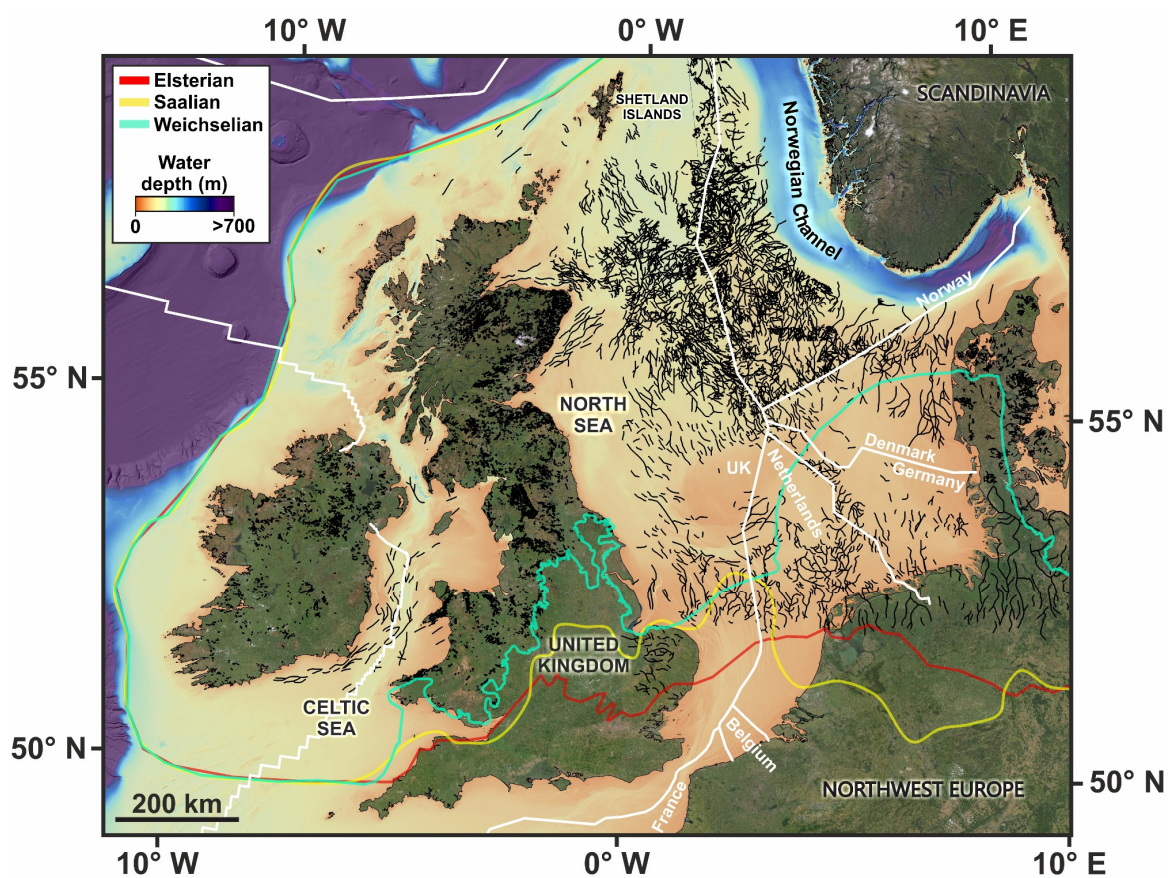


Figure 2.9. Distribution of tunnel valleys and meltwater channels in the North Sea and northwest Europe. Tunnel valleys buried beneath the seafloor of the North Sea (van der Vegt et al., 2012; Ottesen et al., 2020) and meltwater channels on the UK mainland (Clark et al., 2018) are displayed as black lines. Best estimate former ice-margin positions for the Weichselian, Saalian, and Elsterian glaciations are shown from Batchelor et al. (2019). Regional bathymetry is from GEBCO (<https://www.gebco.net>). Solid white lines delineate national maritime territorial boundaries.

However, as spatial coverage of 3D seismic data has grown, greater numbers of buried tunnel valleys have been mapped beneath the North Sea. Many of these valleys cross-cut one another, with more recent tunnel valleys incising older ones. The cross-cutting character of these tunnel valleys has been used to assign relative chronologies to them, in which each generation of tunnel valley is correlated to a different glaciation (Stewart and Lonergan, 2011). As a result of increasing investigation of 3D seismic data, up to five cross-cutting generations of tunnel valleys have now been mapped in the eastern North Sea (Kristensen et al., 2007), whilst up to seven generations are present in the central North Sea (Stewart and Lonergan, 2011; Stewart et al., 2013; Ottesen et al., 2020). Complex patterns of tunnel valley incision and cross cutting have been used to argue that the former tripartite classification of North Sea glacial history is likely too simplistic (Stewart and Lonergan, 2011). It is difficult to accurately establish the age of many tunnel valleys due to a paucity of datable material (Ehlers and Linke, 1989; Praeg, 2003), but palaeomagnetic evidence from a single British Geological Survey borehole (77/03; Stoker et al., 1983) has been used to infer that most tunnel valleys in the central North Sea are younger than the Brunhes-Matuyama magnetic reversal event at 780 ka (Stewart and Lonergan, 2011). The North Sea tunnel valleys, and their sedimentary infill, therefore record a complex history of continental ice-sheet growth, retreat, and subglacial water flow over at least the past 500,000 years.

2.5.3 Tunnel valley infill

2.5.3.1 General infill patterns

The internal infill lithologies and sedimentary architectures of tunnel valleys are notoriously complex due to the potential range of sedimentary and erosional processes that can affect the valley fill during both glacial and post-glacial times (Figures 2.10, 2.11) (Kehew et al., 2012; van der Vegt et al., 2012; Atkinson et al., 2013). The sedimentary structures preserved within infilled tunnel valleys thus provide records of the flow conditions experienced by the channel when it was active and the sedimentary deposystems influencing the channels after they were abandoned (Praeg, 2003; Hepp et al., 2012; Stewart et al., 2012). Tunnel valley infill sequences are often separated into stratigraphically distinct base (primary) and upper (secondary) fill units which reflect differing degrees of glacial influence (Kehew et al., 2012; van der Vegt et al., 2012). van der Vegt et al. (2012) argued that the sedimentary architecture of tunnel valleys is primarily dictated by their available accommodation space. In this model, smaller tunnel valleys will become rapidly infilled with glacial sediments, whereas larger valleys will contain glacially-derived sediments at their base and sediments of decreasing glacial

influence towards their top — reflecting a pattern of ice-margin retreat. Some tunnel valleys may also be only partially infilled, or lack infill entirely, such as those present on the seabed of the central North Sea (Stewart and Lonergan, 2011; Stewart, 2016).

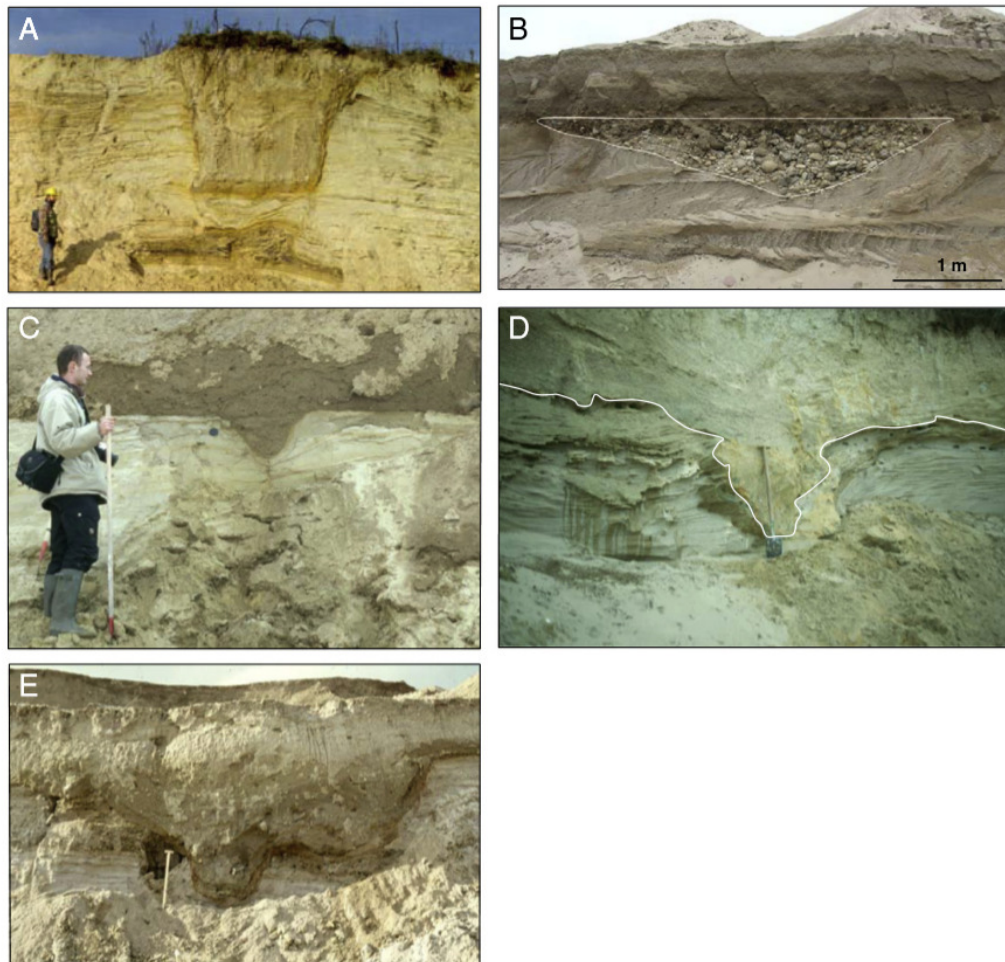


Figure 2.10. Examples of buried and infilled tunnel valleys exposed in outcrops from Germany and Denmark. The tunnel valleys are characterised by a variety of dimensions and infill lithologies. The tunnel valley in (A) is from eastern Germany and is of Saalian age (Piotrowski et al., 1999). The valleys shown in B–E were produced in the Weichselian glaciation, and are found in Denmark (B–C) (Larsen et al., 2004; Lesemann et al., 2010a) and Germany (D–E) (Piotrowski, 1999). Figure is taken from Kehew et al. (2012).

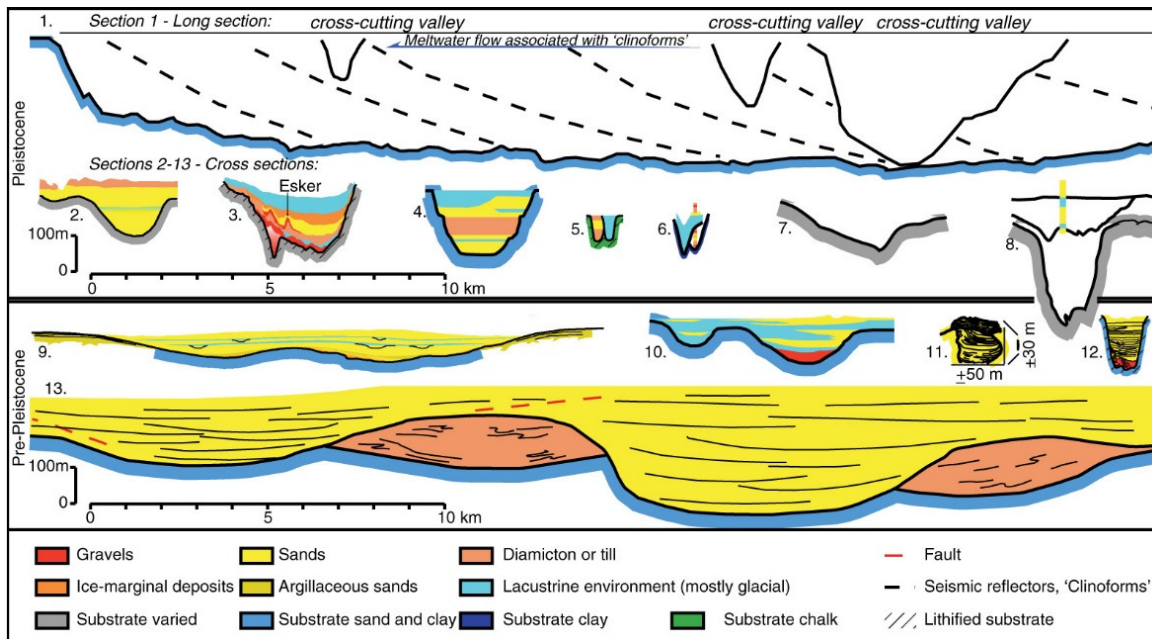


Figure 2.11. Examples of tunnel valley cross sections and infill structures. The upper panel displays tunnel valleys of Pleistocene age, whilst the lower panel displays tunnel valleys of Pre-Pleistocene age. All images show cross sections perpendicular to the tunnel valley long axis, except example (1) which displays a long profile down a tunnel valley thalweg. Text in square brackets describes the method(s) in which the infill composition was determined. (1) Tunnel valley long profile from the eastern North Sea containing 'clinoform' reflections [seismic-reflection data] (Kristensen et al., 2007). (2) Tunnel valley from Oak Ridges Moraine, Canada [seismic-reflection data and boreholes] (Russell et al., 2003). (3) Tunnel valley containing an esker in Lake Geneva, Switzerland [seismic-reflection data and boreholes] (Moscarriello et al., 1998). (4) Bornhöved Valley, Germany, containing diamicton from a subsequent ice advance [borehole data] (Piotrowski, 1994). (5) Tunnel valleys from the Upper Cam Valley, England [borehole data] (Baker, 1977). (6) Hornsyld Valley, Denmark, [borehole, seismic, and transient electromagnetic data] (Jørgensen and Sandersen, 2006). (7) Subglacial channel formed under Breiðamerkurjökull in Iceland during the Little Ice Age [radio-echo soundings] (Björnsson, 1996; Boulton et al., 2007). (8) Tunnel valleys on the Scotian Shelf, Canada [seismic-reflection data and boreholes] (Boyd et al., 1988). (9) Cross-section of two confluent tunnel valleys in Gargaf Arch, Libya [field outcrop observations] (Le Heron et al., 2004). (10) Tassili N'Ajjer, Algeria [outcrop data] (Eschard et al., 2005). (11) Subglacial or possibly proglacial channel in Tassili du Tufassasset, Algeria [field observations] (Beuf et al., 1971). (12) Tunnel valley in Adrar Mauritania [field observations] (Ghienne and Deynoux, 1998). (13) Cross-cutting tunnel valleys in Saudi Arabia [field observations] (Vaslet, 1990). Figure is reproduced from van der Vegt et al. (2012).

The basal fill of tunnel valleys is often glacial in origin and may contain diamictites of heterogeneous grain size (Ehlers and Linke, 1989; van der Vegt et al., 2012). Evidence of glacial deformation and high subglacial meltwater pressures at the base of some tunnel valleys is implied through the presence of faults, folds, injections, and compaction structures which are well preserved in outcrops of ancient Ordovician tunnel valleys (Le Heron et al., 2004; Le Heron et al., 2005; Ravier et al., 2014; Ravier et al., 2015). Many tunnel valleys contain thick sequences of massive gravels and sands as their primary fill unit (Figure 2.11; Ehlers and Linke, 1989; Ghienne and Deynoux, 1998; Le Heron et al., 2004); these have been interpreted as products of subglacial meltwater deposition or gravity-flow activity released in an ice-proximal setting (van der Vegt et al., 2012; Clerc et al., 2013). Instances where gravel-dominated bedforms are present within tunnel valleys, or where the channels terminate in outwash fans containing large boulders, have been used to link these infill facies to specific sediment transport processes as these coarser materials would require high discharge fluxes to be transported effectively (Brennan and Shaw, 1994; Cutler et al., 2002).

The secondary fill sequences of tunnel valleys are not always exclusively glacial in origin and, as a consequence, secondary infill units are comparatively more varied than those comprising the basal (primary) fill of the tunnel valleys (Kehew et al., 2012; van der Vegt et al., 2012). If ice-sheet retreat is characterised by abundant sediment expulsion, the secondary infill units of tunnel valleys are often associated with thick sequences of glacial deposits such as outwash sands and gravels released at the margin of the receding ice sheet, or turbidity-current sequences deposited in proglacial lacustrine or marine environments (Ehlers et al., 1984; Ehlers and Linke, 1989; Janszen et al., 2012a; Kehew et al., 2012). Where tunnel valleys are not entirely filled by glacial outwash sediments during ice-sheet retreat, laminated clays and silts may be deposited which reflect a glacial-marine or glacial-lacustrine environment during marine transgression. Coarser material may also be incorporated into the secondary infill facies if the tunnel valleys are overridden by grounded ice during subsequent glacial (re)advances, or through other mechanisms such as the collapse of the tunnel valley sides, meltout of stagnant ice buried within the valleys, or through iceberg rafting (Hepp et al., 2012; Kehew et al., 2012; Stewart et al., 2012; van der Vegt et al., 2012; Clerc et al., 2013; Benvenuti et al., 2018).

2.5.3.2 The infill of tunnel valleys in the North Sea

Categorising the infill of the buried tunnel valleys in the North Sea is complex as infill patterns vary spatially between different regions (Huuse and Lykke-Andersen, 2000b;

Kristensen et al., 2008; Kristensen and Huuse, 2012; Stewart et al., 2012). Consequently, many different models have been proposed to explain the tunnel valley infill. As the tunnel valleys in this region have been either buried by sediments or inundated by seawater, seismic-reflection methods (Chapter 3) are the predominant method through which their infill architecture is studied.

The infill of most tunnel valleys in the North Sea is characterised by two or three facies in seismic-reflection profiles. The lowermost facies is often the most volumetrically significant, and is characterised by a seismically unstructured or chaotic unit. These are overlain by a well-layered unit characterised by sub-horizontal reflections. In some instances, a third unit, which displays a chaotic seismic structure, overlays the well layered second unit (Huuse and Lykke-Andersen, 2000b; Kristensen et al., 2007; Hepp et al., 2012; Kristensen and Huuse, 2012; Stewart et al., 2012). However, in other locations, the entire valley fill sequence can be completely chaotic or contain onlapping fill (Wingfield, 1989; Huuse and Lykke-Andersen, 2000b; Stewart et al., 2012).

Based on a comparison with buried Elsterian valleys onshore northern Europe, the seismic facies characterised by chaotic and disrupted reflections has been interpreted as glacialfluvial sands and silts, whilst the well-layered unit has been interpreted as silts and clays deposited in an ice-free glacialmarine setting (Ehlers et al., 1984; Kristensen et al., 2008). These interpretations are supported by the small number of boreholes in the northern and central North Sea, which have recovered sands, silts, and some localised gravel and diamictons in the lower facies, and glacialmarine muds from the upper infill facies (Hepp et al., 2012). The lower facies often consists of thick (<180 m), fining-up cycles of gravels and sands, suggesting a continuous decrease in transport energy from proximal to distal in relation to a retreating ice sheet (Kluiving et al., 2003; Hepp et al., 2012; van der Vegt et al., 2012). Rarely, small deposits of diamictons or till are found at the base or at the sides of the tunnel valleys, and have been interpreted to have either slumped from the ice-sheet base, been deposited by overriding ice, or represent subglacial deformation till (Lonergan et al., 2006).

Tunnel valleys buried in the southern and southeastern North Sea are distinct from tunnel valleys in other regions of the North Sea because they are infilled with hundreds of metres of kilometre long northward dipping clinofolds (Figure 2.12A)(e.g., Praeg, 2003; Kristensen et al., 2007; Kristensen et al., 2008; Moreau and Huuse, 2014; Benvenuti et al., 2018). These structures have not been confidently observed in outcrops onshore in northwest Europe (Ehlers et al., 1984; Benvenuti et al., 2018), although clinofold-like geometries have been recognised in outcrops of Late Ordovician tunnel valleys preserved

in north Africa (Le Heron et al., 2004). The processes responsible for the deposition of these clinoforms has been a source of controversy and puzzlement for the Quaternary community for decades as the northward dip of the clinoforms is opposite to the expected direction that glacial sediments should dip if they were deposited by the north European Elsterian Ice Sheet (Benvenuti et al., 2018). Different authors have proposed contrasting and contradictory explanations for these unique infill features, with some favouring glaci-fluvial or subglacial processes (e.g., Praeg, 1996; Kluiving et al., 2003; Kristensen et al., 2007; Kristensen et al., 2008; Passchier et al., 2010; Benvenuti and Moscariello, 2016), whilst others have challenged these interpretations by suggesting a riverine origin for the clinoforms following ice-sheet retreat (Moreau and Huuse, 2014).

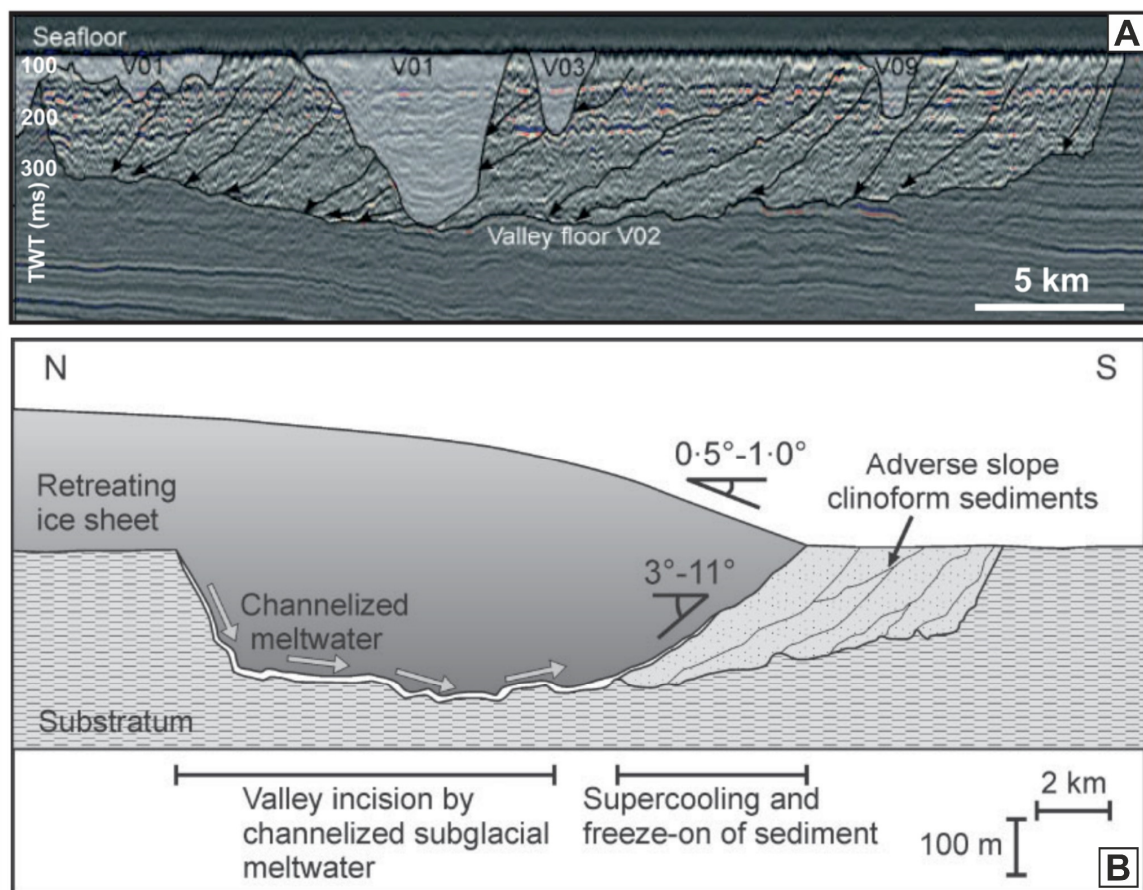


Figure 2.12. Example of the northward-dipping clinoforms found to infill tunnel valleys in the southern and southeastern sectors of the North Sea. (A) Seismic profile line along the thalweg of a tunnel valley in the southern North Sea exhibiting clinoform infill structures (black arrows). **(B)** Conceptual schematic of the ‘backfilling’ tunnel valley infill hypothesis. Sediment is eroded and transported by channelised meltwater beneath the retreating ice-sheet margin. As the subglacial meltwater reaches the terminus, sediment-laden water is plastered onto adverse slopes due to supercooling beneath the ice margin. Figures are reproduced from Kristensen et al. (2008). TWT — two-way travel time.

The up-valley dipping clinoforms may be explained by a time transgressive glacifluvial back-filling hypothesis in which a channelised drainage system erodes sediments up ice and deposits them along the adverse slope at the valley end as the ice sheet retreats (Praeg, 2003). Kristensen et al. (2008) suggested that this ‘conveyor belt’ system of tunnel valley incision and infill near the ice-sheet margin was enabled by supercooled sediment-laden meltwater affected by pressure changes along the undulating tunnel valley floors (Figure 2.12B). When these are steeper than 1.2–1.7 times the ice-surface slope, the threshold required for supercooling to occur is passed (Alley et al., 2003; Cook et al., 2006) and debris will start to accrete at the ice/water interface which may lead to channel plugging and the deposition of the diagnostic up-valley dipping clinoforms (Kristensen et al., 2007; Kristensen et al., 2008).

This ‘back-filling’ model is attractive as it links together tunnel valley incision and infill processes (Benvenuti et al., 2018). However, southwest of the area studied by Kristensen et al. (2008), Moreau and Huuse (2014) found that over 95 % of clinoform dips were less than 3°, the minimum required for supercooling to take place. Based on the extension of the clinoforms above the tunnel valley shoulders, Moreau and Huuse (2014) thus argued that the infill was unconfined, separate to the incision of the tunnel valleys, and was more likely to correspond to postglacial sedimentation from northwest Europe’s river deltas. However, sediment provenance analysis on infill samples from a large tunnel valley in the Dutch sector of the southern North Sea demonstrates that the sediment infilling the base of the tunnel valley was glacially recycled from the local area and was transported southward by the action of subglacial meltwater flows (Benvenuti and Moscarriello, 2016; Benvenuti et al., 2018), supporting a subglacial origin for the clinoforms.

2.6 Summary

The movement and storage of water beneath ice sheets and glaciers has been of interest to glaciologists for over half a century because of its potential to affect ice flow and ultimately impact rates of sea-level rise. The influence of meltwater on ice-sheet dynamics is likely to increase in the future as the Earth’s climate continues to warm. Water can be transported beneath ice sheets and glaciers through a number of efficient and inefficient mechanisms; the distribution of these mechanisms varies depending on factors including water availability, basal substrate type, and the hydraulic potential gradient.

Beneath the Antarctic Ice Sheet, water may be transferred between systems of subglacial lakes which can influence ice-sheet dynamics. Groundwater storage also represents a key, and currently under-explored, element of ice-sheet hydrology. In contrast to Antarctica,

the Greenland Ice Sheet is characterised by abundant surface meltwater production. Hydrological connectivity between the ice-sheet surface and bed results in the efficient transport of surface meltwater to the ice-sheet bed, where the water drives marked seasonal variations in ice-sheet dynamics.

The beds of the Antarctic and Greenland ice sheets, in addition to former mid-latitude ice sheets, contain abundant evidence for water flow that occurred in the past. These records sometimes indicate that water transport was many orders of magnitude larger than has been observed in the recent satellite era of glaciological observations. Some of the most striking evidence for water flow beneath past ice sheets takes the form of large channels known as tunnel valleys that can attain widths of several kilometres and depths of hundreds of metres. Tunnel valleys have a near global distribution in formerly glaciated regions and can be studied in sedimentary sequences both onshore in outcrops and offshore in the marine geological record. These features are of interest as records of past glacial history, as reservoirs of water, ore minerals and hydrocarbons, and as hazards to seafloor infrastructure installation.

However, despite being discovered over a century ago, the mechanisms in which tunnel valleys are formed and infilled remain poorly constrained, whilst their influence on ice-sheet dynamics has only been loosely hypothesised. Addressing these shortcomings is important as contemporary observations of ice-sheet change are short, and analogues are required to understand how extant ice sheets will respond to sustained climate warming in the future. New geophysical data, combined with novel analytical approaches, offer opportunities to address these questions. The following chapters will adopt this approach to quantify the routing and fluxes of subglacial meltwater beneath former ice sheets that have previously undergone retreat over centennial to millennial timescales. The new geophysical data will provide unprecedented insight into the linkages between subglacial hydrology and ice-sheet dynamics during deglaciation; this information will inform about how the subglacial hydrological system of contemporary ice sheets may evolve in response to climatic warming.

Chapter 3

Methodology and datasets

3.1 Background: Marine acoustic methods and glaciology

Landforms and sediments in formerly glaciated regions are records of inaccessible processes that operated, and continue to operate, beneath ice sheets (e.g., Ottesen and Dowdeswell, 2006; Larter *et al.*, 2009; Ottesen and Dowdeswell, 2009; Batchelor *et al.*, 2013; Dowdeswell *et al.*, 2016b; Ottesen *et al.*, 2017; Larter *et al.*, 2019; Batchelor *et al.*, 2020; Hogan *et al.*, 2020). Marine acoustic methods allow glaciologists to image the geological imprint of past glacial periods that are now preserved on the seafloor and to reconstruct the extent, dynamics, and flow history of former ice sheets (Dowdeswell *et al.*, 2007; Rea *et al.*, 2018).

Since the early development of relatively high-resolution marine geophysical tools in the 1980s and 1990s (e.g., Loncarevic *et al.*, 1994), together with the increasing availability of ice-strengthened research vessels, an explosion of interest in marine geophysical methods for glaciological purposes has driven greater data acquisition in formerly glaciated regions (Dowdeswell *et al.*, 2016a; Jakobsson *et al.*, 2016). The resulting new data have yielded significant insights into otherwise inaccessible glaciological processes. Beyond determining former ice-margin positions and flow paths, examples of novel insights include constraining maximum ice-retreat rates during deglaciation (Dowdeswell *et al.*, 2020), providing evidence for critical processes that may accelerate future ice-sheet collapse (Jakobsson *et al.*, 2011; Wise *et al.*, 2017), and elucidating complex mechanical and hydrodynamic processes that are likely to operate at the base of modern ice sheets (e.g., Wellner *et al.*, 2001; Graham *et al.*, 2009a; Larter *et al.*, 2009; Arndt *et al.*, 2018; Larter *et al.*, 2019; Hogan *et al.*, 2020).

Despite the global coverage of marine survey data being low (18 % of grid cells within the General Bathymetric Chart of the Oceans [GEBCO] contain multibeam bathymetric soundings), especially within the Polar Regions (11 % and 22 % within the Arctic and Southern oceans, respectively), initiatives designed to increase data coverage such as the Nippon Foundation-GEBCO Seabed 2030 Project mean that the potential of marine acoustic technologies for glaciological applications continues to grow (Arndt *et al.*, 2013; Jakobsson *et al.*, 2016; Mayer *et al.*, 2018; Wöfl *et al.*, 2019). This chapter summarises the methodology behind the two marine acoustic methods used in this thesis: multibeam bathymetry and 3D seismic reflection surveys.

3.2 Multibeam-bathymetric data

3.2.1 Introduction

Multibeam echo-sounding works on the principle of emitting a short pulse of sound from an acoustic source and measuring the time that the sound takes to return after being reflected off the seafloor. Two-way travel time (TWT) is then calculated and can be converted to depth, D , if the velocity of sound through water, v , is known:

$$D = v \times \frac{\text{TWT}}{2} \quad (3.1)$$

The comparatively high acoustic frequency of the emitted sound (typically 12–15 kHz for deep water systems and up to 700 kHz for shallow water systems (Jakobsson *et al.*, 2016)) distinguishes this method from other acoustic imaging technologies, such as 3D seismic reflection techniques (typically 3–125 Hz; Mosher *et al.* (2006)), and ensures that the sound waves typically reflect only off the seafloor rather than penetrating the subsurface (Figure 3.1). Multiple pulses of sound, or ‘pings’, are emitted from a transducer attached to the keel of a ship as a broad fan with typical angles of 130–150°, allowing large tracts or swathes of the seafloor to be mapped in a single run (Wöfl *et al.*, 2019). Motion sensors are used to measure and correct for the heave, pitch, yaw, and roll of the vessel as the multibeam-bathymetric survey is undertaken. Resolving a survey vessel’s rapidly changing geometry provides one of the main challenges to resolving the shape of the seafloor accurately (Jakobsson *et al.*, 2016). Regular measurements of water column properties must also be undertaken in order to correctly model the path and rate of travel of each ping through the water mass to the seafloor and back to the receiving transducer array.

The swath width of multibeam bathymetry data is proportional to the water depth due to the spreading of the pattern of beams as they travel through the water column (Wöfl *et al.*, 2019). Accordingly, the horizontal resolution of multibeam data decreases as water

depth increases owing to the lower density of pings reflected per unit area of the seafloor. Horizontal resolution is also influenced by vessel speed, ping rate, and the mode of bottom detection (e.g., amplitude, phase) (Jakobsson *et al.*, 2016). Once acquired, the multibeam-bathymetric data are processed and errors are removed by identifying and eliminating individual soundings that differ significantly from the surrounding point cloud of pings that constitute the multibeam-bathymetric data. The sounding data are then gridded to produce a digital terrain model (DTM) of the seafloor with a grid size specified according to the considerations outlined above.

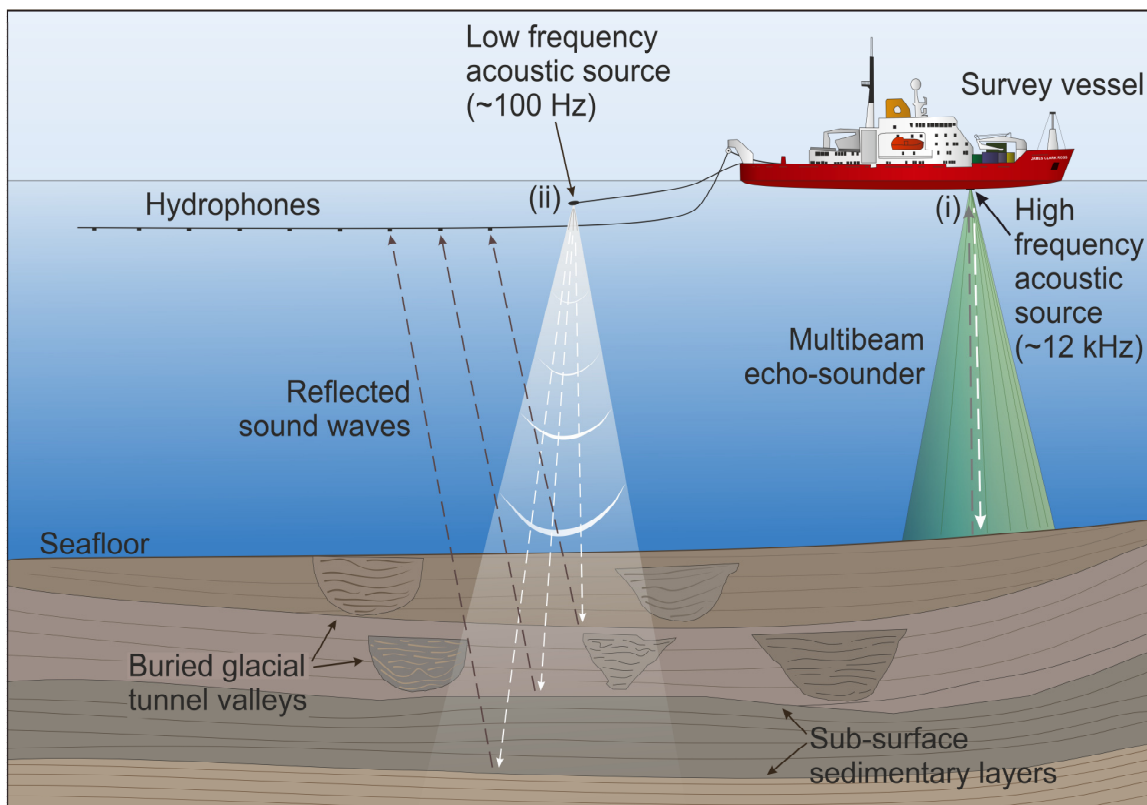


Figure 3.1. Acoustic methods used to image submarine glacial landforms. (i) A survey vessel, equipped with acoustic instruments, sails across the ocean. Beneath the vessel, a multibeam echo-sounder emits a broad fan of high frequency sound from a transducer mounted on the ship's keel. These sound waves travel through the water column and reflect off the seafloor to a receiver mounted on the keel of the ship, where the data are processed to image a large swath of the seafloor. (ii) A low frequency acoustic seismic source is towed behind the vessel, producing pressure pulses which penetrate the seafloor and reflect off layers in the subsurface. The reflected pulses are then captured and converted to electrical signals by an array of hydrophones in the streamer travelling behind the acoustic source. This permits buried features such as glacial deposits, and oil and gas reservoirs, to be visualised.

For the majority of shipborne multibeam echo-sounders, these constraints result in a typical horizontal resolution of 5–50 m and a vertical resolution of a few metres (Wellner *et al.*, 2006; Jakobsson *et al.*, 2016). However, to achieve higher resolution imagery of

the seafloor in deep water than is possible using shipborne echo-sounders, high-resolution shallow water echo-sounding systems have been attached to autonomous underwater vehicles that are capable of navigating close to the seafloor even at considerable water depths (>1 km; Dowdeswell *et al.*, 2008). Deploying these instruments can produce surveys with horizontal and vertical resolutions in the order of centimetres (Batchelor *et al.*, 2020). This can yield unprecedented insights into glacial erosional and depositional landforms and identify delicate seafloor features that cannot be resolved using conventional shipborne echo-sounding technology (Graham *et al.*, 2013, 2022; Dowdeswell *et al.*, 2020).

3.2.2 Multibeam-bathymetric data used in this thesis

This thesis utilised two types of multibeam-bathymetric data, distinguishable by their extent and resolution. Relatively small areas ($\sim 20,000$ km²) of high resolution multibeam-bathymetric data were used to study seafloor geomorphology and identify submarine glacial landforms that record processes operating within the basal environments of ice sheets. These high-resolution bathymetric data were contextualised by coarser scale regional bathymetric compilations; these also served as a basis for the numerical modelling experiments conducted in Chapter 4 and Chapter 6.

The high resolution multibeam-bathymetric data used to study several areas of the West Antarctic seafloor in Chapter 4 were collected over the last two decades by multiple scientific research expeditions. Owing to the variety of vessels from which the data were acquired, a range of multibeam systems were used to gather the data. These included Kongsberg EM120/EM122 multibeam echo-sounders with a transmission frequency of 11.25–12.75 kHz and a swath angle of up to 150° (for data collected by the RRS *James Clark Ross* and, post-2002, the RVIB *Nathaniel B. Palmer*); Krupp-Atlas Hydrosweep DS multibeam echo-sounders with a transmission frequency of ~ 15 kHz and a swath angle of up to 120° (for data collected by the RV *Polarstern*); and Seabeam 2112 multibeam sonar systems with a transmission frequency of 12 kHz and a swath angle of up to 120° (for data collected by the RVIB *Nathaniel B. Palmer* until 2002) (Nitsche *et al.*, 2007).

Data were processed onboard the vessels during each respective cruise in order to apply representative sound velocity profiles of the water column measured during data acquisition. The cleaned and calibrated bathymetric data were then gridded into a DTM using open access MB-System software (Caress and Chayes, 1996; Caress *et al.*, 2021). Interpolation was used to fill any small gaps between data points. Interpolation was applied conservatively and limited to four cell widths (~ 80 m) away from any data-filled cell in order to limit spurious bathymetric data generation.

Regional scale bathymetric data for Antarctica were derived from the 500 m resolution BedMachine Antarctica dataset (Morlighem *et al.*, 2019). BedMachine Antarctica employs a mass conservation approach to calculate the basal topography of the Antarctic Ice Sheet. The majority of the terrestrial (beneath grounded ice) measurements are derived from ice-penetrating radar profiles and satellite-derived ice velocity measurements (Rignot *et al.*, 2011). The bathymetry of the continental shelf and those areas of the seafloor beneath floating ice shelves is derived from gravity (Millan *et al.*, 2017), seismic (Greenbaum *et al.*, 2015; Rosier *et al.*, 2018), and multibeam-bathymetric data (Arndt *et al.*, 2013).

For the region of West Antarctica studied in Chapter 4, most of the multibeam data have been previously collated in the International Bathymetric Chart of the Southern Ocean (IBCSO) (Arndt *et al.*, 2013; Dorschel *et al.*, 2022) with additional input from gravity inversions beneath the Pine Island, Thwaites, Dotson, Crosson, and Getz ice shelves (Millan *et al.*, 2017). The IBCSO dataset consists of over 4200 million data points collected primarily using multibeam echo-sounding over 177 cruises — in addition to over 50 million depth soundings acquired by single beam echo-sounders. Data quality varies substantially depending on the age and type of system used, and the amount of processing applied to the data after collection. The IBCSO data were gridded into 500×500 m cells using an iterative method in which results are gridded, visualised, cleaned, and re-gridded until a satisfactory solution is found (Arndt *et al.*, 2013).

In the Northern Hemisphere, the bathymetry of the North Sea and the elevation of its surrounding landmasses were derived from the European Marine Observation and Data Network (EMODnet) Bathymetry DTM (EMODnet Bathymetry Consortium, 2018). The EMODnet Bathymetry DTM is a publically available bathymetric dataset for the European seas compiled from over 9400 bathymetric surveys gathered from 49 providers. Additional nearshore bathymetric measurements, derived from Landsat 8 satellite data, were also incorporated into the data compilation to create a DTM with a gridded horizontal resolution of approximately 115×115 m.

3.3 Seismic-reflection methods

3.3.1 Introduction

Seismic-reflection data can be used to identify buried glacial surfaces, often past continental shelves, beneath hundreds to thousands of metres of sediment. They provide information about older ice advances across the continental shelf than those revealed by the seafloor record visible with multibeam-bathymetric data (e.g., Dowdeswell *et al.*,

2007; Graham *et al.*, 2009b, 2010; Batchelor *et al.*, 2013; Dowdeswell and Ottesen, 2013; Bellwald *et al.*, 2018; Rea *et al.*, 2018). Since its origins in the 1920s, reflection seismology has developed into a hugely valuable tool for visualising and understanding the structure of sedimentary basins (Stoker *et al.*, 1997; Cartwright and Huuse, 2005; Brown, 2011). Over time, driven largely by the advent of major hydrocarbon exploration programmes and enabled by technological advances in computer processing power and improvements in precision navigation, the use of these methods has led to significant insights into geological processes such as rock-fluid interactions, soft-sediment deformation, shallow-gas hazards, fault growth, and fluid flow (Cartwright and Huuse, 2005; Mosher *et al.*, 2006; Cartwright, 2007). Many of these advances came about with the development of 3D seismic technology in the 1980s — a so-called ‘geological Hubble’ moment (Cartwright and Huuse, 2005) which enabled the sub-surface to be visualised in three, or even four, dimensions if repeat 3D surveys are undertaken over time.

The basic principle of reflection seismology relies on measuring the time taken for a low frequency acoustic pulse, generated at a known time using an artificial source, to be returned after being reflected off different layers of the sub-surface (Figure 3.1). Individual layers can be distinguished by contrasts in their acoustic impedance (the product of material density and seismic velocity) and the results are typically visualised in two-way travel time (Stoker *et al.*, 1997; Brown, 2011). A key difference between seismic studies and those using multibeam echo-sounders is that, due to the latter’s higher frequency acoustic source (~12 kHz for deep water systems but up to 700 kHz for shallow water systems), there is little or no signal penetration of the seafloor at these higher frequencies (Jakobsson *et al.*, 2016).

For ship-based seismic systems, the acoustic source and receiver array are towed behind the survey vessel, separated in space. Several techniques exist to generate acoustic pulses, including injecting compressed air into the water column, displacing water, or using sparks. The method chosen affects the extent of substrate penetration and the vertical resolution of the data collected. Seismic ‘boomers’ produce a relatively high frequency (500–1500 Hz) pressure pulse using the displacement of water by rapidly flexing a metal plate. The higher frequencies associated with this method produce data with higher vertical resolutions (decimetres) but relatively shallow penetration into the substrate. Conversely, the lower frequency pulses generated by air and sleeve guns (typically with most energy in the range of 20–100 Hz), which release high-pressure air into the water, yield greater sub-surface penetration at the expense of vertical resolution. Additionally, sparker systems can be used to generate acoustic pulses with most energy between 20–200 Hz by imploding bubbles (Jakobsson *et al.*, 2016).

The vertical resolution of seismic-reflection data can be understood as the distance that two geological entities have to be separated by before they can be detected as distinct reflection events (Cox *et al.*, 2020). Vertical resolution is determined by many factors including the source spectrum, signal absorption, receiver depth, water depth, single element spacing and temporal noise spectrum (Stoker *et al.*, 1997; Mosher *et al.*, 2006; Brown, 2011). In practice, the limit of separability — the capability to resolve the top and base of a sedimentary layer — can be approximated using the Rayleigh Criterion in which resolution equals roughly one quarter of the dominant wavelength, λ , of the seismic signal (Kallweit and Wood, 1982). The dominant wavelength is determined by the frequency of the wavelet, F , and the velocity of the rock unit, V :

$$\lambda = V/F \quad (3.2)$$

Accordingly, the vertical resolution of a given seismic-reflection dataset, R , is:

$$R = \lambda/4 \quad (3.3)$$

Once an acoustic pulse has been produced, it travels through the water column and encounters the sub-surface layers, where part of the pulse is reflected back towards the vessel. Here, returned signals are captured by a single or an array of streamers, consisting of hydrophones made of piezoelectric materials, towed behind the acoustic source. The hydrophones convert the reflected pressure wave into an electrical signal which is relayed to the survey vessel where it is processed. Hydrophones may either be connected together to constitute one channel or in groups to produce multiple channels. A multi-channel setup has the advantage of being capable of providing information on the seismic velocities (material densities) of sedimentary layers below the seafloor. Single-channel streamers are typically tens of metres in length, whilst a multi-channel streamer can be hundreds of metres to kilometres long. In general, deeper objectives require longer cables.

The depth at which the seismic source and receivers are towed affects the data resolution due to interference with signals reflected from the sea surface (Jakobsson *et al.*, 2016). This interference results in the suppression of seismic frequencies for which the towing depth is equal to half the wavelength of the signal, whilst those at half that frequency are reinforced. Thus, for a setup towing streamers at a depth of 5 m below the sea surface, a sound wave travelling at a velocity of 1500 m s⁻¹ will have frequencies around 150 Hz suppressed, whilst those around 75 Hz will be reinforced (Jakobsson *et al.*, 2016). Typically, a modern setup designed to acquire 3D seismic data will consist of multiple streamers (potentially >20), each of which can be up to 6–8 km in length, towed at a depth of 5–8 m below the sea surface (Figure 3.2) (Games and Wakefield, 2014).



Figure 3.2. Example of a modern marine setup for large-scale 3D seismic data collection. The image depicts the *Ramform Atlas*, a 104 m long, 70 m wide seismic survey vessel owned by the marine geophysical company Petroleum Geo-Services (PGS). The survey vessel is capable of towing up to 24 streamer reels, allowing it to gather up to 200 km² of data in a single day (Jakobsson *et al.*, 2016). Photograph courtesy of PGS.

3.3.2 3D seismic data

Seismic reflection mapping can be conducted in both two and three dimensions. In 2D surveys, seismic-reflection data are collected along a single profile, whereas 3D surveys tie together a set of closely spaced profiles, typically spaced tens of metres apart and parallel from one another, to produce a three dimensional representation of the sub-surface (Figure 3.3) (Jakobsson *et al.*, 2016). The first offshore 3D seismic reflection survey was completed by Exxon in 1967 (Cleveland and Morris, 2014). Due to the extremely high cost of data collection, most 3D seismic surveys are carried out for the purpose of hydrocarbon exploration, although more compact high-resolution 3D seismic systems are increasingly being deployed by the academic community (e.g., Bellwald *et al.*, 2018; Lebedeva-Ivanova *et al.*, 2018; Tasianas *et al.*, 2018; Bellwald *et al.*, 2019).

The 3D seismic technology employed for exploration purposes typically relies on the reflection of broadband, non-rectified sound in the low frequency range (3–125 Hz) (Mosher *et al.*, 2006). The horizontal resolution of the data collected is dependent on the source wavelet frequency, the acoustic aperture (length of the array), hydrophone element spacing, spatial noise power spectrum, pattern responses, group interval, and

the accuracy of the positioning system (Power and Clarke, 2019). Of these, frequency and acoustic aperture are the most significant parameters; larger apertures and wider source bandwidths improve horizontal resolution (Mosher *et al.*, 2006).

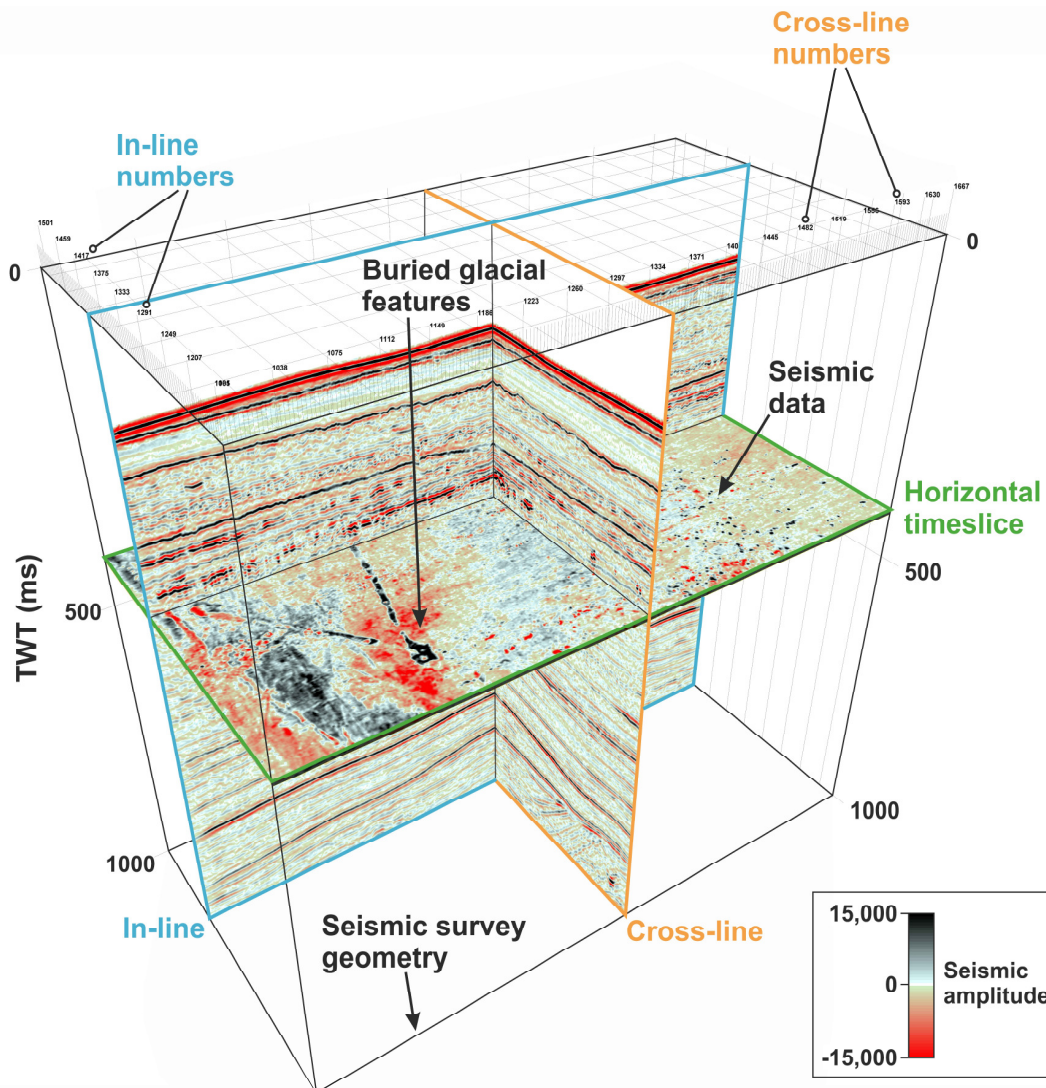


Figure 3.3. A 3D seismic volume displayed within seismic interpretation software. Example in-line, cross-line and horizontal seismic profiles demonstrate how 3D seismic data can be sliced and interrogated from multiple angles to examine glacial landforms buried on past continental shelves and slopes. The overall survey geometry is outlined within a black box with depth shown in two-way travel time (TWT). A seismic amplitude colour bar shows the polarity and amplitude of the seismic reflections.

3D seismic reflection technology offers two main improvements over 2D seismic methods. First, the spacing between profiles is dramatically reduced from ~ 1 km to < 25 m, offering much higher horizontal resolution. As a result of this improvement, it is now possible to image the seafloor as a 3D seismic horizon to a comparable level of detail as when surveyed using a multibeam echo-sounder (Mosher *et al.*, 2006; Power and Clarke, 2019).

An additional advantage of 3D seismic data is that the density of the sampled data (bin spacing) is independent of water depth; instead, this is controlled by the streamer spacing, channel spacing within the streamers and the shot interval of the acoustic source (Mosher *et al.*, 2006). In contrast, the density of multibeam echo-sounder data decreases with water column thickness. Accordingly, in deep water, 3D seismic methods may even outperform multibeam echo-sounders in terms of horizontal spatial resolution, especially in areas where seafloor bathymetry lacks particularly steep slope angles (Bulat, 2005; Cartwright and Huuse, 2005; Mosher *et al.*, 2006; Cartwright, 2007; Power and Clarke, 2019).

The second advantage of 3D seismic over 2D seismic data is that the dense 3D grid of data points generated by this technique allows seismic migration algorithms to be applied which reposition reflected arrivals to their true source points (Jakobsson *et al.*, 2016; Cox *et al.*, 2020). The spatial resolution of unmigrated seismic data is generally limited by the dimensions of the first Fresnel zone — a region of constructive interference surrounding the geometrically predicted reflection point determined by the dominant wavelength of the source wavelet. The ability to apply migration algorithms to 3D seismic data collapses the Fresnel zone in two dimensions, improving the accuracy of reflection positioning and facilitating the accurate alignment and imaging of three dimensional geological structures (Cartwright and Huuse, 2005; Mosher *et al.*, 2006).

3.3.3 High-resolution 3D seismic data

Continued improvements in the resolution of 3D seismic data over time (e.g., Lebedeva-Ivanova *et al.*, 2018) have given rise to the field of seismic geomorphology (Posamentier *et al.*, 2007). This sub-discipline identifies and characterises assemblages of buried landforms to attempt to understand the former sea bed (Bellwald *et al.*, 2019). The approach has been employed widely at high-to-mid latitudes to reconstruct past glacial influence and former ocean circulation patterns throughout the Quaternary (e.g., Todd *et al.*, 1988; Dowdeswell *et al.*, 2007; Dowdeswell and Ottesen, 2013; Newton *et al.*, 2016; Rea *et al.*, 2018).

Conventional 3D seismic data are associated with two main drawbacks. First, the low frequency range of the source means that the frequency content of the data is low (typically ~60 Hz). This limits the vertical resolution of the data to several tens of metres. Second, because of the large offsets between the source and the streamers, any ‘shallow’ data in the first 5–600 ms TWT is poorly imaged (Games and Wakefield, 2014). Many buried glacial landforms from the Quaternary are present at these depths (e.g., Montelli *et al.*, 2017; Newton and Huuse, 2017). The seafloor and near-seafloor signal returns from

longer offsets are also muted to preserve temporal frequencies; however, this practice limits the spatial resolution achievable with this method (Mosher *et al.*, 2006).

The need for greater vertical and horizontal resolution than that offered by conventional seismic exploration methods has recently led to the development of techniques capable of gathering high- or even ultra-high-resolution 3D seismic data (e.g., Games, 2012; Games and Wakefield, 2014; Bellwald *et al.*, 2018; Lebedeva-Ivanova *et al.*, 2018; Bellwald *et al.*, 2019). These advances are facilitated by the use of a high frequency seismic source towed no deeper than 3 m, closely spaced streamers with group lengths less than 12.5 m and recording intervals of <1 ms (Games, 2012). Together, this setup improves the effective spatial and vertical resolution of the data at the expense of the rate of data acquisition being reduced by a factor of ~ 6 compared to exploration data (Games, 2012; Games and Wakefield, 2014; Games and Self, 2017). Higher recorded frequencies permit the bin size of the data to be reduced, resulting in an increase in horizontal resolution from the ~ 12.5 –100 m range typical of commercial 3D seismic surveys to 3–6 m, whilst vertical resolution is improved from ~ 8 m to 1–5 m (Figure 3.4; e.g., Games and Wakefield, 2014; Bellwald *et al.*, 2018; Lebedeva-Ivanova *et al.*, 2018; Tasianas *et al.*, 2018). Accordingly, these technologies now mean that buried horizons can be imaged at a similar resolution to that of the seafloor when using multibeam-bathymetric data, even in shallow water (Figure 3.5; Bellwald *et al.* (2019)).

One example of high-resolution 3D seismic technology is the P-cable seismic system. P-cable is a lightweight high-resolution 3D seismic system that has been used to identify a wide variety of metre-scale glacial features in Arctic and sub-Arctic settings (Jakobsson *et al.*, 2016; Lebedeva-Ivanova *et al.*, 2018). Examples of the features imaged using this technique include iceberg ploughmarks, hill-hole pairs, streamlined glacial landforms, shallow gas pockets, fluid leakage pathways and erosional surfaces (e.g., Petersen *et al.*, 2010; Plaza-Faverola *et al.*, 2011; Brookshire *et al.*, 2015; Bellwald *et al.*, 2018, 2019, 2023; Tasianas *et al.*, 2018). The system consists of a cross-cable that is towed perpendicular to the ship's course between two paravanes, to which 12 or more 25–100 m long streamers are attached (Jakobsson *et al.*, 2016). When towed behind the vessel at a depth of 1–3 m, P-cable can acquire a high-resolution (50–300 Hz) swath of 3D seismic data up to 150 m wide in water depths of 300–3000 m. Real-time Global Positioning System (GPS) positioning is used to accurately locate the data in space. The use of relatively high frequencies, small offsets and close streamers means that the data can be binned at 6×6 m or less (Jakobsson *et al.*, 2016), and configurations to reduce bin size down to 1×1 m have even been proposed (Lebedeva-Ivanova *et al.*, 2018). The high-resolution data are gathered at the expense of a narrower swath width compared to

conventional exploration seismic data. As a result, 3–5 days of ship time may be required to cover a 10–50 km² area, whereas modern exploration seismic setups may gather up to 200 km² of data in a single day (Jakobsson *et al.*, 2016; PGS, 2017).

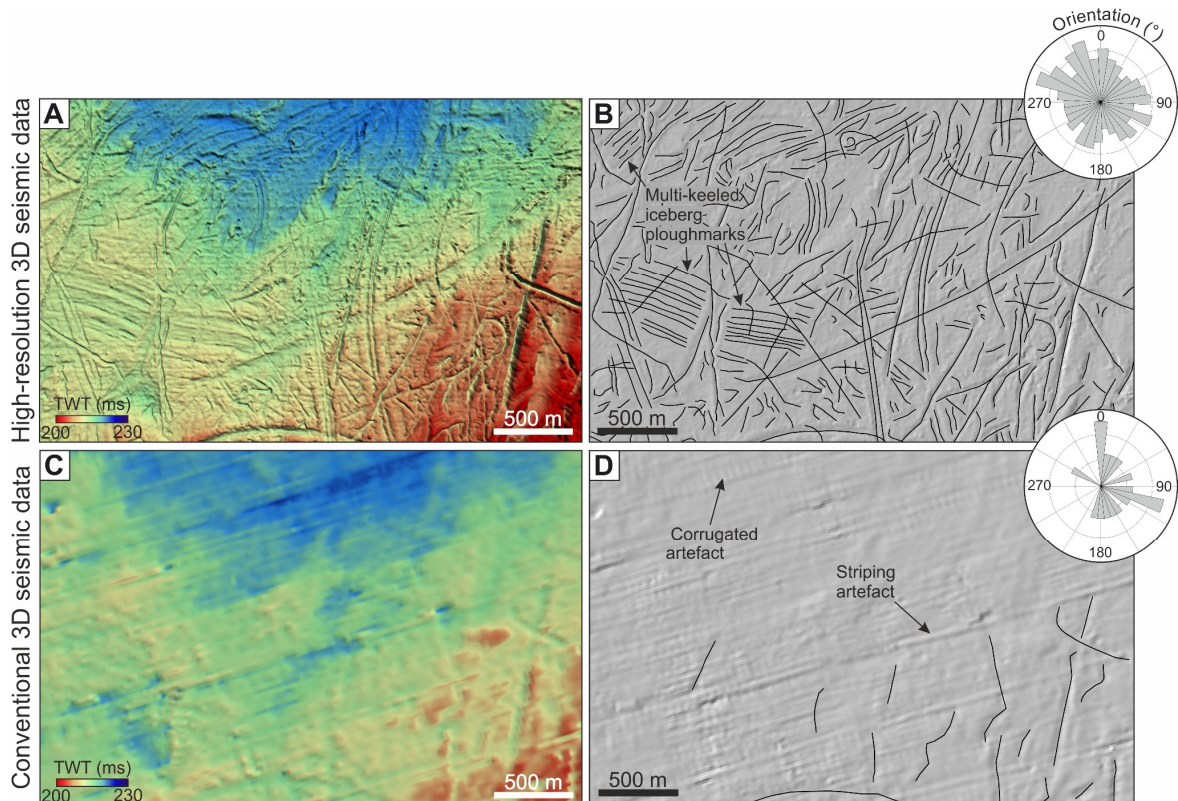


Figure 3.4. Differences between high-resolution 3D seismic-reflection data and conventional 3D seismic-reflection data. (A) A glacial surface buried ~30 m beneath the modern-day seafloor mapped using high-resolution 3D seismic data (6.25×6.25 m bin size) and (B) geomorphological mapping of iceberg ploughmarks from the surface shown in (A), inset with their respective orientations in degrees north. Note the multi-keeled iceberg ploughmarks. (C) The same area and horizon mapped using exploration quality 3D seismic-reflection data (12.5×12.5 m bin size). (D) Mapped iceberg ploughmarks visible in (C) and their respective orientations. Note the presence of artefact stripes and corrugations.

3.4 Seismic methods employed in this thesis

The seismic data used in this thesis were collected using two classes of acquisition systems with different horizontal and vertical resolutions. Small areas of high-resolution 3D seismic data were used to examine the infill architecture of glacial tunnel valleys buried beneath the North Sea seafloor at a much higher resolution than has been conducted previously. Due to the small areal coverage of the high-resolution 3D seismic data (typically between 1.5–40 km² per dataset), a regional scale 3D seismic survey was used to contextualise the high-resolution data and extend the interpretations over a regional scale.

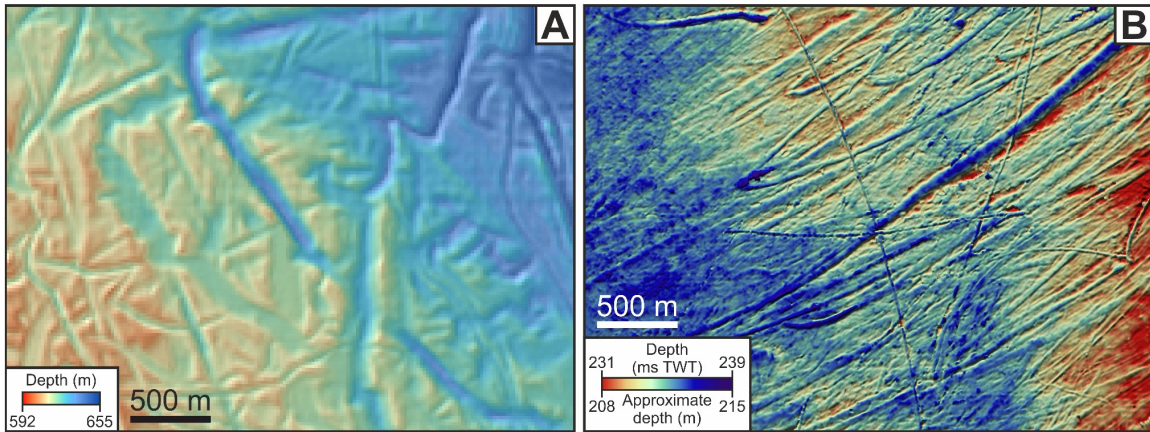


Figure 3.5. Comparison between seafloor iceberg scours mapped using multibeam bathymetric data and buried iceberg ploughmarks mapped using high-resolution 3D seismic data. (A) Multibeam-bathymetric data showing iceberg ploughmarks in Pine Island Bay, West Antarctica (Jakobsson *et al.*, 2011; Eriksson *et al.*, 2021). The data are gridded at a 20-m horizontal resolution. (B) Iceberg ploughmarks buried ~30 m beneath the modern day seafloor of the North Sea, imaged using high-resolution 3D seismic data. Depths were converted using Equation 3.1. The horizontal scale on both images is identical.

3.4.1 GSeis³ high-resolution 3D seismic data

In this thesis, high-resolution 3D seismic data were used, acquired using the GSeis³ seismic setup. The GSeis³ acquisition system was developed by the Gardline Limited, a marine geotechnical and environmental surveying company, for the assessment of geohazards including shallow gas. The acquisition system has been operational since 2013 and utilises two 1200-m-long streamers towed 1–3 m beneath the sea surface from the vessel MV *Ocean Reliance* (Figure 3.6; Games and Wakefield, 2014). The streamers have 96 traces with 12.5 m groups, and data are collected with a shot interval of 6.25 m and a sample rate of 1 ms. The seismic source consists of two 4×40 inch³ sleeve airguns, fired in flip-flop formation, with a signal frequency range between ~20–250 Hz (Games, 2012; Games and Wakefield, 2014; Games and Self, 2017).

The main benefit of this particular technique over other high-resolution 3D seismic acquisition systems is the exact positioning of the source and streamers. This is due to the positions of the acoustic source, head buoys and tail buoys being precisely known from GPS positioning and laser tracking from the rear of the survey vessel. Compass birds are also attached to the streamers at 150 m intervals; these, combined with the laser tracking and GPS positioning, allow the movement of the streamers in the water to be modelled in detail and the data to be accurately binned at a high resolution (Games, 2012; Games and Wakefield, 2014; Games and Self, 2017). In addition to the benefit of

precise streamer and source locations, the long streamer lengths employed by GSeis³ enable velocity analysis to be conducted. This is crucial for the removal of seismic multiples, especially in shallow-water areas such as the North Sea. It is not possible to conduct velocity analysis using systems that employ shorter streamer lengths, such as P-Cable.

The processed 3D seismic data consist of time-migrated stacks with a 1 ms sample rate and a bin size of 6.25×6.25 m. The vertical resolution of the data is ~ 4 m, with a detection limit along individual reflectors of ~ 0.5 m. The data were processed using ProMAX 3D software. During processing, noise from seismic interference and swell was first removed using the common-P removal technique and a time-frequency domain (TFD) filter. Surface Related Multiple Elimination (SRME) was then applied to remove seismic multiples from the data. Global Navigation Satellite System (GNSS) calculated tides were used to correct the data for tidal induced fluctuations in water depth. The remaining processing workflow included normal-moveout correction, two passes of velocity analysis run at 250×250 m intervals, the application of Kirchhoff pre-stack Time Migration to the common offset gathers, and low-cut/high-cut bandpass filtering. The final processed data effectively have the quality of high-resolution 2D seismic data in a 3D format which allows buried surfaces to be examined in three dimensions. These processed seismic data were handled using S&P Global Kingdom Software.

3.4.2 Regional scale 3D seismic data

The high-resolution 3D datasets are supplemented by the Central North Sea (CNS) MegaSurveyPlus, a merged regional scale 3D seismic dataset covering an area of 23,650 km² in the central North Sea produced by the marine geophysical company Petroleum Geo-Services (PGS). Over the last 20 years, PGS has collected 3D seismic data in the central North Sea using a variety of acquisition systems and, since 2002, has delivered a merged regional 3D seismic dataset known as the MegaSurvey (PGS, 2020). The CNS MegaSurveyPlus builds on areas where previous data coverage is already good by including legacy data from field tapes and data that are now of release age. These data have been reprocessed and merged with the existing data using state-of-the-art processing techniques to provide better structural imaging and improved signal-to-noise ratios (PGS, 2020). The data consists of a 3D pre-stack time-migrated seismic cube that stretches ~ 200 km from north to south and ~ 140 km from east to west. The data have a bin size of 12.5×12.5 m and a vertical resolution of ~ 8 –20 m depending on the original acquisition system used and the conditions in which the data were collected. Data were provided down to 1 s TWT.

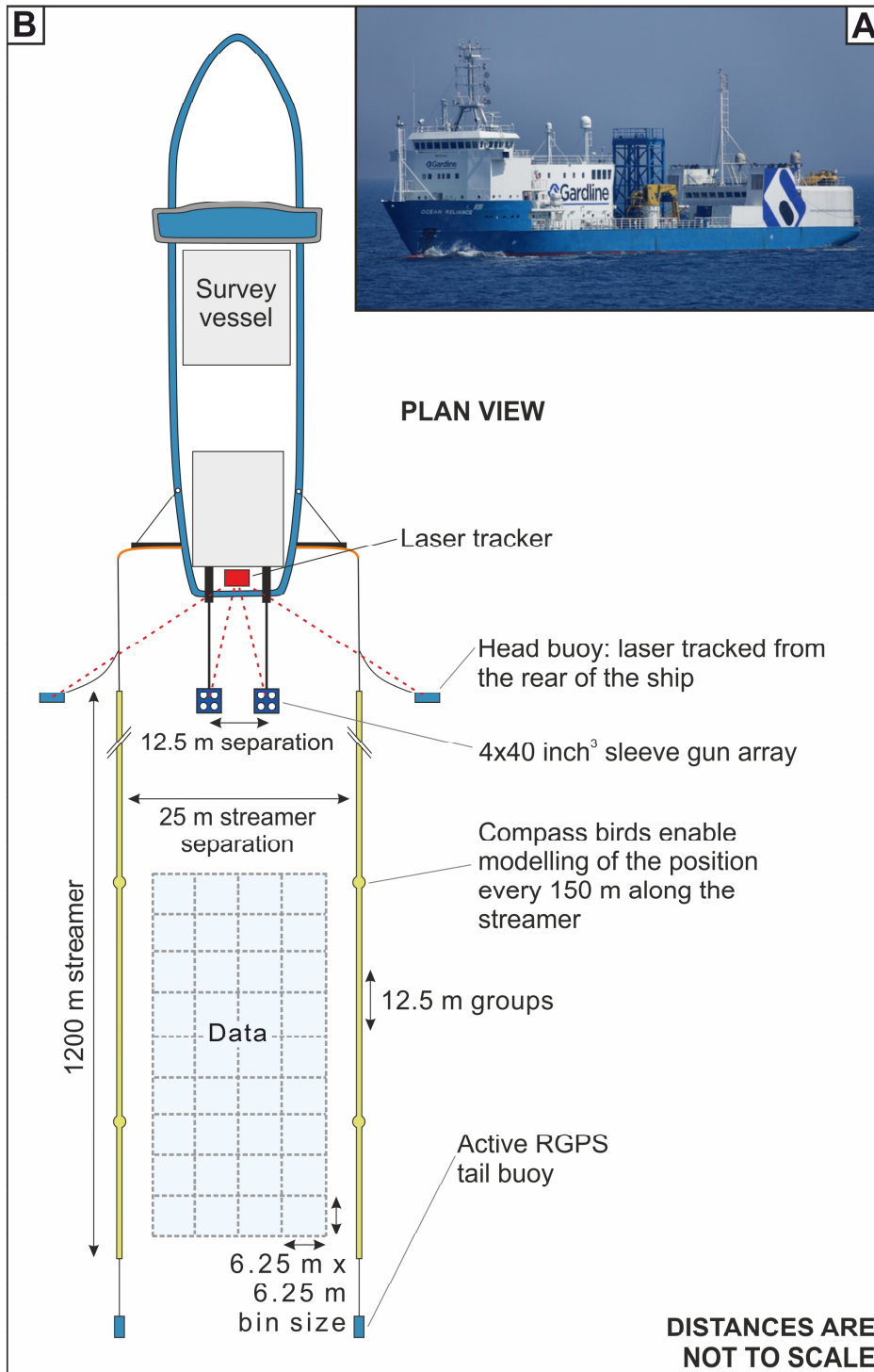


Figure 3.6. The GSeis³ acquisition system. **(A)** Photograph of the MV *Ocean Reliance* — the vessel from which the high-resolution 3D seismic data used in this thesis were collected. **(B)** Plan view schematic of the GSeis³ acquisition system. The system consists of two 1200 m streamers with 12.5 m groups towed behind a survey vessel. Compass birds are attached every 150 m along the length of the streamers which, along with laser tracking of the head buoys and GPS positioning of the tail buoys, allows the movement of the streamers in the water to be modelled. Two 4×40 inch³ sleeve airguns arrays provide an acoustic source with a frequency range of ~ 20 – 250 Hz.

Chapter 4

Past water flow beneath Pine Island and Thwaites glaciers, West Antarctica

Abstract

Outburst floods from subglacial lakes beneath the Antarctic Ice Sheet modulate ice-flow velocities over periods of months to years. Although subglacial lake drainage events have been observed from satellite-altimetric data, little is known about their role in the long-term evolution of ice-sheet basal hydrology. In this chapter, past water flow is systematically mapped and modelled through an extensive area containing over 1000 subglacial channels and 19 former lake basins exposed on over 19,000 km² of seafloor by the retreat of Pine Island and Thwaites glaciers in West Antarctica. At 507 m wide and 43 m deep on average, the channels offshore of present-day Pine Island and Thwaites glaciers are approximately twice as deep, three times as wide, and cover an area over 400 times larger than the terrestrial meltwater channels comprising the Labyrinth in the Antarctic Dry Valleys. The channels incised into bedrock offshore of contemporary Pine Island and Thwaites glaciers would have been capable of accommodating discharges of up to $8.8 \times 10^6 \text{ m}^3 \text{ s}^{-1}$. The channels are inferred to have formed from episodic discharges from subglacial lakes trapped during ice-sheet advance and retreat over multiple glacial periods. These results document the widespread influence of episodic subglacial drainage events during past glacial periods, in particular beneath large ice streams similar to those that continue to dominate contemporary ice-sheet discharge.

4.1 Introduction

The widespread and accelerating retreat of Pine Island and Thwaites glaciers constitutes a potential threat to the stability of the West Antarctic Ice Sheet (WAIS) (Rignot et al., 2008; Joughin et al., 2014; Rignot et al., 2014; Feldmann and Levermann, 2015; Shepherd et al., 2018; Yu et al., 2018). The routing, storage, and expulsion of subglacial water from beneath the WAIS directly influences its mass-loss rates and, accordingly, sea-level rise (Joughin et al., 2002; Alley et al., 2006; Bell et al., 2007; Stearns et al., 2008). Variability in subglacial water supply can lead to ice-sheet instability (Schoof, 2010). However, the effect of subglacial water as a lubricant at the basal ice-sheet boundary is still insufficiently understood to be accurately incorporated into the current generation of ice-sheet models, and is thus presently absent from assessments of future ice-sheet behaviour (Fricker and Scambos, 2009; Flowers, 2015; Fricker et al., 2016).

Over recent decades, ice-penetrating radio-echo sounding surveys and satellite altimetry have revealed an intricate subglacial network of water storage and transfer beneath the contemporary Antarctic Ice Sheet. Over 670 ponded water bodies, termed subglacial lakes, have been detected beneath the ice (Figure 4.1) (Robin et al., 1970; Oswald and Robin, 1973; Siegert et al., 1996; Siegert et al., 2005; Siegert et al., 2016b; Livingstone et al., 2022), about a quarter of which have been observed to fill and drain over sub-decadal timescales (Gray et al., 2005; Wingham et al., 2006; Fricker et al., 2007; Smith et al., 2009a; Smith et al., 2017). The subglacial routing of the water released from this special class of “active” subglacial lakes can be traced for hundreds of kilometres, often triggering a cascade of further subglacial lake drainage downstream (Wingham et al., 2006; Fricker et al., 2007; Flament et al., 2014; Fricker et al., 2014). In some instances, active lake drainage has been associated with temporary accelerations in ice velocity (Stearns et al., 2008; Siegfried et al., 2016). Active Antarctic subglacial lakes typically discharge relatively small volumes of water over several months, with peak discharges of tens of cubic metres per second. For example, lakes detected in the Adventure subglacial trench, East Antarctica, discharged 1.8 km^3 of water over 16 months with a peak discharge of $\sim 50\text{ m}^3\text{ s}^{-1}$ (Wingham et al., 2006), whilst 3.7 km^3 of water was released from a system of subglacial lakes beneath Thwaites Glacier between June 2013 and January 2014 (Smith et al., 2017). To date, the largest contemporary subglacial lake drainage event observed in Antarctica was the loss of $5.2 \pm 1.5\text{ km}^3$ of water from Lake Cook, East Antarctica, over a 2-year period (Flament et al., 2014).

Geomorphological evidence suggests that subglacial water movement, substantially larger than that documented in the satellite era, has occurred beneath the Antarctic Ice Sheet in the past. The mountains flanking the Antarctic Dry Valleys in southern Victoria Land and the ice-free margin of the East Antarctic Soya Coast contain abundant features formed by the flow of subglacial meltwater (Denton et al., 1984; Sawagaki and Hirakawa, 1997). Channel systems that are kilometres long and hundreds of metres wide are present in the Asgard Range (Sugden et al., 1991), in the foothills of the Royal Society Range (Sugden et al., 1999), and in the Convoy Range of the Transantarctic Mountains (Denton and Sugden, 2005; Lewis et al., 2006) (Figure 4.1). One of the most spectacular relict Antarctic landscapes carved by subglacial water is a 5 km long anastomosing system of terrestrial channels in Wright Valley termed the Labyrinth (Selby and Wilson, 1971). The Labyrinth channels can exceed 500 m in width and are incised over 150 m into a 300 m thick sill of Ferrar Dolerite (Lewis et al., 2006). Channel formation has been attributed to repeated subglacial outburst floods, with estimated discharges of up to $1.6\text{--}2.2 \times 10^6 \text{ m}^3 \text{ s}^{-1}$, sourced from one or more subglacial lakes that became trapped as the Antarctic Ice Sheet overrode the Transantarctic Mountains during the Miocene epoch (23–5.3 Ma) (Marchant et al., 1993; Marchant and Denton, 1996; Denton and Sugden, 2005; Lewis et al., 2006). The irregular reverse gradients, anastomosing structure, and the potholes and plunge pools associated with the channel systems in southern Victoria Land are consistent with formation by pressurised subglacial meltwater (Shreve, 1972; Denton and Sugden, 2005; Marchant et al., 2011) on a scale that is perhaps unequalled outside of the Channeled Scablands landscape of eastern Washington state — produced by some of the largest subaerial floods on Earth from Pleistocene proglacial Lake Missoula (Bretz, 1923, 1969).

Channels with similar dimensions have been identified submerged offshore on the largely bedrock-dominated inner continental shelves of the western Antarctic Peninsula (e.g., Ó Cofaigh et al., 2002; Ó Cofaigh et al., 2005; Domack et al., 2006; Anderson and Fretwell, 2008), West Antarctica (e.g., Lowe and Anderson, 2002, 2003; Larter et al., 2009; Nitsche et al., 2013), and eroded into soft sediments in the inner Ross Sea (Simkins et al., 2017). The observed landforms are typically hundreds of metres wide, tens of metres deep, and possess undulating thalwegs that indicate incision by pressurised subglacial meltwater (Lowe and Anderson, 2002). The size and widespread distribution of the offshore channels implies that substantial quantities of subglacial meltwater were required for their formation; this inference is fundamentally inconsistent with the quantity of meltwater produced at the Antarctic ice–bed interface currently (Nitsche et al., 2013; Rose et al., 2014) and the discharges associated with active subglacial lake water transfer

(Wingham et al., 2006; Stearns et al., 2008). The physical process responsible for the formation of the large channel systems on the Antarctic continental shelf thus remains unresolved, limiting our understanding of ice-sheet hydrology and future ice-sheet behaviour.

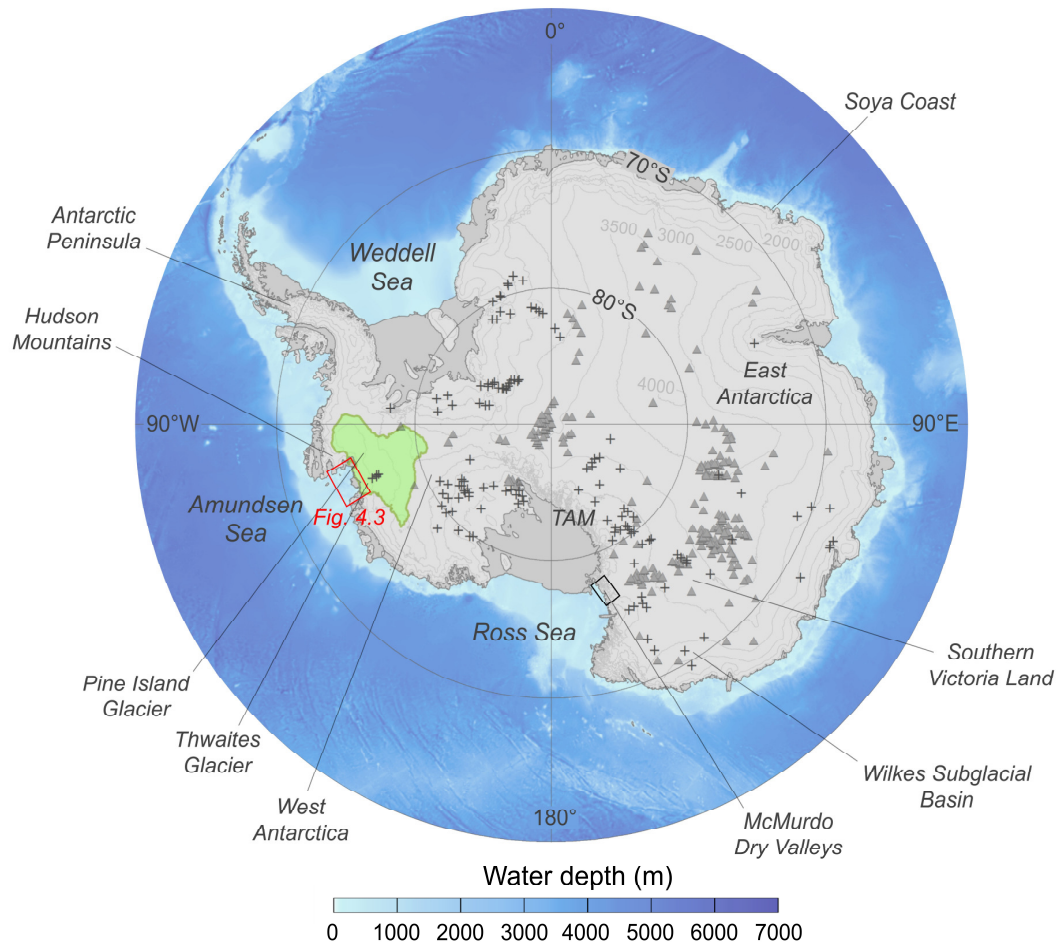


Figure 4.1. Overview map displaying the location of the features and regions referred to in the text. The catchment drained by contemporary Pine Island and Thwaites glaciers is highlighted in green. The black box shows the portion of the Transantarctic Mountains (TAM) containing Wright Valley, the Royal Society Range, the Convoy Range and the Asgard Range, in which channel features have been observed. The area shown in Figure 4.3 is displayed as a red box. The locations of subglacial lakes observed from radio-echo sounding (grey triangles) and actively draining subglacial lakes observed from satellite altimetry (+) are shown from Wright and Siegert (2012) and Smith et al. (2017). Regional bathymetry and ice surface elevation is from BEDMAP2 (Fretwell et al., 2013).

In this chapter, the origin and formation of a huge system of submarine channels, covering an area $>19,000 \text{ km}^2$ (over twice the size of Yellowstone National Park) and located within 200 km of the present-day margins of Pine Island and Thwaites glaciers, is examined. The channel network is mapped in detail and a quantitative morphometric comparison is made between the channels in Pine Island Bay and the terrestrial channels comprising the Labyrinth. A numerical model is then used to simulate the subglacial hydrological conditions and water routing beneath Pine Island and Thwaites glaciers during the Last Glacial Maximum (LGM), and provides constraints on the possible mechanisms and timescales over which the submarine channels formed.

4.2 Methods

4.2.1 Bathymetric and terrestrial data

Multibeam-bathymetric data, collected over two decades by extensive shipborne surveys in Pine Island Bay, were used to produce a comprehensive high-resolution digital elevation model (DEM) of the seafloor offshore from modern Pine Island and Thwaites glaciers (Table 4.1). The multibeam-bathymetric data were gridded at a 20 m resolution. A conservative degree of interpolation, applied up to four cell widths away from a data-filled cell, was used to fill small missing gaps in the grids when proximal to existing bathymetry data. This was the highest resolution that could be achieved without requiring interpolation to fill more than 10% of the study area's grid cells. In addition to the bathymetric data, a 2 m horizontal resolution DEM of Wright Valley, in the McMurdo Dry Valleys of Antarctica, was obtained from the National Aeronautics and Space Administration's 2001 Airborne Topographic Mapper laser altimetry survey to examine the morphology of the Labyrinth (Schenk et al., 2004).

Table 4.1. Details of the geophysical cruise data used in this Chapter.

Cruise / ID	Ship	Year	Multibeam system	Principal investigator
ANT-XXIII/4	Polarstern	2006	Hydrosweep DS2	Gohl, K.
JR179	James Clark Ross	2008	EM120	Larter, R.
JR294	James Clark Ross	2014	EM122	Heywood, K.
NBP0001	N.B. Palmer	2000	SeaBeam 2112	Jacobs, S.
NBP0702	N.B. Palmer	2007	EM120	Jacobs, S.
NBP0901	N.B. Palmer	2009	EM120	Jacobs, S.
NBP1210	N.B. Palmer	2013	EM120	Halanych, K.
NBP9902	N.B. Palmer	1999	SeaBeam 2112	Anderson, J.

4.2.2 Derivation of channel metrics

Channels were digitised manually using hill-shaded DEMs in ArcGIS 10.4. Comparison with a three-dimensional representation of the study area, in which the digitised channel outlines were draped over the projected DEM, ensured that the boundaries of the channels were demarcated accurately (Mayer et al., 2000). This technique permitted the routing pathway of each individual channel to be established. Channels were defined to terminate when they were intersected by a larger, deeper routing pathway. This analysis was repeated for the Labyrinth channels, which, because of their size and anastomosing structure, are arguably the closest analogue for the channels submerged offshore of Pine Island and Thwaites glaciers.

More than 4200 cross sections were analysed to determine the morphological characteristics of the now-submarine Pine Island and Thwaites glacier channels, whilst more than 1600 were used to analyse the subaerially exposed Labyrinth channels. Based on Noormets et al. (2009), a semi-automated algorithm was developed to quantify the width, depth, cross-sectional area, and symmetry of each channel cross section (Figure 4.2). Channel width was defined as the distance between the highest point of each of the channel sides. The greatest vertical distance between the base of the channel and a line intersecting the two channel edges defines the channel depth, D . The horizontal distances from the deepest point of the channel to each of the channel sides, $W1$ and $W2$, were calculated using an idealised triangular representation of the channel. The normalised ratio of $W1$ to $W2$ was used to assess the symmetry of the channel, which can range between 0 and 2. Symmetry values of 1 indicate a symmetrical cross section, whilst values greater than 1 signify a left-skewed channel and values less than 1 indicate a right-skewed channel cross section. Trapezoidal numerical integration was used to approximate the internal area of the channel, bounded by the line intersecting the channel edges. The ratio of channel depth to channel width was used to enable comparison between the vertical and horizontal proportions of each cross section.

In addition to the channel depth–width ratio, the cross-sectional shape of each sample was assessed using the General Power Law (GPL) program (Pattyn and Van Huele, 1998). The GPL program applies a general form of the power-law equation to derive a best-fit approximation of a shape parameter, b , which summarises the geometric shape of the channel:

$$y - y_0 = a |x - x_0|^b, \quad (4.1)$$

where a and b are constants, x_0 and y_0 are the coordinates of the origin of the cross section, and x and y are the horizontal and vertical components of the channel cross section, respectively. A general least-squares method was used to derive the best-fit values of a and b . The value of the shape parameter, b , generally varies from 1 to 2 according to cross-sectional shape, with b -values of 1 indicating a “V-shaped” cross section and values of 2 denoting a perfectly “U-shaped” channel geometry (Pattyn and Van Huele, 1998). Composite channel forms are typically associated with b -values between these two values. Shape-parameter values exceeding 2 are associated with more box-shaped channel cross-sectional profiles, whereas geometries characterised by b -values less than 1 indicate channel flanks with a convex-upward form (Gales et al., 2013).

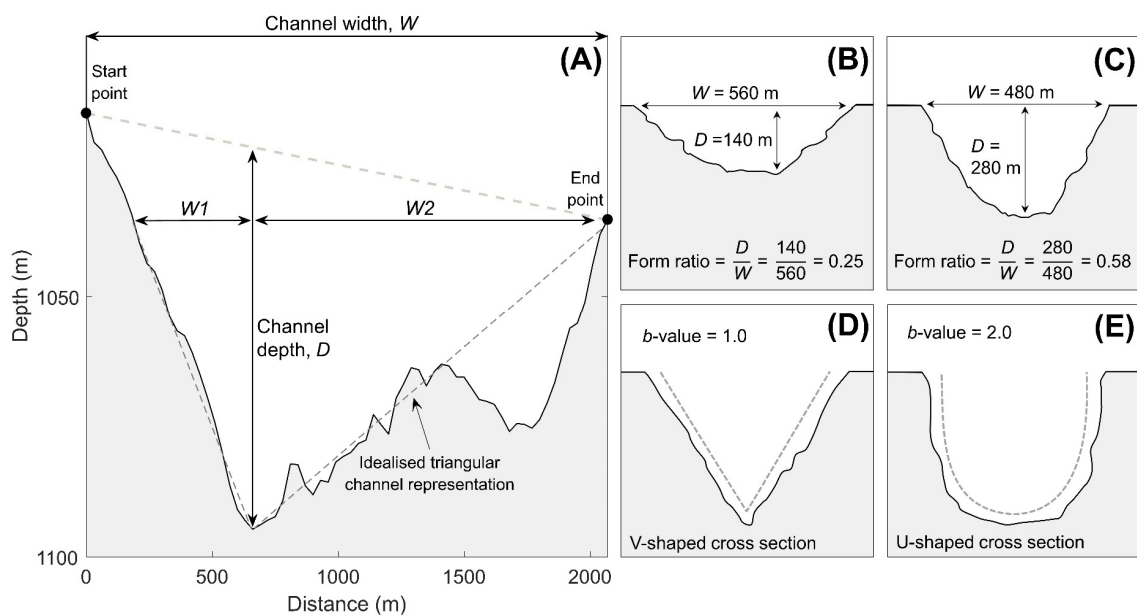


Figure 4.2. Methods of quantifying channel morphometry. (A) Output of the semi-automated algorithm used to derive channel cross-sectional metrics, after Noormets et al. (2009). Plots (B) and (C) illustrate the concept of channel form ratio: the ratio of channel depth to channel width. Wider, shallower channels will be characterised by lower form ratios. Plots (D) and (E) show the variation in channel b -value according to channel shape. V-shaped channels will exhibit a b -value of ~ 1 , whilst U-shaped channels will be characterised by b -values of ~ 2 . Vertical exaggeration in (A) is $20\times$.

4.2.3 Modelling past subglacial water flow

To assess the rates at which subglacial water could be produced, stored, and routed beneath the former Pine Island and Thwaites glaciers, hydrological modelling simulations were performed for the full-glacial configuration of the Pine Island–Thwaites catchment, accounting for isostatic loading under the expanded WAIS, at 20 ka.

4.2.3.1 Palaeo ice-sheet reconstruction and data

The thickness and surface slope of the LGM configuration of the WAIS was derived from a series of palaeo ice-sheet reconstructions produced using the Parallel Ice Sheet Model (PISM) (Golledge et al., 2012). PISM is a three-dimensional, thermomechanical ice-sheet model constrained by geological observations that has been widely used to simulate the dynamics of the Antarctic ice sheets (e.g., Golledge et al., 2012; Golledge et al., 2013; Fogwill et al., 2014; Golledge et al., 2014). PISM combines shallow-ice and shallow-shelf approximations for grounded ice to capture the dynamic behaviour of grounded ice and is able to simulate ice-stream flow and ice drawdown at a relatively high 5 km resolution (Golledge et al., 2012; Fogwill et al., 2014).

Simulation results from Golledge et al. (2012) provided the data required to calculate the routing and flux of subglacial water flowing under hydrostatic pressure beneath Pine Island and Thwaites glaciers at the LGM. A nested modelling approach was adopted in which catchment-wide water fluxes were first calculated at a 500 m resolution. These model results were then input at the edges of the higher-resolution bathymetric DEM covering the offshore channels. The bathymetric DEM was resampled to 90 m for the sake of computational efficiency. Ice-surface topography at the LGM was interpolated from the Golledge et al. (2012) reconstructions to the appropriate resolution (500 or 90 m). Bed topography for the majority of the catchment was derived from the 500 m resolution BedMachine Antarctica dataset of the contemporary Antarctic Ice Sheet's bed (Millan et al., 2017; Morlighem et al., 2019). These data were corrected for isostasy by calculating the isostatic deflection at the LGM from the Golledge et al. (2012) results, and then adding the interpolated deflection values to the bed-topography data to produce a 500 m resolution, isostatically corrected DEM. Ice thickness was calculated by subtracting the interpolated ice-sheet surface from the isostatically corrected bed topography. Subglacial topography and ice thickness were then used to calculate the subglacial hydraulic potential within the study region.

Basal meltwater production was calculated using the modelled basal frictional heating from the Golledge et al. (2012) reconstruction, added to the geothermal heat flux of the

LGM Pine Island and Thwaites glaciers catchment. Geothermal heat flux values were derived from Martos et al. (2017) for the portion covered by the contemporary ice sheet and from Davies (2013) for the offshore portion of formerly ice-covered land. The geothermal heat flux of the catchment ranges between ~ 70 and $\sim 130 \text{ mW m}^{-2}$, whilst frictional heating values range from ~ 0 to $\sim 500 \text{ mW m}^{-2}$. For areas of the bed calculated to be at the pressure melting point in the Golledge et al. (2012) results, the sum of these heat sources was used to calculate the basal melt rate in each DEM cell, which can then be multiplied by the cell area to give a water volume per unit time. For cold-based ice where basal meltwater is absent, the production of basal meltwater was set to zero.

4.2.3.2 Flow routing

Meltwater routing beneath the $\sim 600,000 \text{ km}^2$ area drained by the LGM Pine Island and Thwaites glaciers catchment was modelled using a weighted upstream catchment area algorithm (Arnold, 2010; Willis et al., 2016). Subglacial hydraulic potential, ϕ , dictates the flow and routing of water beneath ice masses (Shreve, 1972). The subglacial hydraulic potential of water flowing beneath an ice sheet is a function of bed topography and ice thickness:

$$\phi = \rho_w gh + k\rho_i gZ \quad (4.2)$$

where ρ_w and ρ_i are the densities of water and ice (kg m^{-3}) respectively, g is the acceleration due to gravity (m s^{-2}), h is bed elevation (m), Z is ice thickness (m), and k is a dimensionless parameter (referred to as the uniform floatation factor) that can be varied from 0 to 1 to simulate variations in subglacial water pressure. Higher k values represent greater subglacial water pressure, with $k = 1$ denoting that water pressure is equal to the overburden pressure exerted by the overlying ice, and $k = 0$ representing water flowing at atmospheric pressure. Seismic (Alley et al., 1986; Blankenship et al., 1986) and borehole (Engelhardt et al., 1990; Kamb, 2001; Tulaczyk et al., 2001) investigations of the basal properties of Antarctic ice streams demonstrate that, where present, the pressure of subglacial meltwater is typically close to the ice-overburden pressure. Multibeam swath bathymetry, sub-bottom profiler, and sediment coring studies have previously established that the now-submarine study area in Pine Island Bay was occupied by a major ice stream during the LGM (e.g., Graham et al., 2010). A k value of 0.995 was therefore chosen to parameterise subglacial water pressures within the numerical model simulations to approximate the subglacial water pressures observed under contemporary Antarctic ice streams.

The upstream area model is described fully in Arnold (2010), and its adaptation for calculating the volume, throughput water discharge, and possible residence time of subglacial lakes is described in Willis et al. (2016). Briefly, the algorithm first identifies all cells in a hydraulic potential surface that have a lower potential than their neighbours. Such “sink” cells allow local subglacial catchments (a group of contiguous cells which all drain toward the sink) to be determined, and also form the nucleus for potential subglacial lakes. The algorithm “floods” each sink cell to find the elevation of the lowest cell in the catchment surrounding the sink over which water would spill into a lower potential downstream cell (and hence into an adjacent catchment). This spill point cell defines the maximum depth (relative to the sink), area, and volume of each potential lake, and also allows the routing algorithm to pass the total catchment area (or cumulative subglacial melt) from catchment to catchment downstream until the model reaches the edge of the DEM. In this way, the algorithm builds up the topology of subglacial water flow, linking the individual catchments together into arborescent structures. The algorithm thus calculates the volume and direction of subglacial water flow; however, it is not capable of predicting physical flow conditions within individual channels.

Rather than simply accumulating the DEM cell areas, the algorithm is weighted such that each cell contributes its modelled basal melt flux (see Section 4.2.3.1). This enables the steady-state subglacial water flux in each cell within the DEM, and the total discharge flowing into each potential subglacial lake, to be calculated. For each lake, the outflow discharge into the adjacent downstream catchment is set to be equal to the inflow discharge, as the algorithm assumes steady-state flow through each lake (which is assumed to be at maximum volume) in order to maintain topological continuity. By dividing the volume of each lake by the input water flux, the total time to refill the lake (again assuming steady flow) can be calculated. This effectively gives the minimum duration of any possible fill–drain cycle for each lake.

The modelled continuous subglacial water fluxes are then compared to the theoretical discharge that could be accommodated by the channels if sufficient water were available based on channel cross-sectional area (Walder, 1986; Wingham et al., 2006; Jordan et al., 2010). The maximum discharge, Q_{max} , capable of being carried by a semi-circular cross section, S , is equal to:

$$Q_{max} = 2\left(\frac{\pi}{2}\right)^{\frac{1}{3}} S^{\frac{4}{3}} m^{-1} \left(\frac{\phi'}{p_w g}\right)^{\frac{1}{2}} \quad (4.3)$$

where ϕ' is the hydraulic potential gradient, ρ_w is the density of water (kg m^{-3}), g is acceleration due to gravity (m s^{-2}), and m is the Manning coefficient ($\text{m}^{-1/3} \text{s}$). The value of S is derived from the measured cross-sectional area of the channels in the multibeam-bathymetric data and along-channel estimates of ϕ' were estimated using Equation 4.2. As the channels were unlikely to have been completely ice-free during periods of occupation by subglacial water, three possible scenarios were used to calculate the hypothetical discharge under in which the channel cross sections are: (1) ice-free, (2) 50% occupied by ice, and (3) 90% occupied by ice.

4.3 Results

4.3.1 Morphology of channels in Pine Island Bay

Over 1000 channels were mapped within Pine Island Bay, covering an area of $\sim 19,000 \text{ km}^2$ (Figure 4.3). This represents a $>40\%$ increase over previous mappings (Figures 4.4A, 4.4B; Kirkham, 2017). The channels are arranged in a complex anastomosing pattern that often appears to follow lines of geological weakness in the inner-shelf bedrock. No channels are visible beyond the transition from the inner-shelf bedrock to the sedimentary strata on the outer continental shelf (e.g., Lowe and Anderson, 2003; Graham et al., 2010; Gohl et al., 2013; Nitsche et al., 2013), $\sim 200 \text{ km}$ from the present ice margin. The channels are characterised by undulating long-axis profiles (thalwegs) containing multiple reverse gradients along their lengths. The majority of channels are less than 5000 m long, range in width from 80 to 3600 m , and are incised into bedrock by between 3 and 330 m . The channels are 507 m wide and 43 m deep on average, with a typical cross-sectional area of $17,000 \text{ m}^2$ (Figure 4.5).

The bedrock channel system in Pine Island Bay is interspersed with a series of 19 flat-bottomed depressions with steep sides relative to the gradient of their central floor. The depressions resemble a series of basins connected, and sometimes cross-cut, by the channels. The basins range in planimetric area between 5 and 159 km^2 and descend several hundred metres beneath the average depth of the surrounding topography. The basin floors contain subdued glacial landforms (Nitsche et al., 2013) that appear to be partially buried by sedimentary infill.

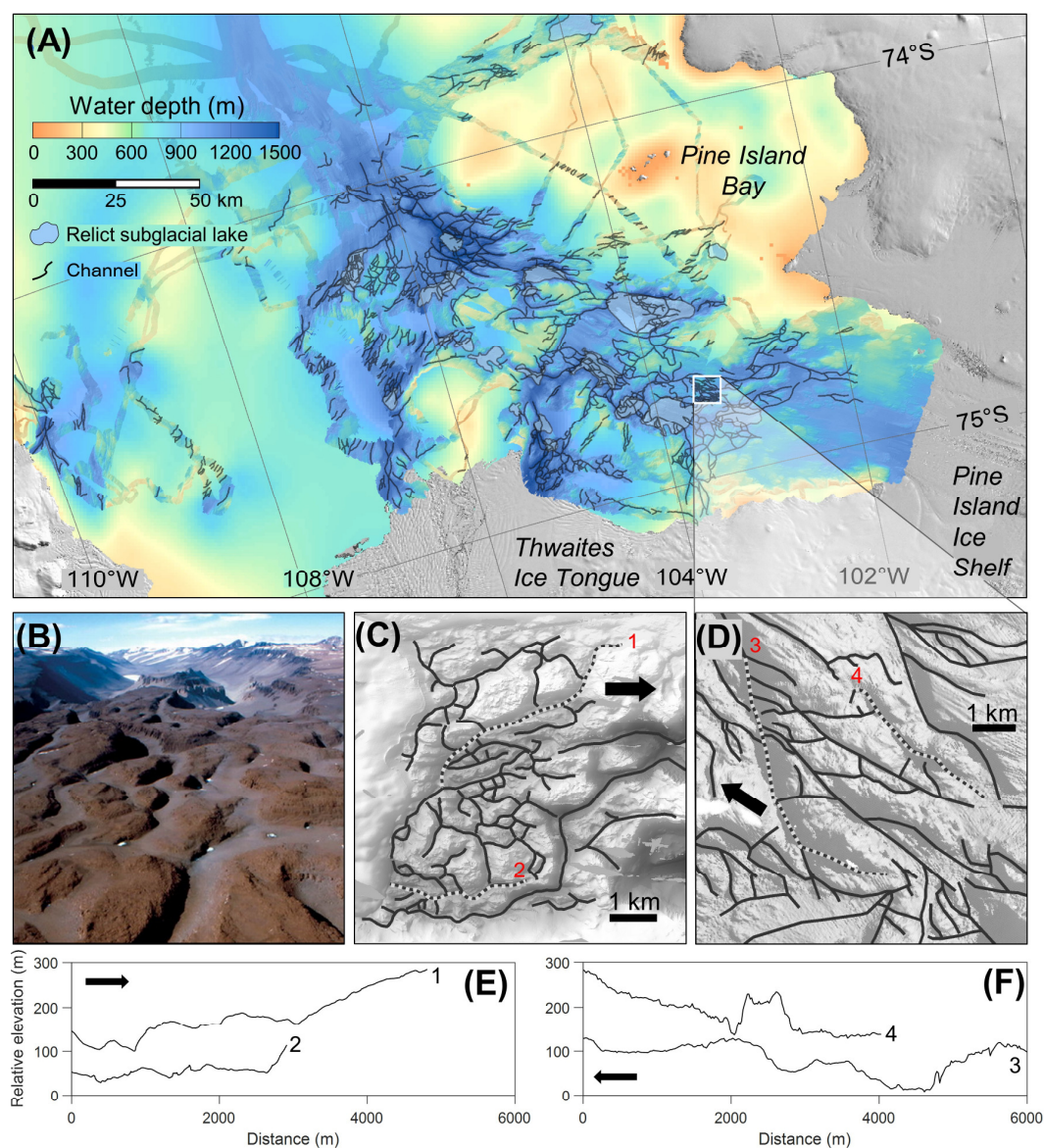


Figure 4.3. Channelised bathymetry of the region offshore of Pine Island and Thwaites glaciers. (A) Inner continental shelf bathymetry within Pine Island Bay, gridded at a 20 m cell size with sun illumination from the northeast. Mapped channels are displayed as black lines, and mapped relict subglacial lake basins are displayed as blue polygons. Onshore topography is displayed as a shaded Landsat Image Mosaic of Antarctica (LIMA) (U.S. Geological Survey, 2007). The white square in (A) is scaled to the same dimensions as the Labyrinth, displayed in (B) and (C). (B) Oblique aerial photograph of the channel system comprising the Labyrinth (Lewis et al., 2006). Channels in the foreground are ~100 m wide. (C) Digital elevation model of the Labyrinth with channels displayed as black lines. (D) Subset of the Pine Island Bay bathymetry, scaled to the same dimensions as the Labyrinth, exhibiting a series of channels. Black arrows denote the inferred direction of palaeo-ice flow. Selected long-profiles of the channels comprising the Labyrinth (E) and in Pine Island Bay (F) with numbers donating their locations in (C) and (D). Vertical exaggeration in (E) and (F) is 50x.

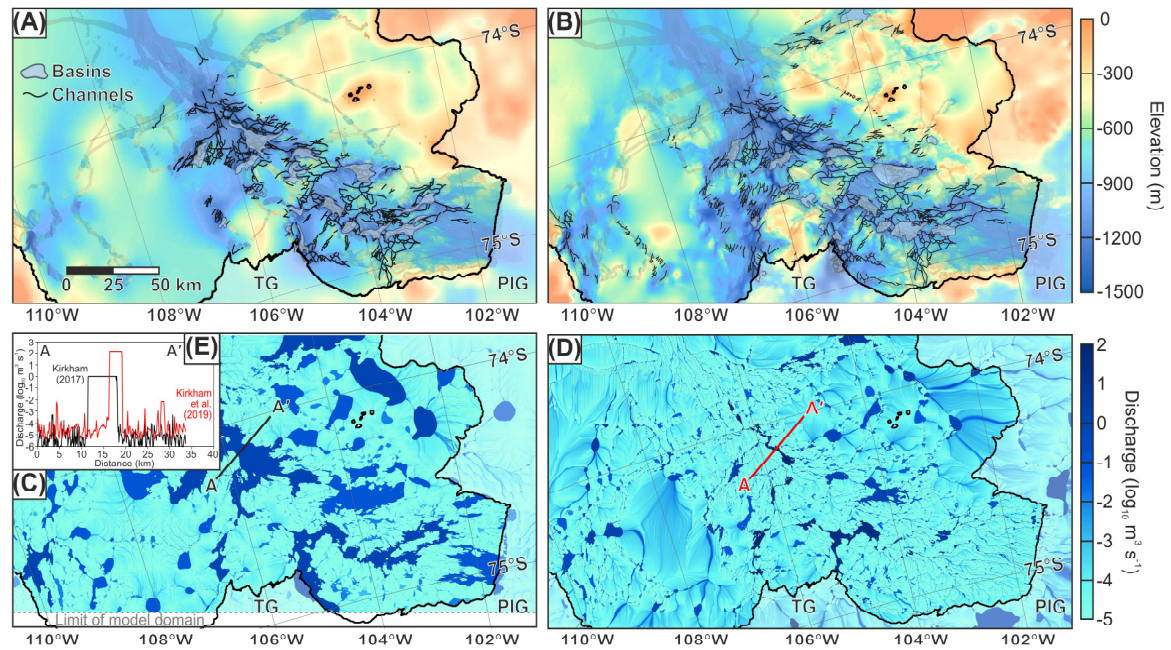


Figure 4.4. Comparison between the results of Kirkham (2017) and Kirkham et al. (2019). (A) Distribution of mapped bedrock channels and basins mapped by Kirkham (2017) and (B) the expansion of mappings in Kirkham et al. (2019). (C) Modelled subglacial water fluxes by Kirkham (2017) for comparison to the full glacier catchments modelled in (D) Kirkham et al. (2019). The limit of the model domain in (C) is displayed as a dotted grey line. (E) Comparison of calculated subglacial water fluxes in transect A–A' in (C) and (D). The present-day ice margin from LIMA (U.S. Geological Survey, 2007) is displayed in all panels as a semi-transparent polygon outlined in black. Regional topography is derived from Fretwell et al. (2013) in (A) and from Morlighem et al. (2019) in (B). The labels ‘PIG’ and ‘TG’ mark the contemporary margins of Pine Island Glacier and Thwaites Glacier, respectively.

4.3.2 Comparison with the Labyrinth

The channels offshore of present Pine Island and Thwaites glaciers are substantially larger than those comprising the Labyrinth, which consists of a series of 80 channels that are generally less than 1000 m in length, 20 to 600 m wide, and 2 to 150 m deep (Figure 4.5). The mean cross-sectional area of the Labyrinth channels is 3000 m². On average, the Labyrinth channels are about half as deep and a third as wide as the Pine Island Bay channels at 23 and 160 m, respectively. The two channel inventories are comparable in terms of their channel density, sinuosity, and characteristic undulating longitudinal channel profiles; however, the channelised region of Pine Island Bay covers an area more than 400 times larger than the size of the Labyrinth (Figures 4.3A–D).

Both the Labyrinth and the Pine Island Bay channels tend to have asymmetric V-shaped (b -value=1), rather than U-shaped (b -value=2), cross sections. The base of the cross sections are commonly more V-shaped than the upper sections of the channels. Channel cross section depth-to-width ratios are also comparable in both regions, with the Labyrinth channels typically 5–12 times as wide as they are deep, whilst the channels in Pine Island Bay are slightly wider in relation to their depth, at 7–25 times as wide as they are deep (Figure 4.5). For the Labyrinth channels, increasing cross-sectional area is more strongly correlated with channel depth than channel width, suggesting that channel enlargement predominantly results from disproportionate overdeepening of the larger channels with respect to their width. In contrast, increases in the Pine Island Bay channel area are due to both widening and deepening of channel cross sections.

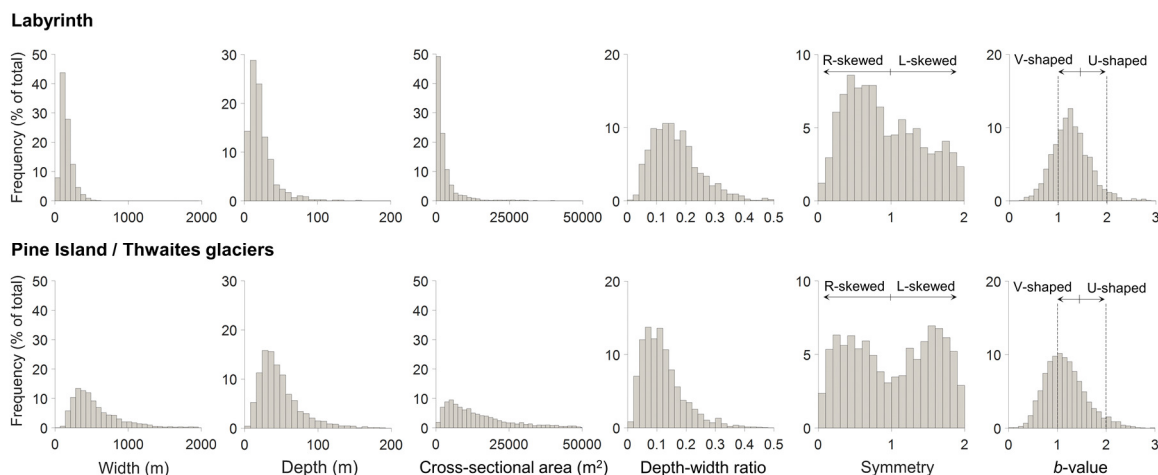


Figure 4.5. Size-frequency distributions of the morphometric characteristics of the channels comprising the Labyrinth and those present offshore from Pine Island and Thwaites glaciers. The channels offshore from Pine Island and Thwaites glaciers from which the distributions in the lower panel are derived are displayed in Figure 4.3. The dotted lines in the b -value plots correspond to where idealised V-shaped ($b = 1$) and U-shaped ($b = 2$) cross sections would fall on the histogram.

4.3.3 Modelled subglacial hydrology

The numerical model results reveal an intricate system of water transfer and storage beneath the LGM configuration of Pine Island and Thwaites glaciers (Figure 4.6). The majority of the LGM catchment is estimated to be at the pressure melting point. Predicted basal melt rates, which are dependent on ice-sheet thickness as well as geothermal and strain heating, are greatest along the thick central and tributary trunks of the expanded Pine Island–Thwaites glaciers, reaching values $>50 \text{ mm yr}^{-1}$. The basin-

wide average melt rate for the LGM catchment is $\sim 20 \text{ mm yr}^{-1}$, producing a total meltwater volume of $12.2 \text{ km}^3 \text{ yr}^{-1}$. The hydraulic potential gradient of the LGM WAIS forces water northwards, forming an arborescent drainage structure that converges into the main trunk of the formerly expanded Pine Island and Thwaites glaciers. Numerous ponded water bodies are predicted to occur within the LGM catchment, several of which fall within areas where subglacial water has been observed to transfer between subglacial lakes beneath the contemporary WAIS (Smith et al., 2017; Figure 4.6B).

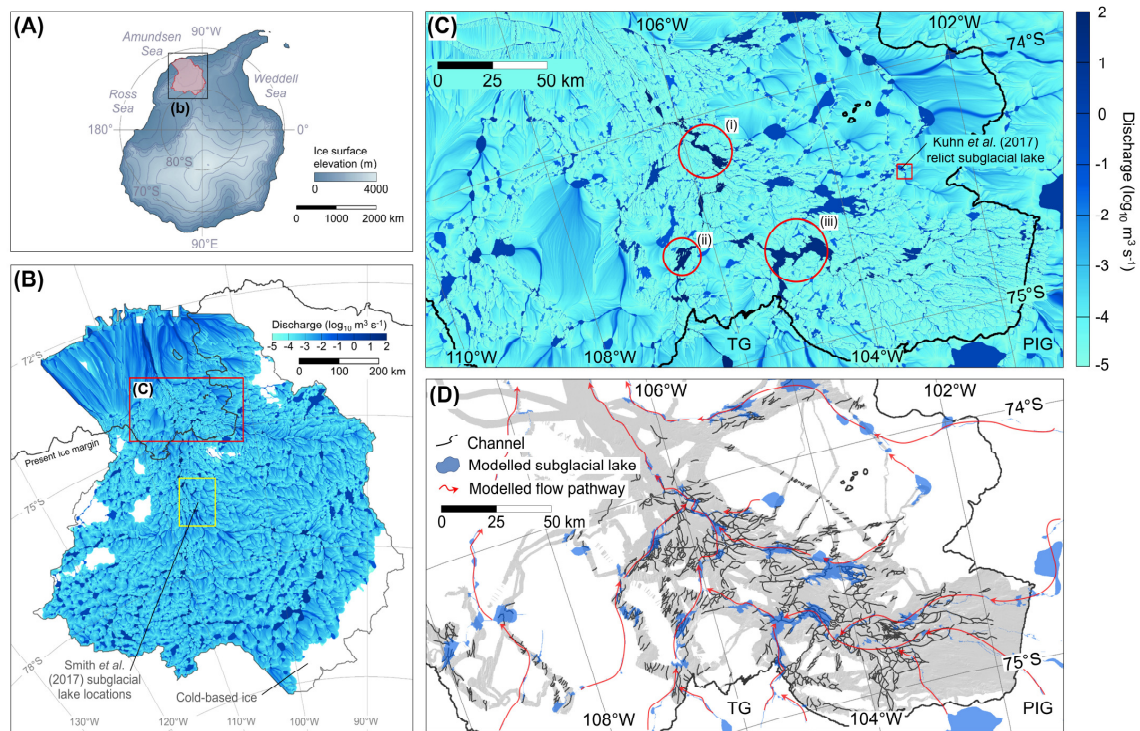


Figure 4.6. Modelled water flow beneath Pine Island and Thwaites glaciers at the LGM. (A) Modelled ice-sheet surface at 20 ka (Golledge et al., 2012), showing the calculated drainage catchment of Pine Island and Thwaites glaciers in red. (B) Water discharge and flow routing paths for the entire Pine Island/Thwaites catchment at the LGM, calculated at a 500 m grid resolution. The location of actively filling and draining subglacial lakes beneath the contemporary WAIS (Smith et al., 2017) is outlined in yellow. Areas of cold-based ice are displayed in white. (C) Modelled subglacial water discharges within the channelised inner shelf region covered by high-resolution (90 m) multibeam-bathymetric data. The locations of four predicted lakes, referred to as examples in the text, are shown. The present-day ice margin from LIMA (U.S. Geological Survey, 2007) is displayed in (B), (C) and (D) as a solid black line. (D) Geomorphologically mapped channel network within the high-resolution bathymetric data and modelled subglacial drainage network. The major flow routing pathways and subglacial lake locations calculated in (C) are displayed as red arrows and blue polygons in (D), respectively. Only subglacial lakes with a steady-state discharge $>3 \text{ m}^3 \text{ s}^{-1}$ are displayed for visual simplicity. The labels ‘PIG’ and ‘TG’ mark the contemporary margins of Pine Island Glacier and Thwaites Glacier, respectively.

Increasing the extent of the subglacial hydrological catchment from the area offshore of the contemporary ice-sheet margin previously modelled (Figure 4.4C; Kirkham, 2017) to the LGM configuration of Pine Island and Thwaites glaciers (Figure 4.6B) significantly elevates the predicted steady-state water fluxes (Figures 4.4D, 4.4E). This change results in subglacial discharge increasing by up to three orders of magnitude compared to the previous results (Kirkham, 2017). The updated basal topography also results in subtle variations in subglacial water routing patterns and ponding locations (Figures 4.4C, 4.4D).

The predicted subglacial water routing converges from across the interior regions of the catchment into the channelised region of Pine Island Bay covered by high-resolution multibeam bathymetry (Figure 4.6C). The majority of this water flow is routed preferentially from beneath the present-day glacier margins and into the inner-shelf trough through the bedrock channels (Figure 4.6D). Most channels have a modelled steady-state water discharge of less than $20 \text{ m}^3 \text{ s}^{-1}$. The highest calculated continuous meltwater flux occurs in a channel situated in the centre of the trough with a discharge of $139 \text{ m}^3 \text{ s}^{-1}$ (Figure 4.6C, location i). Channels that are wide and deep and have a large cross-sectional area are generally associated with higher steady-state discharges; these tend to occur in the centre of the trough occupied by the former Pine Island–Thwaites Ice Stream during the LGM (Figure 4.7A). Similarly, smaller channels located perpendicular to the former ice stream margins are associated with lower steady-state discharges. No relationship is present between channel symmetry or *b*-value and modelled steady-state water discharge. The largest channels occur in close proximity to the basins in which water is predicted to pond (Figure 4.7B). However, although larger channels are associated with higher discharges, this does not hold true in all cases as some of the smallest channels (cross-sectional area $< 5000 \text{ m}^2$) are calculated to carry some of the highest discharges ($\sim 130 \text{ m}^3 \text{ s}^{-1}$), whilst many of the largest channels contain discharges $< 0.1 \text{ m}^3 \text{ s}^{-1}$ (Figure 4.7C). This discrepancy is emphasised at location (i). Here, four tributary channels flow into a basin which then outflows into one large channel that has the highest calculated water flux in the catchment (Figure 4.8A). The four tributary channels have approximately the same cross-sectional area as the main outflow channel but have steady-state discharges over 3 orders of magnitude less than those of the main channel, demonstrating that not all large channels are associated with high steady-state discharges.

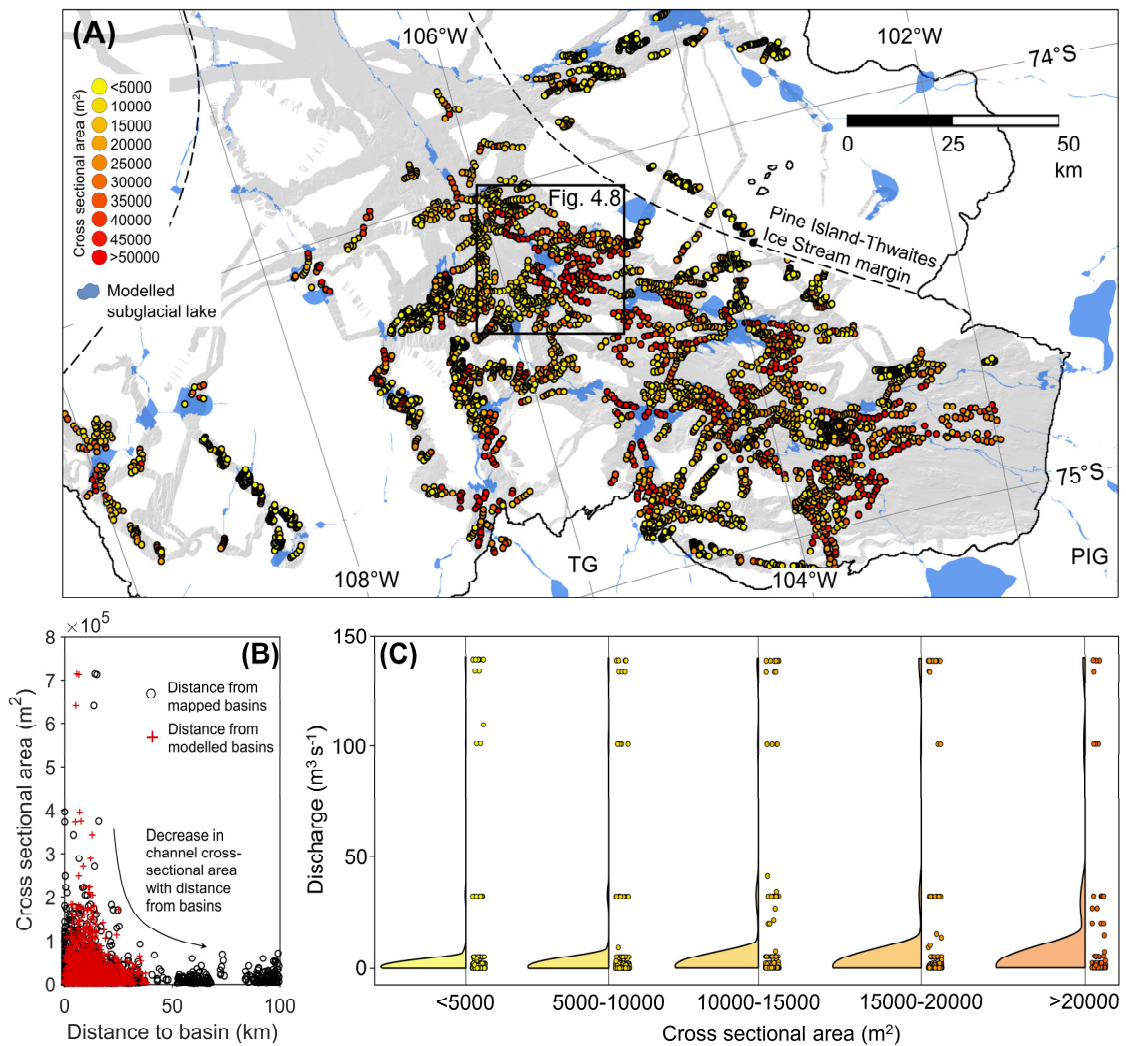


Figure 4.7. Spatial variation of channel size within Pine Island Bay. (A) Spatial variation of channel cross-sectional area in relation to the location of modelled subglacial lakes. Channel cross sections used to analyse channel geometry are displayed as dots coloured by channel cross-sectional area. The margins of the former Pine Island-Thwaites Ice Stream (Graham et al., 2010) and the location of Figure 4.8 are shown. The present-day ice margin from LIMA (U.S. Geological Survey, 2007) is displayed as a solid black line. (B) Variation in channel cross-sectional area with distance to the nearest mapped and modelled subglacial lake basin. (C) Raincloud plot showing the data and distributional shape of modelled steady-state discharges through channels of different cross-sectional areas. Rainclouds were produced using code from Allen et al. (2019).

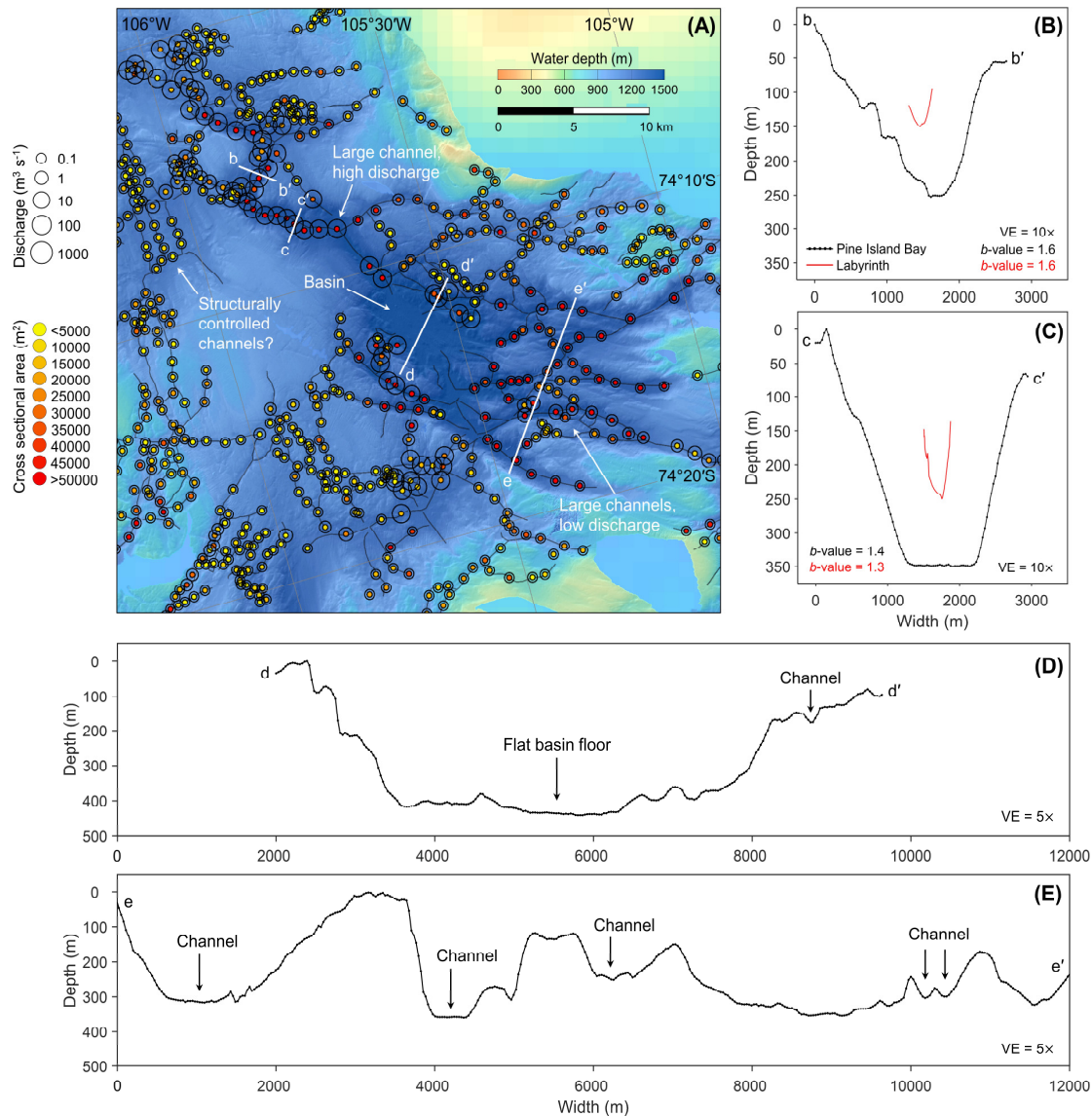


Figure 4.8. Relationship between modelled water flux and channel size through a channel-basin system. (A) Example channel-basin system in Pine Island Bay. Mapped channels are displayed as black lines. Cross sections used to calculate channel geometries are displayed as dots coloured by channel cross-sectional area. The size of the circle surrounding the dots represents the calculated steady-state water flux through the channels. The locations of the cross profiles displayed in B-E are shown. Note the contrast between the large, high discharge channel to the northwest of the basin and the equally large, but low discharge, channels flowing into the basin from the southeast. (B-C) Cross-sectional profiles of a large channel in Pine Island Bay compared to some of the largest channels in the Labyrinth. (D) Cross section of a basin in Pine Island Bay. (E) Cross section of a series of channels feeding the basin from the southeast. Vertical exaggeration (VE) is 10× in (B-C) and 5× in (D-E).

Multiple lakes are predicted to occur in the bedrock depressions in Pine Island Bay under LGM conditions. Once the lakes are filled to their spill point, water is transferred through the bedrock channels into further lakes downstream. The modelled fluxes, volumes, and recharge rates of the lakes are examined using four examples displayed in Figure 4.6C. Lake (i) occurs at the confluence of the main streams that drain the Pine Island and Thwaites glacier catchments; lake (ii) is the furthest downstream lake in the Thwaites catchment, and lake (iii) is the furthest downstream lake in the Pine Island catchment. The fourth example lake occurs within the relict subglacial lake basin described by Kuhn et al. (2017). The four example lakes have volumes between 0.33 and 19.9 km³ when filled to their spill points. The majority of the water routed into Pine Island Bay is directed from beneath Thwaites Glacier, flowing into lake (ii) at a steady-state rate of 101 m³ s⁻¹. When combined with the steady-state flux of water contributed by the Pine Island Glacier catchment (32.2 m³ s⁻¹), the two catchments yield a steady-state discharge of 139 m³ s⁻¹ through lake (i). Under these continuous flow rates, the three lakes would fill to their spill points on annual to decadal timescales (Table 4.2). The basin described by Kuhn et al. (2017) is smaller than the lakes draining the main glacier catchments and is modelled to accumulate water at a steady-state rate of 0.23 m³ s⁻¹, filling to its spill point every 45 years. If these example lakes were to drain over a ~16-month period, typical of subglacial water transfer beneath the contemporary Antarctic Ice Sheet (Wingham et al., 2006), water would be released from the lakes at an average rate of ~10–80 m³ s⁻¹ for the three smaller lakes (i, ii, iv) and ~470 m³ s⁻¹ for lake (iii) at the edge of the individual Pine Island glacier catchment (Table 4.2).

We quantify the largest possible discharge that could occur through the channels by considering a scenario in which a large modelled lake, situated upstream in the Pine Island–Thwaites catchment, drains within 16 months and triggers a cascade of catastrophic lake drainages downstream. This scenario represents the most extreme discharge that could have been generated beneath the LGM configuration of Pine Island and Thwaites glaciers. Under this scenario, the mean flood discharge through the inner-shelf channels would be ~5.5–6.6 × 10⁴ m³ s⁻¹. However, these are mean discharges. In a modelling study of water transfer between subglacial lakes in the Adventure subglacial trench, using data from Wingham et al. (2006), Peters et al. (2009) found that subglacial discharge between the lakes was highly sensitive to the model parameters used, especially the assumed channel roughness, and short-lived peak fluxes of around 10 times the mean discharge were quite conceivable. Given this uncertainty, it may have been possible to produce short-lived outbursts up to ~5 × 10⁵ m³ s⁻¹ through the Pine Island Bay channels. This estimate is of the order of 10% to 50% of the maximum carrying capacity of the

channels (Equation 4.3). Under the hydraulic potential gradient of the LGM configuration of the WAIS, channels filled with water to the bankfull stage would be capable of accommodating flows with an average discharge of $\sim 8.8 \times 10^6 \text{ m}^3 \text{ s}^{-1}$. This carrying capacity would be reduced to $3.5 \times 10^6 \text{ m}^3 \text{ s}^{-1}$ if the channels were 50 % ice filled and to $2.8 \times 10^5 \text{ m}^3 \text{ s}^{-1}$ if they were 90 % ice filled.

Table 4.2. Volume, filling time, local steady-state discharge, and potential mean flood discharge of lakes displayed in Figure 4.6.

Lake	Local steady-state water discharge ($\text{m}^3 \text{ s}^{-1}$)	Lake volume (km^3)	Time to fill (years)	Local potential mean discharge ($\text{m}^3 \text{ s}^{-1}$)*	Total upstream volume (km^3)	Potential mean flood discharge** ($\text{m}^3 \text{ s}^{-1}$)
(i)	139	3.29	0.73	78.2	2762	65690
(ii)	101	3.47	1.09	82.5	2329	55390
(iii)	32.2	19.9	19.6	473	389	9251
(iv)***	0.23	0.33	45.1	7.8	0.58	13.8

*Local mean discharge calculated by assuming drainage of the lake in 16 months, assuming no further inflow into the basin during drainage (c.f. Wingham *et al.* 2006).

**Potential mean flood discharge calculated by assuming drainage of a large upstream lake in 16 months (c.f. Wingham *et al.* 2006) which triggers the cascading drainage of all lakes downstream from that initial event.

***Basin suggested to be a relict subglacial lake by Kuhn *et al.* (2017).

4.4 Discussion

4.4.1 Channel formation

The morphology, discharge carrying capacity, and form distributions of the Pine Island Bay and Labyrinth channels are strikingly similar despite the former being significantly larger. Channel form ratios and b -values demonstrate that both sets of channels tend to have broad and shallow V-shaped cross-sectional profiles (Figure 4.5), indicative of subglacial meltwater erosion, rather than the U-shaped morphology associated with direct glacial erosion (Pattyn and Van Huele, 1998; Rose *et al.*, 2014). Some of the channels also have trapezoidal cross-sectional forms (b -values ~ 1.3 – 1.6 ; Figure 4.8C). This cross-sectional shape has been associated with high-magnitude discharges of water (Bretz, 1923, 1969; Gupta *et al.*, 2007; Larsen and Lamb, 2016), although the shape of the channels in Pine Island Bay, and accordingly their b -values, may be unrepresentative where significant sediment infill of the base of the channel is present (e.g., Smith *et al.*, 2009b). The undulating long-axis profiles and reverse gradients associated with both sets of channel inventories combined with their size, shape, and incision into bedrock suggests that they were formed by high-velocity subglacial meltwater flowing under hydrostatic

pressure (Shreve, 1972; Sugden et al., 1991; Lowe and Anderson, 2003; Lewis et al., 2006; Smith et al., 2009b; van der Vegt et al., 2012; Nitsche et al., 2013). Morphometric evidence thus indicates a similar formative process for both sets of channels; that is, incision by pressurised subglacial water, albeit executed over a vastly larger scale beneath Pine Island and Thwaites glaciers than at the Labyrinth (Figures 4.3, 4.8B, 4.8C).

The dimensions and the extensive area over which the submarine channels are observed indicate that the hydrological system beneath the formerly expanded Pine Island and Thwaites glaciers at times transported substantial volumes of pressurised water along consistent routing pathways. The inner-shelf substrate in Pine Island Bay consists mainly of hard granitoid bedrock and porphyritic dykes (e.g., Pankhurst et al., 1993; Kipf et al., 2012; Gohl et al., 2013; Lindow et al., 2016) that would be resistant to erosion by subglacial meltwater. The transportation of coarse bedload permits water to rapidly incise bedrock (Cook et al., 2013). In order to mobilise such suitable sediment loads, large fluxes of water would have been required to excavate channels of the size observed in Pine Island Bay (Alley et al., 1997). Although it is likely that infilling with ice prevented all of the channels from being active contemporaneously (Nitsche et al., 2013), even if half of the channel cross sections were filled with grounded ice, at $3.5 \times 10^6 \text{ m}^3 \text{ s}^{-1}$, their carrying capacity would still have been larger than the maximum bankfull discharge estimated for the Labyrinth ($1.6\text{--}2.2 \times 10^6 \text{ m}^3 \text{ s}^{-1}$) (Lewis et al., 2006). Constraining the age of the submarine channels, and determining whether any resculpting by ice occurs within a glacial cycle or over shorter timescales, is difficult. However, the presence of deformation till in some of the channels indicates that they have been overridden by wet-based ice since their incision so may be the outcome of several advances and retreats of grounded ice through Pine Island Bay (Smith et al., 2009b; Nitsche et al., 2013).

Unlike the channels in Pine Island Bay, the age and formation of the Labyrinth is better constrained, and has been attributed to one or more subglacial floods sourced from a subglacial lake trapped as the Antarctic Ice Sheet overrode the Transantarctic Mountains during the Miocene (Lewis et al., 2006). The last period of Labyrinth channel incision occurred between 14.4 and 12.4 Ma (Marchant et al., 1993; Marchant and Denton, 1996; Denton and Sugden, 2005; Lewis et al., 2006). Around this time, the region experienced strong climatic cooling of at least $8 \text{ }^\circ\text{C}$ (Lewis et al., 2007; Lewis et al., 2008). This period of cooling changed the basal thermal regime of the ice in the vicinity of the Labyrinth to minimally erosive cold-based ice, potentially protecting the channels from any substantial further erosion (Atkins and Dickinson, 2007). The absence of post-incisional reworking of the top of the channels by wet-based ice may explain the tendency for the

Labyrinth channels to be less wide in relation to their depth than the channels in Pine Island Bay (Figure 4.5), and for increased Labyrinth channel cross-sectional area to be more strongly correlated with channel depth than channel width. In contrast, increasing cross-sectional area of the channels in Pine Island Bay is correlated with both channel width and depth, suggesting that glacial erosion of the sides of the channels has been a significant additional process influencing the morphology of the channels. This supports the notion that the channels have been formed and reoccupied over multiple glacial cycles, allowing subglacial erosion to enlarge the top of the channels and produce composite features (Figure 4.9). Interestingly, this implies that the Labyrinth channels may represent “purer” meltwater signatures than the larger features observed in Pine Island Bay.

4.4.2 Channel water sources

The polar desert climate characterising the contemporary Antarctic Ice Sheet largely confines the influence of surface melting to the Antarctic Peninsula and the ice shelves fringing the continent (e.g., Tedesco, 2009; Tedesco and Monaghan, 2009; Barrand et al., 2013; Trusel et al., 2013; Bell et al., 2017; Bell et al., 2018). Where present, surface meltwater can be transported efficiently across the ice surface through the action of surficial meltwater rivers (Bell et al., 2017; Kingslake et al., 2017) or even enter the englacial system and be stored as shallow subsurface lakes in some ice shelves (Lenaerts et al., 2016). However, the absence of surface melting for the majority of the grounded ice sheet results in the water present within the Antarctic subglacial hydrological system being sourced from processes that operate almost exclusively at the ice-sheet bed (Rose et al., 2014). The undulating long profiles of the channels (Figure 4.3F) indicate that they were formed beneath grounded ice and not from water that propagated through an ice shelf (Nitsche et al., 2013). Thus, the hydrological conditions characterising the grounded interior of the contemporary ice sheet offers the best analogue for former subglacial water generation. With average summer temperatures around -10°C at the present-day coast around Pine Island Bay (King and Turner, 2007), the contribution of surface meltwater to the subglacial hydrological system can be considered negligible if the past climate were similar to present, or more likely colder, under late Pleistocene full-glacial conditions (Trusel et al., 2013). Therefore, even assuming a climate similar to present, the subglacial meltwater responsible for bedrock-channel formation could only have been generated by geothermal and strain heating at the ice-sheet bed.

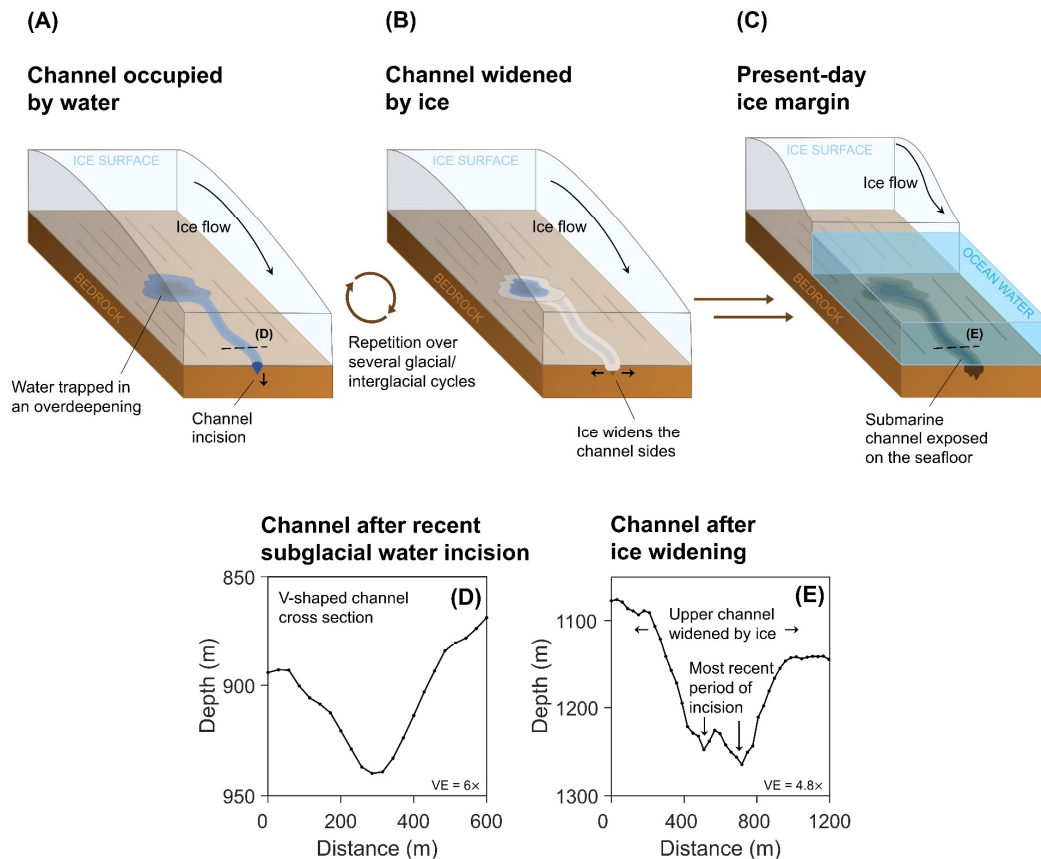


Figure 4.9. Schematic of channel formation over multiple glacial-interglacial cycles. (A) Channels are incised by short-lived episodes of fast-flowing subglacial meltwater, potentially released from lakes trapped in overdeepenings during ice sheet advance and retreat. (B) Repeated periods of ice overriding widens the top of the channels. (C) A composite channel feature, produced over multiple glaciations, is left exposed on the seafloor. (D) Example of a more recently incised channel, characterised by a V-shaped cross section. (E) Cross section of a channel persisting from previous glacial periods containing both V-shaped meltwater signatures and a wide upper channel section eroded by ice. Vertical exaggeration (VE) is $6\times$ in (D) and $4.8\times$ in (E).

The geothermal heat flux beneath West Antarctica is larger than for the remainder of the continent due to its location on the West Antarctic Rift System — an extensional volcanic rift system that stretches across Marie Byrd Land from Pine Island Glacier and into the Ross Sea (Blankenship et al., 1993; LeMasurier, 2013; Loose et al., 2018). Despite this elevated geothermal heat flux, the quantity of subglacial meltwater produced by geothermal heating is estimated to be only $4\text{--}10\text{ mm yr}^{-1}$ (Dowdeswell et al., 2016a) — 2 orders of magnitude less than the maximum rates of surface melt observed on the Antarctic Peninsula today ($>400\text{ mm yr}^{-1}$ w.e.) (Trusel et al., 2013). Although basal melt rates may be elevated by strain heating at the lateral shear-margins of ice streams (Bell, 2008; Graham et al., 2009), the combination of these processes would only yield subglacial melt rates of up to $90\text{--}180\text{ mm yr}^{-1}$ (Dowdeswell et al., 2016a).

The basin-wide average basal meltwater production rate beneath Pine Island and Thwaites glaciers is $\sim 28 \text{ mm yr}^{-1}$ at present, generating 5.2 km^3 of meltwater per year (Joughin et al., 2009). The model used in this chapter calculates that under the LGM configuration of these glaciers, meltwater would have been produced at $\sim 20 \text{ mm yr}^{-1}$ on average, although elevated melt rates $> 50 \text{ mm yr}^{-1}$ would have occurred beneath the thick central trunk of the ice stream. Combined, these melt rates would have generated a total volume of $12.2 \text{ km}^3 \text{ yr}^{-1}$ across the entire LGM catchment. These rates are too low to transport sediment efficiently and would therefore preclude significant erosion of bedrock (Alley et al., 1997). This interpretation is supported by the relationship between channel cross-sectional area and modelled steady-state discharge as, if the channels were incised by the continuous flow of meltwater beneath the former Pine Island–Thwaites Ice Stream, all large channels would be expected to be associated with a high discharge whereas this is not the case for all channels (e.g., Figures 4.8A). Furthermore, there is a discrepancy between the potential carrying capacity of the channels and the predicted discharges through the channels if the subglacial water-transfer system is assumed to be in steady state. This discrepancy occurs because the channels, even if 90 % full of ice, would be capable of accommodating discharges over 3 orders of magnitude larger ($2.8 \times 10^5 \text{ m}^3 \text{ s}^{-1}$) than the largest steady-state water fluxes predicted to occur by the numerical model ($139 \text{ m}^3 \text{ s}^{-1}$). The continuous production of basal meltwater beneath former Pine Island and Thwaites glaciers is therefore insufficient to incise channels of the size present in Pine Island Bay (Lowe and Anderson, 2003; Nitsche et al., 2013). Consequently, another mechanism, capable of mobilising coarse bedload, is required to explain their formation.

Episodic, but high-magnitude, subglacial volcanic activity occurring over multi-millennial timescales may have supplied large volumes of meltwater to the subglacial hydrological system of Pine Island and Thwaites glaciers in the past (Wilch et al., 1999; Nitsche et al., 2013). West Antarctica contains 138 volcanoes, including three extensively eroded Miocene volcanoes and other younger parasitic cones in the Hudson Mountains, 150 km east of Pine Island Bay (Nitsche et al., 2013; Loose et al., 2018; van Wyk de Vries et al., 2018). The most recent volcanic eruption in this region occurred ~ 2200 years ago (Corr and Vaughan, 2008). Analogies from subglacial volcanic eruptions in Iceland demonstrate that these events commonly cause meltwater to accumulate in unstable subglacial lakes incised upwards into the ice (Björnsson, 1992, 2002). When hydrostatic pressure exceeds the strength of the ice damming the lake, jökulhlaup outburst floods may occur with observed discharges of up to $5 \times 10^4 \text{ m}^3 \text{ s}^{-1}$ (Björnsson, 2002). Jökulhlaups transport huge amounts of sediment, on

the order of 10,000,000 tonnes per event (Nye, 1976; Roberts, 2005), allowing them to impose a significant geomorphic imprint upon the landscape, including the incision of large subglacial channels (Björnsson, 2002; Russell, 2007). However, although it is possible that volcanically induced subglacial floods supplied large volumes of water to the beds of Pine Island and Thwaites glaciers in the past, this mechanism does not explain the occurrence of channelised landforms observed in different, less volcanically active, regions of Antarctica such as the East Antarctic Soya Coast (Sawagaki and Hirakawa, 1997) and the western Antarctic Peninsula (e.g., Ó Cofaigh et al., 2002; Ó Cofaigh et al., 2005; Domack et al., 2006; Anderson and Fretwell, 2008). Hence, although episodic volcanism may have contributed water to the formation of the channel system present in Pine Island Bay, it is unlikely to represent the sole or dominant mechanism through which the channels formed.

Meltwater features, similar to the channels in Pine Island Bay, have been mapped and modelled beneath other former ice sheets such as the Fennoscandian and Barents Sea ice sheets (Greenwood et al., 2016; Bjarnadóttir et al., 2017; Greenwood et al., 2017; Shackleton et al., 2018) and the Laurentide Ice Sheet (Mullins and Hinchey, 1989; Kor et al., 1991; Brennand and Shaw, 1994; Livingstone and Clark, 2016; Livingstone et al., 2016; Lewington et al., 2020). The deglacial configuration of these former ice sheets was likely conducive to producing large volumes of surface meltwater that may have propagated to the bed (Carlson et al., 2008; Jansen et al., 2014), similar to that observed on the margins of the contemporary Greenland Ice Sheet (Zwally et al., 2002; Das et al., 2008; Bartholomew et al., 2011a). Subglacial streams fed by surface melt have high discharges and exceptional sediment transport capacities due to the short time period in which supraglacial drainage occurs (Alley et al., 1997). When this water is delivered to areas of the bed where unconsolidated sediments have been stripped away, these high water fluxes will have large unsatisfied transport capacities and will be able to rapidly erode bedrock if paired with a suitable bedload (Alley et al., 1997; Cook et al., 2013). Exceptionally high erosion rates have been associated with supraglacial water input to the Greenland subglacial hydrological system ($4.8 \pm 2.6 \text{ mm yr}^{-1}$; 1–2 orders of magnitude larger than long-term estimates of denudation rates beneath the Greenland Ice Sheet) (Cowton et al., 2012; Andrews et al., 2014), and the input of supraglacial meltwater into the subglacial hydrological system of the deglaciating Fennoscandian Ice Sheet has been proposed to have cut large gorges into bedrock in northern Sweden (Jansen et al., 2014).

Although the injection of surface meltwater to the bed of the Antarctic Ice Sheet through hydrofracture is potentially forecast under future climate warming scenarios (Bell et

al., 2018), the extent to which surface melting of the Antarctic Ice Sheet may have occurred in the past is poorly constrained. However, evidence from environmental proxies (Escutia et al., 2009; Cook et al., 2013), sea-level reconstructions (Miller et al., 2012), and numerical modelling simulations (DeConto and Pollard, 2003) indicates that significant circum-Antarctic warming occurred during the Miocene and the Pliocene (5.3–2.6 Ma) epochs. This climate warming may have raised surface temperatures sufficiently to facilitate surface melt across significant portions of the Antarctic interior (Rose et al., 2014). However, numerical model simulations suggest that despite peak Miocene air temperatures being sufficiently warm to facilitate surface melting, it is unlikely that the WAIS was developed enough at this time to allow large-scale grounded ice to extend onto the inner continental shelf of the Amundsen Sea, precluding the possibility of subglacial channel formation in Pine Island Bay (DeConto and Pollard, 2003).

The establishment of a more expansive, yet dynamic (Cook et al., 2013), WAIS during the Pliocene (Pollard and DeConto, 2009; DeConto and Pollard, 2016), combined with temperatures 2 to 3°C warmer than present (Dowsett, 2007), makes this epoch a potential candidate for when substantial quantities of surficial meltwater could propagate to the bed of the WAIS and form the meltwater channels. Ice-sheet modelling by Raymo et al. (2006) predicts that the extent of Pliocene summer melting on the East Antarctic Ice Sheet margin would have been comparable to the considerable quantities of supraglacial meltwater produced during the summer ablation season of the contemporary Greenland Ice Sheet (e.g., Abdalati and Steffen, 2001; Zwally et al., 2002; Hanna et al., 2008). If a comparable level of surface melt also occurred on the surface of the WAIS at this time, substantial quantities of supraglacial meltwater could have propagated to the expanded ice sheet's bed, facilitating channel incision (Rose et al., 2014). Although bedrock channels exist on the Greenland continental shelf (Ó Cofaigh et al., 2004; Dowdeswell et al., 2010) and beneath the contemporary Greenland Ice Sheet (Bamber et al., 2013; Livingstone et al., 2017), they are not nearly as common as those offshore of the WAIS and the formation of many has been attributed to turbidity currents or fluvial activity predating the inception of the Greenland Ice Sheet (e.g., Cooper et al., 2016; Batchelor et al., 2018). Accordingly, if supraglacial water injection is responsible for the incision of the Antarctic channels, it raises the question of why these features are not more common on the margin of the Greenland Ice Sheet where this process is known to occur, or why channels have not been observed forming beneath the ice sheet today.

An alternative source of water with which the channels could have formed is subglacial lakes produced by the accumulation of subglacial meltwater in hydraulic potential lows.

The seafloor of Pine Island Bay and the bed of the LGM catchment contain multiple bedrock basins where low hydraulic potential provides favourable locations for water to pond beneath the WAIS at the LGM (Figures 4.6, 4.8D). The dimensions of the basins beyond the current Pine Island–Thwaites glacier margins are of the same order of magnitude as many contemporary subglacial lakes occupying bedrock basins. For example, Lake Ellsworth has an area of 29 km² (Siegert et al., 2004) whereas the basins beyond Pine Island Glacier and Thwaites Glacier have planimetric areas between 5 and 160 km². The modelled water bodies have volumes, filling–draining times, and steady-state inflow and outflow fluxes that are comparable to contemporary subglacial lake drainage events observed using satellite altimetry (Wingham et al., 2006; Fricker et al., 2007; Flament et al., 2014; Smith et al., 2017). The bedrock basins in Pine Island Bay are infilled with several to tens of metres of sediment (Nitsche et al., 2013). Sediments recovered from one of these basins suggest deposition in a low-energy freshwater subglacial lake environment during the last glacial period (Kuhn et al., 2017), an interpretation that is consistent with the low-magnitude water flux modelled for the basin sampled (0.23 m³s⁻¹). The fact that the largest channels are located at the edge of the subglacial lakes (Figure 4.7B) strongly supports the notion that channel genesis is connected to the basins, possibly through episodic outbursts of water from former subglacial lakes. Consequently, similar to other areas offshore of the Antarctic Peninsula (Domack et al., 2006; Larter et al., 2019), it is possible that the bedrock basins in Pine Island Bay may represent the locations of relict subglacial lakes in past glacial periods that episodically drained to form the subglacial channels (Domack et al., 2006; Livingstone et al., 2013b; Kuhn et al., 2017).

Although multiple subglacial lake drainage events have been observed beneath the contemporary Antarctic Ice Sheet (e.g., Gray et al., 2005; Wingham et al., 2006; Fricker et al., 2007; Smith et al., 2009a; Smith et al., 2017), the peak discharge and volume of water displaced during contemporary lake drainage is 4 to 5 orders of magnitude smaller than the amount that the channels in Pine Island Bay could potentially accommodate, even when mostly filled with ice. Furthermore, models of active subglacial lake drainage most closely replicate observed subglacial lake behaviour when water mechanically erodes shallow canals into the underlying deformable sediment rather than producing an R-channel (Röthlisberger, 1972; Carter et al., 2009; Fowler, 2009; Carter et al., 2017). These results are consistent with measured pore water pressures beneath Whillans Ice Stream (Blankenship et al., 1987; Engelhardt et al., 1990; Walder and Fowler, 1994; Alley et al., 1997) and radar specular analysis of present-day Thwaites Glacier, although, in the case of the latter, it is possible that a focused channelised system exists further

downstream (Schroeder et al., 2013). These observations may imply that many active subglacial lakes require soft bedded sediments to form and drain (Carter et al., 2017), explaining the tendency for these features to lack the characteristic basal reflection properties used to identify subglacial lakes with radio-echo sounding (Siegert et al., 2016a; Carter et al., 2017; Humbert et al., 2018). However, it may be possible to produce, and temporarily sustain, R channels with cross-sectional areas of $\sim 20 \text{ m}^2$ when water is transferred between a system of bedrock overdeepenings by pressure waves that propagate along the length of an ice stream over several years (Fricker et al., 2014; Dow et al., 2018), or along ice-stream shear margins where basal meltwater production rates are high (Perol et al., 2015; Elsworth and Suckale, 2016; Meyer et al., 2016; Bougamont et al., 2019).

The extent to which the active subglacial lake drainage events observed in the satellite era are representative of the behaviour of the Antarctic subglacial hydrological system over a full-glacial–interglacial cycle, especially during ice-sheet advance and retreat, is unknown. Differences in discharge magnitude and their association with soft sediments limit the use of present-day subglacial lake drainage as an analogy for the mechanism which incised channels into hard crystalline bedrock in Pine Island Bay. However, past outburst flooding from subglacial lakes has been suggested to have had a substantial impact on the landscape elsewhere in Antarctica (e.g., Domack et al., 2006; Lewis et al., 2006; Jordan et al., 2010; Larter et al., 2019). Jordan et al. (2010) proposed that outbursts sourced from a palaeo-subglacial lake with a volume of 850 km^3 were responsible for the formation of a series of kilometre-wide bedrock canyons in the Wilkes Subglacial Basin. This lake is proposed to have accumulated and catastrophically drained during the expansion of the East Antarctic Ice Sheet in the Miocene epoch, at a similar time to when the Labyrinth and the other channel systems in Victoria Land are suggested to have formed (Denton et al., 1984; Denton et al., 1993; Sugden et al., 1999; Sugden and Denton, 2004; Denton and Sugden, 2005). Morphological evidence for past outburst flood occurrence also exists elsewhere in Scandinavia (Mannerfelt, 1945; Holtedahl, 1967), in North America (Bretz, 1923; Ives, 1958; Wright, 1973), and in Scotland (Sissons, 1958). The largest of these floods was the release of $\sim 2500 \text{ km}^3$ of water during the Missoula floods in eastern Washington state, USA, which have been estimated to have attained peak discharges of $\sim 1.7 \times 10^7 \text{ m}^3 \text{ s}^{-1}$ (Waite, 1985; O'Connor and Baker, 1992). Although the Missoula floods were released from a proglacial, rather than subglacial, source, their estimated volume is similar to the amount of water that could have drained from beneath former Pine Island and Thwaites glaciers if a cascade of upstream lake drainage were to occur (Table 4.2).

Two models of how Antarctic lakes could form and then drain catastrophically have been hypothesised. Alley et al. (2006) proposed a model in which seawater becomes trapped in bedrock basins by the advance and thickening of an ice shelf over the sill of bedrock overdeepenings. Water pressure in the basins would build until the hydraulic potential exceeds that of the next basin downstream, culminating in short-lived, high-magnitude water drainage events, or floods. An alternative hypothesis was put forward by Jordan et al. (2010) in which subglacial water ponds in hydraulic-potential lows produced by the reduced ice-surface slope associated with an advancing ice sheet, with flooding occurring during ice-sheet retreat. Both of these lake drainage models occur during either large-scale ice sheet advance or retreat, so are outside of the subglacial hydrodynamics captured by modern observations. Numerical calculations show that these types of event are capable of producing peak discharges of $\sim 10^5 \text{ m}^3 \text{ s}^{-1}$ (Evatt et al., 2006). The numerical model results presented in this chapter demonstrate that the cascading release of water trapped in a large upstream basin could initiate a flood with a peak discharge of $\sim 5 \times 10^5 \text{ m}^3 \text{ s}^{-1}$. This discharge is approximately equal to the potential carrying capacity of the channels if they were partially ice filled at the time of the flood.

Although high-magnitude fluxes of water could have been released beneath Pine Island and Thwaites glaciers through cascades of subglacial lake drainage, recent modelling by Beaud et al. (2018b) suggests that significant erosion can be achieved by relatively low influxes ($\sim 20 \text{ m}^3 \text{ s}^{-1}$) of seasonal meltwater into the subglacial system when repeated regularly throughout a glacial cycle. For an idealised ice-sheet geometry, these simulations demonstrate that small but regular influxes of meltwater are able to excavate channels up to $\sim 20 \text{ m}$ deep and 100 m wide into a bedrock substrate over the course of 7500 years (Beaud et al., 2018b). Although the model omits plucking, which may play a significant role in the erosion of fractured bedrock by large floods (e.g., Lamb and Fonstad, 2010; Larsen and Lamb, 2016), the substrate eroded in the model is similar to the hard bedrock present in Pine Island Bay and can therefore be used to assess the formation timescale of the submarine channels. With an average depth of 43 m and a mean width of 507 m , the channels present in Pine Island Bay are substantially larger than the channels that Beaud et al. (2018b) are able to erode in a single glacial cycle. This supports the interpretation that the huge channels observed beyond the present margins of Pine Island and Thwaites glaciers must have formed over more than one glacial period. The fluxes of meltwater produced by subglacial lake drainage beneath Pine Island and Thwaites glaciers in the past span discharges similar to those used in the Beaud et al. (2018b) simulations to several of orders of magnitude more depending on whether the drainage was cascading or only sourced from a single lake. Accordingly,

it is possible to envisage a scenario in which recurrent releases of subglacial meltwater trapped in bedrock basins, ranging from frequent gradual drainages to larger outburst floods, could have cut large channels into bedrock over the course of several glacial cycles. The former lake basins may have acted as sedimentary depocentres which supplied bedload during subglacial lake discharge to enhance the erosive potential of the floods. Thus, when paired with a suitable sediment load for channel erosion, outbursts from a population of subglacial lakes occupying large bedrock basins, occurring as either repeated small outbursts or larger, less frequent, drainage cascades triggered by ice sheet advance or retreat, may have been sufficiently erosive to excavate huge channels in the bedrock of Pine Island Bay.

4.5 Conclusions

The huge palaeo-channel-and-basin systems beyond modern Pine Island and Thwaites glaciers are evidence for an organised and dynamic subglacial hydrological system beneath former major outlets of the WAIS. Channels of greater dimensions than those in the Labyrinth can only have been incised by large discharges of water flowing under subglacial hydraulic pressure. The numerical model used in this chapter produces similar steady-state discharges and filling and drainage timescales to those that are observed for subglacial lakes beneath the contemporary Antarctic Ice Sheet. However, the fluxes of water flowing in continuous steady state beneath the LGM ice sheet are too low to have formed channels of the scale observed in Pine Island Bay. Rather, a higher-magnitude, lower-frequency mechanism is required to explain the formation of the channels. Many mechanisms could have been responsible for channel formation, including propagation of surface melt to the bed and subglacial volcanic eruptions. However, based on their geomorphological similarity to features known to have been formed by outburst flooding and their ability to accommodate discharges of at least $2.8 \times 10^5 \text{ m}^3 \text{ s}^{-1}$, even when mostly filled with ice, the most likely candidate for the formation of the Pine Island Bay channel system was episodic releases of meltwater trapped in upstream subglacial lakes, potentially triggered by ice-sheet advance or retreat. This mechanism may be outside the range of processes captured by modern observations of subglacial hydrology, but is likely to have had an impact on the flow regime of these large ice streams that continue to dominate ice-sheet discharge today. Further observations of the duration and frequency of contemporary subglacial drainage events and the incorporation of more detailed bed topographies into numerical models will help elucidate the role that organised, episodic outburst flooding plays in the dynamics of the Antarctic Ice Sheet.

Chapter 5

Tunnel valley infill and genesis revealed by high-resolution 3D seismic data

Abstract

Landforms produced beneath former ice sheets offer insights into inaccessible subglacial processes and present analogues for how current ice masses may evolve in a warming climate. Large subglacial channels cut by meltwater erosion (tunnel valleys) have the potential to provide valuable empirical constraints for numerical ice-sheet models concerning realistic melt rates, water routing, and the interplay between basal hydrology and ice dynamics. However, the information gleaned from these features has thus far been limited by an inability to adequately resolve their internal structures. In this chapter, high-resolution three-dimensional (HR3D) seismic data (6.25 m bin size, ~ 4 m vertical resolution) are used to analyse the infill of buried tunnel valleys in the North Sea. The HR3D seismic data represent a step-change in our ability to investigate the mechanisms and rates at which tunnel valleys are formed and filled. Over 40 % of the tunnel valleys examined contain buried glacial landforms including eskers, crevasse-squeeze ridges, glacitectonic structures, and kettle holes. As most of these landforms had not been detected previously using conventional 3D seismic-reflection methods, the mechanisms that formed them are currently absent from models of tunnel valley genesis. The ability to observe such intricate internal structures opens the possibility of using tunnel valleys to reconstruct the hydrological regimes of former mid-latitude ice sheets as analogues for contemporary ones.

5.1 Introduction

Throughout the Quaternary, the growth and retreat of ice sheets across high- and mid-latitude continental shelves drove major changes to topographic relief and global sea level (e.g., Batchelor et al., 2019). Subglacial water flow to the margins of these ice sheets excavated huge channels, sometimes kilometres wide and hundreds of meters deep, which are referred to as tunnel valleys (Ó Cofaigh, 1996; Huuse and Lykke-Andersen, 2000b; Kehew et al., 2012). Multiple cross-cutting generations of tunnel valleys, potentially correlated with seven glacial cycles, are buried beneath the seafloor in the North Sea (Kristensen et al., 2007; Stewart and Lonergan, 2011). Tunnel valleys provide a unique opportunity to investigate the subglacial plumbing system of the ice sheets that formerly covered north-western Europe and to learn more about inaccessible basal processes that regulate ice-sheet flow and retreat. However, there is currently no consensus on the timescales and mechanisms through which glacial meltwater forms tunnel valleys or their impact on ice-sheet dynamics, and theories about their formation range from rapid erosion during catastrophic floods to more gradual development through multiple incision events (Kehew et al., 2012).

The infill of tunnel valleys is similarly complex; some models propose that tunnel valleys were cut and filled incrementally (e.g., Jørgensen and Sandersen, 2006), whereas others favour simultaneous cutting and infilling in a conveyor-like fashion tracking ice front recession (Praeg, 2003; Kristensen et al., 2008). Disagreement over tunnel valley infill reflects spatial heterogeneity in tunnel valley form and sedimentary composition in outcrops, a scarcity of borehole samples, and data resolution constraints that limit the extent to which their internal architecture can be analysed in three dimensions (3D; Huuse and Lykke-Andersen, 2000b; Praeg, 2003). In this chapter, novel high-resolution 3D (HR3D) seismic data from the North Sea are used to examine the infill of tunnel valleys in unprecedented detail and discuss the implications for tunnel valley genesis.

5.2 Data and methods

Six HR3D seismic data sets, covering ~ 60 km², were examined from the central North Sea (Figures 5.1A and 5.1B). The acquisition system comprised two 1200-m-long streamers towed 3 m beneath the sea surface with 96 hydrophone groups at 12.5 m spacing, a 6.25 m shot interval, and a 1 ms sample rate (Games, 2012). The seismic source consisted of two 160-inch³ sleeve air gun clusters with a 20–250 Hz signal frequency. Data processing included swell noise attenuation, tide correction, multiple suppression, two passes of velocity analyses run at 250×250 m intervals, normal

moveout correction, and bandpass filtering. The final processed data sets consist of time-migrated 3D stacks with a 1 ms sample rate, a 6.25×6.25 m bin size, a vertical resolution of ~ 4 m, and a detection limit along individual reflectors of ~ 0.5 m. In comparison, the 3D seismic data previously used to examine tunnel valleys in this region typically have bin sizes of 12.5–50 m and a vertical resolution of ~ 8 –16 m (Stewart et al., 2013). Depth conversions used a velocity of 1800 m s^{-1} (Stoker et al., 1985). Seismic interpretation was carried out using S&P Global Kingdom Software.

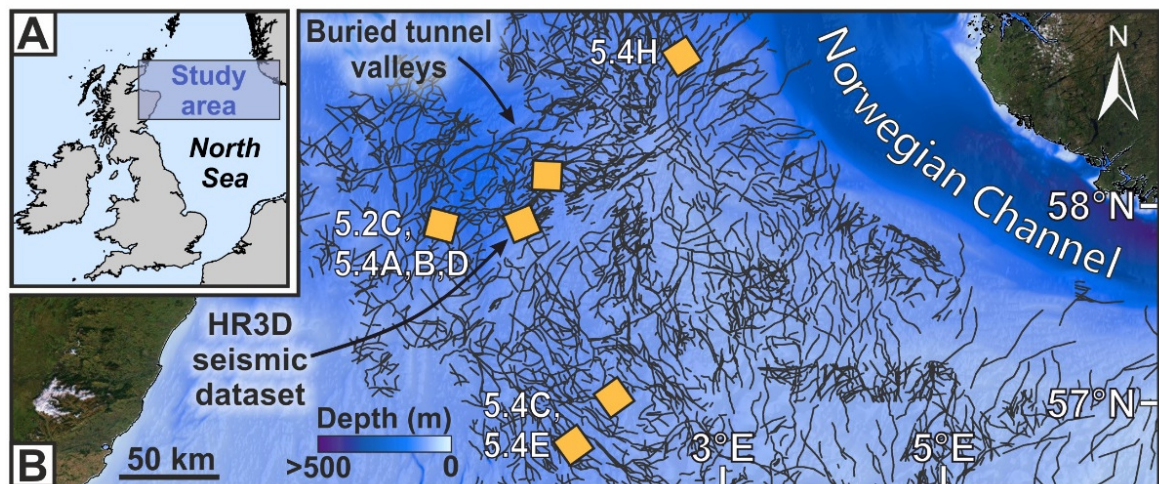


Figure 5.1. Distribution of buried tunnel valleys in the central North Sea. (A) Study area. **(B)** Bathymetry of the central North Sea (GEBCO: <https://www.gebco.net>) and the locations of buried tunnel valleys (Ottesen et al., 2020) and the six high-resolution 3D (HR3D) seismic datasets used in this chapter (squares). White labels refer to the locations of other figures shown in this chapter.

5.3 Buried landforms within tunnel valleys

The six HR3D seismic data sets image 19 cross-cutting incisions that are 300–3000 m wide, up to 300 m deep, and possess undulating thalwegs. These incisions are interpreted as tunnel valleys formed by subglacial meltwater based on their distinctive morphology (e.g., Stewart et al., 2013). The tunnel valleys contain between one to four discrete fill units, and most consist of two seismic facies. The infill is highly variable and lacks consistent patterning between each tunnel valley, although some common facies are present (Figures 5.2A and 5.2B). Over 50 % of the tunnel valleys contain a chaotic, largely homogenous fill package that often overtops the tunnel valley shoulders (light brown shading in Figure 5.2B). This facies is interpreted as subaqueous or subaerial outwash. In addition, the lowermost facies of ~ 60 % of tunnel valleys contains discontinuous sub-parallel reflections that are interpreted as clays and sands deposited in a subglacial or proglacial subaqueous setting (dark brown shading in Figure 5.2B).

Approximately twice the number of infill units can be resolved in the HR3D seismic data compared to conventional 3D seismic data; this improvement represents a step-change in our ability to observe fine-scale tunnel valley infill structures (Figure 5.3).

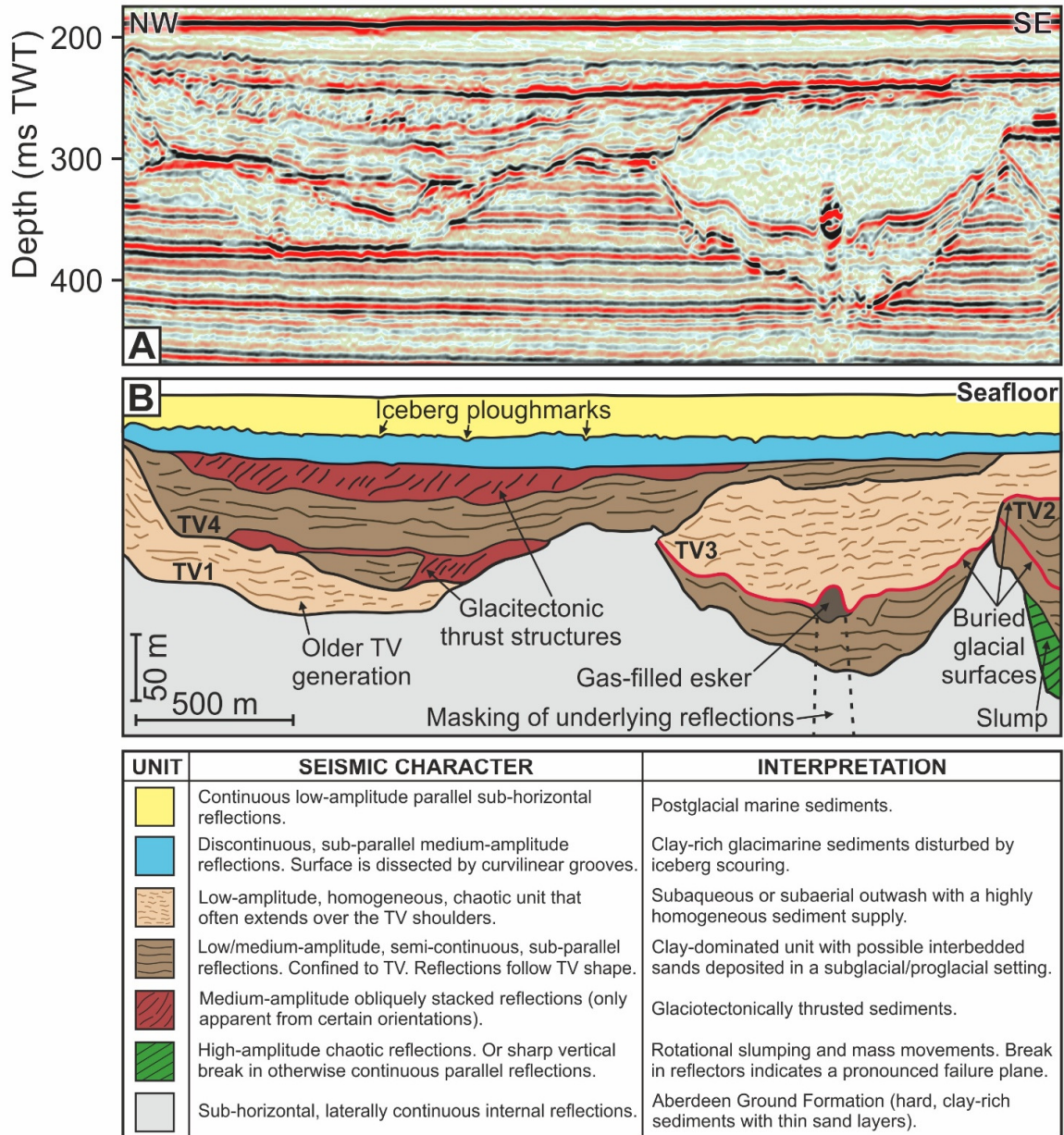


Figure 5.2. Seismic character of buried tunnel valleys in the central North Sea. (A) Example of a seismic section displaying cross-cutting tunnel valleys with variable infill character. (B) Stratigraphic interpretation of the tunnel valleys and their infill (see table for legend). Solid red lines correspond to buried glacial surfaces mapped within the tunnel valleys. Four tunnel valley generations are present; TV1 is the oldest stratigraphically, followed by TV2, TV3, and TV4. TWT—two-way travel time. TV—tunnel valley.

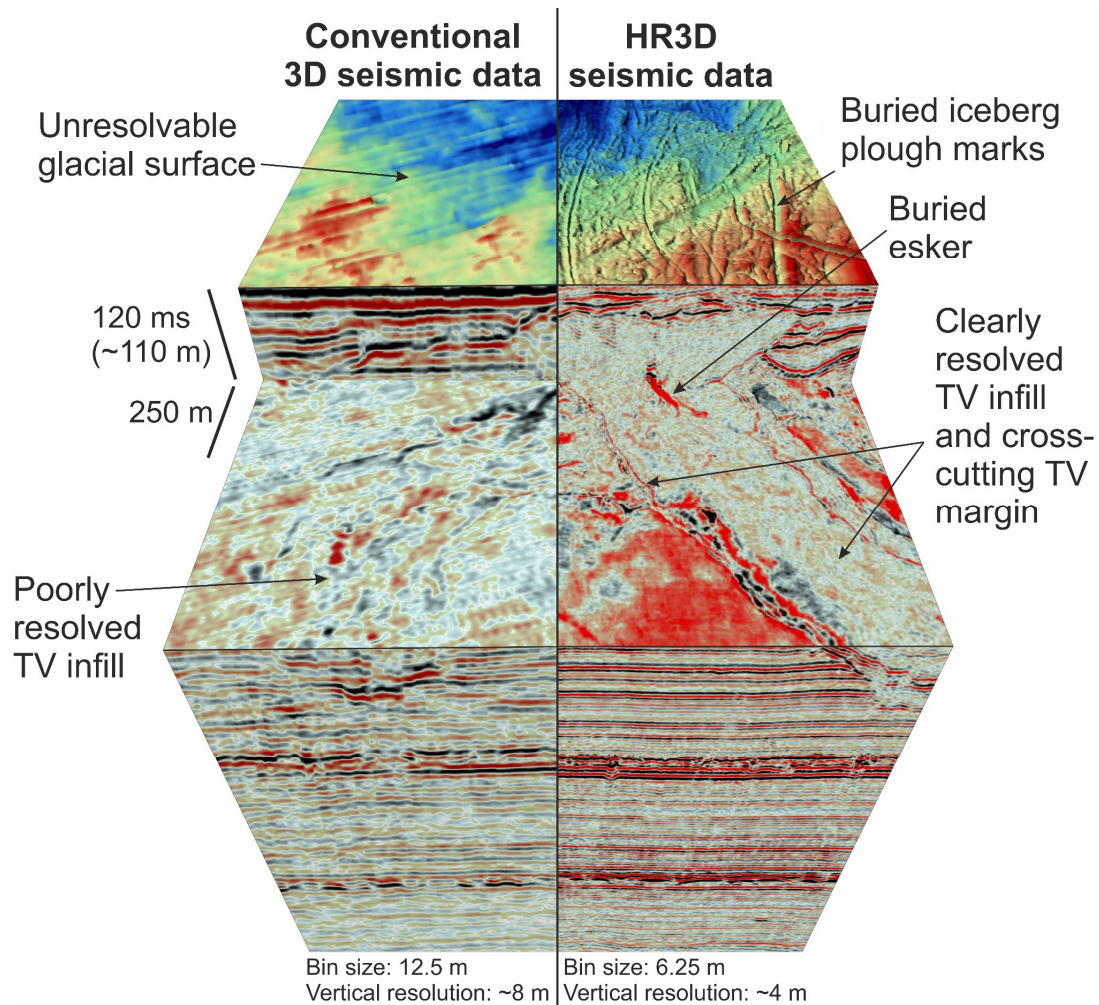


Figure 5.3. Comparison of conventional 3D seismic-reflection data (left) and high-resolution 3D seismic-reflection data (right). Both datasets cover the same region of the central North Sea and the figure shows a continuation of the same buried surfaces for each dataset. The top surface is a horizon mapped at ~ 220 ms depth and shows buried iceberg ploughmarks (seafloor is at ~ 190 ms). TV—tunnel valley. Data courtesy of PGS and Gardline Limited.

Several tunnel valleys contain high-amplitude reflections between their upper and lower fill units. When mapped in 3D, these reflections delineate sinuous ridges that are up to 2.8 km long, 30–150 m wide, and 5 m high on average (Figure 5.4A). The ridges display striking morphological similarity to eskers deposited in meltwater conduits present at the base of an ice sheet (e.g., Storrar et al., 2014; Figure 5.5), and are interpreted as such. The absence of eskers shorter than 400 m in the North Sea likely reflects the relatively small areal coverage of the 3D seismic data which is considerably lower than the terrestrial datasets used to produce previous esker morphology inventories (e.g. Storrar et al., 2014).

Small hollows containing well-layered fill are observed buried within the outwash unit that caps some tunnel valleys. The hollows are 100–300 m wide, 200–750 m long and have side slopes of 10–35° (Figures 5.4B and 5.4F). The hollows are interpreted as kettle holes that formed when stagnant ice blocks were stranded in shallow water, as discussed using examples exposed by the retreat of Svalbard tidewater glaciers (e.g., Ottesen et al., 2017). Their well-layered internal structure likely reflects infilling with fine-grained sediments once the ice blocks melted in place or floated off in a marine setting.

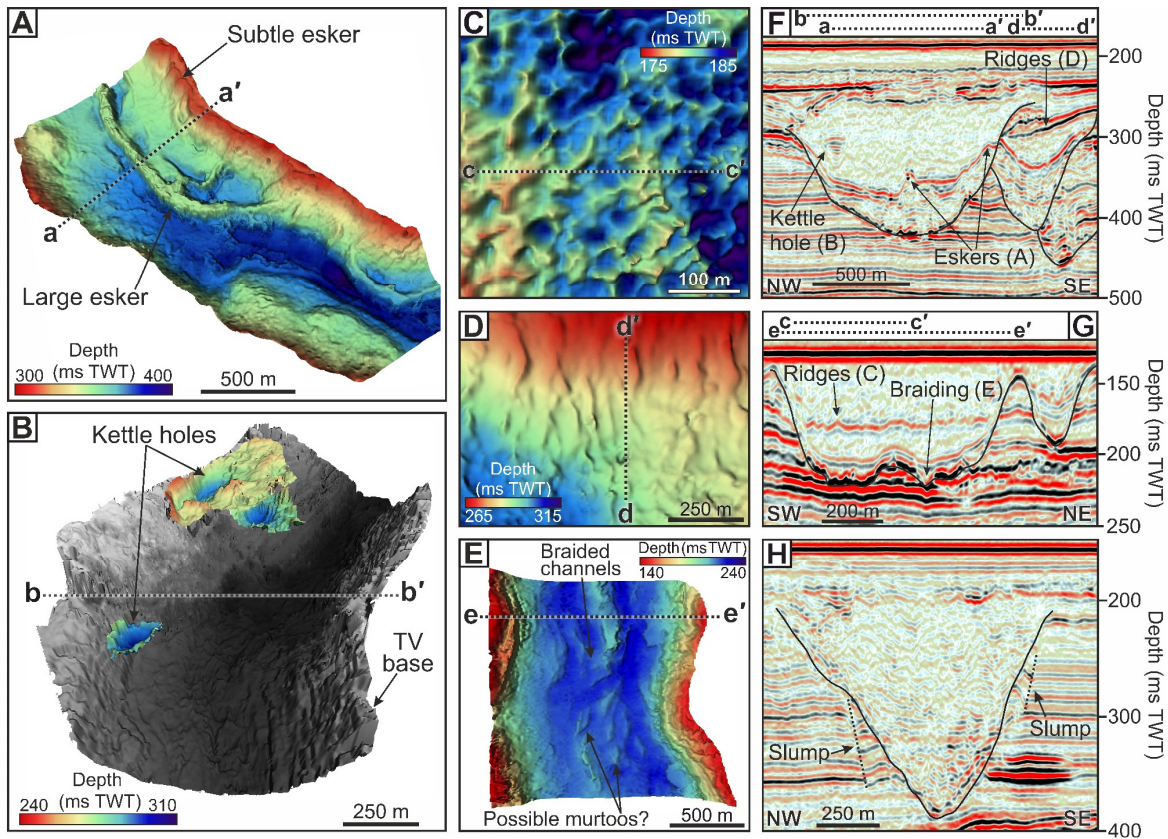


Figure 5.4. Glacial landforms buried inside tunnel valleys. (A) Curvilinear ridges ~ 5 m high, ~ 70 m wide, and up to 2.8 km long are interpreted as eskers. (B) Localised pockets of onlapping fill occupy sub-rounded depressions with side slopes of 10–35° and are interpreted as kettle holes. The tunnel valley base is shaded in grey (deeper = darker). (C) Rhombohedral ridges arranged in a honeycomb structure and (D) curvilinear ridges perpendicular to the tunnel valley long axis are interpreted as crevasse-squeeze ridges. (E) The base of the tunnel valley in (G) exhibits a braided structure with channels diverging around bar-like features. (F–G) Seismic sections across tunnel valleys (outlined by thin black lines) that contain buried landforms. (H) Slumps inside a tunnel valley. Vertical exaggeration in F–H is $\sim 5\times$. TWT—two-way travel time.

Subtle ridge patterns of two morphologies are buried within the tunnel valleys and appear as undulating reflections with high acoustic amplitude. The first features form irregular networks of four- to six-sided polygons that are rhombohedral in planform

morphology, 40–80 m in diameter, and slightly hollow in the centre. Individual ridges are 20–250 m long, 20–30 m wide, and <4 m high from base to crest (Figures 5.4C and 5.4G). Several processes have been documented to produce rhombohedral ridges, including fluid escape, diagenesis, glacier surging, and permafrost processes (e.g., Ottesen and Dowdeswell, 2006; Morley et al., 2017; Bellwald et al., 2019). Fluid escape may be ruled out due to the absence of visible chimneys or pipes above the features and suggest that substantial diagenetic change is unlikely to occur at such shallow depths (<250 m below seabed). The fact that the ridges are confined to the tunnel valley rather than extending onto the surrounding banks, combined with their irregular rims, suggests these landforms do not result from permafrost processes.

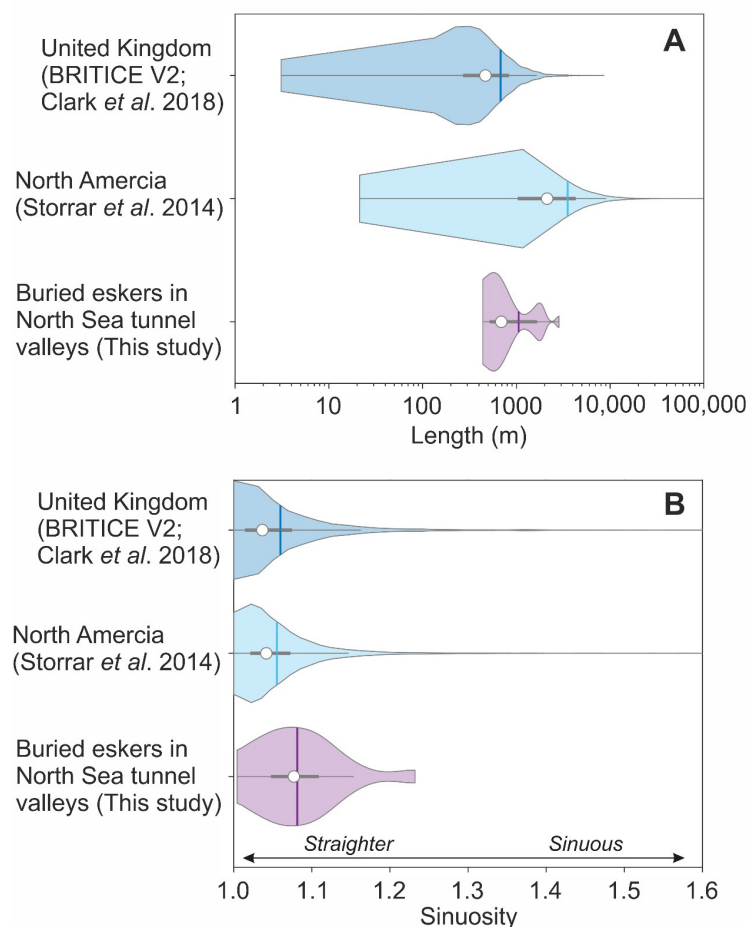


Figure 5.5. Comparison between the morphology of eskers buried within tunnel valleys in the North Sea and those in other locations. (A) Violin plots of the length of terrestrial eskers in the United Kingdom, North America and those found buried within North Sea tunnel valleys. **(B)** Comparison between the sinuosity of terrestrial eskers in the United Kingdom, North America and those found buried within North Sea tunnel valleys. Data on the characteristics of eskers in the United Kingdom and North America were derived from the inventories of Storrar et al. (2014) and Clark et al. (2018). White dots = median value. Vertical lines = mean value. Internal grey boxes show the first–third quartiles of the data. For more information about how to interpret violin plots see Hintze and Nelson (1998).

Rather, based on a morphological comparison to 298 ridges mapped on formerly glaciated terrains imaged on the Svalbard seafloor (Ottesen and Dowdeswell, 2006; Figure 5.6), these landforms are interpreted as crevasse-squeeze ridges that formed through sediment injection upwards into basal fractures beneath grounded ice (Rea and Evans, 2011; Evans et al., 2016). The height, width, length, cross-sectional area, and orientation of the ridges imaged within the North Sea tunnel valleys are highly similar to the crevasse-squeeze ridges mapped in Svalbard (Figures 5.6C–J). The comparative reduction in cross-sectional area for the buried examples in the North Sea may relate to post-depositional compaction of these features once buried. The dominant orientation of crevasse-squeeze ridges is thought to relate to the stress field of the overlying ice. Linear extension of the ice has been hypothesised to lead to relatively straight crevasse-squeeze ridges, whilst radial extension of ice, potentially encouraged by close proximity to a relatively unconfined ice margin (Kurjanski et al., 2019), is hypothesised to result in rhombohedral crevasse-squeeze ridge morphologies.

Groups of sub-parallel curvilinear ridges, commonly located in the upper third of tunnel valley infill, constitute the second type of ridge pattern (Figure 5.4D). The symmetrical ridges are spaced 50–100 m apart, 100–300 m long, <3 m high, terminate sharply, and are oriented perpendicular to the long axis of the tunnel valleys (Figure 5.4D). These are interpreted as crevasse-squeeze ridges formed at the grounding zone as ice retreated through the tunnel valleys.

Distinctive features are also found at the base of the tunnel valleys in the form of networks of anabranching braided channels (80 m wide and ~6 m deep on average) incised around streamlined bars 55–540 m long and 30–165 m wide (Figure 5.4E). The streamlined bars found in the tunnel valleys resemble a distinctive triangular glacial landform recently identified on the former bed of the last Fennoscandian Ice Sheet (Seppälä, 2016; Mäkinen et al., 2017). Ojala et al. (2019) termed these features as ‘murtoos’; they are typically 30–200 m long and 30–200 m wide, which is similar to the dimensions of the bars imaged at the base of the North Sea tunnel valleys. Although the exact mechanism responsible for the formation of murtoos is not well understood, they are suggested to form from subglacial meltwater erosion when large quantities of meltwater are delivered to the bed (Ojala et al., 2019), potentially simultaneously with tunnel valley incision (Peterson et al., 2018). The thalweg of the tunnel valley displayed in Figure 5.4E undulates, which suggests a subglacial rather than subaerial fluvial origin. Several tunnel valleys also contain chaotic and displaced reflections along the sides and bases, which are interpreted as evidence of slumping (Figure 5.4H), faulting, and glacitectonic thrusting (Figure 5.2B).

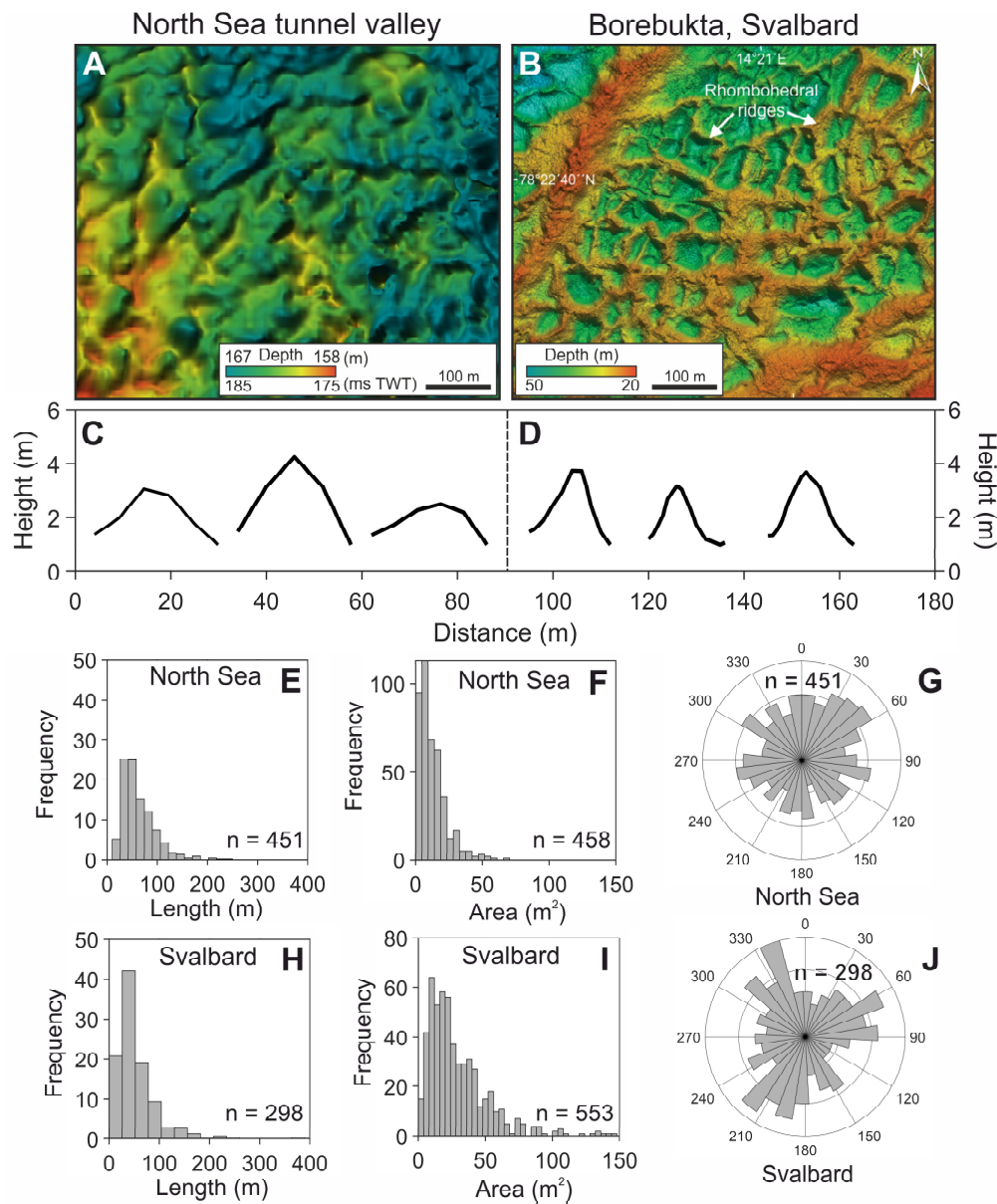


Figure 5.6. Comparison between ridges found buried within North Sea tunnel valleys and rhombohedral crevasse-squeeze ridges in Svalbard. (A) Ridges arranged in a honeycomb structure present midway within the infill of a tunnel valley (see Figure 5.4G) in the central North Sea. (B) Rhombohedral crevasse-squeeze ridges formed by a surging glacier in Borebukta, Svalbard (reproduced from Dowdeswell et al. (2016)). Typical examples of ridge cross sections are shown for those present in the tunnel valleys (C), and in Svalbard (D). (E) Along profile length of the 451 ridges present inside the tunnel valley. (F) Distribution of tunnel valley ridge cross-sectional areas, based on a sample of 458 cross sections (some ridges were sampled more than once). (G) Compass orientation, relative to north (0°), of the 451 ridges present inside the tunnel valley. (H) Along profile length of the 298 crevasse-squeeze ridges present in Borebukta, Svalbard. (I) Distribution of crevasse-squeeze ridge cross-sectional areas, based on a sample of 553 cross sections in Borebukta, Svalbard. (J) Compass orientation, relative to north (0°), of the 298 ridges present in Borebukta, Svalbard.

5.4 Discussion

Over 40 % of the tunnel valleys examined here contain buried landforms of glacial origin (Figure 5.4), whose morphology has been described previously in terrestrial glaciated landscapes and in multibeam-bathymetric imagery of the formerly glaciated seafloor (e.g., Benn and Evans, 2010; Dowdeswell et al., 2016a). Most of these features are too small to interpret using conventional 3D seismic data and would be difficult to detect using 2-D seismic data or boreholes alone (Figure 5.3). Accordingly, glacial landforms, both erosional and depositional in nature, are likely far more common inside tunnel valleys than previously recognised.

The ice sheets formerly occupying the North Sea Basin were underlain by thick sequences of flat-lying unconsolidated sediments (e.g., Ziegler, 1990; Lamb et al., 2018). In such settings, subglacial water is thought to be transported in networks of broad and shallow sedimentary channels (Walder and Fowler, 1994) that may resemble the braided channels observed at the base of some tunnel valleys (Figure 5.4E). Braided channel systems may be eroded into the substrate surrounding a subglacial conduit when the latter drainage system is temporarily overwhelmed by pulses of meltwater supplied from the ice-sheet surface (Lewington et al., 2020; Figure 5.7A). This could be achieved by supraglacial lake drainage via hydrofracture (e.g., Das et al., 2008). Repeated transfer of surface meltwater to the bed, coupled with lateral enlargement by overriding ice, would gradually excavate a tunnel valley and induce glacetectonic deformation structures and mass movements along its sides (Figure 5.4H); these processes have also been inferred from tunnel valleys exposed in sections of Late Ordovician glacial rocks in, for example, North Africa (Hirst et al., 2002; Le Heron et al., 2004).

Although eskers have been documented along the base of unfilled subaerial tunnel valleys in North America (e.g., Brennand and Shaw, 1994), these features are rarely reported inside filled tunnel valleys (van der Vegt et al., 2012). Traditionally, eskers and tunnel valleys were thought to coexist only rarely, as eskers were associated mainly with hard bed substrates whereas tunnel valleys formed in poorly consolidated sediments (Clark and Walder, 1994; Huuse and Lykke-Andersen, 2000b). The eskers observed within the tunnel valleys here indicate that this association probably reflects the poor preservation potential of eskers on soft substrates (Storrar et al., 2019). The near-central stratigraphic position of the eskers within the tunnel valley infill is significant, as it demonstrates that grounded ice occupied the tunnel valley until the channel filled to approximately half of its accommodation space. This finding contrasts with many previous models of tunnel valley genesis (van der Vegt et al., 2012) which posit that the influence of grounded ice

is largely restricted to near the base of the tunnel valley infill succession (during incision). Instead, new observations presented in this chapter imply that grounded ice continues to influence tunnel valley formation over much longer time periods — in some cases until the point where 50 % of the channel has been infilled.

It is possible that the eskers in the tunnel valleys represent the final sedimentary cast of migrating meltwater conduits that were filled during the last stages of deglaciation under a thinning ice-sheet terminus (Storrar et al., 2014; Beaud et al., 2018a). Lateral continuity and a high degree of esker preservation implies gradual ice retreat from these tunnel valleys and precludes reworking by ice readvances before the eskers were buried by outwash sediments. As esker continuity reflects the ice dynamics at the time that they were formed (Storrar et al., 2014), further investigation into the degree of esker fragmentation within tunnel valleys may hint at the style and rate of past ice-sheet retreat (Livingstone et al., 2020).

Crevasse-squeeze ridges are typically diagnostic of surging glaciers (Sharp, 1985). These features form at the termination of a surge through sediment injection into basal crevasses and are preserved by the stagnation and in-situ downwasting of the overlying ice (Rea and Evans, 2011). Kettle holes can also form from ice stagnation and meltout during the quiescent phase of tidewater glacier surges (Ottesen et al., 2017).

The presence of landforms indicative of glacier surging within some tunnel valleys may imply that they acted as conduits for fast ice flow prior to being fully infilled. The absence of these landforms beyond the tunnel valleys indicates that either surges were confined to the tunnel valleys due to hydrological factors that initiated the fast flow or that such delicate features were not preserved outside of the tunnel valleys. Experiments with silicon models of the subglacial hydrological system demonstrate that tunnel valley formation often coincides with surges in the velocity of the model glacier that are triggered by increases in basal water pressure, causing the ice to decouple from its bed (Lelandais et al., 2016). The glacial landforms observed here support a link between the transport of water in tunnel valleys and dynamic ice behaviour.

The variety of landform assemblages preserved inside the cross-cutting tunnel valleys hints at the diverse ice-sheet regimes that formed and filled them. The schematic illustrations displayed in Figure 5.7 summarise the implications that the novel HR3D seismic observations have for the genesis and infilling mechanisms of tunnel valleys. The HR3D seismic data suggest that tunnel valleys are incised gradually by migrating subglacial meltwater channels driven by pulses of meltwater from the ice-sheet surface (Figure 5.7A). These pulses of surface meltwater resulted in the formation of braided

channel networks and potentially the co-production of murtoos-like features at the base of some tunnel valleys (Peterson et al., 2018; Ojala et al., 2019) (Figure 5.4E). Once established, the tunnel valleys were enlarged by the flow of basal ice which had deformed into the top of the valleys, inducing deformation structures and mass movements along their sides (Prins et al., 2020) (Figure 5.7B). Gradual ice retreat from tunnel valleys may fill and preserve the most recently active channels as laterally continuous eskers (Figure 5.7C). In contrast, dynamic ice flow through the tunnel valleys, possibly as surges or readvances, followed by stagnation and downwasting, may be indicated by the presence and preservation of crevasse-squeeze ridges and kettle holes (Figure 5.7D). Consecutive generations of cross-cutting tunnel valleys are produced in response to subsequent glaciations or ice (re)advances across the same area after the tunnel valleys are infilled. If combined with more robust chronological constraints from shallow boreholes, the ability to observe such intricate internal structures opens the possibility of using tunnel valleys to reconstruct the hydrological regimes and dynamics of former mid-latitude ice sheets — information that can be used as an analogue for how contemporary ice sheets may respond to future climatic warming.

5.5 Conclusions

This chapter marks the first time that abundant glacial landforms have been convincingly imaged within buried tunnel valleys in the North Sea. The presence of eskers and crevasse-squeeze ridges within the mid–upper tunnel valley fill packages demonstrates that grounded ice played an active role in tunnel valley incision and was present for a substantial time during filling. For these delicate landforms to have been preserved in the geological record, reoccupation of the tunnel valleys between different glacial cycles must have been limited, although localised ice readvances may have occurred. This result constrains the formation and infilling of each tunnel valley generation to a single glaciation and supports the notion that the multiple generations of tunnel valleys present in the North Sea record at least seven glacial advances across north-western Europe (Stewart and Lonergan, 2011). Greater coverage of HR3D seismic data on formerly glaciated continental margins, combined with chronological constraints from shallow drilling, may permit tunnel valleys to become a resource to improve understanding of the hydrological systems and dynamics of former ice sheets.

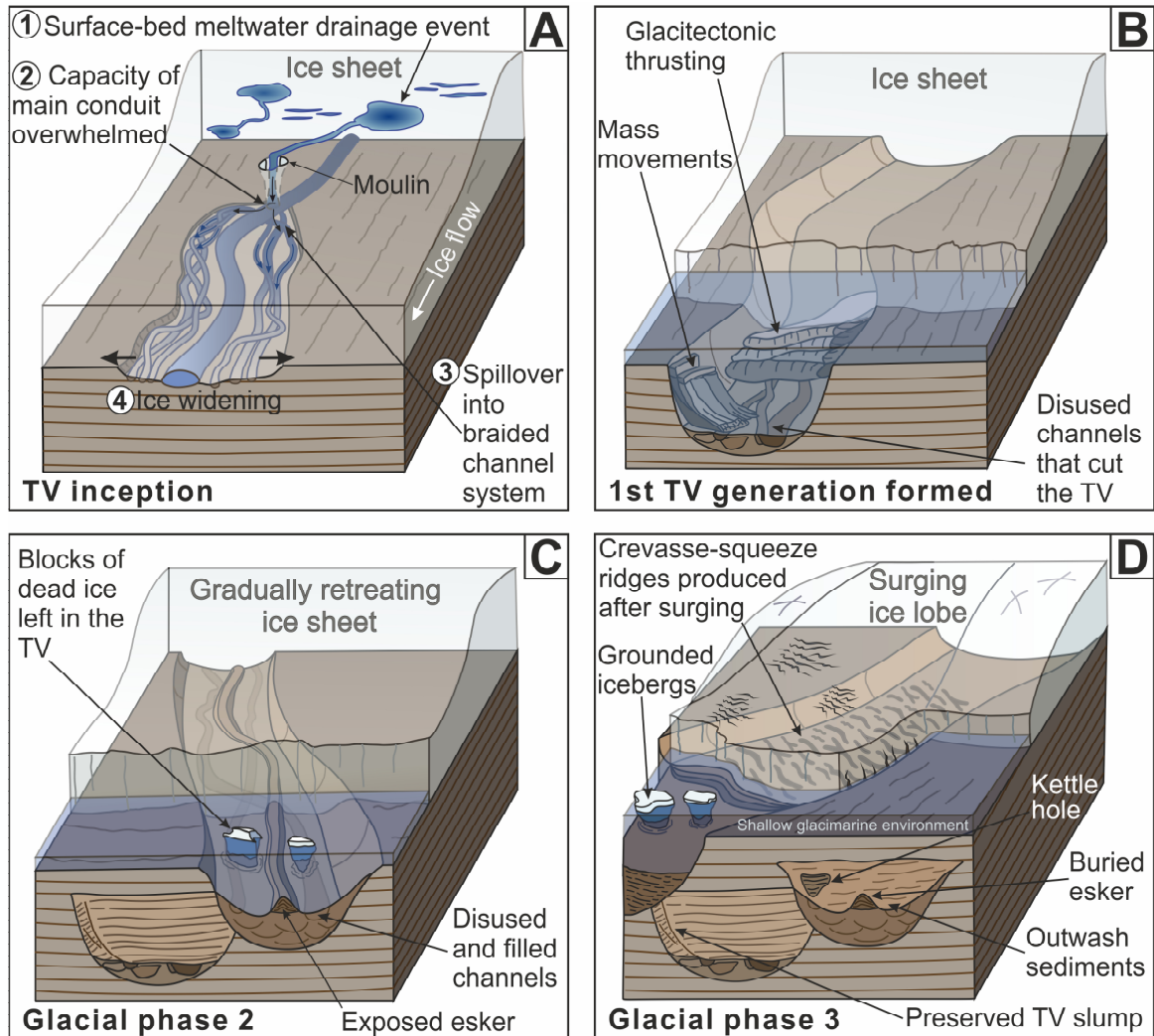


Figure 5.7. Ice-sheet regimes implied by landform assemblages and stratigraphic relationships inside tunnel valleys. (A) Tunnel valley inception triggered by surface meltwater drainage and (B) enlargement by overriding grounded ice. (C) A second glaciation/ice (re)advance results in the incision of migrating channels across the previous tunnel valley (now filled with glacimarine infill). As ice gradually recedes, eskers are left behind that represent sedimentary casts of the most recently active channels. Abandoned blocks of dead ice later form kettle holes. (D) A third glaciation/readvance is affected by more dynamic ice flow and results in crevasse-squeeze ridges that are found near the termini of modern surge-type glaciers.

Chapter 6

Tunnel valley formation beneath deglaciating mid-latitude ice sheets: Observations and modelling

Abstract

The geological record of landforms and sediments produced beneath deglaciating ice sheets offers insights into inaccessible glacial processes. Large subglacial valleys formed by meltwater erosion of sediments (tunnel valleys) are widespread in formerly glaciated regions such as the North Sea. Obtaining a better understanding of these features should assist with the parameterisation of basal melt rates and the interplay between basal hydrology and ice dynamics in numerical models of past, present, and future ice-sheet configurations. However, the mechanisms and timescales over which tunnel valleys form remain poorly constrained. In this chapter, a series of numerical modelling experiments, informed by new observations from high-resolution 3D seismic data (6.25 m bin size, ~4 m vertical resolution), are presented which test different hypotheses of tunnel valley formation and calculate subglacial water routing, seasonal water discharges, and the rates at which tunnel valleys are eroded beneath deglaciating ice sheets. Networks of smaller or abandoned channels, pervasive slump deposits, and subglacial landforms are imaged inside and at the base of larger tunnel valleys, indicating that these tunnel valleys were carved through the action of migrating smaller channels within tens of kilometres of the ice margin and were later widened by ice-contact erosion. The model results imply that the drainage of extensive surface meltwater to the ice-sheet bed is the dominant

mechanism responsible for tunnel valley formation; this process can drive rapid incision of networks of regularly spaced subglacial tunnel valleys beneath the fringes of retreating ice sheets within hundreds to thousands of years during deglaciation. Combined, the observations and modelling results presented in this chapter identify how tunnel valleys form beneath deglaciating mid-latitude ice sheets and have implications for how the subglacial hydrological systems of contemporary ice sheets may respond to sustained climate warming.

6.1 Introduction

Subglacial hydrology exerts a major control on ice-sheet dynamics, sedimentation rates, and landscape evolution. Currently, mass losses from the Antarctic and Greenland ice sheets are accelerating (Shepherd et al., 2018; Mouginot et al., 2019; Rignot et al., 2019; Shepherd et al., 2020). Increasing numbers of lakes on the surface of the Greenland Ice Sheet are forming further inland (Leeson et al., 2015; Gledhill and Williamson, 2017). These lakes can drain, sometimes rapidly (e.g., Zwally et al., 2002; Das et al., 2008; Selmes et al., 2011; Smith et al., 2015; Chudley et al., 2019), transporting large and sometimes quantifiable volumes of meltwater to the base of the ice sheet. Widespread melting events have also been observed around the fringes of the Antarctic Ice Sheet and these are predicted to increase in extent in the future (Scambos et al., 2000; Tedesco, 2009; Tedesco and Monaghan, 2009; Trusel et al., 2015; Kingslake et al., 2017; Bell et al., 2018). Subglacial hydrology will play an increasingly important role in the fate and behaviour of these ice sheets as the climate continues to warm. However, the subglacial hydrological system of modern ice sheets is highly inaccessible, and models of how the subglacial drainage system will adapt to future climate warming are poorly constrained. Consequently, there is great value in examining what can be learnt about subglacial hydrology from the geological record of the demise of former ice sheets.

Some of the most striking landforms associated with subglacial meltwater in formerly glaciated regions take the form of elongate depressions known as tunnel valleys. Tunnel valleys typically form on low relief beds near former ice-sheet margins and can be incised into both unlithified sediments and bedrock (Kehew et al., 2012; van der Vegt et al., 2012; Livingstone and Clark, 2016). They are commonly hundreds to thousands of metres wide, tens to hundreds of metres deep and form semi-regularly spaced channel networks with spacings of ~2–9 km (Kehew et al., 2012; van der Vegt et al., 2012; Livingstone and Clark, 2016; Ottesen et al., 2020). Tunnel valleys are ubiquitous deglacial landforms which are observed frequently in the geological record in both the Quaternary (e.g., Woodland, 1970; Wright, 1973; Mooers, 1989; Praeg, 1996; Huuse and Lykke-Andersen,

2000b; Kristensen et al., 2007; Müther et al., 2012; Stewart et al., 2012; Moreau and Huuse, 2014; Montelli et al., 2020) and pre-Quaternary glacial periods (e.g., Ghienne and Deynoux, 1998; Hirst et al., 2002; Le Heron et al., 2004; Douillet et al., 2012; Montelli et al., 2019). They can transport large quantities of water and sediment (Livingstone and Clark, 2016) and may play a critical role in regulating ice-stream stability during deglaciation by draining meltwater away that might otherwise have reduced basal friction and increased basal sliding (Lelandais et al., 2018). The termini of tunnel valleys are often used as markers to locate the position of former ice margins (e.g., Wingfield, 1989; Huuse and Lykke-Andersen, 2000b; Sandersen et al., 2009; Lohrberg et al., 2020; Ottesen et al., 2020). In some regions, multiple generations of buried cross-cutting tunnel valleys exist; information from which may be used to reconstruct the history of glaciations that occurred prior to the last glacial period (Jørgensen and Sandersen, 2006; Kristensen et al., 2007; Stewart and Lonergan, 2011; Douillet et al., 2012; Atkinson et al., 2013; Stewart et al., 2013; Pugin et al., 2014; Montelli et al., 2020).

Although the origin of tunnel valleys has been attributed to erosion by pressurised subglacial meltwater for over 100 years (Jentzsch, 1884; Ussing, 1903, 1907), the rates at which they form and the processes involved and their impact on ice-sheet dynamics are still subjects of intense debate (Ó Cofaigh, 1996; Huuse and Lykke-Andersen, 2000b; Kehew et al., 2012; van der Vegt et al., 2012). Theories explaining tunnel valley formation can be broadly divided into two genetic models: formation through (i) ‘outburst’ flooding and (ii) ‘gradual’ or ‘seasonal’ incision by relatively small water fluxes (e.g., Ó Cofaigh, 1996; Praeg, 1996; Kehew et al., 2012; van der Vegt et al., 2012; Figure 6.1).

Due to their large dimensions and extensive geographical distribution, many authors have suggested that large volumes of water must have been involved in tunnel valley formation. This has led to a proposed mechanism in which outburst floods from trapped, subglacially stored reservoirs erode large volumes of material rapidly under high discharges (e.g., Wright, 1973; Wingfield, 1990; Piotrowski, 1994; Cutler et al., 2002; Jørgensen and Sandersen, 2006). The water reservoirs for these floods may reside in subglacial basins or be trapped behind frozen toes of permafrost near the ice margin, releasing water as the ice edge retreats (Figure 6.1A; Piotrowski, 1994).

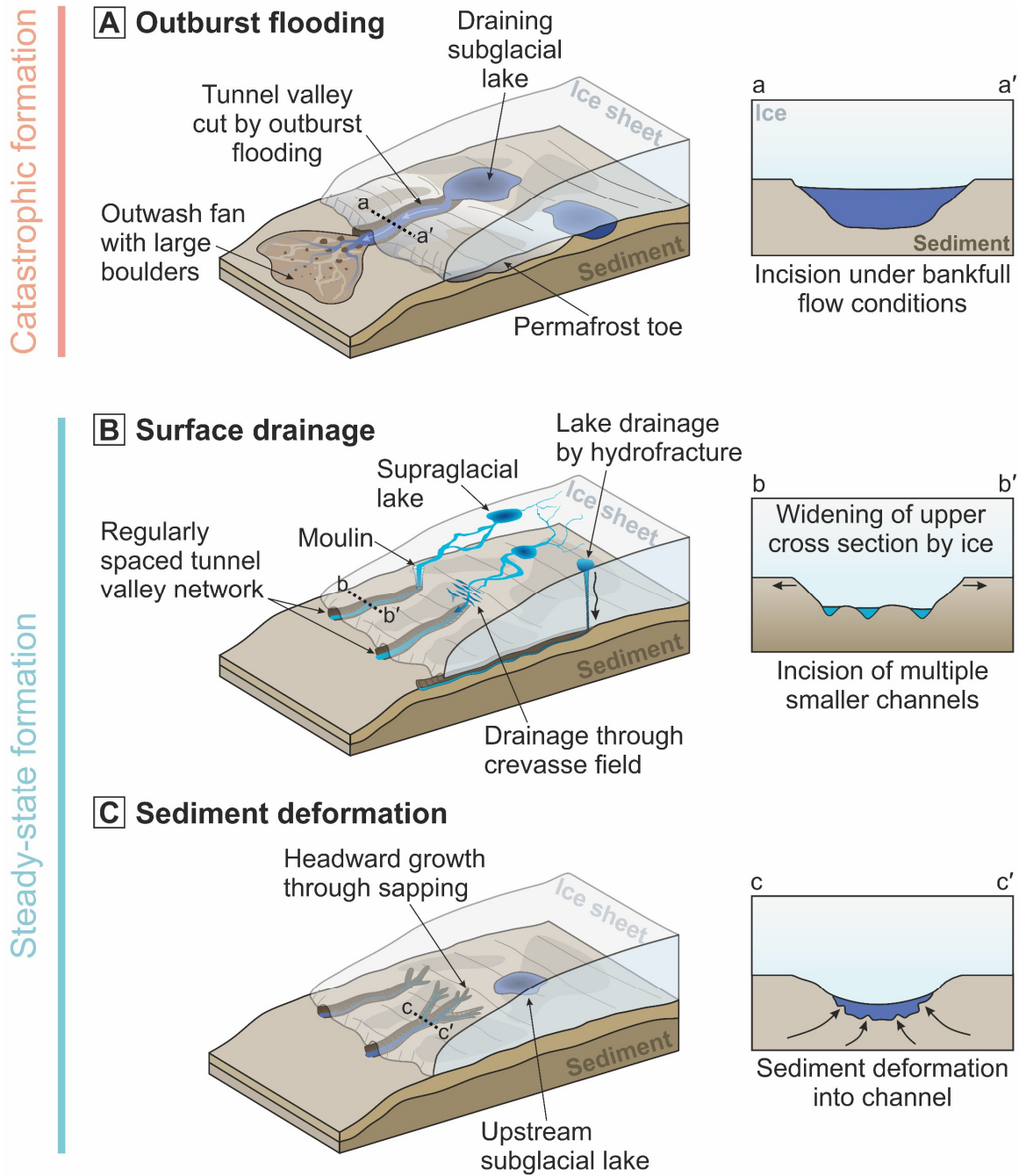


Figure 6.1. Previously proposed mechanisms of tunnel valley formation. (A) Catastrophic formation via outburst flooding from subglacial lakes trapped behind a frozen toe of permafrost. High water discharges and bankfull flow conditions result in the deposition of an outwash fan containing large boulders at the ice-sheet terminus. (B) Steady-state formation close to the ice margin, with water sourced from surface melting, resulting in the formation of regularly spaced tunnel valley networks. Surficial streams drain meltwater to the ice-sheet bed where smaller channels, possibly arranged in a braided structure, gradually incise a larger valley. (C) Gradual headward growth by sapping, possibly towards subglacial lakes trapped upstream. Tunnel valleys grow as sediment deforms into the low pressure channel, and sediment is removed by the transport of meltwater towards the ice-sheet terminus.

The magnitude of flooding, or the number of flood repetitions required for tunnel valley genesis, is not well constrained. Repeated low to moderate magnitude floods that reoccupy the same narrow meltwater pathway, potentially during multiple glaciations, have been offered as an explanation for the superposition of smaller channel infill structures within larger tunnel valley tracts (Jørgensen and Sandersen, 2006; Sandersen et al., 2009). In contrast, much larger discharges capable of forming entire networks of tunnel valleys in massive sheet floods have also been proposed (e.g., Shaw and Gilbert, 1990; Brennard and Shaw, 1994) but this hypothesis is not widely accepted due to the enormous quantities of water required and absence of supporting evidence in the distal sedimentary record (Ó Cofaigh, 1996).

The alternative group of hypotheses proposed to explain tunnel valley formation build around the concept that tunnel valleys are formed incrementally by meltwater flowing under steady-state conditions rather than catastrophically, allowing their extensive incisions to build up time-transgressively. Theories comprising this hypothesis focus around the seasonal propagation of surface meltwater to the bed through an efficient supra-to-subglacial drainage system connection (Figure 6.1B), or sediment creep into a low pressure channel driven by high basal porewater pressures alone (Figure 6.1C). Both of these mechanisms imply that meltwater pathways remained relatively stable in space in order for smaller water discharges to gradually incise a large tunnel valley, potentially aided by the enlargement of the upper valley cross section by ice (Huuse and Lykke-Andersen, 2000b; Kehew et al., 2012; van der Vegt et al., 2012). Pervasive slumping of the tunnel valley flanks may also have enhanced the lateral expansion of the tunnel valleys (Prins et al., 2020; Kirkham et al., 2021).

In the sediment-creep hypothesis (e.g., Shoemaker, 1986; Boulton and Hindmarsh, 1987; Mooers, 1989), headward erosion of a small conduit by piping is triggered in response to increased porewater pressures caused by insufficient evacuation of meltwater from the subglacial environment (Figure 6.1C). As fluid pressures within the conduit are lower than in the surrounding bed, groundwater flows towards the conduit via steady-state Darcian flow, causing the conduit to enlarge into a tunnel valley as sediment is eroded from the channel walls (Boulton and Hindmarsh, 1987). Once established, the conduit may tap into upstream subglacial lakes, further enlarging the channel through outburst flooding (Hooke and Jennings, 2006).

Alternatively, the seasonal input of supraglacial, rather than basal, meltwater to the bed of the ice sheet may gradually incise tunnel valleys (Figure 6.1B). Analogues from the present-day Greenland Ice Sheet demonstrate that large volumes of meltwater are

mobilised during the ablation season; these are transported to the bed through connections such as moulins and crevasses on the ice-sheet surface (Bartholomew et al., 2011a; Tedesco et al., 2013; Smith et al., 2015; Banwell et al., 2016; Koziol et al., 2017; Koziol and Arnold, 2018). Similar, and probably even more extensive, surface-to-bed hydraulic connections were likely present across the surface of former mid-latitude ice sheets as they deglaciated, providing a water source to facilitate tunnel valley incision.

The steady-state body of hypotheses require less specific circumstances than the ‘outburst flood’ hypotheses, such as not needing to invoke large subglacial lakes or permafrost trapping of water. Thus, this formative mechanism is appealing given the widespread geographical distribution of tunnel valleys (Kehew et al., 2012; van der Vegt et al., 2012). Nevertheless, steady-state formation hypotheses have often been disregarded because of the assumption that channels hundreds of metres deep and kilometres wide must require huge discharges in order to form rapidly. However, recent research utilising numerical models of erosion from subglacial water flow and stratigraphic investigations has challenged both of these assumptions.

Sandersen et al. (2009) used lithological and biostratigraphical data from northern Denmark to constrain the age of tunnel valleys formed during the recession of the Late Weichselian Eurasian Ice Sheet across this region. The tunnel valleys were incised during temporary stillstands of the retreating ice-sheet margin between ~19 ka and 18 ka, leaving only a few hundred years at each ice-margin position for the features to form (Sandersen et al., 2009). The formation of a series of ~1–2 km wide, 5–10 km long and up to 180 m deep valleys within a few hundred years demonstrates rapid incision of the tunnel valleys near the ice-sheet margin. Similarly, Giglio et al. (2021) inferred that the maximum time available to carve an extensive system of tunnel valleys into lithified bedrock in the Celtic Sea during the last glacial period was ~1–2 kyrs. Erosive meltwater drainage occurred concurrently with a period of rapid retreat of the Irish Sea Ice Stream across the continental shelf (Giglio et al., 2021). These studies provide observational benchmarks against which theories of tunnel valley formation can be tested.

Sandersen et al. (2009) invoked repeated outbursts of meltwater along narrow conduits to explain the rapid formation of the tunnel valleys in northern Denmark. However, recent numerical modelling by Beaud et al. (2018) suggests that small-magnitude discharge events in the form of seasonal influxes of meltwater from the ice-sheet surface can excavate large channels (100s m wide and 10s m deep) into bedrock over thousands of years (Beaud et al., 2016; Beaud et al., 2018). Whilst their model is applicable only to the erosion of bedrock channels, and different governing equations would be needed

to test these findings on poorly consolidated sediments (e.g., Walder and Fowler, 1994), these model results challenge the assumption that high-magnitude subglacial discharges are necessary to erode large tunnel valleys rapidly beneath the margins of deglaciating ice sheets. The results of Sandersen et al. (2009) and Beaud et al. (2018) warrant further investigation of the minimum seasonal meltwater discharges required to erode tunnel valleys into poorly consolidated sediments over hundreds of years. This will help to establish which formation process is most likely, and may elucidate the impact that tunnel valley formation has on ice-sheet dynamics (van der Vegt et al., 2012).

In this chapter, an ice-sheet modelling approach informed by new geomorphological observations from high-resolution 3D seismic analyses of tunnel valley morphology is used to investigate these questions. Possible water fluxes and erosion rates beneath deglaciating ice sheets are quantified and these calculations are used to test previously proposed hypotheses of tunnel valley formation.

6.2 Methods

In this chapter, subglacial water fluxes and routing are simulated beneath the last British-Irish and Fennoscandian ice sheets to provide greater understanding of tunnel valley formation in the North Sea. It is important to note that the tunnel valleys present in this region are largely attributed to glaciations which occurred prior to the last glacial period (particularly the Elsterian Glaciation; 430–450 ka), although some examples from the last glacial period do exist (e.g., Sandersen et al., 2009; Giglio et al., 2021). This chapter deliberately focuses on modelling water flow during the last glacial period because the ice-sheet geometries and climate forcings are considerably better constrained than those of earlier glaciations (e.g., Svendsen et al., 2004; Batchelor et al., 2019; Gowan et al., 2021). Accordingly, this study does not aim to provide a realistic representation of the water routing beneath the ice sheets that formed the majority of tunnel valleys in this region. Instead, it is assumed that the ice sheets present during the last glacial period can provide physically plausible constraints on the ice-sheet geometries and climatic conditions experienced during previous glaciations when most tunnel valleys formed. These relatively well-constrained boundary conditions are used to quantify a realistic range of water fluxes, melt rates and timescales of channel incision which inform about processes of tunnel valley formation.

6.2.1 Detailed channel morphology from high-resolution 3D seismic data

The water routing and erosion modelling experiments are framed in the context of detailed geomorphological observations derived from high-resolution 3D (HR3D) seismic

data. HR3D seismic data are capable of revealing intricate morphological details of buried landforms and deposits, many of which cannot be resolved using conventional 3D seismic methods (Kirkham et al., 2021). These previously unseen details provide new insights into incision processes, realistic water fluxes and the mode of meltwater drainage within the tunnel valleys.

Seven HR3D seismic datasets from the central North Sea were examined (Figure 6.2; Kirkham et al., 2021) covering a combined area of ~ 67 km² and containing a total of 23 tunnel valleys. The acquisition system comprised two 1200-m-long streamers towed 3 m beneath the sea surface with 96 hydrophone groups at 12.5 m spacing, a 6.25 m shot interval and a 1-ms sample rate (Games, 2012). The seismic source was two 160-inch³ (2.62 L) sleeve airgun clusters. Data processing included swell noise attenuation, tide correction, multiple suppression, two passes of velocity analysis run at 250×250 m intervals, normal-moveout correction, bandpass filtering (20–250 Hz), stacking, and migration. The final processed datasets consist of time-migrated 3D stacks with a 1-ms sample rate, a 6.25×6.25 m bin size, a vertical resolution of ~ 4 m, and a detection limit for depth changes along individual reflectors of ~ 0.5 m (King, 2020; Kirkham et al., 2021).

The base, sides, and internal fill packages of each tunnel valley were mapped and traced laterally through the HR3D seismic volumes using S&P Global Kingdom Software. Picking of seismic horizons was largely conducted manually on a seismic line-by-line basis because automated picking algorithms struggled to follow the complex tunnel valley shapes. The mapped tunnel valley seismic horizons were converted from two-way travel time (TWT) to depth using a velocity of 1900 m s⁻¹, which is appropriate for the Pleistocene sediments in this region (Kristensen and Huuse, 2012). Characteristic morphological measurements, such as width, depth and cross-sectional area were then derived for each tunnel valley.

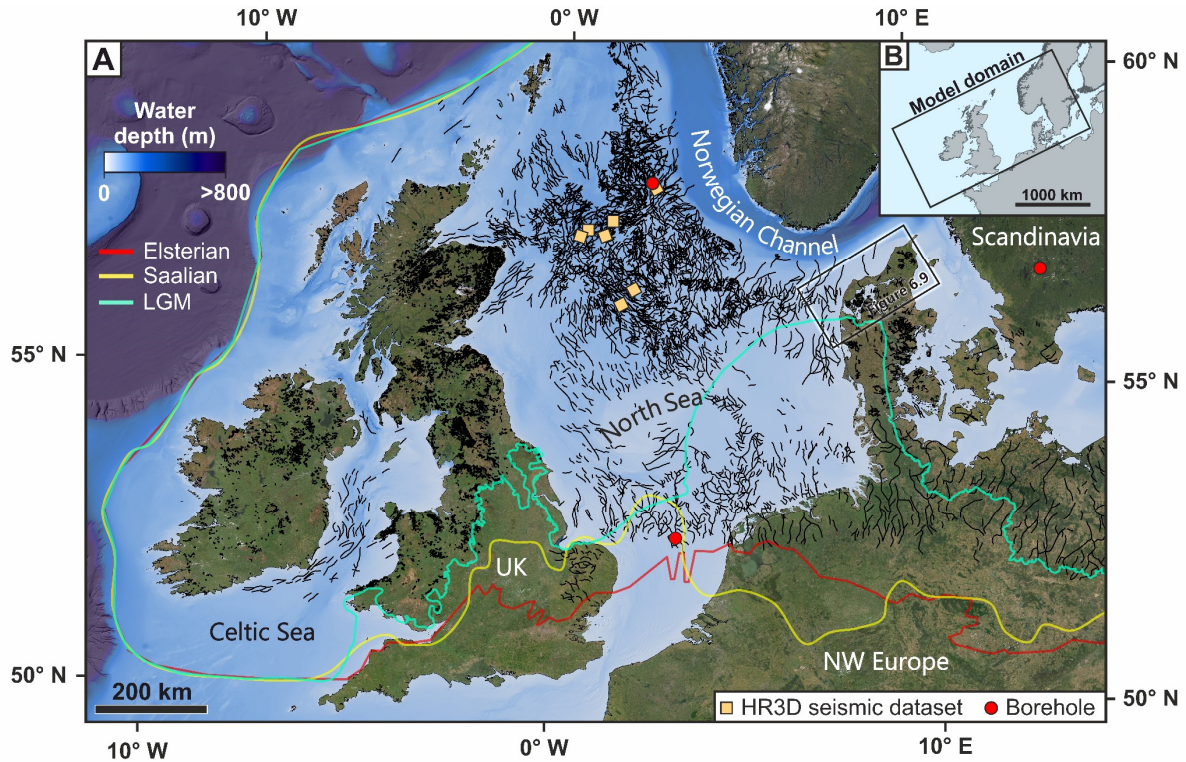


Figure 6.2. Study area. (A) Distribution of tunnel valleys in the North Sea and surrounding landmasses (van der Vegt et al., 2012; Ottesen et al., 2020), and meltwater channels on the UK mainland (Clark et al., 2018), in relation to the high-resolution 3D seismic datasets (orange squares) and boreholes (red circles) used in this chapter. Best estimate former ice margin positions for the Last Glacial Maximum (LGM), Saalian Glaciation (MIS 6), and Elsterian Glaciation (MIS 12) are shown from Batchelor et al. (2019). Regional bathymetry is from GEBCO (<https://www.gebco.net>). (B) Extent of the modelling domain used in this study.

6.2.2 Modelling subglacial water flux and routing

6.2.2.1 BRITICE-CHRONO ice sheet modelling data

The geometry, thickness, surface slope, and the basal and surface melt rates of the last British-Irish Ice Sheet were derived from a series of palaeo ice-sheet reconstructions produced using the Parallel Ice Sheet Model (PISM) as part of the BRITICE-CHRONO project (Clark et al., 2021; Clark et al., 2022b). PISM is a three-dimensional, thermomechanical ice-sheet model constrained by geological observations which combines shallow-ice and shallow-shelf approximations for grounded ice to capture dynamic ice behaviour (Winkelmann et al., 2011). The model was run at a high horizontal resolution of 5 km, with a domain which covers the British Isles and parts of Scandinavia (Figure 6.2B), to capture the interaction between the British-Irish and Fennoscandian ice sheets.

Climate was prescribed using the glacial index method (e.g., Marshall et al., 2000; Tarasov and Peltier, 2004; Zweck and Huybrechts, 2005; Niu et al., 2019), whereby climate was scaled along the Greenland ice core record between different 1 kyr climate reconstructions derived from the PMIP3 simulations and palaeogeographical maps (Clark et al., 2022a; Clark et al., 2022b). Temperature and precipitation from the index approach were converted into surface mass balance through a positive degree day model. For areas of the ice sheet with a negative surface mass balance, the mass balance values were converted into surface melt rates and added to the steady-state basal melt rate derived from geothermal and frictional strain heating (Cuffey and Paterson, 2010). Geothermal heat flux varied spatially and was compiled from data collected by the British Geological Survey and Geological Survey Ireland (see Gandy et al., 2019). This combined melt rate was then used to calculate the subglacial water flux at each grid cell. Following widespread observations of surface meltwater draining to the base of the modern-day Greenland Ice Sheet (e.g., Bartholomew et al., 2011a; Andrews et al., 2014; Smith et al., 2015; Banwell et al., 2016; Koziol et al., 2017; Nienow et al., 2017), a first-order assumption was made that all surface meltwater propagates to the bed of the ice sheet, rather than flowing to the margin in supraglacial streams, for the deglacial scenarios considered here. This assumption is justified given the very high proportion of surface runoff that was observed to enter the subglacial hydrological system of the contemporary Greenland Ice Sheet through moulins fed by supraglacial streams during an extreme melt event in 2012 (Smith et al., 2015); conditions that may be analogous to the meltwater transport regime experienced during deglaciation.

Model outputs were taken at four timeslices (27 ka, 21 ka, 19 ka, and 18 ka) to investigate changes in subglacial discharge and water routing as the last British-Irish and Fennoscandian ice sheets deglaciated. The modern topography of the North Sea and surrounding landmasses was taken from the EMODnet digital bathymetry dataset (EMODnet Bathymetry Consortium, 2018), which has a grid spacing of ~ 115 m. These modern topographic data were corrected for isostasy by applying the results of a new glacial isostatic adjustment model of the British Isles and northwest Europe that is constrained by geomorphological and geochronological data collated by the BRITICE-CHRONO consortium, the DATED-1 project (Hughes et al., 2016), and a recently updated regional sea-level database for the last 20 kyr (Bradley et al., 2018). The model accounts for far field sea-level effects (e.g., gravitational attraction, different glacial histories) and near field ice loading.

6.2.2.2 Subglacial water routing

Water routing over the $\sim 2,750,000$ km² model domain was modelled using an upstream area algorithm (Arnold, 2010) that has been adapted for subglacial water routing (e.g., Willis et al., 2016; Kirkham et al., 2019). The direction in which water is routed beneath ice masses is controlled by gradients of subglacial hydraulic potential (Shreve, 1972). The subglacial hydraulic potential, ϕ , of water flowing beneath an ice sheet is a function of bed topography and ice thickness:

$$\phi = \rho_w gh + k\rho_i gZ \quad (6.1)$$

where ρ_w and ρ_i are the densities of water and ice (kg m⁻³) respectively, g is the acceleration due to gravity (m s⁻²), h is bed elevation (m), Z is ice thickness (m) and k is a dimensionless parameter (referred to as the uniform floatation factor) that represents the ratio between subglacial water pressure and ice overburden pressure (Table 6.1). The value of k varies both spatially and temporally depending on the quantity of meltwater input from the surface, basal ice temperature, the character of the subglacial drainage system and the properties of the underlying substrate (Shreve, 1972; Andrews et al., 2014). A k -value of 0.925 is employed in this chapter. This value has been shown to be realistic when averaged over an entire melt-season, according to empirical studies from several sectors of the Greenland Ice Sheet (Banwell et al., 2013; Lindbäck et al., 2015), and has been used previously to model water flow beneath the former Scandinavian and Barents Sea ice sheets (Shackleton et al., 2018).

The routing algorithm passes the cumulative subglacial water flux, derived from the sum of surface and basal melting from the ice-sheet model, downstream from cell to cell until the routing algorithm reaches the edge of the DEM. This allows the direction and the steady-state subglacial water discharge in each DEM cell to be calculated (Arnold, 2010; Willis et al., 2016). Subglacial water routing across the isostatically corrected bed of the former ice-sheet complex was conducted at a 1500-m resolution, whilst detailed model runs used for calculating tunnel valley erosion rates (Section 6.2.3) were conducted around the fringes of the ice sheet at a 50-m resolution.

6.2.2.3 Tunnel valley carrying capacity

In addition to calculating the steady-state discharges resulting from basal and surface melting, the maximum carrying capacity of the tunnel valleys was calculated based on their cross-sectional area (Walder, 1986; Wingham et al., 2006; Jordan et al., 2010). The maximum discharge capable of being carried by a channel, Q_{max} ($\text{m}^3 \text{s}^{-1}$), is equal to:

$$Q_{max} = 2\left(\frac{\pi}{2}\right)^{\frac{1}{3}} S^{\frac{4}{3}} m^{-1} \left(\frac{\phi'}{p_w g}\right)^{\frac{1}{2}} \quad (6.2)$$

where S is the cross-sectional area (m^2) of a channel, ϕ' is the hydraulic potential gradient, and m is the Manning coefficient ($\text{m}^{-1/3} \text{s}$) describing the internal roughness of the channel. Representative channel cross-sectional areas were derived from measurements of a selection of tunnel valleys imaged in the HR3D seismic-reflection data.

6.2.3 Modelling tunnel valley erosion

6.2.3.1 Erosion model

To better constrain the fluxes of water and the time required to incise tunnel valleys downwards into poorly consolidated sediments, like those of the North Sea Basin (e.g., Ziegler, 1990; Huuse and Lykke-Andersen, 2000b; Lamb et al., 2018), a model of subglacial channel erosion into a deformable substrate developed by Carter et al. (2017), based on the work of Walder and Fowler (1994), was applied. This model has been used previously to simulate the formation of channels through subglacial lake drainage beneath the Antarctic Ice Sheet (Carter et al., 2017), and to estimate incision rates of large subglacial channels in the Green Bay Lobe, Wisconsin, during the last glacial period (Zoet et al., 2019). The model calculates the balance between the water-driven erosion of the base and walls of a soft-bedded subglacial channel and the sediment deposition rate within the channel, estimated using Stokes' settling law (Walder and Fowler, 1994). A viscous substrate rheology was invoked in Walder and Fowler (1994) and Carter et al. (2017) to simulate till flux into the channel, which acts to offset a portion of the mass loss due to water erosion. However, this rheology is inconsistent with laboratory data, numerical experiments and field studies (e.g., Iverson et al., 1998; Tulaczyk et al., 2000a, b; Iverson et al., 2007; Damsgaard et al., 2017; Zoet and Iverson, 2020). Accordingly, this chapter followed Zoet et al. (2019) and omitted the viscous portion of the model.

The erosion rate (m s^{-1}), \dot{E} , of a sedimentary channel is calculated as:

$$\dot{E} = K_1 \left(\frac{v_s}{\alpha_{cc}}\right) \left(\frac{\max(\tau_{cc} - \tau_{k,0}, 0)}{g(\rho_s - \rho_w)D_{15}}\right)^{\frac{3}{2}} \quad (6.3)$$

where v_s is the mean sediment settling velocity, K_1 is an erosion constant (Walder and Fowler, 1994), τ_{cc} is the channel bed shear stress, τ_k is the critical shear stress at the base of the channel, D_{15} is the 15th percentile grain-size diameter of the sediments carried within the flowing water, ρ_s is the density of sediment, ρ_w is the density of water, and α_{cc} is a channel geometry correction factor which can be approximated as (width/depth)³ (Carter et al., 2017). The value of α_{cc} was derived from measurements from the HR3D seismic data, and a range of D_{15} values was investigated guided by the grain-size distribution of tunnel valley infill sediments sampled from boreholes in the North Sea and western Europe (Figures 6.2, 6.3; Benvenuti et al., 2018; Peterson et al., 2018).

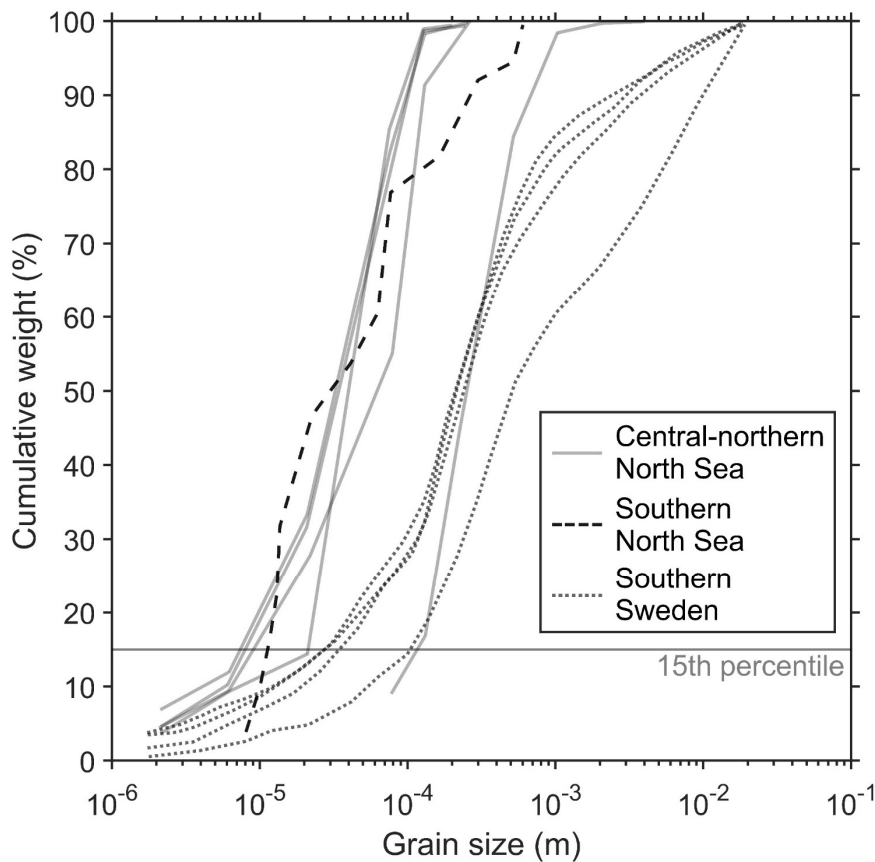


Figure 6.3. Distribution of grain sizes from boreholes drilled into the infill of tunnel valleys in the central-northern North Sea, the southern North Sea (Benvenuti et al., 2018), and southern Sweden (Peterson et al., 2018). See Figure 6.2A for borehole locations. The horizontal grey line indicates the 15th percentile of grain size used as a model parameter (D_{15}) in the water erosion simulations. The grain size distributions for tunnel valleys in the central-northern North Sea were derived from geotechnical boreholes acquired in an area of HR3D seismic data coverage.

The rate of sediment deposition within the channel, \dot{D} (m s⁻¹), is:

$$\dot{D} = K_2 \frac{v_s}{\alpha_{cc}} \bar{c} \sqrt{\frac{g D_{15} (\rho_s - \rho_w)}{\tau_{cc}}} \quad (6.4)$$

where K_2 is a deposition constant (Walder and Fowler, 1994) and \bar{c} is the sediment concentration in subglacial waters which, following Zoet et al. (2019), was estimated from measurements of sediment concentrations in flood-stage rivers (Williams, 1989).

Following Carter et al. (2017), τ_{cc} , τ_k , and v_s are estimated as:

$$\tau_{cc} = \left| \frac{1}{8} f_{cc} \rho_w u_c^2 \right| \quad (6.5)$$

$$\tau_k = 0.025 D_{15} g (\rho_s - \rho_w) \quad (6.6)$$

$$v_s = D_{15}^2 \frac{2(\rho_s - \rho_w)g}{9\mu_w} \quad (6.7)$$

where f_{cc} is a channel roughness parameter (Carter et al., 2017), u_c is the channel water velocity and μ_w is the viscosity of water.

Many of the parameters governing the balance between erosion and deposition within the tunnel valleys can be constrained from the HR3D seismic data or from boreholes drilled into the tunnel valleys (Table 6.1), increasing the confidence in the calculated values of \dot{E} and \dot{D} . Nonetheless, some of the model parameters used in this chapter remain loosely constrained and thus the calculated rates should be treated as order of magnitude estimates to assess the likely timescales in which tunnel valleys form.

6.2.3.2 Testing scenarios of tunnel valley formation: outburst floods versus steady seasonal melt supply

Two scenarios of tunnel valley formation were tested by varying the magnitude and duration of meltwater input into the erosion model:

- (i) Outburst flooding: the hydrograph from the 1938 jökulhlaup at Grímsvötn (Björnsson, 1992) was used to simulate the erosive impact of a short, high magnitude outburst flood spread across a wide (500-m or 1000-m) channel. This flooding event released ~ 4 km³ of water over ~ 10 days, attaining peak discharges of $\sim 20,000$ m³ s⁻¹. A second scenario was also examined in which this flood hydrograph was upscaled to simulate the drainage of a 15-km³ lake over the same time period, attaining peak flow discharges of $\sim 80,000$ m³ s⁻¹.

These hydrographs represent some of the largest subglacial floods documented in observational records (Gudmundsson et al., 1995; Björnsson, 2002).

- (ii) Seasonal surface drainage: total annual surface melt, added to the steady-state basal melt rate from geothermal and frictional strain heating ($\sim 0.01\text{--}0.06\text{ m yr}^{-1}$), was input over a 4-month period to mimic the seasonal input of surface meltwater to the ice-sheet bed over an ablation season, such as is observed on the contemporary Greenland Ice Sheet (e.g., Banwell et al., 2016; Koziol and Arnold, 2018). When input into the subglacial hydrological system, water is routed within smaller 100-m wide channels.

The erosion model was applied to the areas of the ice sheet that experienced surface melting and it was assumed that all supraglacial meltwater propagates to the bed for the seasonal drainage scenario. Although surface meltwater can propagate to the bed through a variety of mechanisms which operate at different rates such as hydrofracturing, seasonally open moulins or through crevasses, these processes are accounted for in a simplified way by inputting surface meltwater at individual grid cells randomly distributed across the area where surface melting is predicted to occur. These input cells essentially operate as synthetic moulins distributed across the ice-sheet surface. The volume of surface meltwater input through each moulin is scaled so that moulins in areas of more negative surface mass balance receive a higher proportion of the total surface melt. For the seasonal scenario, a moulin density of 0.2 km^{-2} was chosen based on the observed distribution of moulins on the ablation zone of present-day Greenland during the summer melt season (Zwally et al., 2002; Colgan and Steffen, 2009; Banwell et al., 2016). Sensitivity of the model to moulin density was tested using densities of $0.05\text{--}0.8\text{ km}^{-2}$; however, this parameter was found to have little impact on the overall magnitude of subglacial discharge downstream (discharge typically varied by $\pm 12\text{--}20\%$, partly due to the randomised placement of moulins).

The modelling approach applied in this chapter assumes that the British-Irish and Fennoscandian ice sheets underwent substantial surface melting during deglaciation. This assumption is justified because modelled deglacial mass balances around the ice-sheet fringes are negative and are of the same order of magnitude as those recorded from regions of present-day Greenland where a substantial volume of surface meltwater is known to drain to the bed (e.g., Zwally et al., 2002; Das et al., 2008; Colgan and Steffen, 2009; Selmes et al., 2011; Leeson et al., 2015; Chudley et al., 2019; Mouginit et al., 2019).

A nested modelling approach was taken whereby subglacial water fluxes resulting from basal melting within the interior of the ice sheet were first calculated at a 1500-m

resolution. The steady-state discharges resulting from basal melt were then input to the edges of a high-resolution 50-m grid covering the ice-sheet ablation zone. Subglacial discharges generated from basal melting were added to the water input derived from surface melt and routed through the finer-scale grid. The resulting subglacial discharges were then used to calculate tunnel valley erosion rates using Equations 6.3 and 6.4. Water inputs from surface melting were typically 3–5 orders of magnitude greater than those from basal melting in the ablation zone of the ice sheet.

A high-resolution (50-m grid) water routing case study was conducted over northern Denmark as the chronology of Weichselian tunnel valley incision is well constrained there (Sandersen et al., 2009). This chronological information allows the different models of tunnel valley formation to be tested in order to investigate which mechanism can achieve the rapid incision rates inferred for 18–19 ka (Sandersen et al., 2009). An initial model run was conducted to assess broad-scale water routing pathways. Water routed along these pathways was assumed to erode channels over time (concurrent with palaeo observations; e.g., Mooers, 1989; Praeg, 1996; Kehew et al., 2012). The maximum length of the channels was defined as the limit at which channelised subglacial discharge no longer exceeded 20 times the average value of the neighbouring cells. Artificial channels with specified widths of 100 m, 500 m and 1000 m were then incised by ~30 m into the isostatically corrected bed topography. These depressions route the majority of the input meltwater into these channels, permitting the erosion rates within the channels to be calculated and the different formation hypotheses relating to water discharge, flow duration and channel size to be tested.

Table 6.1. Definitions, values and sources of parameters used throughout the text.

Symbol	Parameter	Value [units]	Source
α_{cc}	Channel geometry factor	5500–233,000 [unitless]	Carter et al. (2017); HR3D seismic measurements
\bar{c}	Sediment concentration in water	1500 mg L ⁻¹	Observations from flood stage rivers (Williams, 1989)
\dot{D}	Deposition rate	[m s ⁻¹]	Model output
D_{15}	15 th percentile grain size	0.01–0.1 mm	Borehole measurements; Figure 6.3
\dot{E}	Erosion rate	[m s ⁻¹]	Model output
f_{cc}	Channel roughness parameter	0.07 m ^{-2/3} s ²	Carter et al. (2017)
g	Acceleration due to gravity	9.81 m s ⁻²	Constant
h	Bed elevation	[m]	BRITICE-CHRONO model output; EMODnet bathymetry
k	Uniform floatation factor	0.925 [unitless]	(Banwell et al., 2013; Lindbäck et al., 2015; Shackleton et al., 2018)
K_1	Erosion constant	0.1 [unitless]	Walder and Fowler (1994)
K_2	Deposition constant	6 [unitless]	Walder and Fowler (1994)
m	Manning coefficient	0.025 m ^{-1/3} s	Constant
ρ_i	Density of ice	918 kg m ⁻³	Constant
ρ_s	Density of sediment	2150 kg m ⁻³	Borehole measurements
ρ_w	Density of water	1000 kg m ⁻³	Constant
Q_{max}	Maximum tunnel valley carrying capacity	[m ³ s ⁻¹]	Calculated
S	Channel cross-sectional area	[m ²]	HR3D seismic measurements
τ_{cc}	Channel bed shear stress	[Pa]	Calculated
τ_k	Critical shear stress	[Pa]	Calculated
u_c	Channel flow velocity	[m s ⁻¹]	Water routing model output
μ_w	Viscosity of water	1.78e ⁻³ Pa s	Constant
v_s	Mean sediment settling velocity	[m s ⁻¹]	Calculated
Z	Ice thickness	[m]	BRITICE-CHRONO model output
ϕ	Hydraulic potential	[Pa]	Calculated from BRITICE-CHRONO model output
ϕ'	Hydraulic potential gradient	[Pa m ⁻¹]	Calculated from BRITICE-CHRONO model output

6.3 Results

6.3.1 Tunnel valley morphology and discharge

The seven HR3D datasets from the North Sea image 23 cross-cutting elongate incisions, previously interpreted as tunnel valleys (Kirkham et al., 2021). The tunnel valleys are 300–3000 m wide, up to 300 m deep, 10,000–100,000 m² in cross-sectional area, with typical side slopes of 15–40°. The valleys are generally 5–10 times wider than they are deep. Many tunnel valleys are characterised by a narrow V-shaped base and a wider upper cross section (Figure 6.4A). Terraces are sometimes present adjacent to the boundary of the V-shaped incision. Several tunnel valleys also contain chaotic and displaced reflections at their sides and bases, which correspond to slumping and faulting along the sides of the features (Figure 6.4B). Where present, the slumps constitute between ~8–41 % of the tunnel valley infill by cross-sectional area and have slope angles at their outer boundaries of 10–42°.

The mass movements present within the tunnel valleys are sometimes associated with subtle curvilinear ridges which appear as distinct anomalies in seismic coherence attribute analyses (Figure 6.5A, 6.5B). The ridges have symmetrical cross-sections, are often cusped or sinuous in form, and run parallel to the tunnel valley edges. Two subsets of ridge types are identified: the first are 5–8 m high, ~80 m wide and up to 1500 m long (Figure 6.5F). They occur towards and along the edges of the tunnel valleys. The second type of ridge is similar in morphology but is lower in amplitude at <2 m high, 20–50 m wide and up to 600 m long, with an intra-ridge spacing of ~60 m (Figure 6.5F). This type of ridge occurs further from the tunnel valley centre than the first subset of ridges. Sharp and continuous breaks in the seismic reflections beneath the ridges demonstrate that these landforms represent the top surface of retrogressive rotational slope failures within the tunnel valleys (Figure 6.5C). Their morphology is nearly identical to the so-called ‘glacial curvilineations’ (GCLs) identified in Poland and in North America (Figures 6.5D, 6.5E, 6.5F; Lesemann et al., 2010b; Clark and Livingstone, 2018; Adamczyk et al., 2022), suggesting that these are the first subsurface examples of these features to be identified.

The tunnel valleys identified in the HR3D seismic data are characterised by undulating thalwegs (Figure 6.6A) and sometimes contain smaller channels, both individual and organised in networks, incised into their bases (Figures 6.6A, 6.6B, 6.6C). When organised in networks, these smaller channels diverge around bar-like features that are 55–540 m long and 30–165 m wide; the bars are typically narrower than the channels which intersect them. Most of the smaller channels present within the tunnel valleys are

80 m wide and ~6 m deep on average, although some attain widths of up to 250 m and depths of 15 m; they are typically ~5–10 times narrower and 3–15 times shallower than the tunnel valleys in which they are located. These smaller channels are relatively straight with sinuosity indexes <1.4, and sometimes appear to have been abandoned in favour of a more recently incised channel (Figures 6.6A, 6.6C). Under ice-surface slopes typical of the margins of contemporary and palaeo ice sheets, these smaller channels present at the base of some valleys could carry discharges of up to $18,000 \text{ m}^3 \text{ s}^{-1}$ if filled to the bankfull level. In contrast, the entire tunnel valley structures, being several orders of magnitude larger in cross-sectional area, could potentially carry discharges of $0.5\text{--}2 \times 10^7 \text{ m}^3 \text{ s}^{-1}$ if filled to their bankfull capacity.

At the resolution of the HR3D seismic data, the tunnel valleys do not contain any evidence for streamlined ice flow, such as glacial lineations, at their bases or within their infill. However, in one HR3D seismic dataset, elongate bedforms are present adjacent to a tunnel valley (Figures 6.7A, 6.7B). The bedforms are <8 m high, up to 130 m wide (average = 58 m) and taper with distance away from the tunnel valley (Figures 6.7B, 6.7C). They are up to 650 m long (average = 404 m) but extend beyond the boundaries of the HR3D seismic datasets in some cases, making their true length difficult to assess. The bedforms are distinct from GCLs as they are oriented oblique rather than parallel to the tunnel valley sides, are less sinuous in form, and taper with distance away from the tunnel valley. Their tapered morphology and elongation ratios of 5–10:1 are similar to other streamlined subglacial bedforms such as crag-and-tails or drumlins (Ely et al., 2016; Fransner et al., 2016), indicating that they are the imprint of fast-flowing ice over the substrate (Stokes and Clark, 2002). The continuation of the seismic reflection corresponding to the streamlined bedforms within the tunnel valley possibly suggests that they formed at a time when the tunnel valley was operating (Figure 6.7D).

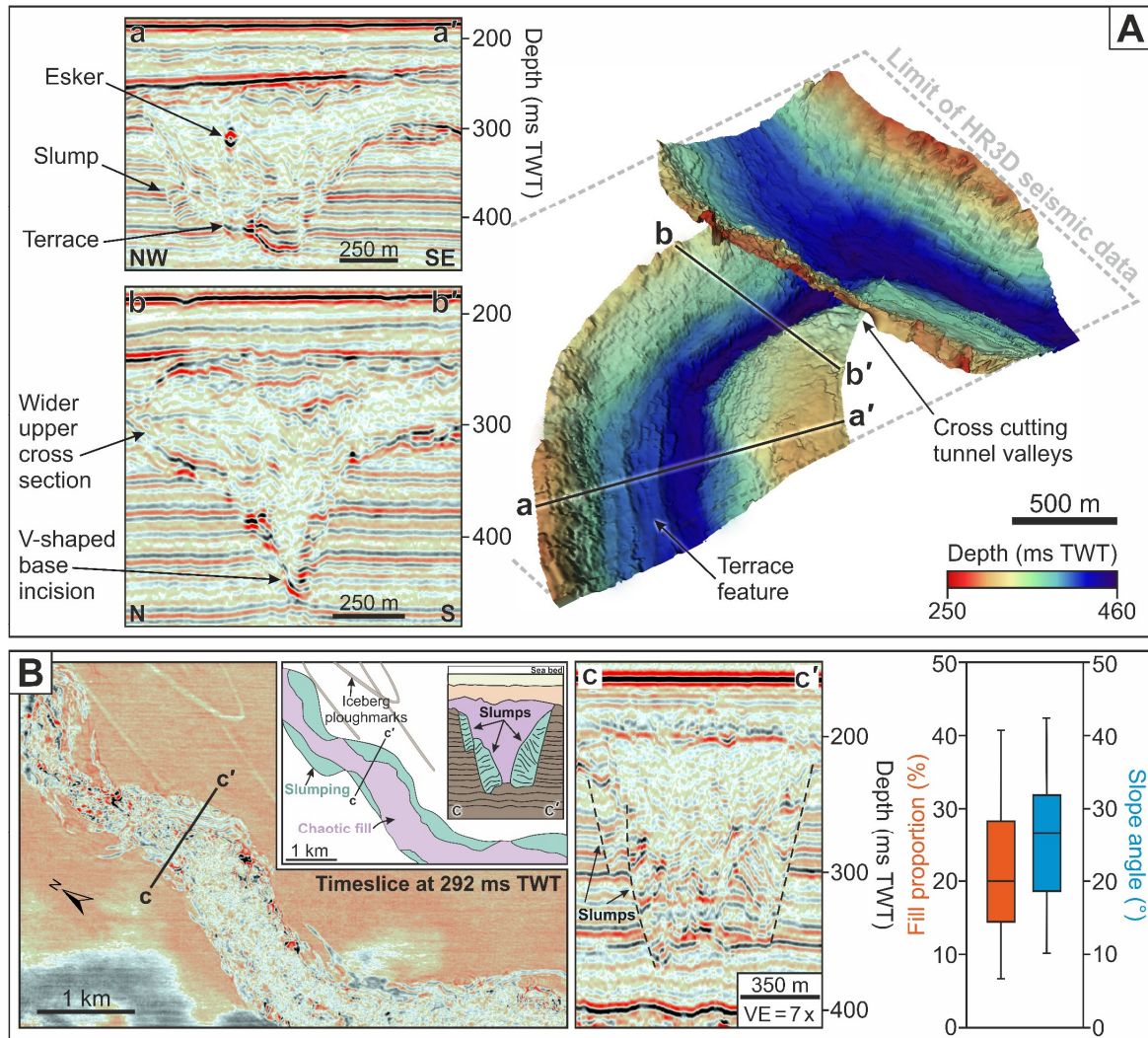


Figure 6.4. Tunnel valley morphology imaged using high-resolution 3D seismic data. (A) Cross cutting tunnel valleys with a V-shaped base and broader upper cross section. The tunnel valleys contain features such as eskers within their infill, sediment slumps along their sides and sometimes terrace-like features like the one shown here near the base of the valley. (B) Examples of substantial mass movements contained within a tunnel valley. Boxplots indicate the proportion of tunnel valley infill comprised of slumped material and the slope angles of mass movements found within the tunnel valleys. VE—vertical exaggeration.

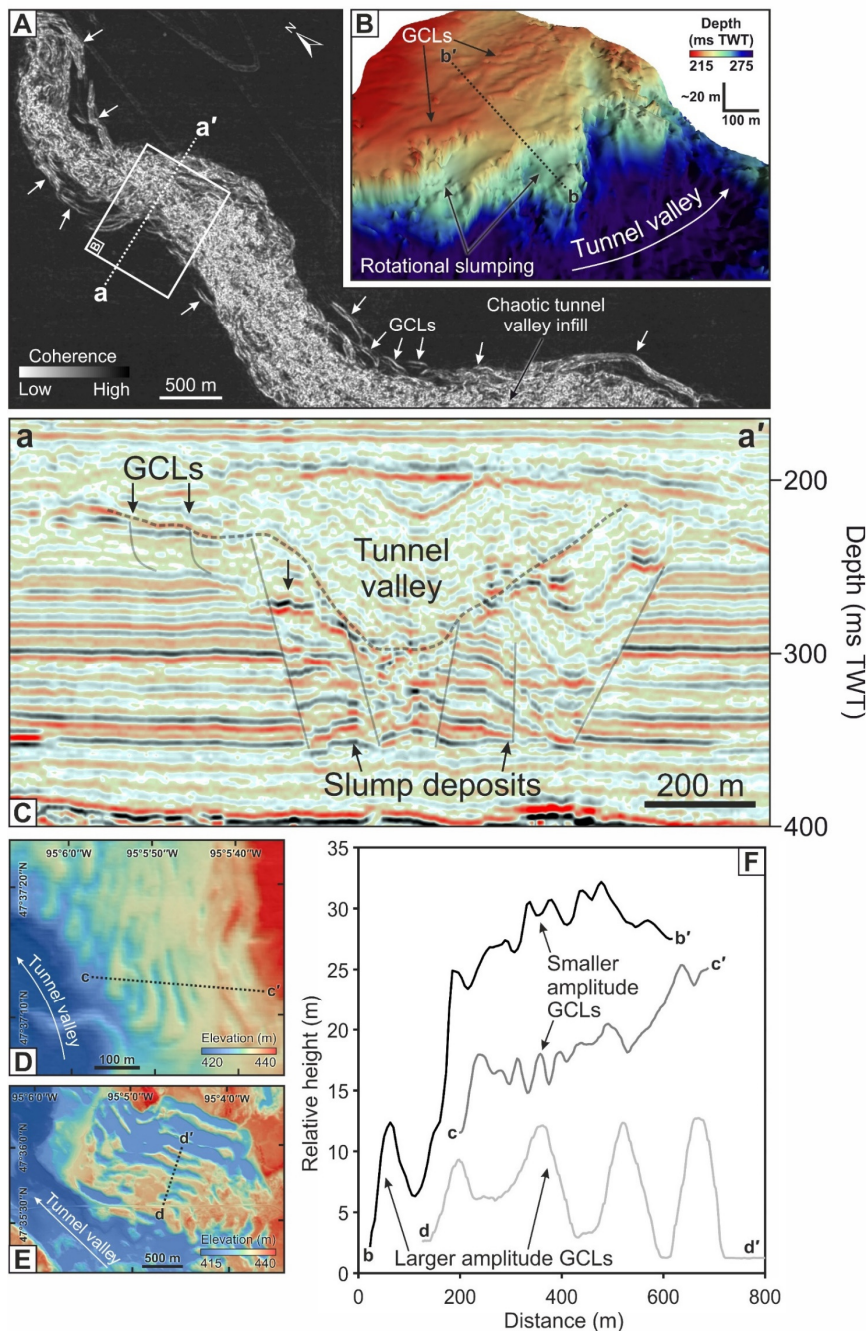


Figure 6.5. Buried glacial curvilinearations (GCLs) imaged within tunnel valleys. (A) Timeslice of seismic coherence at 290 ms TWT displaying curvilinear seismic anomalies (GCLs) along the sides of a tunnel valley in high-resolution 3D seismic data. (B) Oblique view of a picked seismic surface displaying GCLs and rotational slump scars along the tunnel valley sides. (C) Seismic section displaying the location of GCLs, slump deposits and faulting (semi-transparent lines) within the tunnel valley. (D, E) Examples of terrestrial GCLs in North America identified by Clark and Livingstone (2018) using the USA’s national elevation dataset (NED) (<http://nationalmap.gov/elevation.html>). (F) Profiles of relative height across the GCLs present within the tunnel valley compared to terrestrial examples in North America.

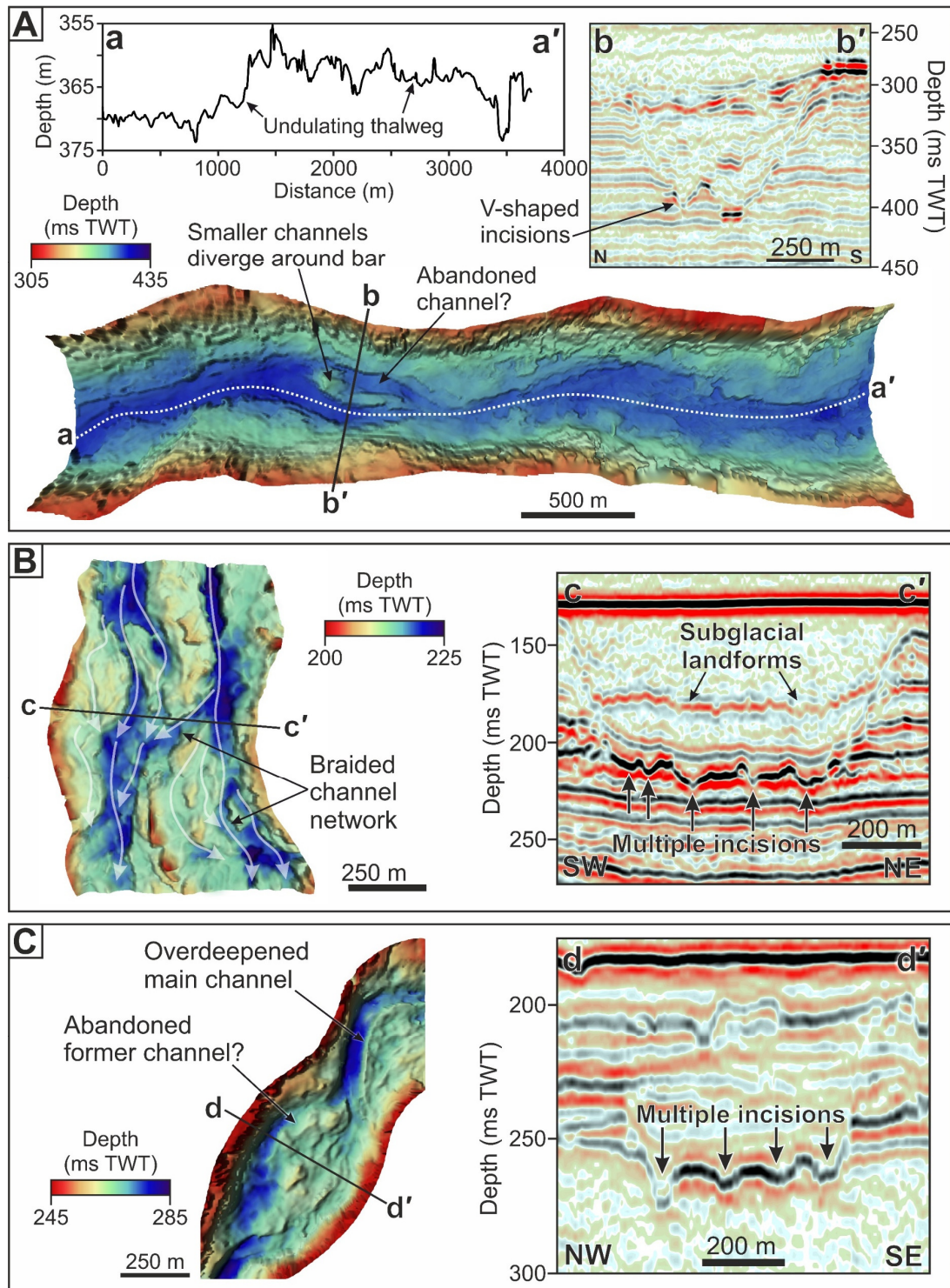


Figure 6.6. Smaller channel systems comprising the base of some tunnel valleys. (A) Base of a tunnel valley displaying smaller channelised V-shaped incisions which diverge around a bar-like feature where a previous channel has been abandoned. The channel thalweg undulates. (B) System of braided channels incised into the base of a tunnel valley. The tunnel valley also contains subglacial landforms buried midway within its infill (see Fig. 3C in Kirkham et al., 2021). (C) Overdeepened channel system at the base of a tunnel valley demonstrating abandonment of a previous channel.

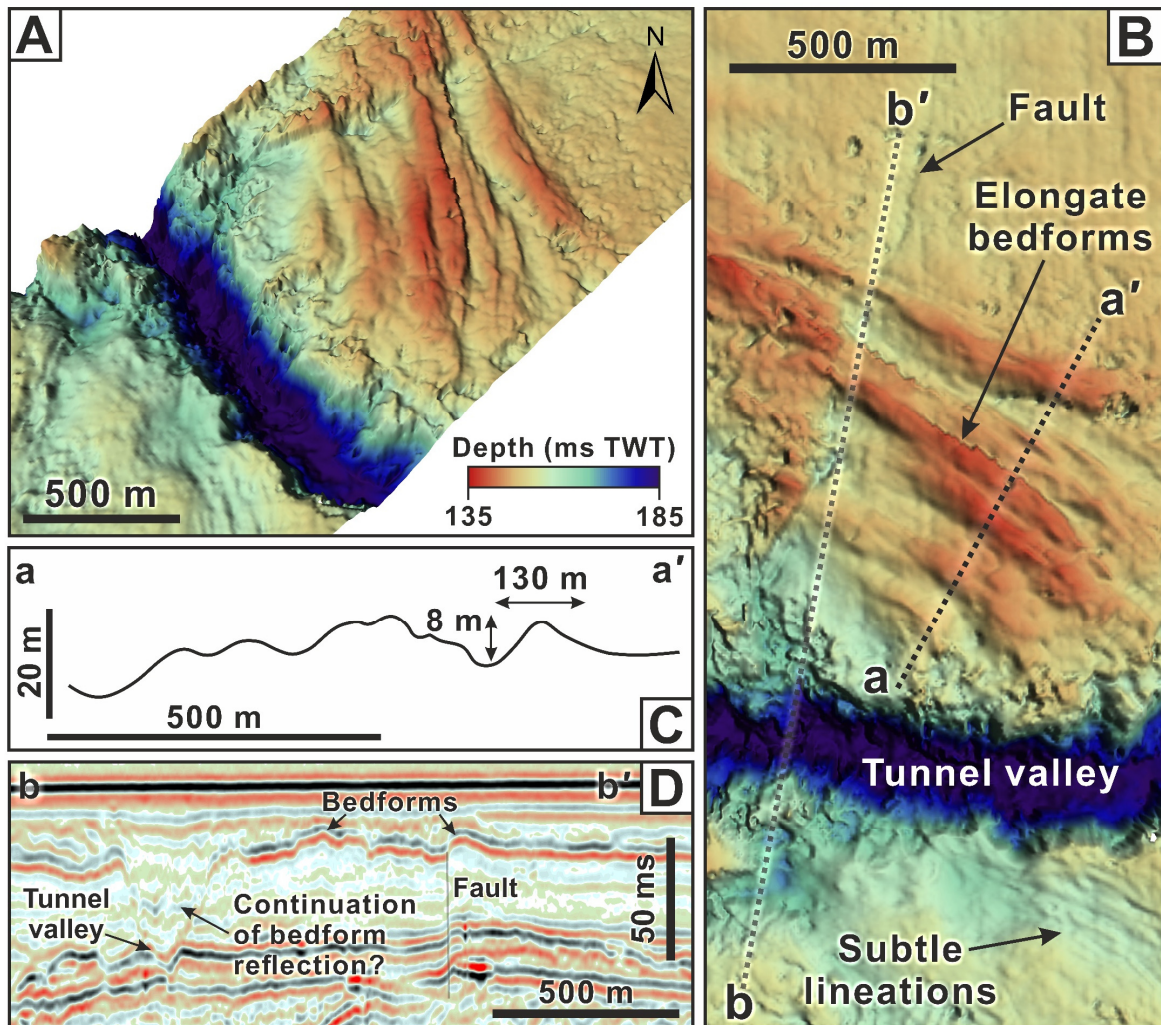


Figure 6.7. Elongate bedforms present adjacent to a tunnel valley. (A) Oblique and (B) plan view of the tunnel valley and onset of the bedforms. (C) Depth-converted profile across the bedforms displaying a series of undulations corresponding to each ridge. (D) Seismic section across the tunnel valley and bedforms — note the continuation of the bedform reflection midway within the tunnel valley infill.

6.3.2 Modelled water routing

The modelled steady-state subglacial water discharges for the British-Irish and Fennoscandian ice sheets as they grew, coalesced, and retreated across the North Sea between 27 ka and 18 ka is shown in Figure 6.8. A large proportion of the ice-sheet bed is predicted to be at the pressure melting point, except at the 21 ka full-glacial time when the majority of the bed beneath the ice sheet in its interior was frozen (white areas). Basal melt rates are, unsurprisingly, predicted to be greatest along fast-flowing ice streams that drain the interior of the ice sheets, attaining rates of 10–60 mm yr⁻¹; these rates are similar to basal melt rates predicted beneath Antarctic ice streams during the Last Glacial Maximum (Golledge et al., 2012; Golledge et al., 2013).

The relatively smooth inferred topography of the central North Sea Plateau provides few opportunities for water to pool, although some water ponding does occur in the Norwegian Channel and in some locations around the terrestrial margins of the UK (Figure 6.8). Instead, hydraulic potential gradients force water towards the ice-sheet margins, forming long dendritic to linear channel networks which flow away from the main ice sheet accumulation centres. Large basal topographic features, such as the Norwegian Channel, also act to steer subglacial water flow. The main pathways of water routing remain relatively consistent throughout deglaciation (Figure 6.8).

The ice-sheet configuration at 27 ka, during ice-sheet build-up, is characterised by low subglacial water discharges of $<0.01 \text{ m}^3 \text{ s}^{-1}$ in its interior where water is derived from basal melting alone. Some surface melting occurs around the fringes of the ice sheet, yielding steady-state subglacial discharges of $1\text{--}2 \text{ m}^3 \text{ s}^{-1}$ if the surface meltwater is assumed to propagate continuously to the bed (Figure 6.8A). Similarly, little to no basal melting is predicted for the interior of the ice sheet during the Last Glacial Maximum at 21 ka, when grounded ice extends fully across the North Sea. Subglacial discharges are $<1 \text{ m}^3 \text{ s}^{-1}$ around the ice sheet periphery despite the cumulative basal melt flux being routed there over long distances from the interior. However, steady-state subglacial discharges at 21 ka increase by orders of magnitude in areas where surface melt is predicted to occur, reaching $5\text{--}10 \text{ m}^3 \text{ s}^{-1}$ in some areas around the fringes of the ice sheet (Figure 6.8B).

The extent and magnitude of melting increases as the ice sheet begins to deglacierate at 19 ka, resulting in subglacial discharges of $5\text{--}15 \text{ m}^3 \text{ s}^{-1}$ in areas of prominent surface melting (Figure 6.8C). Substantial surface melting around the fringes of the retreating ice sheet occurs at 18 ka, generating steady-state subglacial discharges of $10\text{--}100 \text{ m}^3 \text{ s}^{-1}$ near the ice-sheet margin (Figure 6.8D). Basal melt rates remain similar to other timeslices. Where present, subglacial discharges of water concentrated into channelised flow paths are generally $<1 \text{ m}^3 \text{ s}^{-1}$ across the interior, whereas water is routed along the Norwegian Channel at rates of $5\text{--}10 \text{ m}^3 \text{ s}^{-1}$. In the higher resolution case study region of northern Denmark (Figure 6.9), the analysis presented in this chapter reveals that meltwater inputs from the surface, combined with basal melt passed down from the wider catchment, forms networks of $10\text{--}70 \text{ km}$ long channels (Figures 6.9C) that are semi-regularly spaced $\sim 1\text{--}12 \text{ km}$ apart (Figure 6.9D).

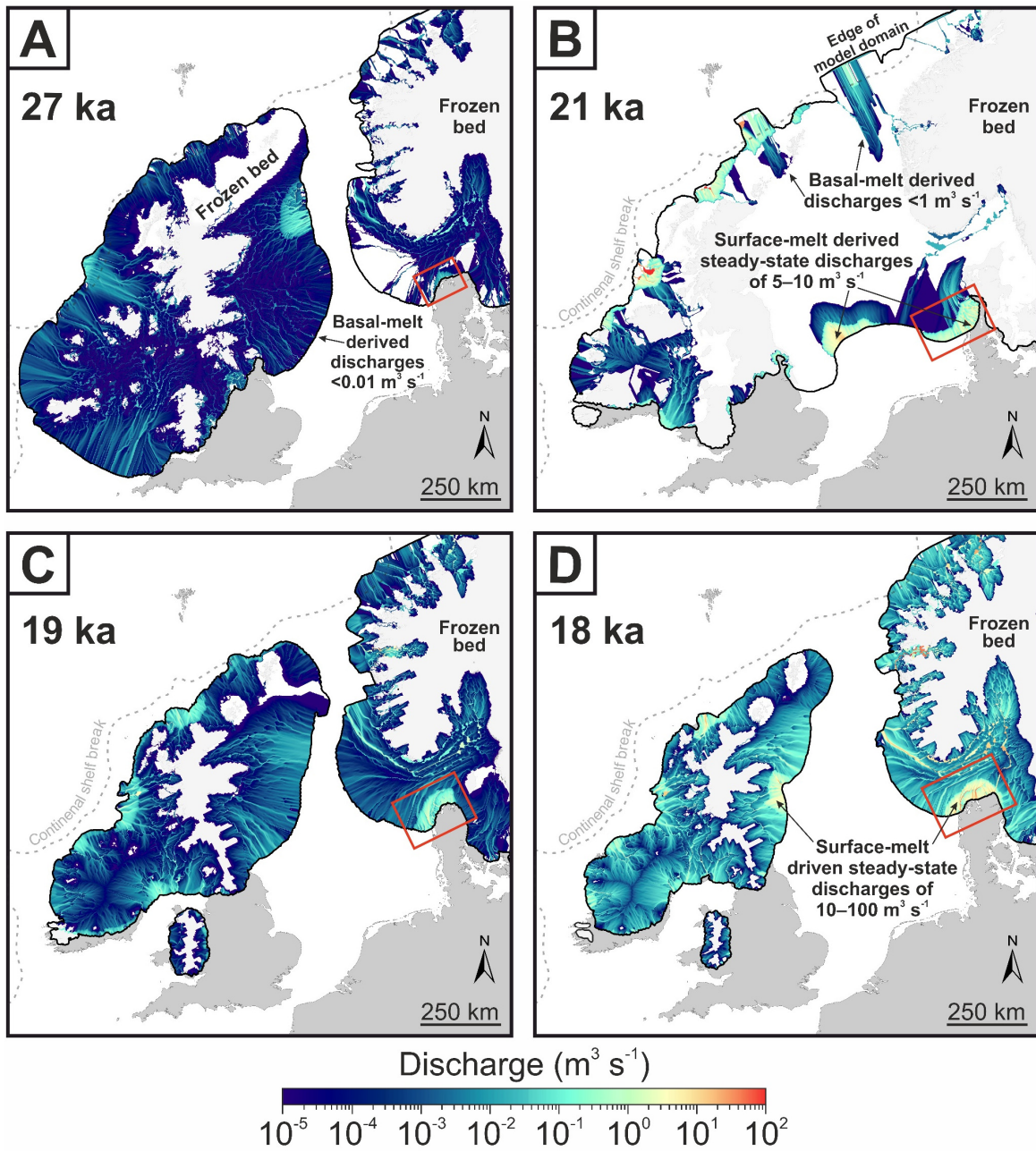


Figure 6.8. Modelled water flow paths and fluxes beneath the British-Irish and Fennoscandian ice sheets. Subglacial water routing and discharge beneath grounded ice calculated at a 1500-m grid resolution at (A) 27 ka, (B) 21 ka, (C) 19 ka, and (D) 18 ka before present day timeslices. Areas of cold-based ice are displayed in white. Stippled grey line indicates the continental shelf break. Inset red boxes display the location of the high-resolution (50-m) model runs conducted across the northern Denmark for each timeslice.

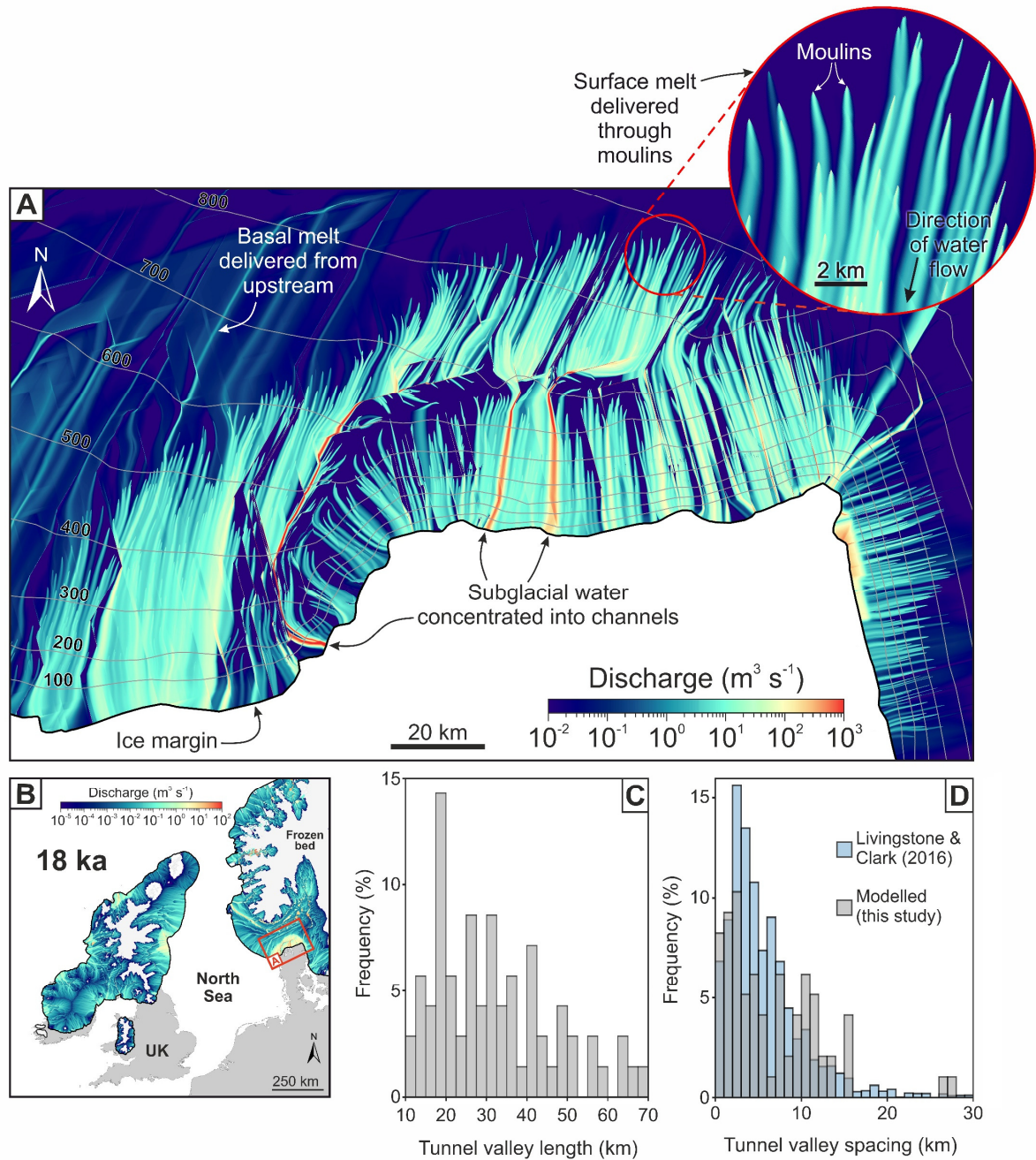


Figure 6.9. Example of a detailed subglacial water routing model run and resulting tunnel valley properties. (A) A 50-m resolution subglacial water routing model run across northern Denmark at 18 ka, displaying the distribution of surface meltwater delivered to the ice-sheet bed through synthetic ‘moulins’ (inset) and the resulting subglacial channels predicted by the model. Contour lines display ice thickness. Panel B displays the location of (A) in the context of the broader water routing modelling run at a 1500-m resolution; note the change in scale bar limits from the main panel. (C) Distribution of the lengths of the simulated tunnel valleys in the high-resolution 50-m model runs between 18 ka–27 ka. (D) Distribution of tunnel valley spacing simulated in the high-resolution 50-m model runs between 18 ka–27 ka compared to those of terrestrial tunnel valleys in North America (from Livingstone and Clark (2016)).

6.3.3 Tunnel valley erosion

6.3.3.1 Erosion from seasonal surface drainage

Erosion rate experiments were run over the region of northern Denmark shown in Figures 6.8 and 6.9A where the high-resolution modelling (50-m grid) of subglacial water flow was conducted. In the seasonal surface drainage scenario, it was assumed that all meltwater propagates to the bed of the ice sheet over a 4-month drainage season where it is routed through networks of 100-m wide channels similar to those observed in the HR3D seismic data (Figure 6.6). This results in average input discharges per moulin of 1–4 m³ s⁻¹ at 27 ka, 5–10 m³ s⁻¹ at 21 ka and 10–20 m³ s⁻¹ at 18 ka and 19 ka. Water discharges are greatest near the ice-sheet margin as the inputs from multiple moulins coalesce, resulting in average channel discharges of <20 m³ s⁻¹ for the 27 ka model run, 50–300 m³ s⁻¹ at 21 ka, and 50–900 m³ s⁻¹ for 18 ka and 19 ka timeslices.

When routed through 100-m wide channels, erosion generally exceeds deposition within the channels for the 18 ka, 19 ka, and 21 ka model runs. However, deposition dominates at 27 ka, especially for coarser ($D_{15} = 0.1$ mm) grain-size distributions due to the relatively low water discharges at this timeslice (Figure 6.10A). It is possible to achieve a small amount of erosion with finer grain size distributions ($D_{15} = 0.01$ mm) within 10 km of the ice-sheet terminus (Figure 6.10E); however, erosion rates remain extremely low (up to 1.2×10^{-6} m d⁻¹) and deposition dominates further up-ice. Thus, little subglacial meltwater erosion is possible at 27 ka.

Channel erosion dominates in the 21 ka simulations. The median erosion rate within the channels increases by up to two orders of magnitude from the start of a channel to positions near the ice-sheet terminus. The last 50 % of the tunnel valley length near the ice-sheet terminus is the most erosive; this corresponds to lengths of ~25–35 km from the ice-sheet margin. Median erosion rates near the ice-sheet terminus are ~0.003 m d⁻¹, with a 75th percentile value of ~0.02 m d⁻¹, and maximum erosion rates of 0.22 m d⁻¹ are calculated for D_{15} grain sizes of 0.1 mm. Reducing the D_{15} grain size parameter to 0.01 mm (medium–fine silts) lowers erosion rates by approximately an order of magnitude (Figures 6.10B, 6.10F). The highest erosion rates are calculated for the 18 ka and 19 ka timeslice model runs. For D_{15} grain sizes of 0.1 mm (very fine sands), median erosion rates near the terminus are ~0.005 m d⁻¹, with a 75th percentile value of ~0.05 m d⁻¹, although erosion rates of up to 0.7 m d⁻¹ are calculated for some channels (Figures 6.10C, 6.10D, 6.10G, 6.10H).

The erosion rates calculated in this chapter (Figure 6.10) would be capable of incising shallow channels into a sedimentary substrate over the course of one melt season during deglaciation. For example, the 75th percentile erosion rate of 0.05 m d⁻¹ at 18 ka and 19 ka would erode a channel ~6 m deep and 100 m wide in a single ablation season. Thus, it would take ~300 years to carve a valley with similar dimensions (1 km wide, 180 m deep) to those observed in northern Denmark or the North Sea if this smaller channel migrated laterally each melt season. Typical median incision rates (0.003–0.005 m d⁻¹) would result in valley formation within ~5,000 years. It is therefore possible to incise large meltwater channels within tens of kilometres of the ice-sheet margin from seasonal surface melt alone over time periods of just hundreds to a few thousands of years.

6.3.3.2 Erosion from outburst floods

When routed down a 500-m wide flood channel, the 10-day drainage of a 4 km³ lake results in total downward erosion of ~0.5–4 m into a sedimentary substrate depending on the grain-size distribution chosen. Scaling this up to the 15 km³ lake drainage scenario, a 500-m wide channel would be eroded downwards by several tens of metres over the 10-day period. However, the erosive impact of these flooding events reduces substantially when the channel width is increased to 1000 m owing to a significant reduction in average water velocity across the channel cross section. In this latter (1000-m wide channel) scenario, total erosion reaches up to ~0.1 m for the 4 km³ lake drainage, and up to 4 m of downward erosion is achieved for the 15 km³ lake drainage scenario.

The basal melt rates calculated from the model reconstructions are up to 10–60 mm yr⁻¹ during the last glacial period, resulting in basal water fluxes that are generally below 0.5 m³ s⁻¹ (Figure 6.8). At these values, minimum lake refilling times are ~250 years for a 4 km³ lake and ~950 years for a 15-km³ lake if the lakes were refilled by basal melting alone. Assuming that the lakes drain when filled to full capacity, it would therefore take ~6000 years to carve a 500-m wide, 100-m deep tunnel valley from a 4 km³ lake, or ~4000 years for a 15 km³ lake. Wider valleys (>1000 m) would take considerably longer to form.

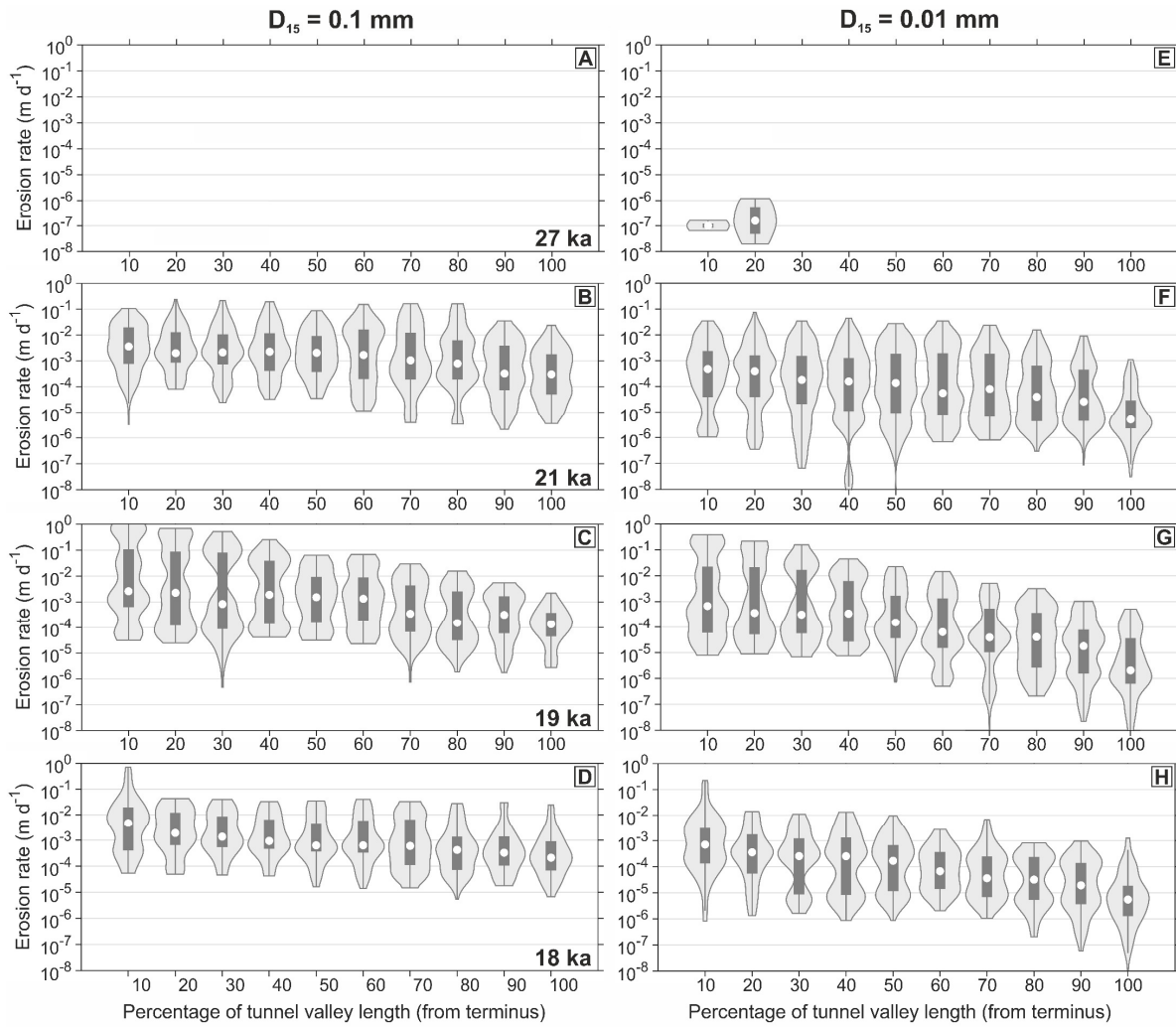


Figure 6.10. Tunnel valley erosion rates into a sedimentary substrate as a proportion of modelled tunnel valley length for the seasonal drainage mechanism (migrating 100 m wide channels). Results are shown for the different model timeslices between 18 ka and 27 ka and D_{15} grain sizes of 0.1 mm and 0.01 mm (A–D and E–H).

6.4 Discussion

6.4.1 Morphological insights into tunnel valley incision processes

Examination of detailed tunnel valley morphology in the HR3D seismic data yields the following observations: (i) the basal portion of tunnel valley cross sections are often several times narrower and more V-shaped compared to the upper cross sections, which are typically more U-shaped (see profile b–b' in Figure 6.4A); (ii) steep slump deposits are often buried inside the tunnel valleys and, when present, comprise ~10–40 % of their infill; (iii) subglacial landforms formed by grounded ice are often buried within the middle of the tunnel valley infill (Kirkham et al., 2021); (iv) networks of smaller channels are sometimes resolvable at the base of the tunnel valleys, typically ~5–10 times narrower and 3–15 times shallower than the larger tunnel valley tracts in which they are situated. Many of these features cannot be resolved using conventional 3D seismic-reflection methods, so the processes they represent may have previously been overlooked in models of tunnel valley genesis (Kirkham et al., 2021).

The composite V/U shaped channel cross-sectional morphology is a commonly observed feature of tunnel valleys incised into unconsolidated sediments and subglacial meltwater channels incised into bedrock (e.g., Hepp et al., 2012; Kirkham et al., 2019; Larter et al., 2019; Kirkham et al., 2020; Lohrberg et al., 2020; Hogan et al., 2022) and likely reflects widening of the upper channel cross section by ice which deformed downwards into the top of the channel. The movement of deforming basal ice through the upper parts of the tunnel valley, or the eventual removal of ice from the valley, may have acted to destabilise the valley sides and trigger the mass movements now contained within the tunnel valleys, enlarging their lateral extent through glacial erosion. This morphology suggests that grounded ice likely persisted within the tunnel valleys as they were incised and filled, and is supported by the deposition of subglacial landforms such as eskers and crevasse squeeze ridges within their infill (Kirkham et al., 2021). Many of these landforms are buried at depths of more than 100 m from the tunnel valley top; based on this, it can be inferred that as much as 65–75 % of the tunnel valley cross section was filled with and sculpted by grounded ice. Ice contact erosion therefore plays an important role in excavating and widening tunnel valleys in unconsolidated sediments.

No deformation structures are resolved along the base and sides of the channels which would suggest that sediment creep into low pressure channels is responsible for the formation of the tunnel valleys (Figure 6.1C; Shoemaker, 1986; Boulton and Hindmarsh, 1987; Mooers, 1989) although it is possible that these features may be unresolvable even in the HR3D seismic data used in this chapter. A similar lack of evidence for extensively

deformed sediment adjacent to tunnel valleys has been reported from terrestrial outcrops (Ó Cofaigh, 1996; Jørgensen and Sandersen, 2006; Kehew et al., 2012). By contrast, the composite V/U-shaped profile of many tunnel valley cross sections (Hepp et al., 2012; Lohrberg et al., 2020; Figure 6.4A), combined with the presence of slump deposits and subglacial landforms buried midway inside the tunnel valley fills (Kirkham et al., 2021), indicate that basal ice likely deformed extensively into the valleys. This process would be conducive to maintaining consistently high water pressures as the tunnel valleys were incised, even after relatively large channel dimensions were attained. The persistent pressurisation of the water at the base of the tunnel valleys by overlying ice, combined with the unconsolidated nature of the sediments into which tunnel valleys are usually incised, may explain how these features attain such characteristically large depths (up to ~500 m deep) (e.g., Praeg, 2003; Montelli et al., 2020). Relatively high basal water pressures within the tunnel valleys also concur with observations gathered from terrestrial outcrops of sediment injections into the preglacial substrates underlying tunnel valleys (e.g., Ghienne et al., 2007; van der Vegt et al., 2012; Ravier et al., 2014).

Relatively high basal water pressures within the tunnel valleys are also supported by the presence of smaller channel networks located at the base of the features (Figure 6.6). It is not clear whether the smaller channel networks observed inside some tunnel valleys indicate that the tunnel valleys experienced pulses of high water discharges released from dammed lakes or from the ice-sheet surface (Lewington et al., 2020; Bellwald et al., 2021) or may simply reflect the expected mechanism for subglacial water flow over unconsolidated thick sedimentary beds (Walder and Fowler, 1994), such as those comprising the North Sea Basin (Lamb et al., 2018; Ottesen et al., 2018; Ottesen et al., 2020). Similar braided channel structures have been replicated in laboratory experiments simulating pressurised water flow over an erodible non-cohesive bed (Catania and Paola, 2001). However, the abandonment of smaller channels in favour of others within some tunnel valleys (Figures 6.6A, 6.6C) may suggest that the smaller channel networks reflect lateral switching between different channels. This abandonment and wandering behaviour has been observed in laboratory experiments of tunnel valley formation (Lelandais et al., 2016), and may be analogous, albeit on a smaller scale, to the ‘cut-and-fill’ structures reported inside some terrestrial tunnel valleys (Jørgensen and Sandersen, 2006). These observations are consistent with the gradual incision of a much larger tunnel valley tract through focussed, yet relatively small, fluxes of water rather than incision by catastrophic floods.

6.4.1.2 The origin of glacial curvilineations

Glacial Curvilineations (GCLs) were first identified in Poland (Nechay, 1927) and were later genetically associated with tunnel valleys based on their typical parallelism to the valley sides (Lesemann et al., 2010b). Two competing theories have been suggested to explain the origin of GCLs in relation to tunnel valley formation. The first suggests that GCLs represent the erosional remnants of longitudinal vortices in water flow that developed during catastrophic outburst floods that produced the tunnel valleys (Lesemann et al., 2010b; Lesemann et al., 2014). However, abrupt changes in observed GCL direction which mimic the tunnel valley edge are difficult to reconcile with this hypothesis as the vortices would become disrupted with such sudden changes in flow routing direction (Clark and Livingstone, 2018). This observation led Clark and Livingstone (2018) to propose an alternative hypothesis in which GCLs form through incremental mass movements at the sides of the tunnel valleys. In this hypothesis, GCLs reflect the widening of tunnel valley sides through slope failures. However, this hypothesis was proposed solely on the basis of morphological properties, and the authors note that further structural and sedimentological information is required to determine the origin of GCLs.

The HR3D seismic data examined in this chapter allow the formation of GCLs to be definitively linked to slope failure processes along the sides of tunnel valleys (Figure 6.5C). The largest GCLs observed within the tunnel valleys are associated with bulbous headwall scarps as described in other locations (Figure 6.5B; Clark and Livingstone, 2018). Sharp breaks in seismic reflections beneath these ridges demonstrate that they formed through retrogressive rotational slope failures, propagating from the centre of the tunnel valley toward its sides, resulting in localised valley widening. The smaller ridges reflect a continuation of the same process, but with less disruption to the underlying sediments, as the slope failures began to stabilise with increasing distance from the tunnel valley centre. The Polish and North American examples of GCLs occur within tunnel valleys that are not entirely infilled, making it difficult to untangle the timing of their formation relative to tunnel valley incision and infilling. HR3D seismic data demonstrate that the formation of the GCLs occurred prior to tunnel valley infilling, linking slope destabilisation and failure to tunnel valley downcutting. The formation of GCLs through slope failure of the underlying strata is also consistent with the variable internal composition of these features on land (Lesemann et al., 2014), implying that their composition will change according to the underlying substrate type rather than reflecting their formative process. The HR3D seismic data therefore strongly support the association between GCL genesis and slope failures triggered in response to tunnel valley

incision, rather than the alternative interpretation in which broad sheet-like floods are invoked to explain their formation.

6.4.2 Mechanisms and rates of tunnel valley erosion

The results presented in this chapter demonstrate that the contribution of basal melt to the subglacial hydrological system is generally small, often 3–5 orders of magnitude smaller than the contribution from surface melting in the ablation zone. Accordingly, steady-state water fluxes derived from basal melting alone are too low (typically $<1 \text{ m}^3 \text{ s}^{-1}$) to facilitate tunnel valley erosion. This finding is consistent with ideas about channel erosion beneath past ice sheets elsewhere (e.g., Lowe and Anderson, 2003; Nitsche et al., 2013; Dowdeswell et al., 2016a; Kirkham et al., 2019). The dimensions of the smaller channel networks within the tunnel valleys constrain the likely discharges responsible for valley incision. At 80 m wide and ~ 6 m deep on average, the smaller channels could carry a maximum discharge of $\sim 18,000 \text{ m}^3 \text{ s}^{-1}$ if filled to the bankfull level beneath a steep ice-sheet margin. Channels of these dimensions would be capable of accommodating small outburst floods from trapped lakes, such as the 4 km^3 lake drainage scenario (peak discharge of $\sim 20,000 \text{ m}^3 \text{ s}^{-1}$). Alternatively, these smaller channel networks might reflect the cumulative erosive imprint of seasonal surface meltwater drainage. The conservative seasonal erosion rates predicted by the numerical model used in this chapter demonstrate that it would be possible to erode 100-m wide channels that are several metres deep in one ablation season. Therefore, the smaller channels sometimes observed at the base of tunnel valleys may also reflect a single ablation season's erosion.

In contrast, the tunnel valleys, being several orders of magnitude larger in cross-sectional area, could hold maximum discharges of $0.5\text{--}2 \times 10^7 \text{ m}^3 \text{ s}^{-1}$ if filled to the bankfull stage. Floods of this size would be amongst the largest floods ever reported on Earth (O'Connor and Costa, 2004). It is highly unlikely that the extensive networks of tunnel valleys observed in the North Sea, and elsewhere, were eroded by such huge discharges given the absence of large water reservoirs in any of the model predictions presented in this chapter (Figure 6.8), and the fact that the geophysical observations suggest that the tunnel valleys were largely filled by ice as they were incised. These arguments rule out the formation of entire tunnel valleys (kilometres wide, hundreds of metres deep) from single mega outburst flooding events in the North Sea.

The modelling results presented in this chapter demonstrate that both the seasonal input of surface meltwater and outburst flooding from smaller trapped lakes are viable mechanisms of incising large channels into thick sequences of unconsolidated soft

sediments on timescales of hundreds to thousands of years. However, whilst seasonal surface drainage can produce networks of semi-regularly spaced tunnel valleys, outburst flooding is only capable of forming one channel in association with a specific lake. The spacing of the channels predicted in the high-resolution seasonal water routing model runs is similar to other inventories of terrestrial tunnel valleys (Figure 6.9D) (Livingstone and Clark, 2016). Such spacings are not reproduced when lake drainage is invoked. These results suggest that whilst both processes may operate during the deglaciation of ice sheets, the dominant mechanism responsible for tunnel valley formation is the drainage of surface meltwater to the bed with relatively small water fluxes.

The inference that outburst flooding assumes a relatively minor role in forming tunnel valleys during deglaciation is supported by the low number of terrestrial tunnel valleys which terminate in outwash fans in North America (Livingstone and Clark, 2016). The presence of large boulders (>2 m diameter) comprising proglacial fans at the termination of some tunnel valleys is often taken as evidence for formation in catastrophic outbursts, because the transportation of such large clasts would require discharges of at least several hundred $\text{m}^3 \text{s}^{-1}$ (Cutler et al., 2002). However, systematic mapping of tunnel valleys across the southern sector of the former Laurentide Ice Sheet by Livingstone and Clark (2016) revealed that only a small percentage of tunnel valleys in this region (~10 %) actually terminated in outwash fans. This observation is consistent with the scarcity of lakes predicted during the last deglaciation across the North Sea (Figure 6.8), in particular because relatively large volumes of water (>4 km^3) are required to form just a single tunnel valley within the timescales implied by Sandersen et al. (2009). Furthermore, the regular spacing of many tunnel valley networks implies that multiple valleys were operating simultaneously across a broad spatial area as they were incised. This observation is difficult to reconcile with episodic outbursts of water released from independent reservoirs (Livingstone and Clark, 2016). Thus, although outburst flooding may play a role in the formation of some tunnel valleys (e.g., Piotrowski, 1994; Cutler et al., 2002; Livingstone and Clark, 2016; Zoet et al., 2019), this mechanism does not appear to be a pre-requisite for their formation.

In contrast, the modelling results presented in this chapter demonstrate that, when focussed in relatively narrow channels operating within larger valley tracts, the input of surface meltwater to the subglacial hydrological system during deglaciation is capable of incising large tunnel valleys within hundreds to thousands of years (Figure 6.11). The erosion modelling supports previous interpretations of tunnel valleys being formed within tens of kilometres of the margins of receding ice sheets in the presence of steep surface slopes (Kristensen et al., 2008; van der Vegt et al., 2012; Livingstone and Clark, 2016),

as the predicted erosion rates are highest within the 20–30 km region upstream of the ice-sheet terminus (Figure 6.10). These relatively steep ice surface slopes would produce steep hydraulic potential gradients and drive subglacial water towards the ice-sheet margin with high water velocities; this may permit relatively low water discharges to rapidly erode sediment (Beaud et al., 2016; Beaud et al., 2018). Accounting for ice margin retreat rates of 50–100 m yr⁻¹ across northern Denmark, this zone of maximum subglacial meltwater erosion would have had 200–600 years to erode the tunnel valleys before grounded ice retreated from the area. The calculated erosion rates from seasonal meltwater inputs are therefore capable of incising large tunnel valleys within the timescales constrained by Sandersen et al. (2009), particularly if glacial erosion (by ice) of the upper tunnel valley cross section also contributed to valley widening.

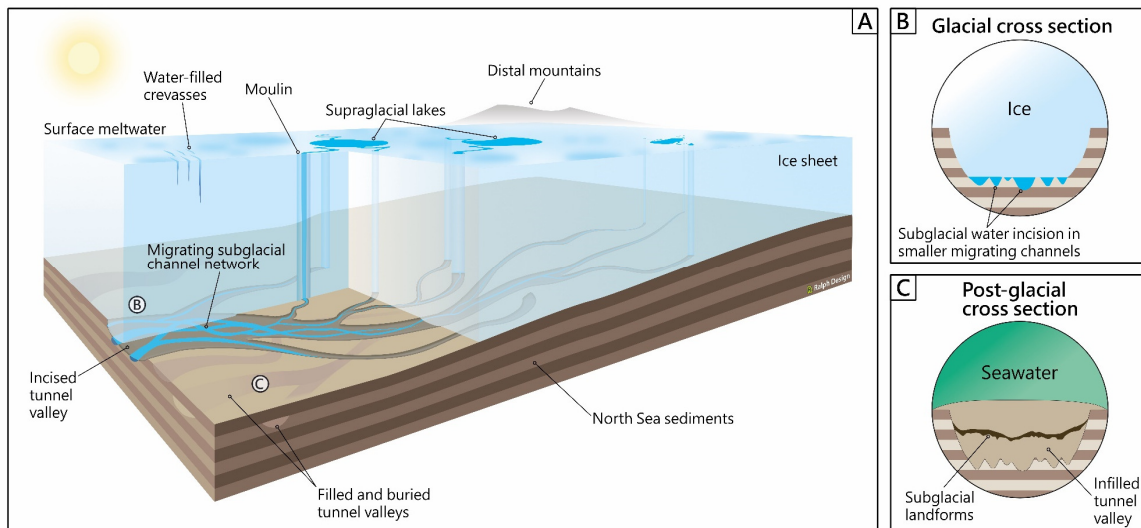


Figure 6.11. Tunnel valley formation beneath a deglaciating mid-latitude ice sheet. (A) Idealised cutaway schematic demonstrating tunnel valley incision through the action of a network of migrating subglacial channels fed by the regular seasonal input of supraglacial meltwater into the subglacial hydrological system. (B) Idealised cross section of a tunnel valley being incised by smaller migrating subglacial channels during a glacial period. (C) Idealised cross section of a buried tunnel valley (now submerged) in a post-glacial configuration. The tunnel valley is infilled and contains subglacial landforms within it.

In addition to the input of surface meltwater through perennially open moulins and crevasses, subglacial meltwater erosion rates may have been temporarily elevated by the sudden release of water trapped in supraglacial lakes through rapid drainage events. When hydrographs from rapid Greenland supraglacial lake drainage events (e.g., Das et al., 2008; Chudley et al., 2019) are used to force the erosion model, these short-lived (hours to days) water influxes could rapidly erode decimetres to metres of sediment if focussed within a pre-existing 100–500 m wide channel. These events may therefore help

to elevate erosion rates within the tunnel valleys. However, these must be taken as maximum rates as models of the input of supraglacial lake water into the subglacial hydrological system have demonstrated that these large floods tend to form a several-kilometre wide turbulent blister beneath the ice sheet (Dow et al., 2015), which would reduce water velocities compared to a situation in which the water was directly concentrated into a channel.

Despite elevated erosion rates caused by supraglacial lake drainage, this mechanism is unlikely to represent the dominant manner in which tunnel valleys are formed. This is because rapid supraglacial lake drainage events observed on present-day ice sheets only transport a small fraction of the total meltwater available from the ice-sheet surface (Koziol et al., 2017). For example, a Greenland-wide survey of supraglacial lakes between 2005 and 2009 demonstrated that only $\sim 13\%$ of lakes drained rapidly (Selmes et al., 2011), with the remainder draining through overtopping into meltwater streams which route water into moulins (Smith et al., 2015). Supraglacial meltwater streams are also capable of transporting far larger volumes of water into the subglacial system than even the largest supraglacial lake drainage events. For example, after the 2012 melt event which briefly thawed 97% of the surface of the Greenland Ice Sheet, the total volume of water transported in supraglacial river networks in a region of south west Greenland over a 5-day period ($0.19 \pm 0.05 \text{ km}^3$; Smith et al. (2015)) was many times greater than the volume of water delivered to the ice-sheet bed during large supraglacial lake drainage events (0.044 km^3 for Das et al., 2008).

Similar, albeit probably more extreme, conditions are likely experienced during ice-sheet deglaciation, providing a mechanism in which tunnel valleys are incised by an abundance of supraglacial meltwater released and transported to the bed by the wastage of the ice sheet. This mechanism is supported by the tendency for tunnel valleys to increase in density towards recessional ice-sheet margins (Mooers, 1989). As the timescales associated with surface melting on glaciers varies from days to hundreds of years, it is likely that the input of surface meltwater to the subglacial hydrological system regularly fluctuated with events such as the addition of surface meltwater from supraglacial lake overtopping (Tedesco et al., 2013; Smith et al., 2015), supraglacial lake drainage via hydrofracture (Das et al., 2008; Chudley et al., 2019), or intense rainfall events (e.g., Doyle et al., 2015). Such pulses of water would have resulted in enhanced erosion as high discharges entered the basal hydrological system (Huuse and Lykke-Andersen, 2000b). Furthermore, the conversion of gravitational potential energy to heat in the basal drainage system as surface meltwater drains to the ice-sheet bed can increase basal melt rates by up to two orders of magnitude during periods of intense surface melting or

rainfall events (Young et al., 2022). Although this process is not included in the model setup used here, this mechanism would increase the erosive potential of surface meltwater drainage events for tunnel valley incision; therefore, the tunnel valley incision rates reported here are likely conservative.

The burial of subglacial landforms at significant depths (>100 m) within the tunnel valleys examined here (Figures 6.4A, 6.6B; Kirkham et al., 2021) demonstrates extensive deformation of ice into the tunnel valleys. This deformation would likely have caused a surface expression in the overlying ice sheet. Basal channels observed beneath Antarctic ice shelves have surface expressions in the form of localised ice lowering along their lengths which can divert surface meltwater into supraglacial rivers and contribute to hydrofracturing (Dow et al., 2018a). A similar feedback mechanism might be expected in the case of tunnel valleys; as ice deforms into the incising tunnel valley, greater amounts of water are focussed into surficial troughs expressed on the ice-sheet surface — contributing to hydrofracturing and supplying additional meltwater that can be used to further incise the tunnel valley. This feedback mechanism might help to explain the great depths that tunnel valleys are capable of incising during relatively short periods of time.

The results of this chapter demonstrate that tunnel valleys can be incised over hundreds to thousands of years by the action of smaller channels fed by the regular seasonal input of supraglacial meltwater into the subglacial hydrological system (Figure 6.11). Combined with ice widening of the upper channel cross section, this process could erode extensive tunnel valley networks, mostly filled with ice as they were incised (Nordmann, 1958; Smed, 1962; Krüger, 1989; Smed, 1998; Huuse and Lykke-Andersen, 2000b).

6.4.3 Implications for tunnel valley genesis and ice-sheet dynamics

The long-standing debate regarding the genesis of tunnel valleys has focussed on the viability of catastrophic versus steady-state formation hypotheses. The results presented in this chapter confirm that both of these mechanisms are possible and may lead to similar valley forms. Some authors have previously made a distinction between tunnel valleys and tunnel channels, whereby tunnel channels are genetically associated with bankfull flooding conditions, a single ice margin, lack tributaries and have consistent dimensions along their length, whereas tunnel valleys may have more complex morphologies and infill (Clayton et al., 1999; Kehew et al., 2012). The geophysical observations and numerical modelling results presented in this chapter support this genetic difference, and potentially provide additional criteria with which these different landforms can be distinguished. The HR3D seismic data reveal that tunnel valleys may

have smaller channels buried inside them and often contain evidence of glacitectonism and extensive ice widening within the upper section of the valleys (Figures 6.4, 6.6; Kirkham et al., 2021). In contrast, tunnel channels are likely to be smaller, straighter, and associated with an individual reservoir (Clayton et al., 1999; Kehew and Kozłowski, 2007; Kehew et al., 2012). For example, tunnel channels formed by subglacial lake drainage in the Green Bay Lobe, Wisconsin, are 450 m wide and 65 m deep (Zoet et al., 2019). They are considerably smaller than other tunnel valleys formed from surface meltwater during the same glacial period elsewhere (e.g., kilometres wide and 100s m deep; Sandersen et al. (2009)).

Accordingly, tunnel channel formation can be viewed as an isolated process that occurs under specific circumstances, such as that in which basal topography permits large scale impounding of water. In contrast, the injection of large volumes of surface meltwater to the ice-sheet bed over a broad area is capable of rapidly generating regularly spaced networks of tunnel valleys if surface melt rates are high enough. This mechanism likely explains the majority of tunnel valley formation in formerly glaciated regions of soft-sediment substrates such as the North Sea. Whilst tunnel valleys buried in the North Sea are notoriously difficult to date, they can be separated into multiple generations by their crosscutting patterns and superposition (Lonergan et al., 2006; Kristensen et al., 2007; Stewart and Lonergan, 2011; Stewart et al., 2013; Ottesen et al., 2020). The results presented in this chapter demonstrate that it would be possible to erode each of these tunnel valley generations within a single glacial-deglacial cycle — and possibly multiple tunnel valley generations if ice readvances occurred in the presence of significant meltwater availability. Consequently, it may be reasonable to associate each generation of tunnel valleys with a particular glaciation, and from this reconstruct ice-sheet extents and the hydrological conditions experienced during each deglaciation based on the distribution and form of that generation of tunnel valleys (Stewart and Lonergan, 2011; Stewart et al., 2013; Ottesen et al., 2020; Kirkham et al., 2021).

The analyses conducted in this chapter supports a growing body of work which suggests that subglacial meltwater is an extremely powerful geomorphic agent, capable of carving large channels into unconsolidated substrates over hundreds to thousands of years (Sandersen et al., 2009; Beaud et al., 2016; Beaud et al., 2018). The rapid formation of large subglacial valleys over potentially just hundreds of years has implications for ice-sheet dynamics. Previous laboratory experiments have suggested that tunnel valley formation may act to stabilise portions of ice sheets undergoing deglaciation through the rapid evacuation of basal water, potentially preventing catastrophic ice-sheet collapse (Lelandais et al., 2018). Similar conclusions have been drawn from the palaeo-record in

some locations (Patterson, 1997). The numerical modelling results indicate that stable evacuation of such water is possible within timescales of hundreds of years — rapid when viewed in the context of deglacial timescales. However, contrasting assemblages of landforms imaged inside and around some tunnel valleys imply that the formation of these channels may be associated with both stable and dynamic ice behaviour (Figure 5.7; Kirkham et al., 2021). Thus, further work, including modelling of the overlying ice response, is needed to elucidate the impact that tunnel valley formation has on the dynamics of deglaciating ice sheets. This could inform on a potentially key process that may regulate the stability of deglaciating ice sheets in the future (e.g., Hulbe, 2017).

6.5 Conclusions

In this chapter, a series of numerical experiments informed by new observations from high-resolution 3D seismic analysis were performed to explore the rates and mechanisms at which tunnel valleys are formed beneath deglaciating mid-latitude ice sheets. These new seismic observations reveal a number of morphological clues as to the mechanisms of tunnel valley formation that are not resolvable using conventional 3D seismic-reflection methods. Smaller abandoned channel systems and braided channel networks present at the base of larger tunnel valley tracts indicate that these features are carved through the action of migrating smaller channels. In addition, extensive slump deposits and subglacial landforms buried within the tunnel valleys demonstrate that pervasive ice contact erosion was a key process regulating their morphology and dimensions.

Numerical modelling of subglacial water flux and sediment erosion demonstrates that migrating narrow channels fed by seasonal surface meltwater are capable of incising networks of tunnel valleys 1–2 km wide and hundreds of metres deep over just hundreds to thousands of years during deglaciation — timescales that are commensurate with independent geological evidence of rapid tunnel valley formation in this region. Modelled erosion rates reach maximum values within tens of kilometres of the ice-sheet terminus, implying that tunnel valleys form time-transgressively close to the margins of retreating ice sheets. This mechanism likely accounts for the formation of most regularly spaced tunnel valley networks found in formerly glaciated regions. Outburst floods from topographically confined basins can also lead to large-scale channel incision over thousands of years; however, this process is only likely to apply in specific circumstances, some of which may now be decipherable using advances in HR3D seismic data. Further incorporation of palaeo-subglacial hydrological evidence into ice-sheet models will help to elucidate the role that tunnel valley formation may have on the dynamics of past and contemporary ice sheets during deglaciation.

Chapter 7

The infill of buried tunnel valleys in the North Sea: Implications for sedimentary processes and ice-sheet dynamics

Abstract

Tunnel valleys are widespread in formerly glaciated regions such as the North Sea and record past meltwater flow, glacial erosion and sediment transport beneath ice sheets undergoing deglaciation. In this chapter, high-resolution 3D (HR3D) seismic data, improved-resolution 3D seismic-reflection data, and geotechnical information from industry-acquired boreholes are used to image the infill architecture of buried Quaternary tunnel valleys in the North Sea in unprecedented detail. Ten cross-cutting generations of tunnel valleys are mapped beneath the seafloor of the North Sea where only seven were visible previously. These mappings indicate that the glacial history of western Europe is more complex than considered previously, and suggest that it is possible to rapidly erode and infill multiple generations of tunnel valleys within a single glacial cycle. The infill of earlier tunnel valley generations reflects sedimentation during relatively gradual ice-sheet retreat with occasional episodes of overriding by re-advancing grounded ice. Tunnel valleys formed in later glaciations are characterised by more variable sedimentation patterns that reflect dynamic fluctuations of the ice margin, including readvances and stagnation, during valley filling and ice retreat. Numerous subglacial landforms are also imaged within the tunnel valleys; these sometimes contain shallow gas accumulations that represent a hazard for seafloor installations and could reduce the efficiency of carbon capture and storage efforts in areas where tunnel valleys are present.

7.1 Introduction

Tunnel valleys record water flow, glacial erosion and sediment transport beneath ice sheets undergoing deglaciation. Obtaining a better understanding of the processes responsible for the formation and infilling of tunnel valleys is of interest for a broad spectrum of reasons. In a glaciological context, understanding the processes involved in tunnel valley formation may inform the parameterisation of realistic melt rates, water routing, and the interplay between basal hydrology and ice dynamics in numerical ice-sheet models. Their location can also be used to reconstruct the position of former ice-sheet margins (e.g., Ehlers et al., 1984; Huuse and Lykke-Andersen, 2000b; Stewart et al., 2013). Tunnel valleys are also important reservoirs of water, ore minerals and hydrocarbons; however, their variable infill can produce difficulties when interpreting seismic profiles of the subsurface (Kristensen and Huuse, 2012; Frahm et al., 2020) and sometimes contains shallow gas accumulations which represent hazards to drilling and increases the risks associated with installing seabed infrastructure (Lohrberg et al., 2020; Ottesen et al., 2020). In addition, the large dimensions of tunnel valleys allow them to capture potentially long-lived sedimentary successions that may otherwise be eroded or reworked by overriding glaciers on land, so they may contain valuable and potentially continuous records of sedimentary depositional history in otherwise poor-preservation settings (Hepp et al., 2012; Huuse et al., 2012; Coughlan et al., 2018). Obtaining a complete understanding of the processes responsible for tunnel valley formation is also important when planning the locations of deep geological repositories for nuclear waste in regions which may become glaciated again in the future (Iverson and Person, 2012; Beaud et al., 2016).

Despite over a century of research, tunnel valleys remain relatively enigmatic glacial landforms because very few modern analogues for them exist beneath extant ice sheets. Whilst their geographical distribution and dimensions are relatively well known (van der Vegt et al., 2012; Ottesen et al., 2020), and recent advances have been made in understanding the manner and timescales over which tunnel valleys form (Beaud et al., 2018b; Giglio et al., 2021; Kirkham et al., 2021, 2022), the processes responsible for their infilling remain poorly constrained. The internal infill lithologies and sedimentary architectures of tunnel valleys are notoriously complex as they can reflect a range of sedimentary and erosional processes that occurred during both glacial and post-glacial times (Kehew et al., 2012; Atkinson et al., 2013). The timing of tunnel valley infill deposits is often poorly constrained due to reworking or a lack of datable material with which the age of the infill can be constrained (Ehlers and Linke, 1989; Praeg, 2003). Tunnel valley infill sequences tend to be dominated by sediment gravity-flow deposits,

glacifluvial sands and gravels, and suspension deposits consisting of fine-grained silts and clays (Ó Cofaigh, 1996). Their infill is often separated into base (primary) and upper (secondary) fill units, which are distinct in terms of their stratigraphy and their relation to the processes which cut the channels (Kehew et al., 2012; van der Vegt et al., 2012).

The basal fill is generally interpreted to be glacial in origin and often contains diamictons (Ehlers and Linke, 1989; van der Vegt et al., 2012). Evidence of faulting, folding, injections and compaction structures observed in outcrops of ancient Ordovician tunnel valleys (Le Heron et al., 2004; Le Heron et al., 2005; Ravier et al., 2014; Ravier et al., 2015) indicate that the base of these tunnel valleys experienced glacial deformation and high subglacial meltwater pressures. The base of other tunnel valleys are filled with massive gravels and sands (Ehlers and Linke, 1989; Ghienne and Deynoux, 1998; Le Heron et al., 2004), which may relate to subglacial deposition or gravity-flow activity in an ice-proximal setting. Many seismic investigations of tunnel valley infill describe a ‘chaotic’ unit present along the base of the valleys which sometimes entirely fills the features (e.g., Mullins and Hinchey, 1989; Huuse and Lykke-Andersen, 2000b; Praeg, 2003; Lonergan et al., 2006; Stewart et al., 2012); in some instances, this unit has been suggested to relate to the collapse and slumping of unstable sediments along the valley sides (Ó Cofaigh, 1996).

The secondary fill sequences of tunnel valleys are generally more varied than those comprising the basal fill as these deposits are not exclusively glacial in origin but rather were deposited in glacially-influenced settings. Thick sequences of glacifluvial sands and gravels are frequently found within the tunnel valleys, relating to outwash fans and glacifluvial deposits expelled at the margin of a receding ice sheet, or turbidity-current sequences deposited in proglacial lacustrine or marine environments (Ehlers et al., 1984; Ehlers and Linke, 1989; Janszen et al., 2012a; Kehew et al., 2012). Laminated clays and silts are also commonly observed, and are interpreted as having been deposited in more distal glacial-marine or glacial-lacustrine environments. Glacial (re)advances, slumping of the tunnel valley sides, melt out of stagnant ice, or iceberg rafting can also deposit diamictons within the secondary infill of tunnel valleys.

The infill of tunnel valleys is thus extremely diverse and varies according to the subglacial sedimentary processes active at that location, the amount and type of sediment load transported by the ice, and the interplay between ice movement, melting and grounding, as well as other post-glacial depositional processes. Moreover, in accordance with their variable infill nature, some tunnel valleys are only partially infilled, such as those exposed on the seabed of the central North Sea (Stewart and Lonergan, 2011; Stewart, 2016).

Others contain gravel-dominated bedforms or terminate in outwash fans containing large boulders which would require high discharge fluxes to transport such a coarse bedload (Brennand and Shaw, 1994; Cutler et al., 2002). Genetic models of tunnel valley infill are therefore difficult to formulate in a manner which is fully compatible with their diverse range of stratigraphic and sedimentological observations. Moreover, the genetic models which do exist often contrast. For example, van der Vegt et al. (2012) proposed a model in which the infill of tunnel valleys relates to their available accommodation space; smaller tunnel valleys are more likely to become entirely filled by glacial sediments, whereas larger valleys would be filled by sequences of ice-proximal deposits, followed by ice-distal sediments as the ice margin retreated back along the valleys. Other models attempt to explain the complex infill of tunnel valleys by multiple erosion and filling events, potentially beneath different ice sheets, with stagnant ice protecting portions of the valleys during retreat (Jørgensen and Sandersen, 2006); however, this model is less applicable in locations where clear upward fining sequences are evident.

This chapter re-examines the infill of tunnel valleys in the central North Sea using state-of-the-art high-resolution 3D (HR3D) seismic data, improved regional scale 3D seismic-reflection data, and geotechnical information from industry-acquired boreholes. Although the patterns of tunnel valley infill in this region are complex, recent improvements in the resolution of 3D seismic data permit a number of subtle patterns to be drawn out which inform about the processes of sedimentation related to deglaciating ice sheets. Delicate subglacial landforms such as eskers and crevasse-squeeze ridges are imaged within the tunnel valleys and imply that tunnel valley formation is linked to dynamic ice-sheet behaviour in areas where meltwater production rates are high. The new HR3D seismic data also reveal a number of new tunnel valley generations (10) which exceeds the maximum number mapped in previous studies (7) (Stewart and Lonergan, 2011; Ottesen et al., 2020). If, as previous studies have concluded (e.g., Passchier et al., 2010; Stewart and Lonergan, 2011; Ottesen et al., 2020), all of the tunnel valleys in the North Sea formed since Marine Isotope Stage 12 (MIS 12), this chapter indicates that more than one generation of tunnel valleys can form within a single glacial stage — pointing towards a more complex glacial history of western Europe than previously recognised.

7.2 Regional setting

The North Sea is a shallow epicontinental sea surrounded by the northwest European, Scandinavian and British landmasses with typical present-day water depths of ~30–150 m (excluding the Norwegian Channel, which is up to 700 m deep). The North Sea Basin formed by lithospheric extension from the Paleozoic to Early Cretaceous (Ziegler,

1990, 1992) and contains up to three kilometres of sediments deposited throughout most of the Cenozoic Era (the last 65 Ma), including a sedimentary sequence up to 1000 m thick deposited during the Quaternary (2.6 Ma onwards) (Lamb et al., 2018; Ottesen et al., 2018). These sediments constitute a vast archive of past environmental conditions, including the build-up, advance and retreat of the Quaternary ice sheets around and into the basin (e.g., Cameron et al., 1987; Huuse and Lykke-Andersen, 2000b; Anell et al., 2012; Lamb et al., 2018; Ottesen et al., 2018; Rea et al., 2018).

The North Sea Basin has been glacially influenced discontinuously throughout most of the Quaternary (Ottesen et al., 2018). Evidence from sediment cores collected in the northern North Sea demonstrates that ice-rafted debris has been present since ~2.7 Ma (Eidvin and Rundberg, 2001; Ottesen et al., 2009), and iceberg ploughmarks have been imaged using seismic reflection data in buried surfaces dated to ~2 Ma in the central and southern part of the basin (Rea et al., 2018). Mega-scale glacial lineations, which are formed subglacially at the base of fast-flowing ice streams (e.g., Clark, 1993), have been observed in buried surfaces dating back to 1.87 Ma (Graham et al., 2010; Buckley, 2012; Rea et al., 2018). These landforms provide evidence for the earliest presence of grounded ice in the centre of the North Sea Basin.

Glacial influence in the North Sea intensified around the time of the Middle Pleistocene Transition (~1 Ma), culminating in three major glaciations which covered the majority of northern Europe and the North Sea. By the time of the Elsterian Stage Glaciation (MIS 12; 430–450 ka), the North Sea Basin was largely infilled and the Fennoscandian and British-Irish ice sheets had coalesced and advanced southward to reach a position close to the present day coastlines of the Netherlands and East Anglia, UK (Figure 7.1A). A similar maximum ice position was attained during the Saalian Glaciation (MIS 10–6), whilst ice was slightly less extensive during the Weichselian Glaciation (MIS 5d–2), extending only as far as northern Denmark and covering the southern central North Sea during the Last Glacial Maximum of MIS 2 (Ehlers, 1990; Ehlers and Wingfield, 1991).

Discrete sets of tunnel valleys identified both onshore and incised into the relatively flat-lying middle to late Quaternary sediments offshore have been used to approximate former ice sheet extents in this three-stage glaciation model despite a notable paucity of stratigraphic dating constraints (Cameron et al., 1987; Wingfield, 1989, 1990; Ehlers and Wingfield, 1991; Praeg, 2003). The largest and most widespread valleys in the North Sea are generally associated with the Elsterian Glaciation, especially in the southern North Sea and adjacent land areas. Tunnel valleys are attributed to this time period based mainly on their large size, which may have been facilitated by the lack of stiff tills

encountered by the ice as it advanced over the substrate for the first time (Passchier et al., 2010). These valleys are infilled with late Elsterian Lauenburg Clay and Holsteinian interglacial deposits, which is similar to other Elsterian tunnel valleys in Denmark and northern Germany (Huuse and Lykke-Andersen, 2000b). Just a few shallower tunnel valleys are interpreted to be Saalian age, mostly in the British and Dutch North Sea sectors of the North Sea, whilst Weichselian tunnel valleys tend to be intermediate size compared to the Saalian and Elsterian valleys (Huuse and Lykke-Andersen, 2000b). However, increasing coverage and analysis of 3D seismic data has permitted buried assemblages of tunnel valleys to be separated into up to seven cross-cutting generations, each of which potentially reflects an individual glaciation; this evidence has been used to argue that the tripartite classification of North Sea glacial history is likely too simplistic (Stewart and Lonergan, 2011).

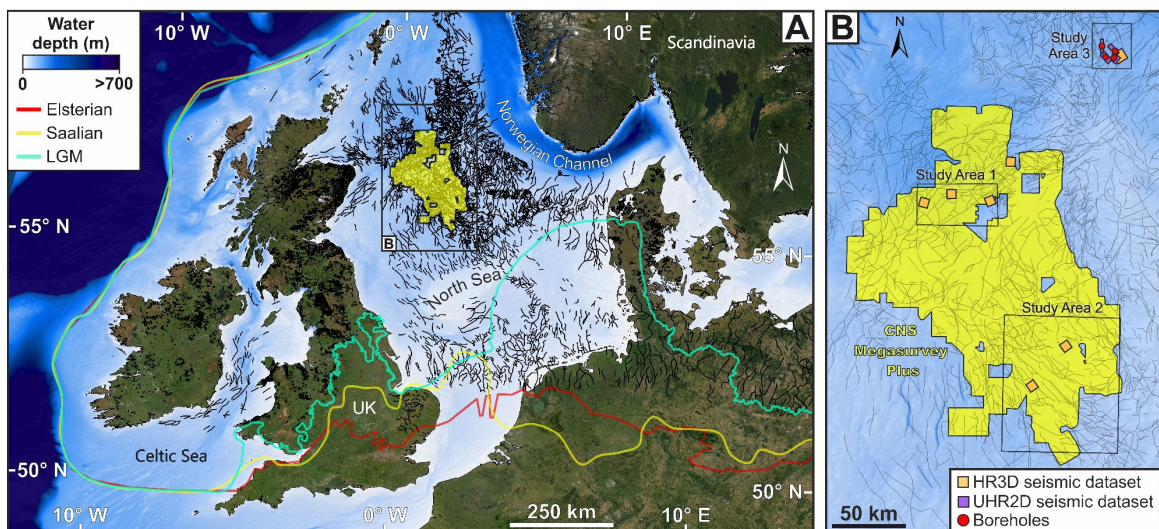


Figure 7.1. Study area. (A) Distribution of tunnel valleys in the North Sea and surrounding landmasses (van der Vegt et al., 2012; Ottesen et al., 2020), and meltwater channels on the UK mainland (Clark et al., 2018). Best estimate former ice-margin positions for the Last Glacial Maximum (MIS 2), Saalian Glaciation (MIS 10–6), and Elsterian Glaciation (MIS 12) are shown from Batchelor et al. (2019). Regional bathymetry is from GEBCO (<https://www.gebco.net>). (B) Distribution of tunnel valleys in the central North Sea displaying the locations of the study areas examined in relation to the conventional 3D seismic data (PGS Central North Sea MegasurveyPlus; yellow polygon), high-resolution 3D (HR3D) seismic datasets (orange squares), ultra-high-resolution 2D (UHR2D) seismic datasets, and boreholes (red circles) used in this chapter.

7.3 Datasets and methods

The seismic data analysed in this chapter were collected using two classes of acquisition system with different horizontal and vertical resolutions. Small areas (typically between 1.5–40 km² per dataset) of HR3D seismic data were used to examine the infill architecture of buried tunnel valleys in unprecedented detail. Due to the small areal coverage of the HR3D seismic data, a regional scale 3D seismic survey was used to contextualise the HR3D seismic analysis and extend the interpretations of tunnel valley infill and architecture to a regional scale.

7.3.1 High-resolution 3D seismic data

HR3D seismic data, originally acquired for the assessment of geohazards such as shallow gas, were used to conduct a detailed examination of the infill and internal architecture of buried tunnel valleys. The acquisition system comprised two 1200-m-long streamers towed 3 m beneath the sea surface. The streamers had 96 hydrophone groups at 12.5 m spacing, a 6.25 m shot interval and a 1-ms sample rate. The seismic source consisted of two 4 × 40 inch³ (2.62 L) sleeve airgun clusters, fired in flip-flop formation (Games, 2012). This acquisition system is particularly well suited for assessing the infill of shallow buried tunnel valleys as precise GPS positioning and laser tracking of the streamers permit data to be binned at a high resolution. In addition, the long length of the streamers enables velocity analyses to be conducted. The resulting velocity data can be used in a range of processes to suppress seismic multiples, which can be prominent in data from formerly glaciated continental shelves such as the North Sea (Games, 2012; Games and Wakefield, 2014; Games and Self, 2017).

Data processing was conducted using ProMAX 3D software and included swell noise attenuation, tide correction, multiple suppression using a combination of SRME, SRWEMA and radon transform methods (all modelled and subtracted), two passes of velocity analysis run at 250 × 250 m intervals, normal-moveout correction and bandpass filtering (20–250 Hz). The final processed datasets consist of time-migrated 3D stacks with a 1-ms sample rate, a 6.25 × 6.25 m bin size and a vertical resolution of ~4 m, given the 100–125 Hz dominant frequency of the seismic-reflection data (Kallweit and Wood, 1982), and a detection limit for depth changes along individual reflectors of ~0.5 m (King, 2020; Kirkham et al., 2021). The final processed seismic data were analysed using S&P Global Kingdom Software. Seven HR3D seismic datasets, covering a combined area of ~67 km², were analysed in this chapter (Figure 7.1B).

7.3.2 Regional scale 3D seismic data

The HR3D seismic datasets are supplemented by the CNS MegaSurveyPlus, a merged regional scale 3D seismic dataset covering an area of 23,650 km² in the central North Sea produced by the marine geophysical company Petroleum Geo-Services (PGS). Over the last 20 years, PGS has collected 3D seismic data in the central North Sea using a variety of acquisition systems and, since 2002, has delivered a merged regional 3D seismic dataset known as the MegaSurvey (PGS, 2020). The CNS MegaSurveyPlus builds on areas where previous data coverage was already good by including legacy data from field tapes and data that is now of release age. These data have been reprocessed and merged with previous data to provide better structural imaging and improved signal to noise ratios (PGS, 2020). The data consist of a 3D pre-stack time-migrated seismic cube that stretches ~200 km from north to south and ~140 km from east to west with a bin size of 12.5 × 12.5 m, although some data gaps are present (Figure 7.1B). The vertical resolution of the MegaSurveyPlus is spatially variable owing to the different acquisition systems and conditions in which the merged data were surveyed; for the burial depths and regions examined here, the vertical resolution of the data is ~8–20 m. Regardless of these variations, the CNS MegaSurveyPlus represents a significant improvement in both horizontal and vertical resolution over older regional scale 3D seismic surveys that have been used previously to study the morphology and infill of tunnel valleys (12.5–100 m bin size; e.g., Lonergan et al., 2006; Stewart and Lonergan, 2011; Stewart et al., 2013), including the previous version of the MegaSurvey (25 × 25 m bin size; Ottesen et al. (2020)).

Two sub-regions of the CNS MegaSurveyPlus were examined in detail in this study. These were chosen based on the locations of clusters of HR3D seismic data containing tunnel valleys which could be linked together using the regional scale 3D seismic survey. The first region, hereafter termed Study Area 1, comprises a 1500 km² area located in the central North Sea at the southern edge of the Witch Ground Basin at a latitude of ~58°N. Study Area 2 consists of a 7,150 km² region located ~150 km southeast of Study Area 1 at a latitude of ~57°N (Figure 7.1B). Study Area 2 contains the three longest tunnel valleys identified to date in the central and northern North Sea (Ottesen et al., 2020). In addition, a third study area in the central northern North Sea is explored where geotechnical information from several boreholes has been obtained. The CNS MegaSurveyPlus coverage does not extend this far north, so in this location a lower resolution (25 × 25 m bin size) legacy 3D seismic dataset covering an area of 1,466 km² was employed to examine the tunnel valleys in this region.

7.3.3 Geotechnical information from industry-acquired boreholes

In addition to the two regions of interest defined within the CNS MegaSurveyPlus, a third study area was chosen outside of the MegaSurveyPlus coverage in an area where a HR3D seismic dataset is accompanied by extensive ultra-high-resolution 2D (UHR2D) seismic data (vertical resolution ~ 2 m) and several geotechnical boreholes which penetrated into and around several tunnel valley fills (Figures 7.1B, 7.2). The boreholes reached depths of up to 100 m below the seafloor, recovering material from approximately one third of the tunnel valley infill by depth. Detailed geotechnical information was derived from the borehole samples, including material lithology, grain size, shear strength and water content; this information was used to aid interpretation of seismic facies and inform about the conditions in which the tunnel valleys were infilled in the region.

7.3.4 Mapping of buried tunnel valleys

An initial digital reconnaissance for the presence of tunnel valleys in the HR3D seismic data was completed by examining sequential horizontal timeslices of the seismic volumes. These provided a planform ‘map’ of the buried tunnel valleys exposed at that depth of the timeslice (Lonergan et al., 2006). The high level of detail present in the HR3D seismic data then permitted the base and sides of each tunnel valley to be laterally traced through the 3D seismic volume and mapped as a horizon in seismic interpretation software. Once the general geometry of the tunnel valleys was established, the facies comprising their infill were examined. In a similar fashion to the base and sides of each valley, the top and base of each infill facies was digitised as an individual seismic horizon and then traced laterally in 3D through each of the HR3D seismic volumes. Any further surfaces, such as stratigraphic discontinuities, present inside the tunnel valley infill were also digitised and examined in 3D. The mapped seismic horizons were converted from two-way travel time (TWT) to depth using a velocity of 1900 m s^{-1} , which is appropriate for the Pleistocene sediments in this region (Kristensen and Huuse, 2012).

Elongate channels surrounding those observed in the HR3D data were mapped from the CNS MegaSurveyPlus using horizontal timeslices at 20 ms intervals. Each channel was confirmed to be a tunnel valley if it satisfied the criteria of having distinctive morphological traits (such as abrupt terminations, steep side slopes) and possessed an undulating thalweg along the length of the valley. Once the regional mapping in the area surrounding the HR3D seismic datasets was complete, tunnel valleys were grouped into generations following the methodology of Stewart (2009). This workflow has been employed by numerous authors to map generations of buried tunnel valleys from 3D seismic data (e.g., Stewart and Lonergan, 2011; Stewart et al., 2013; Ottesen et al., 2020).

In this method, tunnel valleys are assigned a relative age based on their crosscutting stratigraphic relationships and, if this is not well resolved or available, based on their orientation and stratigraphic depth (Stewart, 2009). This method permitted the tunnel valleys observed in the HR3D seismic data, and their infill architecture, to be placed into the regional context of tunnel valley generations, providing them with a relative age.

7.3.5 Examination of tunnel valley infill

The infill of each tunnel valley mapped in the two study areas was examined using vertical cross sections of their infill along the length of the features at 100 m spacing for the CNS MegaSurveyPlus seismic data and at 25 m spacing for the HR3D seismic data. Features of particular interest were examined at the highest possible resolution available for the area whilst seismic attributes, such as coherence, were also computed and analysed to help delineate internal structures within the tunnel valley infill. Horizontal timeslices were used to investigate how the seismic character of their infill varied spatially along the length of the tunnel valleys. For each of the tunnel valleys, the following information was assessed and recorded:

- (i) The number of facies comprising the infill;
- (ii) The detailed seismic character of each infill facies;
- (iii) Whether any landforms (verified by 3D examination of their morphology along mapped seismic horizons) were present;
- (iv) Whether the infill contained any evidence of deformation or thrust structures;
- (v) Whether the infill contained any high-amplitude reflections with additional characteristics such as phase-reversed polarity or acoustic masking of underlying reflectors which suggest the presence of shallow gas accumulations;
- (vi) Whether the infill was internally confined or overtopped the valley shoulders.

7.4 Results and interpretation

7.4.1 Mapped tunnel valleys

In total, 93 tunnel valleys were mapped in Study Area 1, and a further 228 were identified in Study Area 2. The new HR3D seismic data reveal that the tunnel valleys are spaced 2–4 times more densely than reported in previous studies that used lower-resolution datasets (e.g., Lonergan et al., 2006; Stewart and Lonergan, 2011; Stewart et al., 2013; Ottesen et al., 2020). For example, 25 tunnel valleys had previously been mapped in the overlapping portion of Study Area 1 (16 mapped by Stewart, 2009; Stewart et al., 2013, later updated to 25 by Ottesen et al., 2020); this has now been revised to 75 tunnel

valleys for the same area. Furthermore, subtle internal structures are visible within the tunnel valleys using HR3D seismic data — these have not been observed in previous investigations utilising lower-resolution 3D seismic data (Figure 7.2; Lonergan et al., 2006). The main increase in observed tunnel valley density is driven by the discovery of numerous smaller valleys (<500 m wide) that are difficult to detect confidently using lower resolution data. Accordingly, the greater number of tunnel valleys mapped here do not fit into the previous generational framework proposed by Stewart and Lonergan (2011). Instead, the tunnel valleys can be separated into 10 generations based on their cross-cutting relationships (Figures 7.3 and 7.4).

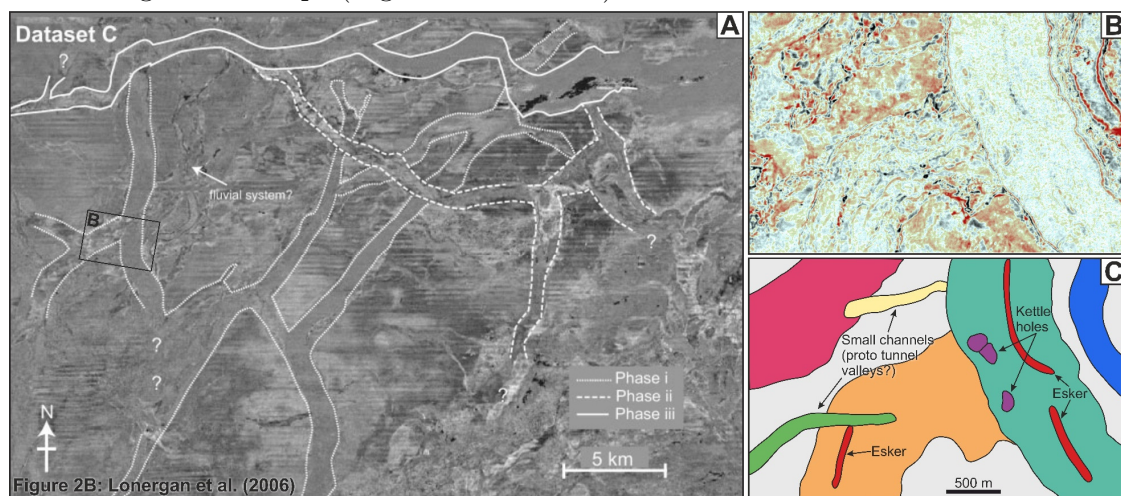


Figure 7.2. Comparison between HR3D seismic data and the conventional 3D seismic data previously used to investigate tunnel valley infill in the central North Sea. (A) Conventional 3D seismic timeslice in the vicinity of Study Area 1 (from Lonergan et al. (2006)). The image is a timeslice of a seismic volume with a bin size of 25×25 m and a vertical resolution of ~ 8 m taken at a depth of 324 ms TWT. **(B)** Timeslice from a HR3D seismic dataset at 324 ms TWT showing the level of detail now attainable using recent seismic methods. **(C)** Interpretation of the HR3D seismic timeslice in (B), displaying 6 tunnel valleys which contain eskers, kettle holes, and smaller channels. These features are invisible in the conventional 3D seismic dataset.

Basic morphological parameters for the tunnel valley generations are similar to those described previously by Stewart et al. (2013) for the central North Sea. In Study Area 1, the tunnel valleys are typically 250–2100 m wide with width-to-depth ratios of 5–10. Generations 1, 2, 4, 5 and 10 are oriented southwest to northeast, whilst generations 3, 7, and 8 are broadly oriented north to south (Figure 7.3A). Generations 6 and 9 are oriented southeast to northwest. Tunnel valleys in Study Area 2 are ~ 200 –3800 m wide with average width-depth ratios of 6–8. Generations 1 and 3 are oriented southwest to northeast, whilst generations 2, 4, 5, 6, 8 and 10 are broadly orientated southeast to northwest (Figure 7.4A). Generations 7 and 9 are orientated north to south. Four

generations of tunnel valleys are distinguished in Study Area 3. The tunnel valleys are 700–2000 m wide and are generally oriented north to south (Figure 7.5). It is not clear whether the less complex pattern of tunnel valleys in this region is because of the lower resolution of the seismic dataset in Study Area 3 compared to the other regions (see Section 7.3.2), or instead relates to regional differences in tunnel valley incidence.

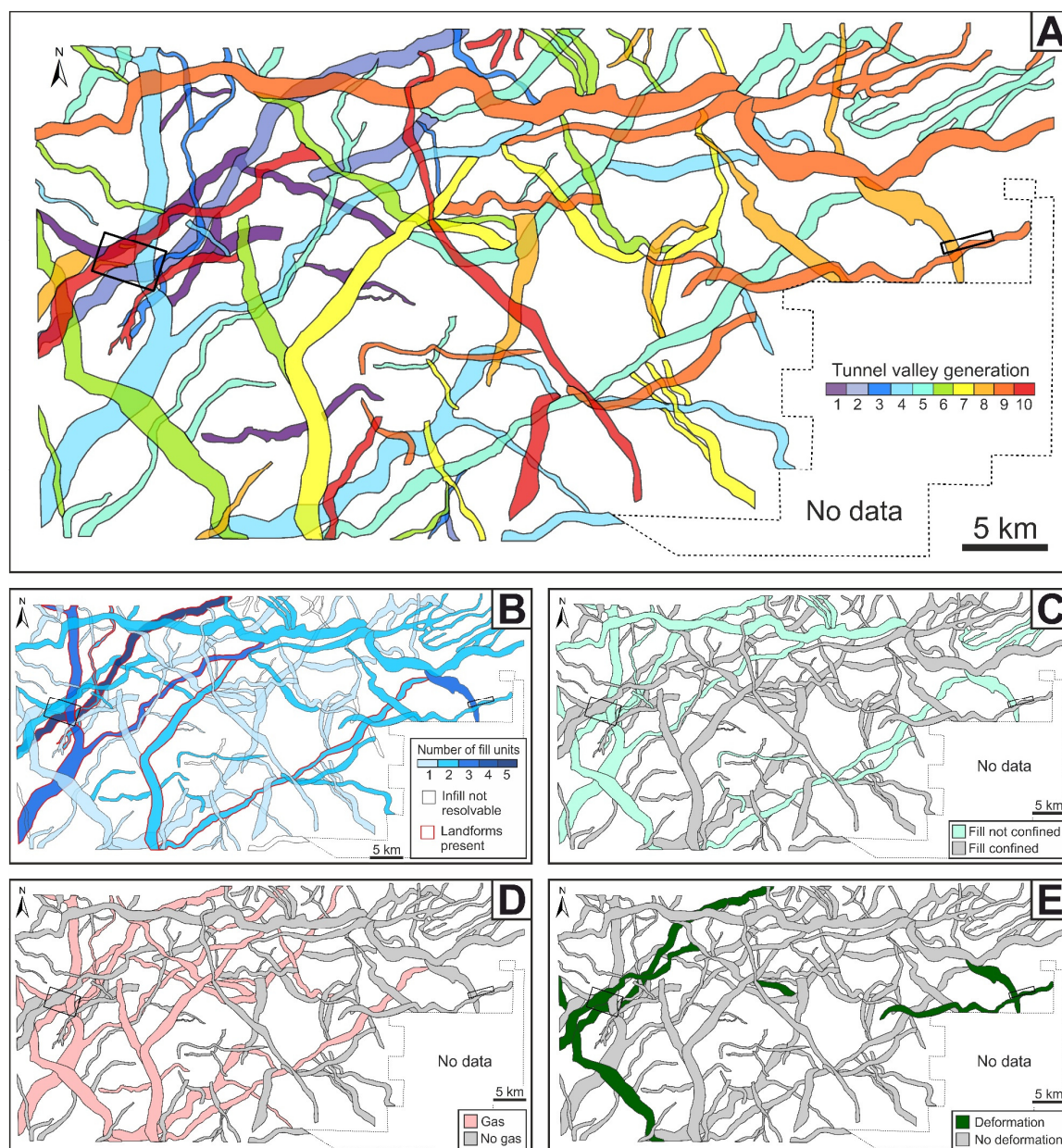
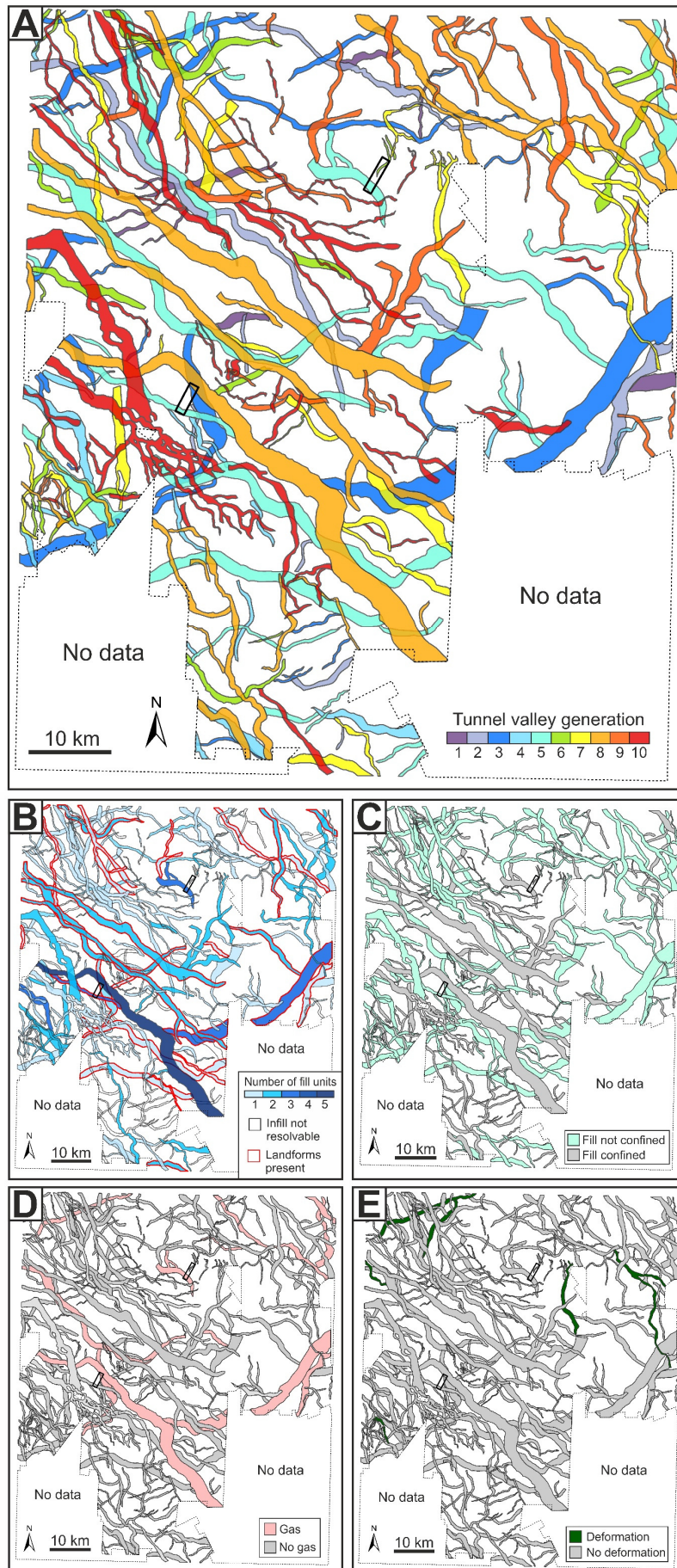


Figure 7.3. Distribution and infill character of tunnel valleys in Study Area 1. (A) Tunnel valleys separated into cross-cutting generations (1 = oldest, 10 = most recent). (B) Number of infill units and distribution of internal landforms (where present). (C) Map of infill which is confined to the tunnel valley sides or overtops the valley shoulders. (D) Presence of high-amplitude, phase-reversed reflections signifying the presence of shallow gas. (E) Presence of deformed sediments comprising the tunnel valley infill. Black boxes delineate the boundaries of HR3D seismic datasets.



(Overleaf) **Figure 7.4. Distribution and infill character of tunnel valleys in Study Area 2.** (A) Tunnel valleys separated into cross-cutting generations. (B) Number of infill units and distribution of internal landforms (where present). (C) Map of infill which is confined to the tunnel valley sides or overtops the valley shoulders. (D) Presence of high-amplitude, phase-reversed reflections signifying the presence of shallow gas. (E) Presence of deformed sediments comprising the tunnel valley infill. Black boxes delineate the boundaries of HR3D seismic datasets.

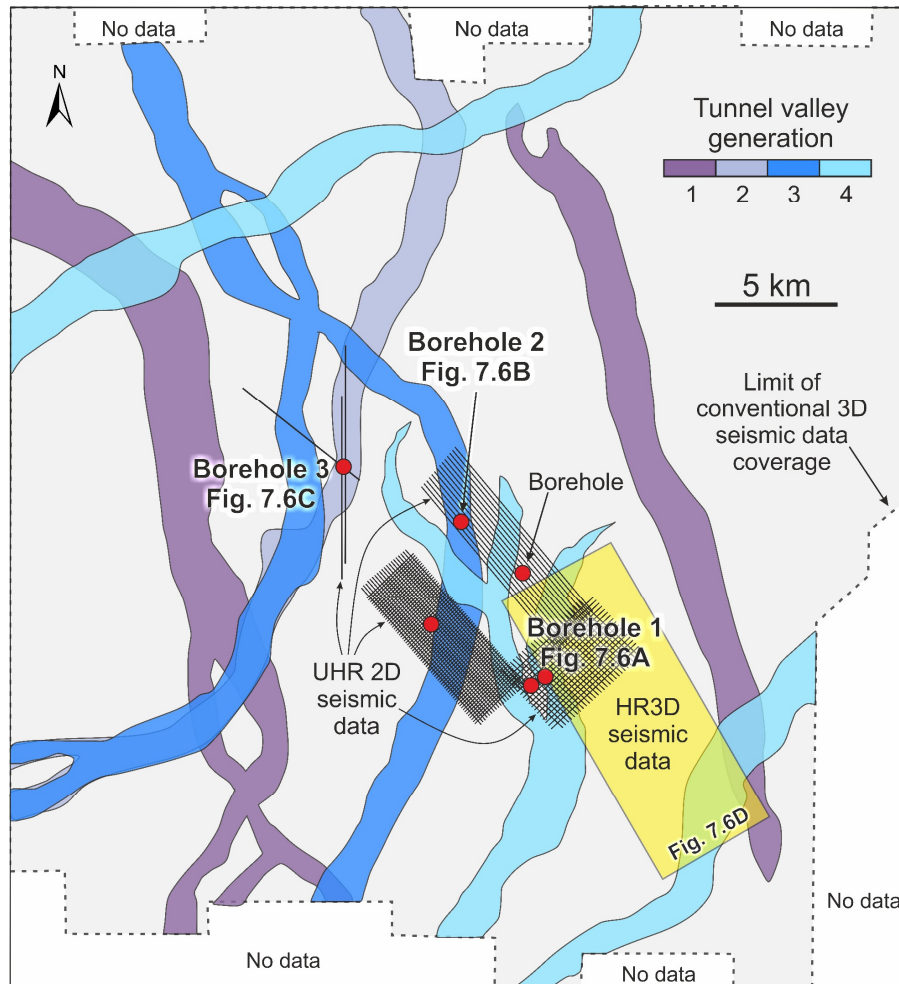


Figure 7.5. Study Area 3. Location of conventional 3D seismic, high-resolution 3D (HR3D) seismic, ultra-high-resolution 2D (UHR2D) seismic data and boreholes in Study Area 3 in relation to the tunnel valleys present in this region. Four generations of tunnel valleys are visible in this region from conventional 3D seismic data.

7.4.2 Types of tunnel valley infill

7.4.2.1 Geotechnical borehole information

Geotechnical information was analysed for six boreholes in Study Area 3. Three boreholes sampled the infill of distinct tunnel valleys in this region and the remainder sampled the substrate immediately adjacent to the channels. The three tunnel valleys are of intermediate size compared to others in the updated inventory presented in this chapter.

The first tunnel valley is 950 m wide, 234 m deep and has a distinctive V-shaped morphometry (Figure 7.6A). In the HR3D seismic data, the infill of this valley is dominated by low amplitude chaotic reflections with a mottled appearance which are extensively faulted along both flanks of the valley. These faults correspond to pervasive slumping of large sediment blocks which fill the valley base (Kirkham et al., 2021), forming glacial curvilineations along the crests of the scarps (Kirkham et al., 2022). The top of the tunnel valley infill is notable as it exhibits a domed upper surface which stands proud of the valley shoulders by ~30 m (based on a velocity of 1900 m s⁻¹; Figure 7.6A). Tracing the reflection corresponding to the top of the tunnel valley into adjacent areas reveals the presence of streamlined glacial landforms indicative of overriding by fast-flowing grounded ice (Figure 7.6D); this fast ice flow appears to have differentially eroded the infill of some filled tunnel valleys, with the softer sediments surrounding the infilled valley being preferentially eroded (Figure 7.6E).

The borehole present at this location (Borehole 1) penetrated 76 m below the seafloor, 45 m of which recovered material from the tunnel valley — approximately one fifth of its total depth. However, given the homogeneous seismic character of the infill facies, it is likely that the sediments sampled are representative of the entire valley infill facies. Borehole 1 reveals that the infill consists of coarse silts and fine sands that are sometimes interbedded with thick layers of coarse silt. Cone penetration tests confirm that the sediments infilling the tunnel valley are very dense with cone resistance values of up to 90 MPa. The proportion of clay (<0.002 mm) within the tunnel valley fill (~4 %) is greatly diminished compared to adjacent sediments into which the tunnel valley is incised (typically 30–60 %). Instead, this fraction of clays is replaced with higher proportions of fine sands (+10–20 %) and coarse silts (+10–30 %) relative to the surrounding substrate at similar depths. Gravel-sized particles (>2 mm) are also absent from the tunnel valley despite small proportions being present in the boreholes surrounding the valley which were probably deposited by ice rafting (e.g., Cameron et al., 1987).

The second tunnel valley is 600 m wide and 55 m deep. When imaged using UHR2D seismic data, the valley infill is characterised by medium to high amplitude semi-continuous reflections that onlap the valley sides (Figure 7.6B). The borehole penetrating this tunnel valley (Borehole 2) reached a depth of 65 m below the seafloor, 15 m of which recovered material from within the valley. Geotechnical information from borehole 2 reveals a greater degree of variability compared to Borehole 1. Samples range between very dense fine sands (100 % of sample), which correspond to high amplitude reflections within the valley, to coarse silts (72 % of sample) with smaller percentages of sands and clays (16 % and 12 %, respectively). Gravel is completely absent from the valley infill,

yet small percentages are present in the surrounding substrate, which are interpreted as ice-rafted debris (e.g., Cameron et al., 1987; Ottesen et al., 2009). The lithology of the tunnel valley infill is relatively similar to neighbouring boreholes located outside of the channel but with slightly higher proportions of silt than the surrounding boreholes. Borehole 2 also lacks the thin laminae and beads of clays and silts that are common in other boreholes located outside of the valley.

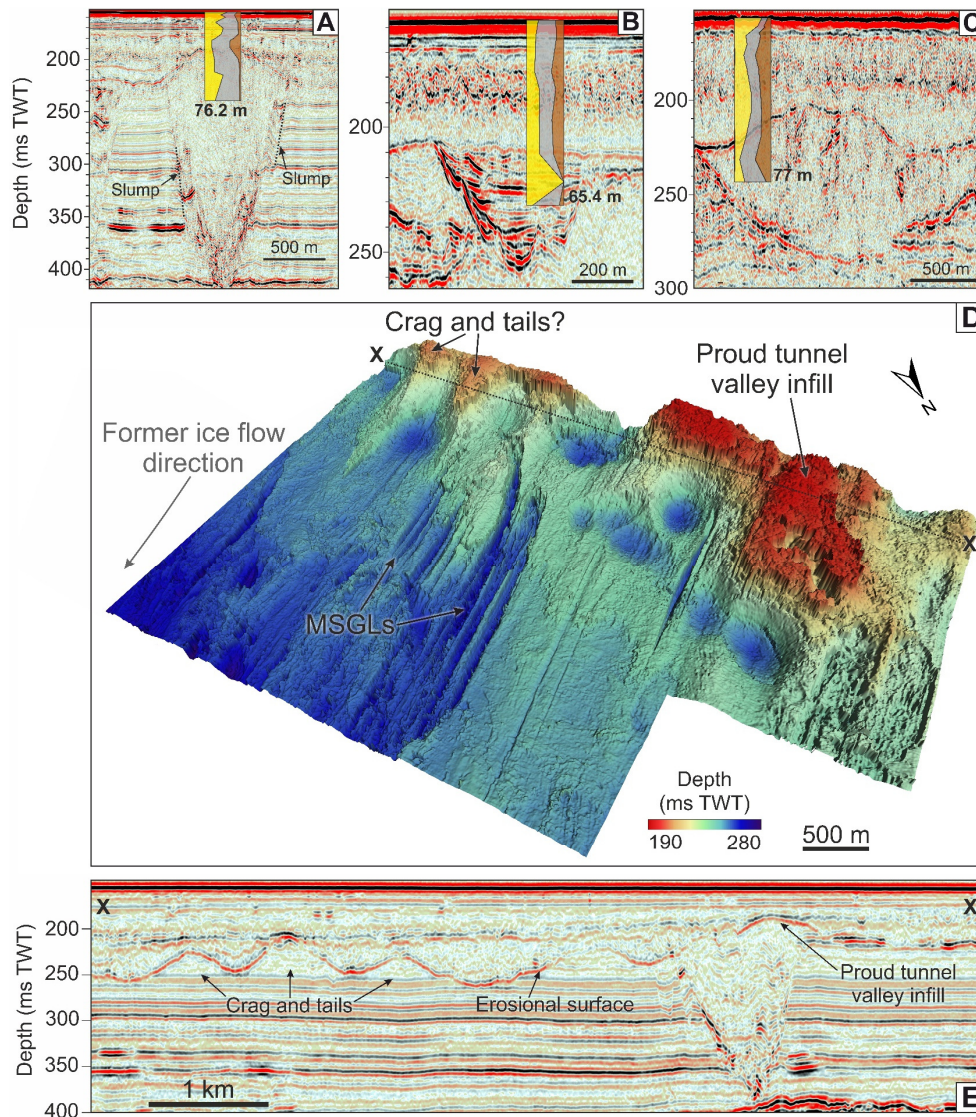


Figure 7.6. Geotechnical boreholes in Study Area 3. (A, B, C) Ultra-high-resolution 2D seismic data displaying the tunnel valleys sampled by geotechnical boreholes. Borehole colours represent the relative concentration of sands, silts and clay throughout the length of the boreholes (sand = yellow, silt = grey, clay = brown). See Figure 7.5 for location of the boreholes. (D) Erosional surface over the top of tunnel valley mapped from high-resolution 3D seismic data. The surface contains the proud-standing tunnel valley infill and streamlined subglacial landforms including megascala glacial lineations (MSGLs) and features resembling crag-and-tails. (E) High-resolution 3D seismic section along the length of the mapped surface displaying the proud tunnel valley infill.

The third tunnel valley is ~1300 m wide, up to 72 m deep and exhibits a domed upper surface similar to the first tunnel valley (Figure 7.6C). The UHR2D seismic data reveals that the valley infill consists of low amplitude chaotic seismic reflections with little internal structure, although some isolated high amplitude reflections are present within the central upper portion of the valley infill. Borehole 3 penetrated the flank of the tunnel valley to a depth of 77 m below seafloor, sampling the upper 18 m of valley infill. Material recovered from this tunnel valley is dominated by silts (43–59 %) and clays (11–42 %) which sometimes contain fractions of fine sand. The valley infill contains a lower fraction of fine sands (13–29 %) than the other valleys sampled.

7.4.2.2 Infill character observed in 3D seismic data

The systematic survey of 321 tunnel valleys imaged in the regional 3D and HR3D seismic data across study areas 1 and 2 reveals that seven types of infill are present (Figure 7.7). Differences in the resolution of HR3D and conventional 3D seismic data result in some notable differences in the seismic character of tunnel valley infill in cases where the spatial coverage of these datasets overlaps. In Study Area 1, overlapping HR3D and conventional 3D seismic data coverage is present for tunnel valley generations 1–4, 6, 8, and 9, whilst overlapping seismic data coverage is present for generations 3, 5, 6, and 8 in Study Area 2.

The first infill type consists of semi-continuous, sub-parallel reflections with low to medium amplitude that onlap onto the tunnel valley sides (Figure 7.7). Type 1 infill is present in 64 % of the tunnel valleys surveyed, and commonly comprises the main basal fill of the valleys if infill Type 7 is absent. Smaller tunnel valleys can be entirely filled by this unit. Geotechnical information from this unit (Borehole 2) demonstrate that these onlapping sub-parallel reflections reflect sedimentary layers consisting of varying fractions of fine sands and coarse silts. These lithological variations would produce more acoustic contrasts and therefore may explain the strong and continuous character of the seismic reflectors associated with this facies. Infill Type 1 may also contain medium- to high-amplitude reflections that correspond to subglacial landforms (see Kirkham et al., 2021) buried within or at the upper boundary of this unit, or deformation within the unit itself. Based on these characteristics, infill Type 1 is interpreted as reflecting ice-proximal sedimentation close to the ice-sheet grounding zone.

A similar facies, described as massive to cross-bedded in structure, is observed along the floors of many Late Ordovician tunnel valleys in northern Africa and Arabia (Le Heron et al., 2004; Clerc et al., 2013). This unit can be up to 40 m thick, although its thickness varies along the length of the valley. Clerc et al. (2013) suggested that this sedimentary

facies was deposited rapidly from granule-rich, high-density turbulent underflow currents expelled from beneath a lightly grounded ice sheet. Deposition of the coarser fraction of the sediment carried by this meltwater would have occurred close to the outlet whilst finer sands, silts, and clays would be carried further in rising meltwater plumes and rain out from suspension further from the outlet (Syvitski, 1989; Mugford and Dowdeswell, 2011; Dowdeswell et al., 2015). These glacial marine deposits sometimes contain evidence of deformation, recording the occasional re-grounding of the ice sheet upon these sediments within the partially grounded zone (Clerc et al., 2013).

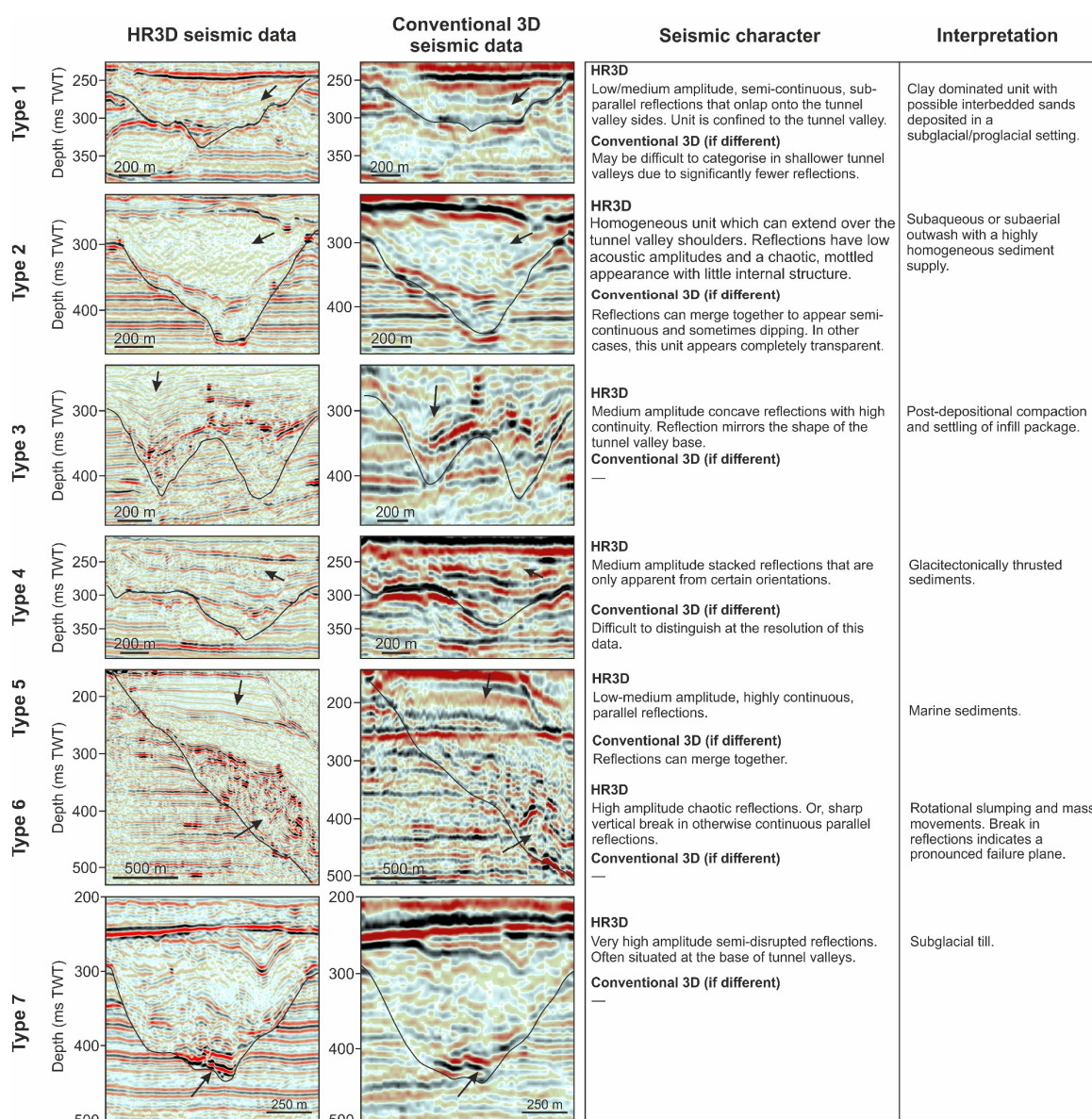


Figure 7.7. Seismic facies identified within the infill of central North Sea tunnel valleys. Differences in seismic character are sometimes present between the high-resolution 3D (HR3D) seismic data and the conventional 3D seismic data. TWT — two-way travel time.

Infill Type 2 consists of a homogeneous unit with low acoustic reflection amplitudes and a chaotic, mottled appearance that indicates very little internal structure at the resolution of the HR3D seismic data (Figure 7.7). Infill Type 2 is present in 31 % of the tunnel valleys surveyed and can overtop the tunnel valley shoulders. In the regional 3D seismic data, these mottled reflections may merge together to form semi-continuous reflections that sometimes dip, potentially making it difficult to distinguish between infill types 1 and 2 using conventional 3D seismic data alone. Structures resembling clinoforms are sometimes visible within this unit (Figure 7.8); however, these are not as easily identifiable as previously recorded examples in tunnel valleys from other areas of the North Sea (Kristensen et al., 2008; Moreau and Huuse, 2014). In other profiles, this unit may appear completely transparent. Samples from Borehole 1 (Figure 7.6) demonstrate that this infill type is comprised of very dense and thick units of homogeneous silty sands with low clay contents.

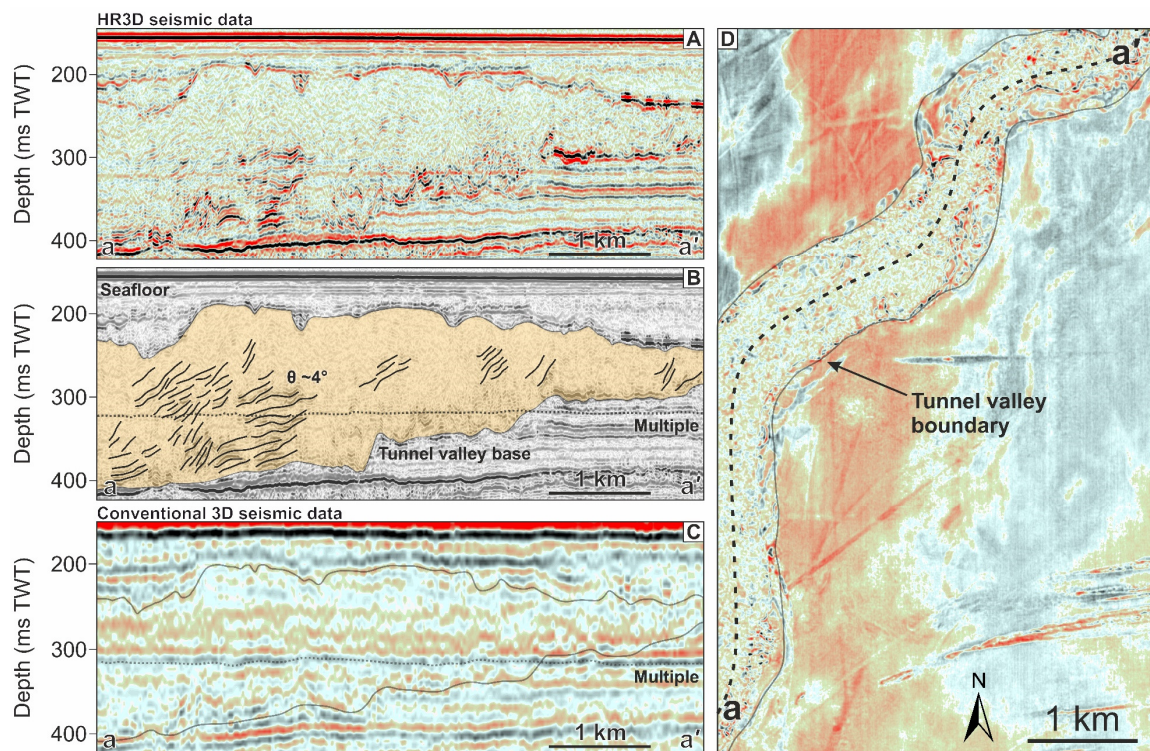


Figure 7.8. Potential clinoform structures imaged within a tunnel valley. (A) High-resolution 3D seismic section taken along the length of a tunnel valley present in Study Area 3. (B) Interpretation of clinoform-like reflections within the tunnel valley infill with a dip angle of $\sim 4^\circ$. (C) Identical seismic profile as in (A) but with conventional 3D seismic data in which clinoform structures are not visible. (D) Horizontal timeslice of the tunnel valley at a depth of 270 ms TWT displaying the location of the seismic profile.

Infill Type 2 is generally absent from the very smallest tunnel valleys and appears to be restricted to valleys that are larger than ~60 m deep and 250 m wide. This facies mostly comprises the upper fill unit in cases where multiple infill facies are present, and is rarely topped by a further seismic facies in the valleys. In instances where overtopping by a further unit does occur, infill Type 2 tends to be overlain by infill types 1, 3, or 5 (ice proximal, deformed, or marine sediments; see below). When infill Type 2 is present in a more complex fill sequence, it tends to comprise over half, and commonly over 70 % of the tunnel valley infill by volume. In rarer cases, this facies comprises the sole infill unit of the valley, especially in tunnel valleys of smaller dimensions.

Based on these characteristics, infill Type 2 is interpreted as subaqueous or subaerial proglacial outwash with a highly homogeneous sediment supply. The morphological, geophysical, and geotechnical characteristics of this unit are similar to upper valley fill deposits recorded in late Ordovician examples of tunnel valleys in northern Africa. These studies describe well-sorted, fine-to coarse-grained sandstones with limited grain-size variations that can extend over the valley shoulders (Le Heron et al., 2004; Clerc et al., 2013). Clinoform-like geometries are sometimes recognised within this unit, and small-scale sedimentary structures such as planar laminae, primary current lineations, convolute lamination, rare antidunes, current ripples and large-scale undulose bedding have been observed (Le Heron et al., 2004; Clerc et al., 2013). An absence of glacitectonic deformation structures suggests that there was no ice contact during the time that this unit was deposited (Clerc et al., 2013). When viewed from a regional perspective, these massive cross-bedded sandstones form a regionally extensive blanket which extends for tens of kilometres and can be several tens of metres thick (Girard et al., 2012; Hirst et al., 2012). This sedimentary unit has been interpreted as proglacial or glacial marine outwash deposited beyond the grounding zone during temporary stillstands punctuating a final, relatively rapid, retreat of the marine-terminating ice-sheet margin (Clerc et al., 2013; Dowdeswell et al., 2015).

The third type of infill unit is characterised by medium amplitude concave-upwards reflections with high continuity that are sub-parallel to the valley floors. Infill Type 3 is present in 26 % of the tunnel valleys surveyed and generally occurs within smaller valleys (<700 m wide, <125 m deep), either as the basal unit or as the only unit filling the valley. In tunnel valleys with multiple infill facies, this unit comprises only a small percentage (15–30 %) of the valley cross-sectional area. The unit does not contain landforms or shallow gas deposits, and is commonly confined to the valley sides. Infill Type 3 is interpreted to represent post-depositional deformation of the infill package driven by factors such as porosity changes or sediment compaction. In some cases, this

unit is associated with salt domes that underlie the tunnel valleys — particularly in the southern central North Sea.

Combined, these three infill classes comprise the bulk of the tunnel valley infill observed within the three study areas. Each of these infill packages is commonly tens of metres thick and is capable of filling the valleys entirely (hundreds of metres thick). A further four infill types are also identified that are less widespread. Of these, the fourth type consists of medium amplitude stacked reflections with dip angles along the valley axis of $\sim 10\text{--}20^\circ$ (Figure 7.7). The reflections are only apparent from certain orientations and can therefore be difficult to detect, particularly in the regional 3D seismic data. This unit is up to several tens of metres thick. Reflections comprising this unit are interpreted as glacitectonic imbricate thrust structures indicating sediment deformation by ice motion, based on comparison to similar features elsewhere (e.g., Huuse and Lykke-Andersen, 2000a).

The fifth infill type observed within the tunnel valleys is characterised by thick sequences of stratified continuous low-medium amplitude parallel reflections that have high continuity. When present, infill Type 5 generally occurs at the top of the valley fill sequence. The infill unit is most commonly observed within larger tunnel valleys, although it may be difficult to distinguish between this unit and ice proximal (Type 1) deposits using conventional 3D seismic data alone due to the similar appearance of these units, with the exception of Type 5 exhibiting more continuous reflections. Infill Type 5 is interpreted as marine sediments deposited near the top of the tunnel valleys.

Infill Type 6 is composed of large blocks of high amplitude chaotic reflections or steep ($10\text{--}42^\circ$) breaks in otherwise continuous parallel reflections that run along the tunnel valley sides. When present, this unit can comprise $\sim 10\text{--}30\%$ of the tunnel valley infill by volume (Kirkham et al., 2022). Infill Type 6 is interpreted as slump and mass-movement deposits. The final infill class (Type 7) consists of discontinuous blocks of very high amplitude semi-disrupted reflections that are often found at the base of the tunnel valleys. The thickness of this unit is typically small ($<10\text{s m}$) compared with the depth of the tunnel valleys in which it is found (100s m). The reflections characterising infill Type 7 are interpreted as the top of discontinuous deposits of subglacial till plastered onto the floors of the tunnel valleys.

7.4.2.3 Study Area 1

The tunnel valleys present in Study Area 1 contain between 1–4 infill facies (Figures 7.3B, 7.9A). The majority of the tunnel valleys are characterised by 1–2 seismic facies,

although this is likely at least partially related to the resolution of the seismic data as tunnel valleys covered by the higher resolution HR3D seismic data typically have greater numbers of seismic facies than the surrounding valleys surveyed by the CNS MegaSurveyPlus (Figure 7.3B). Of the ten generations of tunnel valleys in this region, all contain valleys filled with ice-proximal sediments (Type 1), whilst six generations contain distal outwash sediments (Type 2) and four are associated with compacted infill (Type 3). Rarely, small units of subglacial till (Type 7) are present discontinuously along the base of some tunnel valleys, although it is difficult to confidently image these units without the greater resolution of the HR3D seismic data.

Tunnel valleys in Generations 1 and 2 are mostly composed of a single unit of ice-proximal fill and occasionally contain gassy reflections. However, one particularly large Generation 2 valley contains 4 seismic facies consisting of subglacial till overlain by ice proximal and outwash sediments before being finally capped by a small pocket of sediment with highly continuous concave reflections (Figure 7.9C). This tunnel valley contains fragmented eskers, gassy deposits and some evidence of deformation within its infill, whilst the outwash fill unit is not confined by the valley sides. Generation 3 tunnel valleys contain 1–2 infill units. Seismic infill character is variable with valleys containing onlapping, concave-upwards, or chaotic reflections indicating a mixture of ice-proximal outwash and deformed sediments. One Generation 3 tunnel valley contains high amplitude gassy reflections within its ice-proximal infill package, which is not confined by the valley sides.

The infill of the tunnel valleys in Generation 4 is characterised mainly by ice-proximal sediments with reflections that onlap the valley sides; these valleys contain between 1–3 infill units. Landforms are buried within one tunnel valley (e.g., Figure 7.10), whilst an additional two valleys contain high amplitude gassy reflections within their fill. Two instances of unconfined fill are observed, one where ice-proximal sediments extend over the tunnel valley shoulders and a second where a chaotic outwash unit is not confined to the tunnel valley. Generation 5 contains a highly consistent fill pattern of either 1–2 units of ice-proximal sediments that occasionally contain landforms and gas, or concave-upwards Type 3 reflections at the valley base capped by outwash sediments that are consistently unconfined by the valley sides. Generations 6–8 are mostly composed of 1–2 units of ice-proximal (Type 1) or compacted (Type 3) infill, with occasional instances of outwash sediments (Type 2). The tunnel valleys sometimes contain gassy reflections or evidence of deformation (Type 4 fill); these features are most commonly associated with the Type 1 infill package. In three instances in Generation 6, tunnel valleys contain Type 3 infill capped by unconfined outwash sediments. The infill of Generation 9 tunnel

valleys is similar to that of Generation 5 with Type 1 or Type 3 infill capped by unconfined outwash sediments, whilst the infill of Generation 10 is comprised of a single unit of Type 1 or Type 3 fill, with occasional evidence of glacitectonic thrusting (Type 4).

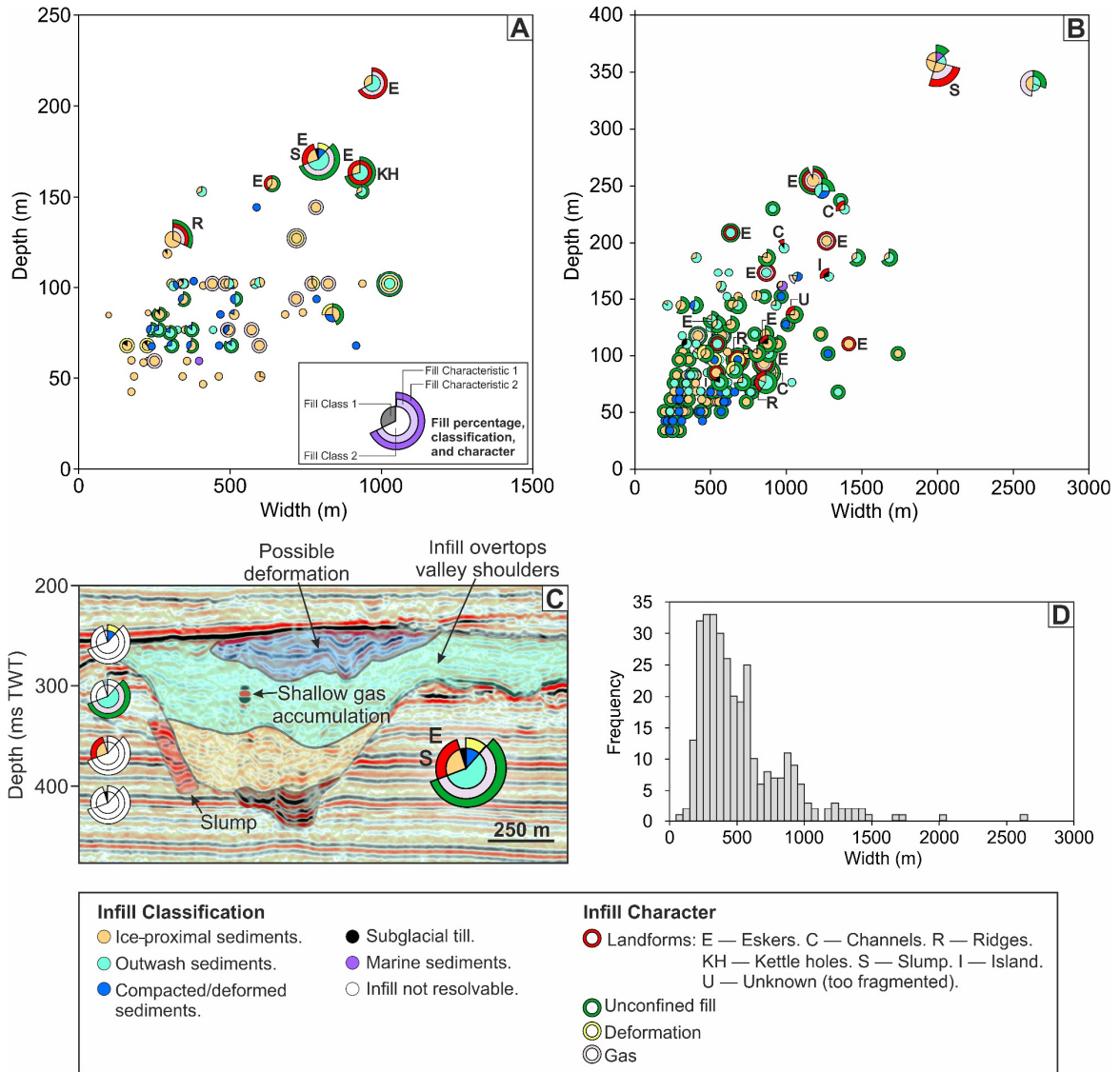


Figure 7.9. Dimensions and infill character of tunnel valleys in the central North Sea. (A) Study Area 1. Inner pie charts display the percentage of each tunnel valley comprised of different fill units, coloured by infill classification. Outer rings surrounding specific pie chart segments indicate the character of the infill of that segment, such as whether the tunnel valley infill is deformed or contains evidence of landforms within it. Fill type is plotted in an anti-clockwise direction from the base of the tunnel valley to its upper fill unit. Larger markers represent more complex infill architecture. (B) Dimensions and infill character of tunnel valleys in Study Area 2. (C) Example tunnel valley cross-section classified into different infill facies and containing characteristics such as slumps, eskers, and shallow gas accumulations. (D) Histogram of tunnel valley widths from both study areas. Note that the figure scales are not consistent between (A) and (B).

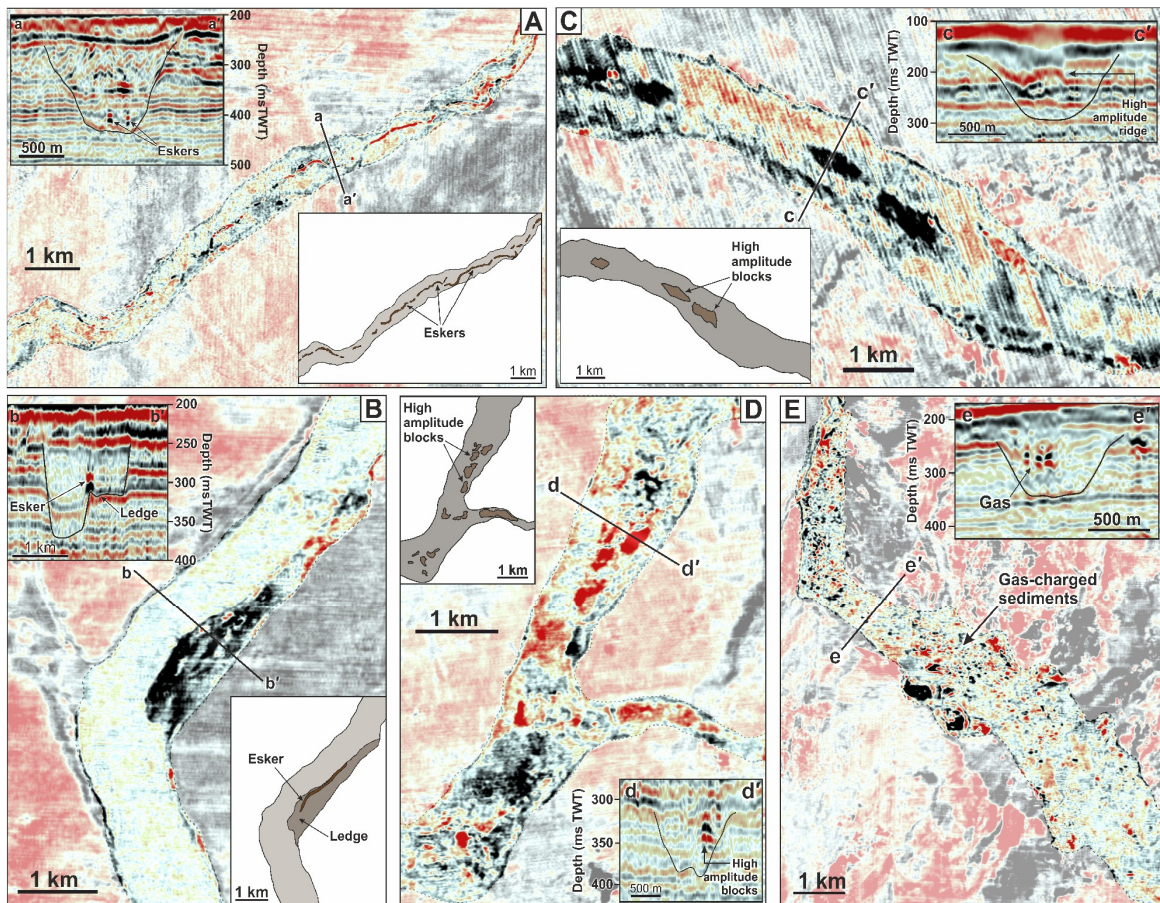


Figure 7.10. High-amplitude reflections associated with subglacial landforms and shallow gas buried within the central North Sea tunnel valleys. (A, B) Examples of eskers and streamlined island-like blocks (C, D) buried within the infill of tunnel valleys. (E) Example of gas-charged tunnel valley infill sediments. All examples are from Study Area 2; however, similar examples are also present in Study Area 1.

7.4.2.4 Study Area 2

The ten generations of tunnel valleys present in Study Area 2 contain up to 5 seismic facies, with most having 1–2 infill units (Figures 7.4B, 7.9B). Larger (both deeper and wider) tunnel valleys generally contain more fill units, although many relatively wide (>1000 m) valleys are also characterised by only 1–2 seismic facies. As with valleys in Study Area 1, subglacial tills are only occasionally present at the base of the tunnel valleys in Study Area 2.

Although tunnel valleys in Generations 1–4 contain up to 3 seismic facies, the majority are dominated by a single unit of Type 1 infill. This unit is typically unconfined by the valley sides and occasionally contains remnant landforms, gas deposits, and some evidence of deformation. A few tunnel valleys are also filled with unconfined concave-upwards (Type 3) or chaotic (Type 2) reflections, with the latter sometimes overlying

the ice-proximal sediments filling the base of the valleys. One instance of glaciectonic thrust stacks (Type 4 fill) is observed in a Generation 3 tunnel valley.

Generation 5 valleys consist mostly of two seismic facies but can contain 1–3 fill units. The majority of the infill is comprised of ice-proximal sediments that are sometimes capped by unconfined outwash deposits. Landforms and gas occur within Generation 5 tunnel valleys at a higher frequency than in other generations; these are mostly associated with Type 1 infill, but in one case landforms are buried within the outwash unit (crevasse-squeeze ridges; Kirkham et al., 2021). Generation 6 tunnel valleys contain 1–2 units of Type 1 or Type 3 infill, many of which are unconfined by the valley sides. Occasional landforms and deformation are associated with valleys filled with ice-proximal sediments. Tunnel valleys in Generation 7 are filled with a variety of infill types, usually as a single unit. In cases where valleys contain two seismic facies, the upper unit is comprised of Type 1 or Type 2 infill which frequently overtops the valley shoulders. Only two instances of glaciectonic thrust sediments (Type 4 fill) are present in tunnel valley Generations 6–7.

Generation 8 contains a massive tunnel valley that is the longest documented in the North Sea (155 km; Ottesen et al., 2020). This tunnel valley is ~360 m deep and contains 5 seismic facies. The lower three facies consist of packages of ice-proximal sediments that are capped by outwash sediments and finally a marine infill package. The valley infill occasionally contains gassy internal reflections. The other tunnel valleys present in this generation have a comparably simple fill architecture of 1–2 fill units of Type 1 or Type 2 infill at the base of the valleys capped by a chaotic, low amplitude outwash unit (Type 2). Where present, the outwash unit is generally unconfined. Landforms, including eskers and island-like blocks, are relatively common within Generation 8 tunnel valleys (Figure 7.10). Generation 9 tunnel valleys are largely infilled with a single unit dominated by ice proximal sediments, although infill Types 2 and 3 are also present in some valleys. The infill of many tunnel valleys of this generation is unconfined. Eskers (e.g., Figure 7.10A, 7.10B) and crudely streamlined island-like features that are up to 1 km long, 300 m wide (e.g., Figure 7.10C, 7.10D) and are interpreted as glaciectonic rafts transported by grounded ice (e.g., Andreassen et al., 2004), are observed within some tunnel valleys, visible as high-amplitude reflections commonly present within the ice-proximal facies. Generation 10 valleys have a higher proportion of Type 3 infill than other generations in this area. Landforms are absent from the valley fills and ~50 % of the fill is unconfined. Most tunnel valleys in this generation contain only one fill unit.

7.5 Discussion

7.5.1 Implications for North Sea glacial history

The revised classification of ten generations of tunnel valleys in the central North Sea is more complex than noted in previous investigations which have identified up to five generations of tunnel valleys in the eastern North Sea (Kristensen et al., 2007) and up to seven generations in the central North Sea (Stewart and Lonergan, 2011; Stewart et al., 2013; Ottesen et al., 2020). This difference derives from the higher-resolution data used to map the buried tunnel valleys in this study. The presence of multiple generations of cross-cutting tunnel valley networks in the central North Sea adds weight to the growing body of evidence that the previous model of northwest Europe's glacial history is too simplistic and likely consists of more than three major glaciations over the last 460 kyr (Stewart and Lonergan, 2011). For example, the Saalian stage likely encompasses 2–3 glacial-interglacial cycles (MIS 10, 8, and 6; Ehlers and Gibbard, 2007), whilst two Elsterian glacial advances are recognised in Germany (Ehlers et al., 1984).

Accurately constraining the age of tunnel valleys in the North Sea is notoriously difficult due to a lack of datable fossils and a general paucity of boreholes from within the tunnel valleys themselves. Characteristic undulations in tunnel valley thalwegs demonstrate that they were formed by pressurised meltwater flowing subglacially beneath a grounded ice sheet (e.g., Shreve, 1972; Ó Cofaigh, 1996). Evidence for grounded ice in the North Sea extends back to 1.87 Ma (Rea et al., 2018), potentially providing a large range of time in which the tunnel valleys could have first been incised. Palaeomagnetic evidence from British Geological Survey borehole 77/03 (Stoker et al., 1983) allowed Stewart and Lonergan (2011) to infer that the oldest of their tunnel valley generations mapped in the central North Sea was younger than the Brunhes-Matuyama magnetic reversal event at 780 ka. As six formally named cold marine isotope stages are observed in the ocean record over this period (Cohen and Gibbard, 2019), Stewart and Lonergan (2011) then correlated each of their seven generations of tunnel valleys to an individual cold stage present in the marine isotope record, with the oldest being of Elsterian age (MIS 12). The third and fourth tunnel valley generations were thought to represent reoccupation of valleys due to local advances and retreats of the ice margin as part of a larger glaciation (MIS 10 or 8). Evidence for valley reoccupation between and during subsequent glaciations has also been found in both onshore and offshore records (e.g., Müther et al., 2012; Roskosch et al., 2015).

The additional tunnel valley generations revealed by the revised mappings presented here complicate this simple correlation. Two explanations could explain the additional

tunnel valley generations identified in this study. First, the extra buried generations may represent additional tunnel valley forming glaciations in the central North Sea that extend further back than the Elsterian (MIS 12). Other cold periods, younger than the Brunhes-Matuyama magnetic reversal event and older than the Elsterian, in which tunnel valleys could have potentially formed occurred in MIS 14, 16, and 18.

An alternative interpretation for the additional tunnel valley generations is that further generations were formed, filled, and re-incised relatively quickly as part of minor retreats and readvances during a larger glacial episode i.e., more than one generation of tunnel valleys formed per glaciation. Although rare, coupled lithological and biostratigraphical data (Sandersen et al., 2009; Giglio et al., 2021), as well as numerical modelling experiments (Chapter 6) suggest that tunnel valleys can form in just a few hundred to a few thousand years during deglaciation. Thus, if sedimentation rates were sufficiently high to infill the tunnel valleys rapidly after they formed, especially with sediments that are resistant to further glacial erosion such as the very dense sands observed in Study Area 3, it would potentially be possible to incise a new generation of cross-cutting tunnel valleys during minor fluctuations of the ice-sheet configuration within a longer glacial period. Episodes of abrupt climate change — Dansgaard–Oeschger events — have been identified in ice-core records from Greenland (Bond et al., 1993; Dansgaard et al., 1993; Andersen et al., 2004), in which temperatures increased rapidly by 10–15°C from cold stadial to warmer interstadial conditions within a few decades (Severinghaus and Brook, 1999; Huber et al., 2006; Kindler et al., 2014). These interstadial states typically lasted for 500–2000 years before gradually cooling — similar to the timescales required to erode tunnel valleys beneath ice sheets experiencing significant surface melting (Kirkham et al., 2022). As the direction of subglacial water drainage on flat and homogeneous ice-sheet beds is controlled by the surface topography of ice sheets (Shreve, 1972), subtle reconfigurations of ice-sheet topography during ice-sheet readvances following a Dansgaard–Oeschger event could produce consecutive generations of tunnel valleys with different orientations and locations within a single glacial period (Lelandais et al., 2018).

If this latter interpretation is correct, it is interesting to note that although the North Sea has been glaciated by grounded ice sheets for up to 1.87 million years, the majority of tunnel valleys appear to have been formed within the last ~500,000 years (Stewart and Lonergan, 2011). This could indicate that the dominant driver of ice-sheet retreat in this setting switched to a meltwater intensive retreat style around 500,000 years ago, leading to the formation of large networks of tunnel valleys in subsequent glaciations. Ice-core records from Antarctica demonstrate that there was less pronounced warmth in interglacial periods prior to 430,000 years ago (Augustin et al., 2004). Interglacials after

the Mid-Brunhes Transition at ~430,000 years ago experienced warmer temperatures, higher concentrations of atmospheric CO₂, and an increase in the amplitude of the 100 kyr climate cycles compared to earlier interglacial periods (Augustin et al., 2004; Jouzel et al., 2007; Lüthi et al., 2008). Recent statistical analysis demonstrates that the Mid-Brunhes Transition was a globally synchronous phenomenon that included other components of the climate system (Barth et al., 2018). The increased amplitude of glacial terminations following the Mid-Brunhes Transition may thus have resulted in a more meltwater intensive regime than in earlier glacial terminations; this climatic change may explain why abundant tunnel valleys began to form in the North Sea at around this time.

In either case, the greater number of tunnel valley generations presented in this chapter is consistent with previous analyses which postulate that tunnel valleys can form rapidly beneath ice sheets (Sandersen et al., 2009; Kirkham et al., 2022), and lends support to a more complex glacial history of northwest Europe than has been assumed in the past. Further absolute dating constraints from boreholes and shallow drilling within tunnel valleys is ultimately required to better constrain their chronology and therefore the glacial history of the North Sea with greater accuracy.

7.5.2 Patterns of tunnel valley sedimentation

The tunnel valley infill sequences mapped in this study are characterised by remarkable facies and architectural heterogeneity. Previous studies have reported a great diversity of tunnel valley infill sequences in the North Sea. These range from clearly partitioned valley fills comprised of coarse glacial fluvial sands and gravels overlain by fine-grained glacial lacustrine or glacial marine sediments, to unstructured sands and silts which fill the entirety of the valleys, or discontinuous deposits of gravelly diamicton present along the erosional unconformity at the base of tunnel valleys (e.g., Cameron et al., 1987; Praeg, 1996; Kluiving et al., 2003; Praeg, 2003; Kristensen et al., 2007; Kristensen et al., 2008; Lutz et al., 2009; Stewart et al., 2012; van der Vegt et al., 2012).

The systematic regional mapping of tunnel valley infill demonstrates that most tunnel valleys are characterised by a relatively simple fill architecture consisting of 1–2 seismic facies, although notably more complex examples of tunnel valley fill exist (up to 5 seismic facies), especially recognised in areas of HR3D seismic data coverage. The more complex infill patterns visible in the HR3D seismic data are more similar to the numerous sedimentary units described in borehole investigations (e.g., Hepp et al., 2012; up to 6 lithological units) than to the simple bi- or tripartite patterns interpreted from conventional 3D seismic data (Kluiving et al., 2003; Lonergan et al., 2006; Stewart et al., 2012). This shows that HR3D seismic data are capable of capturing fine-scale infill

packages not visible in conventional 3D seismic data. Consequently, although the CNS MegaSurveyPlus used for the majority of the tunnel valley infill mapping in this study is higher resolution than previous compilations, the finer detail of tunnel valley fills is probably not fully resolved in the regions where HR3D seismic data coverage is absent. This issue is likely spatially variable because the presence of seismic multiples in some areas and other quality control issues (e.g., poor muting and velocity controls) can make it difficult to interpret the near-seabed interval of the 3D seismic data. Therefore, whilst conventional 3D seismic data are sufficient to map and classify the broad-scale structure of tunnel valley infill facies, HR3D seismic data are needed to reveal the true morphology and infill structures present within buried tunnel valleys.

Tunnel valleys with larger dimensions tend to contain greater numbers of fill units, a trend that is particularly apparent for the more recent generations (Figure 7.9). At a gross scale, many tunnel valleys contain a previously reported deglacial succession of ice-proximal sediments overlain by distal outwash deposits that may overtop the valley shoulders (e.g., Cameron et al., 1987; Huuse and Lykke-Andersen, 2000b; Kluiving et al., 2003; Stewart et al., 2012; van der Vegt et al., 2012). Marine sediments are also present at the top of the largest valleys that were not fully infilled during deglaciation. This pattern of decreasing glacial influence reflects the retreat of the ice sheet front away from the tunnel valleys after these features were incised (Praeg, 1996; Ghienne and Deynoux, 1998; Janszen et al., 2012b; van der Vegt et al., 2012).

In contrast to previous studies, however, the detailed mapping using higher resolution 3D seismic data presented in this chapter allows for a number of additional patterns to be tentatively drawn out. Previous investigations of tunnel valley infill in the North Sea have not been able to distinguish differences in the infill patterns of different tunnel valley generations (e.g., Stewart et al., 2012). The updated mapping suggests that earlier tunnel valley generations (1–2 in Study Area 1 and 1–3 in Study Area 2) are characterised by simpler infill architectures than later tunnel valley generations. These earlier tunnel valley fills consist largely of ice-proximal sediments that sometimes contain evidence of ice overriding. These infill sequences are interpreted to reflect sedimentation during relatively gradual ice-sheet retreat with occasional episodes of overriding by re-advancing grounded ice. Later generations of tunnel valleys (4–10 in both study regions) have more variable sedimentation patterns with a higher incidence of outwash sediments. Many examples of subglacial landforms, deformation structures, and shallow gas deposits are present within these later tunnel valley generations, possibly indicating more dynamic fluctuations of the ice margin (including readvances and stagnation) during valley filling and ice retreat.

In addition, extensive proglacial outwash sediments are particularly common further south in Study Area 2. This infill unit overtops the valley shoulders in over 50 % of the tunnel valleys that contain it — a characteristic that appears to be independent of valley size. The reduced presence of ice-proximal sediments and the deposition of a regionally extensive blanket of unconfined outwash sediments in this region indicates that ice-margin retreat rates in this area were comparatively rapid — a pattern that occurred over multiple glaciations. The thickness and patterns of tunnel valley infill may also be capable of indicating relative retreat rates and the frequency of readvances of the ice margin in the geological record (Janszen et al., 2012b). For example, infill sequences in which distal outwash deposits are overlain by sediments deposited in an ice-proximal setting indicates a substantial readvance of the ice margin following initial ice retreat. In the areas examined in this chapter, incidences of this pattern are rare (<2 %), indicating that substantial readvances of the ice margin followed by a more gradual retreat did not occur frequently during the deglaciation of the North Sea at times when the tunnel valleys were unfilled. However, a greater number of tunnel valleys in Study Area 2 (14 %) are entirely filled with outwash sediments compared to those in Study Area 1 (3 %), a trend that is particularly apparent for more recent tunnel valley generations (8–10). This pattern may indicate that the southern North Sea experienced greater ice-marginal retreat rates compared to the central North Sea where thicker deposits of ice-proximal facies are present. These inferences are supported by numerical model and geomorphological reconstructions of the deglaciation of the North Sea during the last glaciation, which conclude that the unzipping of the British-Irish and Scandinavian ice sheets was rapid and was primarily driven by the retreat of the Norwegian Channel Ice Stream (Gandy et al., 2021; Clark et al., 2022b).

An exception to this pattern is where landforms, in particular crevasse-squeeze ridges, are observed within the valley fills (Figures 7.9, 7.10). Where observed, crevasse-squeeze ridges are buried within the outwash unit. Formatively linked to glacial surging (Sharp, 1985; Solheim and Pfirman, 1985), an absence of ice-proximal sediments above and below these ridges demonstrates that a rapid readvance and retreat of the ice margin occurred before and after ridge deposition, respectively. This suggests that in rare cases, rapid and substantial fluctuations (surges or readvances and stagnation) of the ice margin occurred during deglaciation, potentially facilitated by changing basal hydrological conditions within the tunnel valleys themselves (Kirkham et al., 2021). Other subglacial landforms buried within the tunnel valleys likely reflect minor seasonal readvances of the ice margin. For example, the formation of continuous and often laterally extensive (>14 km) depositional landforms such as eskers (Figure 7.11), rather than more discontinuous

beaded structures, demonstrates that sediment supply outpaced ice retreat in these environments (Livingstone et al., 2020).

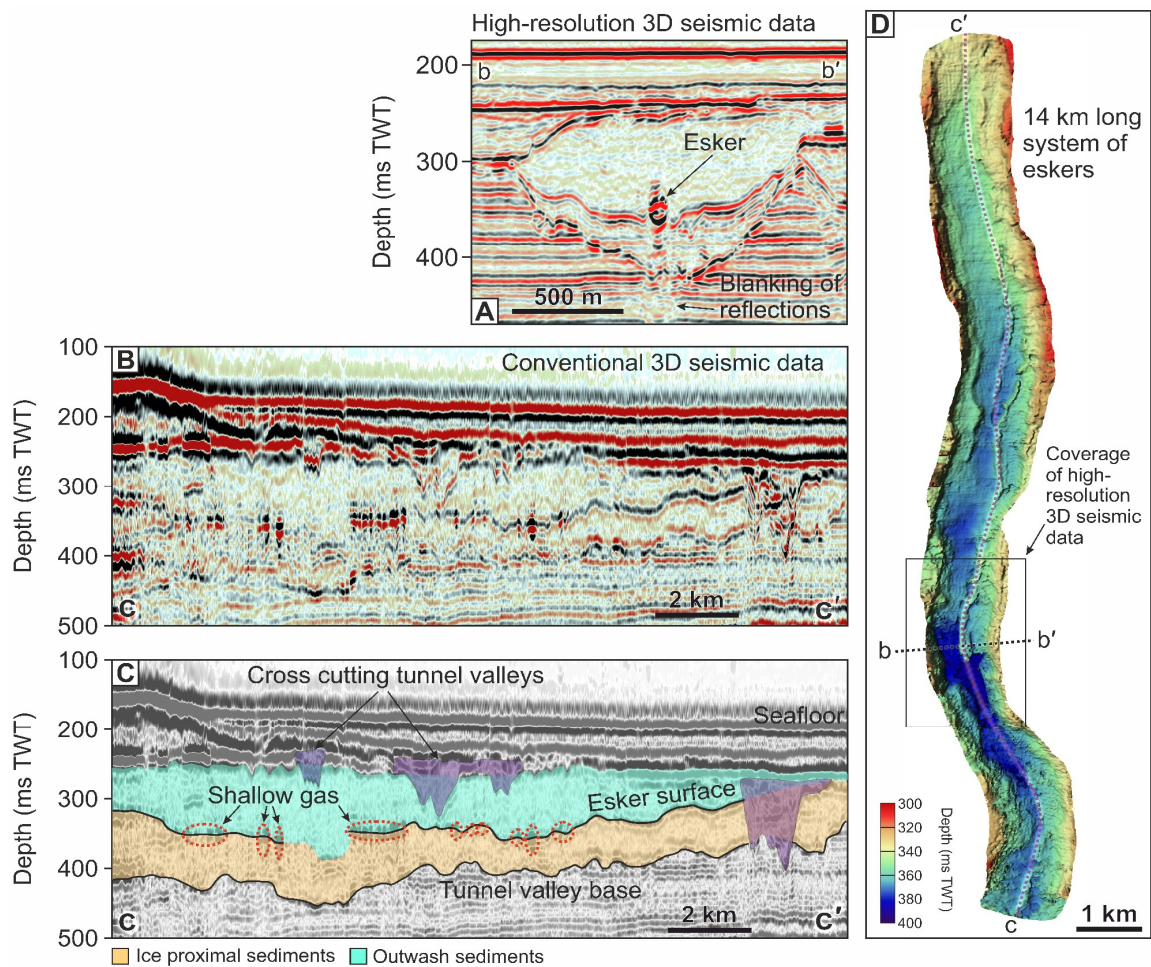


Figure 7.11. Gas-charged eskers buried within tunnel valleys. (A) Cross-section of a tunnel valley in high-resolution 3D seismic data containing an esker characterised by a high-amplitude seismic reflection with phase-reversed polarity over the ridge crest. (B) Seismic profile along the length of the esker using conventional 3D seismic data, interpreted in (C). Stippled red lines indicate the locations of shallow gas anomalies. (D) Mapped seismic horizon in the centre of the tunnel valley infill corresponding to the esker reflection in conventional 3D seismic data. A 14-km long system of eskers can be visualised.

Landforms are most commonly present within larger tunnel valleys (wider than ~400 m and deeper than ~75 m), particularly in the deepest ones, and typically occur within valleys characterised by more complex infill patterns (>2 seismic facies) (Figure 7.9). High-amplitude, phase-reversed seismic reflections and blanking of reflections associated with the presence of shallow gas (Fader, 1997) also occur most frequently within larger tunnel valleys with complex infill architectures. However, in contrast to the landforms which are present in most tunnel valley generations, shallow gas accumulations generally occur within older tunnel valley generations (Figures 7.3D, 7.4D); this observation might

indicate that the shallower sediments covering these tunnel valleys might be ineffective as a trap for gas in the younger valley generations.

The relative position of the subglacial landforms within the sedimentary facies that buries them within the tunnel valleys is capable of indicating relative retreat rates. Approximately 46 % of the buried eskers observed in the tunnel valleys are situated between two layers of ice-proximal sediments. This pattern indicates that a readvance occurred over the first ice-proximal unit. The esker was then formed before the ice gradually retreated from the tunnel valley, depositing the second ice-proximal unit. The preservation of eskers also implies that there was little or no ice flow in the tunnel valley after the eskers formed; this situation could occur if ice margin had surged along the tunnel valley and then stagnated prior to esker formation (Kirkham et al., 2021). In contrast, a pattern of rapid ice-margin retreat following esker deposition is slightly more commonly observed as 54 % of buried eskers are located at the boundary between ice-proximal and outwash sediments. This pattern indicates that a readvance of the ice margin, followed by esker deposition and then rapid lift off and retreat of the ice front, occurred in these settings. The rapid retreat style implied by the presence of thick outwash sediments at the top of the tunnel valleys is supported by the association between this sedimentary facies and the higher continuity of eskers buried by this package compared to those buried by further ice-proximal sediments. This implies that the eskers were exposed from beneath the grounded ice sheet only briefly before being blanketed by outwash sediments, enabling their excellent preservation compared to the slower ice retreat implied by the presence of ice-proximal sediments over these features (Storrar et al., 2014; Storrar et al., 2019).

Eskers buried within the tunnel valleys are characterised by high-amplitude seismic reflections with phase-reversed polarity over the ridge crests (Figures 7.11A, 7.11B, 7.11C, 7.12). Combined with acoustic masking of underlying reflectors, these characteristics suggest that the eskers often contain shallow gas within their constituent sediments (Fader, 1997; Buckley, 2012; Rose et al., 2018). Accordingly, when HR3D seismic data are available to use as a guide, it is possible to image eskers using conventional 3D seismic data as the shallow gas within them highlights them from the surrounding valley infill (Figure 7.11C). Correlation analysis between the eskers and the gas-charged “Crenulate Reflector” beneath them (Fyfe et al., 2003; Stoker et al., 2011) reveals that there is little to no correlation between the location of gas accumulations within these features (Figure 7.12). This lack of correlation may indicate that the shallow gas contained within the eskers is biogenic in origin. However, as the coarse-grained deposits comprising the eskers represent high permeability pathways, gas from the

underlying strata would only need to migrate upwards to the eskers at a single point before migrating along these features to accumulate at local high points or stratigraphic traps. The large shallow gas accumulation at the intersection of the two tunnel valleys (Figure 7.12A) is also notable as it shows that the tunnel valley walls constitute seals that can trap gas in the adjacent strata (Callow et al., 2021). The presence of gas within the North Sea eskers indicates that such structures are potentially a hazard for the installation of near-seafloor infrastructure. In addition, the extensive length (>14 km) and continuity of many of the eskers may also pose a threat to carbon capture and storage attempts. This is because if fluids were ever to migrate from storage reservoirs to the shallower depths in which the eskers are found, they would provide preferential pathways through which trapped gases could migrate laterally through the subsurface.

The inventory of tunnel valley infill presented in this chapter supports the conclusions of previous studies which do not observe clinoform structures within valleys present in the central North Sea (Stewart et al., 2012). However, in the southern North Sea, tunnel valleys are filled with hundreds of metre-high, kilometre-long, clinoforms that dip northward towards the former ice-sheet centre(s) with angles of 0.5–12° (Laban, 1995; Praeg, 2003; Kristensen et al., 2007; Kristensen et al., 2008). These clinoform structures thus appear to be relatively unique to tunnel valleys present in the southern North Sea, as they have not been confidently observed in outcrops onshore in northwest Europe (Ehlers et al., 1984; Benvenuti et al., 2018), although clinoform-like geometries have been recognised in outcrops of late Ordovician tunnel valleys preserved in North Africa (Le Heron et al., 2004). An exception to this trend is one tunnel valley covered by HR3D seismic data in the central northern North Sea (Study Area 3). Here, subtle structures resembling clinoforms are imaged from some orientations along the tunnel valley (Figure 7.8A). The reflections have dip angles <4°, which is within the range of slopes reported from the well-known clinoform examples in the southern North Sea (1–11°), and dip towards the former ice-sheet centre in a similar manner to those filling the tunnel valleys present in the southern North Sea (Praeg, 1996; Kluiving et al., 2003; Kristensen et al., 2008). However, without further HR3D seismic data coverage, it is difficult to assess the scale and prevalence of these features within neighbouring valleys as they are difficult to detect using conventional 3D seismic data alone (Figure 7.8C).

Another unusual feature of the tunnel valleys in Study Area 3 is the differential erosion of some filled tunnel valleys, leading to a domed profile (Figures 7.6A, 7.6C, 7.6E). Streamlined glacial landforms located adjacent to the tunnel valleys demonstrate that they have been overridden by fast-flowing ice subsequent to their infilling with dense sands (e.g., Clark, 1993; Graham et al., 2007; King et al., 2009) (Figure 7.6D). The

dimensions, elongation ratios, and orientation of these landforms suggest that this region was overridden by a tributary of the Norwegian Channel Ice Stream. This fast-ice flow preferentially eroded the softer clay-dominated sediments surrounding the infilled valley, leaving the more resistant tunnel valley infill standing proud of its surroundings (Figure 7.6E). However, even the densely consolidated sands filling the tunnel valleys should have been relatively easy to erode by a grounded ice stream. Consequently, an additional factor potentially facilitated the unusual resistance of this material to glacial erosion, such as freezing or the accumulation of gas-hydrates.

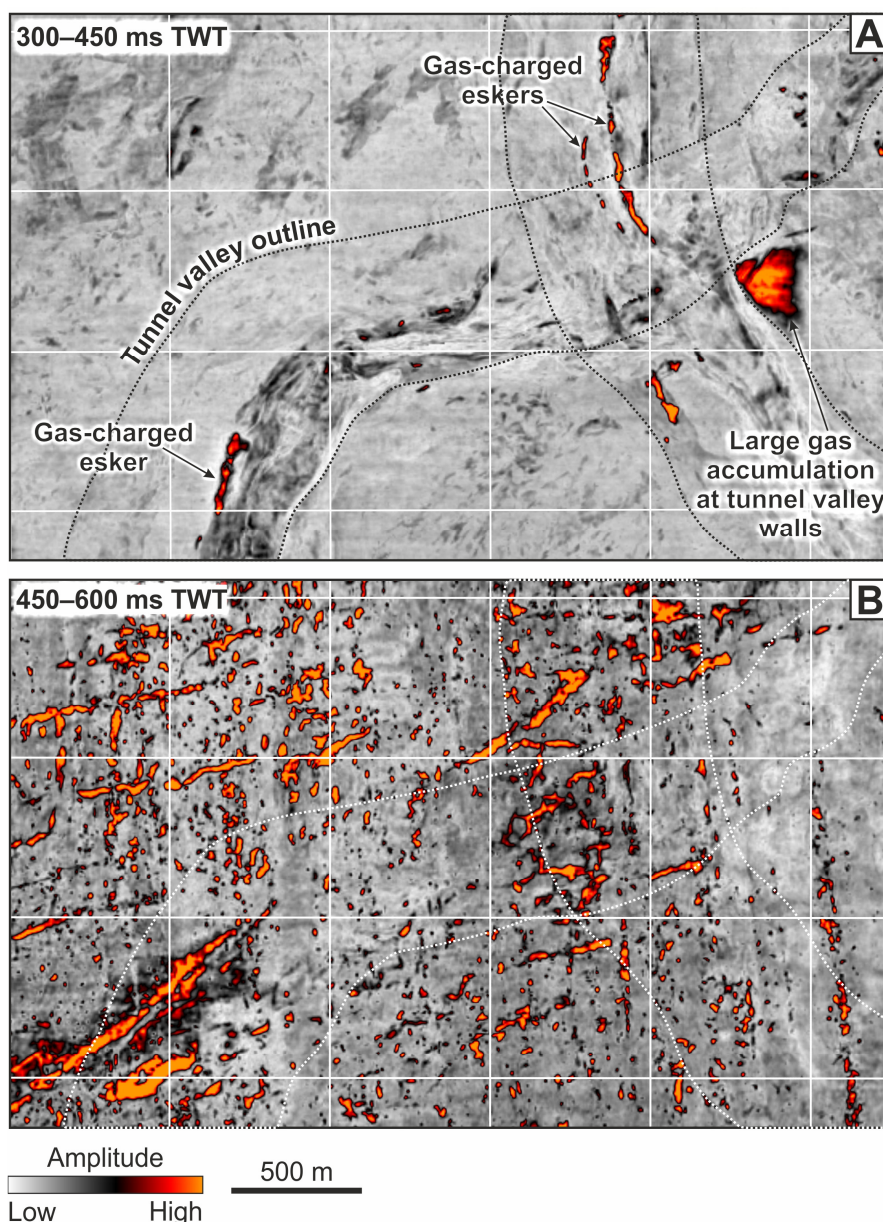


Figure 7.12. Comparison of amplitude anomaly extractions between depths where tunnel valleys are present and the underlying gas-charged Crenulate Reflector. (A) Amplitude anomaly extraction at 300–450 ms TWT highlighting the locations of gas-charged eskers (high amplitudes). (B) Amplitude anomaly extraction at 450–600 ms TWT displaying the gas-charged Crenulate Reflector.

Accumulations of subglacial gas-hydrates have been associated with areas of high basal traction — sticky spots — beneath palaeo ice streams in the Barents Sea (e.g., Winsborrow et al., 2016; Serov et al., 2017). The presence of gas hydrates can lead to an eight-fold increase in sediment shear strength through desiccating and stiffening their host sediments (e.g., Winters et al., 2004; Waite et al., 2009); this increase in sediment stiffness could have protected the tunnel valley sediments from the erosion of overriding ice. However, whilst there is some evidence for gas migration and escape through the tunnel valley sediments in the form of seabed pockmarks, phase-reversed reflections, and the blanking of underlying reflections, these indicators are not widespread in the locality of the tunnel valleys. Furthermore, any pockmarks that are present are not preferentially clustered above the tunnel valley fills as would be expected in the case of extensive gas hydrates being released in this area.

Alternatively, the sediments could have been strengthened through the incorporation of frozen water within them. The clinofolds noted within the southern North Sea tunnel valleys have been used as a basis to propose a ‘backfilling’ model of tunnel valley infilling close to the margin of a retreating ice sheet (Praeg, 2003; Kristensen et al., 2008). This theory postulates that tunnel valleys form and fill as a ‘conveyor-belt’ system, with sediment-laden meltwater produced in the ice-sheet interior being transported and plastered onto steep adverse bed slopes near the ice-sheet margin to form the clinofold structures through the process of glaciohydraulic supercooling. As the water becomes supercooled, thick sections of sediment-laden frazil and platy ice accrete onto the substratum sediments, trapping sediments in the ice (Alley et al., 1998; Lawson et al., 1998). Once deposited, the tunnel valley sediments could remain frozen due to the migration of groundwater from upstream regions, characterised by thicker ice and thus high pressures, towards the thinner ice marginal regions where it may freeze as it enters this lower pressure setting. The importance of tunnel valleys as groundwater reservoirs in many formerly glaciated settings supports this hypothesis (Sharpe et al., 1996; Piotrowski, 1997a; BurVal Working Group, 2006; van der Vegt et al., 2012). Whilst many tunnel valleys mapped in this study contain sandy facies that overtops the valley shoulders, it is notable that the tunnel valleys containing a domed proud-standing infill are also the only ones that contain subtle structures resembling clinofolds within them. If the clinofold-like structures interpreted within the tunnel valley are real, they could suggest that the freezing of water within these sediments, both during and after deposition, helped to protect these dome-shaped tunnel valley fills from subsequent ice-sheet overriding.

7.6 Conclusions

This chapter represents the most detailed attempt to characterise the infill of buried Quaternary tunnel valleys in the central North Sea to date. Improved regional 3D and state-of-the-art HR3D seismic data reveal ten cross-cutting generations of tunnel valleys buried beneath the seafloor of the central and central southern North Sea where only seven were visible previously. These results support models of a more complex glacial history in western Europe than considered previously, and potentially suggest that it is possible to rapidly erode and infill multiple generations of tunnel valleys within a single glacial cycle. Further chronological constraints from boreholes are required to confirm or refute these hypotheses in the future.

Although the infill architecture of the tunnel valleys in the North Sea is immensely variable, advances in the resolution of 3D seismic data permit some subtle patterns to be drawn out which were unresolvable in previous datasets. The number of facies distinguishable in HR3D seismic data is similar to the number of sedimentary units described in borehole investigations; HR3D seismic data are therefore capable of revealing the true morphology and infill structures present within buried tunnel valleys. The overall pattern of tunnel valley infill in the North Sea records decreasing ice-sheet influence towards the top of the tunnel valleys and reflects the retreat of the ice-sheet margin away from the features after they are incised. At a more subtle level, earlier tunnel valley generations contain simpler infill architectures than later tunnel valley generations, reflecting sedimentation during relatively gradual ice-sheet retreat with occasional episodes of overriding by re-advancing grounded ice. Tunnel valleys formed in more recent glaciations have more variable sedimentation patterns with a higher incidence of outwash sediments, buried subglacial landforms, and deformation structures that potentially reflect more dynamic fluctuations of the ice margin (including readvances and stagnation) during valley filling and ice retreat in recent glaciations.

Delicate subglacial landforms such as eskers and crevasse-squeeze ridges are imaged within the tunnel valleys and imply that tunnel valley formation is linked to dynamic ice-sheet behaviour in areas where meltwater production rates are high. These landforms may contain shallow gas accumulations that represent a hazard for seafloor installation and may reduce the efficiency of carbon capture and storage efforts in areas where tunnel valleys are present. These findings underline the importance of considering tunnel valleys as regulators of ice dynamics in models of future ice-sheet change, and the need to survey these features at a high resolution when attempting to install infrastructure in formerly glaciated regions.

Chapter 8

Synthesis and conclusions

8.1 Purpose of this chapter

Subglacial landforms present in formerly glaciated regions record glacial erosion, sediment transport and deposition in otherwise inaccessible environments at the base of past ice sheets. The overall research aim of this thesis was to use the geological record of water flow beneath past ice sheets to understand how the subglacial drainage systems of contemporary ice sheets may evolve in a warming climate. This overarching aim was split into three research objectives: (i) to constrain the routing and fluxes of subglacial water beneath past ice sheets; (ii) to examine the impact of subglacial water flow on ice-sheet dynamics during deglaciation; (iii) to investigate the sedimentation patterns resulting from subglacial water flow and other glacier-influenced processes during deglaciation. These objectives formed the basis of Chapters 4–7. This concluding chapter places the developments made in Chapters 4–7 into a broader context, identifies the limitations of this work, and suggests directions for future research.

8.2 Flux and routing of water beneath deglaciating ice sheets

8.2.1 Advances made in the thesis

The first research objective of the thesis was to constrain the routing and fluxes of subglacial water beneath deglaciating ice sheets. This objective was motivated by the need to improve understanding of the effect of subglacial water as a lubricant at the basal ice-sheet boundary in order to accurately incorporate this process into models of future ice-sheet behaviour with its implications for sea-level rise (Fricker and Scambos,

2009; Flowers, 2015; Fricker et al., 2016). Although the movement of water beneath contemporary ice sheets has been charted from space (Wingham et al., 2006; Fricker and Scambos, 2009; Fricker et al., 2016; Bowling et al., 2019; Livingstone et al., 2022), observations derived from satellite altimetry products are short (decades) compared to the timescales associated with glacial advance and retreat cycles (tens of thousands of years). Furthermore, although theory exists to predict the routing of water in subglacial environments (e.g., Shreve, 1972; Walder and Fowler, 1994; Ng, 2000), models of contemporary water drainage often fail to reproduce the patterns of water movement indicated by surface elevation data from modern ice sheets (Peters et al., 2009), whilst hydrological calculations (e.g., Willis et al., 2016) and geostatistical models (e.g., MacKie et al., 2020) predict numbers of subglacial lakes that are an order of magnitude greater than those currently observed (Livingstone et al., 2022).

Landforms produced by subglacial meltwater provide definitive records of water flow beneath ice sheets. The tangible nature of these records permits the long-term routing of subglacial meltwater to be constrained with greater certainty than when attempting to access inaccessible contemporary ice-sheet beds. Moreover, the morphology of these meltwater features, combined with numerical modelling reconstructions of water flow beneath past ice sheets, can be used to infer the manner in which subglacial meltwater is routed and stored in the subglacial environment. However, until now, the timescales over which subglacial meltwater can incise large channels into the beds of ice sheets has remained poorly constrained (Kehew et al., 2012; van der Vegt et al., 2012), limiting our understanding of how water flow affects ice-sheet dynamics over glacial-interglacial timescales.

In Chapters 4 and 6, a combined geomorphological and numerical modelling approach was employed to constrain the fluxes and routing of subglacial water beneath two very different ice sheets. In Chapter 4, evidence for past water flow was mapped and modelled through a 19,000 km² area containing over 1000 channels and 19 former subglacial lake basins exposed on the seafloor by the retreat of Pine Island and Thwaites glaciers in West Antarctica (Kirkham et al., 2019). A systematic mapping approach revealed that the channels offshore from present-day Pine Island and Thwaites glaciers are approximately twice as deep, 3 times as wide, and cover an area over 400 times larger than the Labyrinth, the largest terrestrial meltwater channel complex described previously in Antarctica (Sugden et al., 1991; Denton and Sugden, 2005; Lewis et al., 2006). By combining analyses of channel morphology with numerical model reconstructions of the Last Glacial Maximum configuration of the West Antarctic Ice Sheet, the analyses conducted in Chapter 4 demonstrated that the channels incised into

bedrock offshore from contemporary Pine Island and Thwaites glaciers could accommodate discharges of up to $8.8 \times 10^6 \text{ m}^3 \text{ s}^{-1}$ if filled to the bankfull level.

In Chapter 6, the morphology and formation of a series of similarly massive channels (300–3000 m wide and up to 300 m deep) were analysed using HR3D seismic data, this time situated in the North Sea (Kirkham et al., 2022). The cross-cutting tunnel valleys present in this region have been incised over multiple glaciations, potentially spanning back to the Brunhes-Matuyama magnetic reversal event $\sim 800,000$ years ago (Stoker et al., 1983; Stewart and Lonergan, 2011). This chapter presented a series of numerical modelling experiments informed by new observations from HR3D seismic data that were used to test different hypotheses of tunnel valley formation and calculate subglacial water routing, water discharges, and the rates at which tunnel valleys are eroded beneath deglaciating ice sheets.

The ice sheets studied in Chapters 4 and 6 vary markedly in terms of their hydrological regimes, with the last British-Irish Ice Sheet being characterised by abundant surface melting whilst the West Antarctic Ice Sheet is primarily a polar ice sheet. In addition, the dominant substrate type in the regions where the channels are situated differs markedly (sedimentary basin versus crystalline bedrock, respectively). Due to a lack of surface meltwater production on the grounded portions of the contemporary Antarctic Ice Sheet (Trusel et al., 2013; Kingslake et al., 2017; Bell et al., 2018), with even less expected during late Pleistocene full-glacial conditions (Golledge et al., 2013), Chapter 4 argued that the channels were formed by episodic discharges from subglacial lakes trapped during ice-sheet advance and retreat over multiple glacial periods. This high-magnitude, low-frequency mechanism is required to explain the formation of the channels as the calculated fluxes of water flowing in continuous steady state beneath the LGM ice sheet are far too low (typically less than $20 \text{ m}^3 \text{ s}^{-1}$ in most channels) to have formed bedrock channels of the scale observed in Pine Island Bay. Due to the long timescales over which this process likely operates (thousands of years), this mechanism may be outside the range of processes captured by modern observations of subglacial hydrology.

In contrast, in the North Sea, networks of smaller or abandoned channels at the base of larger tunnel valley tracts indicate that these tunnel valleys were carved through the action of migrating smaller channels and were later widened by ice-contact erosion. Numerical modelling results demonstrate that the drainage of extensive surface meltwater to the ice-sheet bed was a powerful erosive mechanism and constitutes the dominant driver of tunnel valley formation in this region. The drainage of surface meltwater alone can muster continuous steady-state subglacial water fluxes of 50–

900 m³ s⁻¹ within a single tunnel valley near the ice-sheet margin. These water fluxes are 3–5 orders of magnitude greater than those predicted from basal melting alone. Accordingly, the results of Chapter 6 demonstrate that abundant surface meltwater production and transfer can drive rapid incision of networks of regularly spaced subglacial tunnel valleys beneath the fringes of retreating ice sheets within hundreds to thousands of years during deglaciation.

The crystalline bedrock substrate of the West Antarctic inner continental shelf would be difficult to erode rapidly, even in the presence of high meltwater fluxes (Smith et al., 2009b; Nitsche et al., 2013). The lack of channel cross-cutting observed within the channel network, combined with the low erodibility of the bedrock substrate, indicates that the entire network of anastomosing channels present in Pine Island Bay was likely operational when transporting meltwater from beneath the former expanded catchments of Pine Island and Thwaites glaciers. Consequently, the entire channel network was likely cut cumulatively by meltwater erosion over multiple glaciations, although the routing of water through some channels may be affected by the deformation of ice into the channels from above (Kirkham et al., 2019; Larter et al., 2019; Hogan et al., 2022).

In contrast, the relatively rapid rates of incision observed for tunnel valleys in soft-sedimentary substrates means that entire networks of tunnel valleys can be formed within a single glaciation, or potentially even within warm climate excursions lasting on the order of a millennium during a glaciation if meltwater availability is sufficiently high. Once infilled, subtle changes in the geometry of ice sheets during subsequent glaciations can drive changes in subglacial water routing which may differ from previous glaciations, resulting in the cross-cutting patterns of tunnel valleys observed in many formerly glaciated regions (e.g., Jørgensen and Sandersen, 2006; van der Vegt et al., 2012; Atkinson et al., 2013; Stewart et al., 2013; Ottesen et al., 2020). The morphological similarity between the North Sea tunnel valleys and the bedrock meltwater channels in West Antarctica (see, for example, Figure 9 in Kirkham et al., 2020), despite these channels being formed in markedly different substrates and over radically different timescales, serves as a reminder of the importance of considering equifinality when using glacial landforms to understand the former hydrological dynamics of ice sheets.

8.2.2 Directions for future work

Although the water routing calculations conducted in Chapters 4 and 6 rely on gradients of hydraulic potential to determine water flow direction (Shreve, 1972), the ice-surface topography that dictates the calculated water routing is assumed to be static through time. While Chapter 6 addresses this issue to some extent by examining changes in water

routing at different model time slices (e.g., 21 ka compared to 19 ka), in reality the presence of subglacial water has been intricately linked to ice-sheet dynamics over much shorter timescales (hours to years) (e.g., Alley et al., 1994; Bell, 2008; Stearns et al., 2008; Chandler et al., 2013; Andrews et al., 2014; Chudley et al., 2019; Livingstone et al., 2022). Consequently, time-dependent feedbacks between subglacial water routing, ice flow and surface topography are not captured in the numerical modelling exercises conducted in this thesis. Furthermore, although ice-surface topography exerts approximately 11 times more influence on the direction of water flow than basal topography (Shreve, 1972), changes to basal topography due to subglacial water erosion may still influence water routing directions, particularly if the basal topography exhibits dramatic relief in comparison to the relatively flat ice-sheet surface (i.e., deep meltwater channels). Incorporating actively evolving parameters that represent subglacial water routing and basal erosion into numerical models of ice-sheet flow thus represents a key area for future work. Such increases in model sophistication will be key to accurately estimating how changes in subglacial hydrology will affect contemporary ice sheets in a warming climate.

A second direction for future work relates to the fate of the subglacial water simulated in Chapter 4 after it crosses the boundary from the largely bedrock-dominated inner Antarctic continental shelf to the sedimentary outer shelf. The results of Chapter 4 demonstrate that the bedrock channels present offshore of contemporary Pine Island and Thwaites glaciers could easily accommodate the volume of water produced by basal melting, and even the quantity produced by a drainage cascade of subglacial lakes (Kirkham et al., 2019). However, the manner in which this subglacial meltwater crossed the outer continental shelf, where no channels are present, remains unresolved. Although a small number of buried and infilled channels have been observed beneath soft sediments in the Anvers-Hugo Trough in 2D seismic-reflection profiles (Larter et al., 2019) and several relatively small sedimentary channels have been observed on the seafloor in the Ross Sea (Simkins et al., 2017; Simkins et al., 2021), meltwater channels are generally absent from the softer sediments present on the middle and outer continental shelves around Antarctica (Kirkham et al., 2020). This discrepancy suggests that the transport of subglacial meltwater may have operated via a different mechanism beyond the transition to the softer middle and outer shelf sediments.

An abundance of gullies on the West Antarctic continental slope has been attributed to flows of sediment and subglacial meltwater released from beneath ice-sheets grounded at the continental shelf edge during full-glacial conditions (Gales et al., 2013). Thus, it is unlikely that subglacial water transport halted at the termination of the bedrock

channels. Instead, meltwater could have been evacuated via a canalised drainage mechanism (Walder and Fowler, 1994) or via Darcian flow through the unconsolidated sediments themselves (Graham et al., 2009a). Evidence of these transport mechanisms may then have been subsequently obliterated by ice-sheet retreat (Nitsche et al., 2013), or could have been buried by more recent sediments that obscure any indication of their presence in multibeam bathymetric investigations of seafloor morphology (Kirkham et al., 2020). Detailed HR3D seismic surveys of the outer Antarctic continental shelf may help to delineate any fine-scale sedimentary structures that record how meltwater was transported across this region in the past.

Although seismic surveys are frequently conducted in Antarctica as part of marine geophysical and geological investigations (e.g., Alonso et al., 1992; Gohl, 2012; Gulick et al., 2017; Pérez et al., 2022), these surveys have entirely been conducted in 2D due to the extremely high costs and logistical constraints of acquiring 3D seismic data in ice-infested waters. Evidence for channelised features is sparse within these existing surveys. However, some seismic-reflection surveys have detected features that resemble buried tunnel valleys (Alonso et al., 1992; Montelli et al., 2019) — hinting that these features are likely present in some regions but may be difficult to detect using 2D seismic methods alone. Fully migrated 3D seismic surveys are thus required to confidently detect buried meltwater features with complex geomorphic expressions, and other subtle features that record their corresponding impact on ice-sheet dynamics (Lebedeva-Ivanova et al., 2018; Bellwald et al., 2019; Kirkham et al., 2021). One particularly exciting possibility for future research in this regard is the deployment of the new generation of HR3D seismic survey systems within Antarctic waters (e.g., Petersen et al., 2010; Games and Wakefield, 2014; Bellwald et al., 2018; Lebedeva-Ivanova et al., 2018). These new systems have shorter streamer lengths and are more compact compared to conventional 3D seismic acquisition systems (Figure 8.1), which may permit their effective use even in ice-choked environments (Jakobsson et al., 2016).

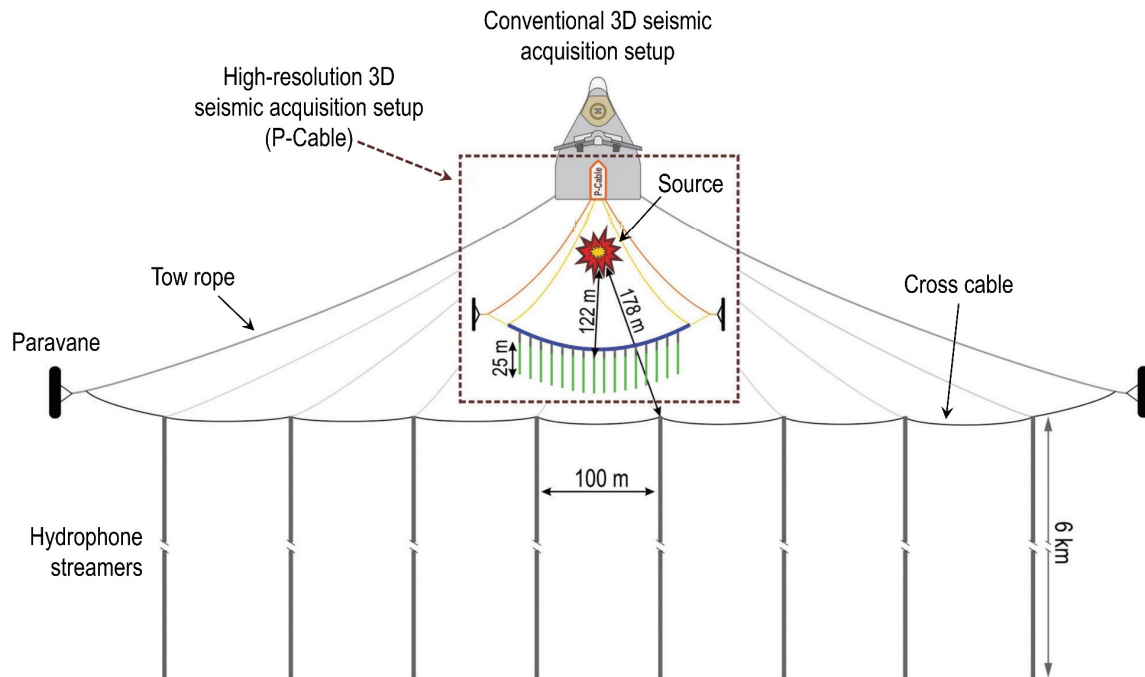


Figure 8.1. Comparison between the size of a conventional 3D seismic acquisition system and the considerably more compact high-resolution 3D seismic P-Cable setup (located within the stippled box). The two systems are drawn at a similar scale. Figure is modified from Lebedeva-Ivanova et al. (2018).

The value of recent technological advances in high-resolution 3D seismic survey design may also be increased by planning where to deploy these systems based on information gleaned from novel machine learning methods. The application of supervised machine learning methods to existing geological and geophysical datasets has recently been used to reveal the spatial distribution of sedimentary basins in Antarctica (Figure 8.2; Li et al., 2022). This novel technique has demonstrated that sedimentary basins are widely distributed across Antarctica, including in the upper catchments of some of Antarctica's most dynamic ice streams such as Pine Island and Thwaites glaciers (Li et al., 2022). These new data provide exciting candidate sites to explore for the presence of tunnel valleys and other subsurface sedimentary features, and underline the importance of understanding basal ice-sheet processes related to the flow of meltwater over sedimentary substrates. In addition, these data could be used to select regions that are most susceptible for tunnel valley formation in the future under meltwater-intensive retreat scenarios.

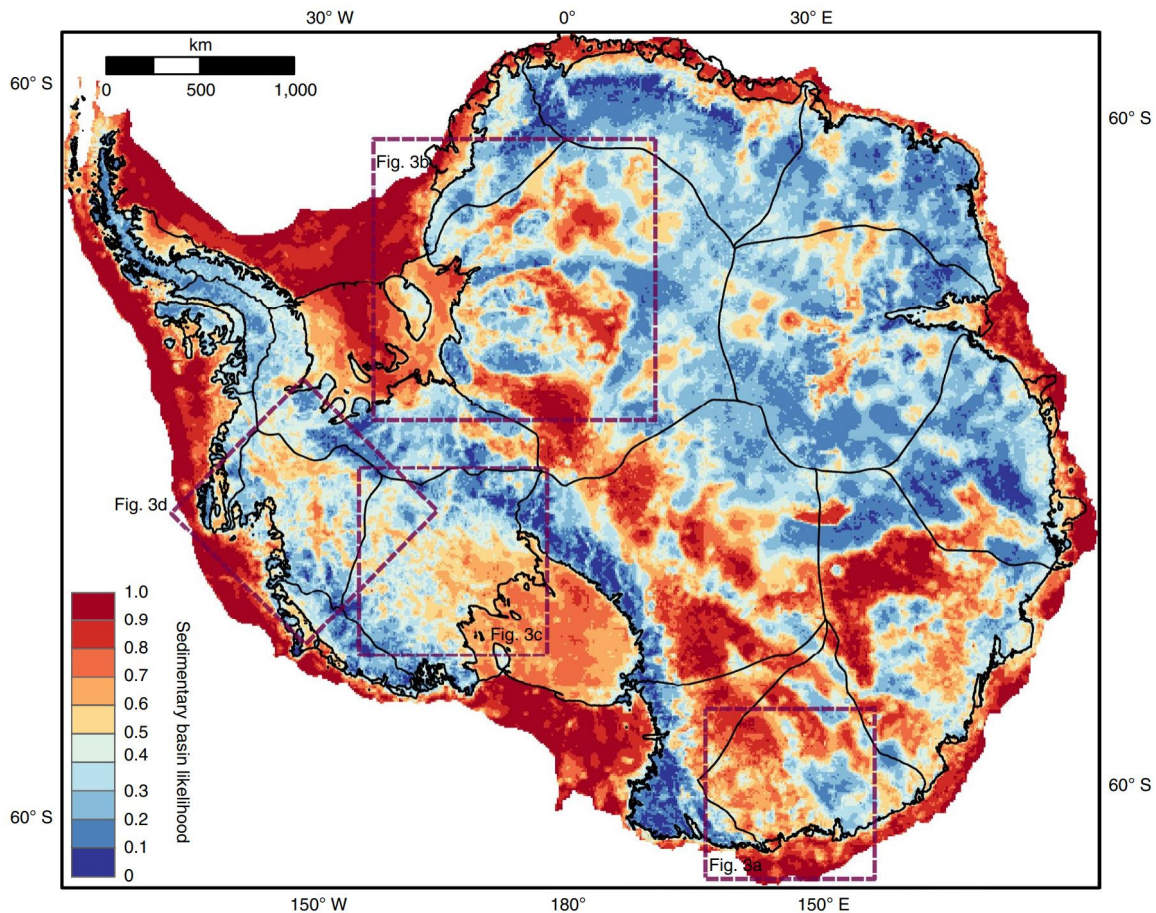


Figure 8.2. Likelihood of sedimentary basins beneath the Antarctic Ice Sheet and the formerly glaciated Antarctic continental shelf. Basin likelihood is calculated by applying a random forest machine learning algorithm to existing geological and geophysical datasets. Black lines delineate major glacier catchments. Figure is reproduced from Li et al. (2022). Stippled boxes refer to the original paper.

8.3 The impact of subglacial water flow on ice-sheet dynamics during deglaciation

8.3.1 Advances made in this thesis

The second research objective of this thesis was to examine the impact of subglacial water flow on ice-sheet dynamics during deglaciation. The movement of water beneath contemporary ice sheets has variable impacts on ice-sheet flow that may enhance (e.g., Stearns et al., 2008; Schoof, 2010; Bartholomew et al., 2011b), reduce (e.g., Sundal et al., 2011; Cowton et al., 2013; Stevens et al., 2016), or have little impact on (e.g., Smith et al., 2017) basal sliding and ice-sheet velocities. However, to date, these linkages have

only been examined over relatively short timescales (days to years) and the effect of basal water on ice-sheet dynamics over longer (>centennial) timescales remains poorly understood (Ashmore and Bingham, 2014; Flowers, 2015).

HR3D seismic data were used in Chapter 5 to analyse the morphology and infill of buried tunnel valleys in the North Sea. These tunnel valleys record meltwater erosion over the last ~800,000 years as multiple ice sheets grew and deglaciated over the United Kingdom and Western Europe in a cyclic fashion (Huuse and Lykke-Andersen, 2000b; Stewart and Lonergan, 2011; Ottesen et al., 2020; Clark et al., 2022b). The tunnel valleys of the North Sea therefore represent a vast and relatively accessible archive of environmental conditions experienced at the beds of ice sheets during deglaciation. This information can be used to understand the effect of basal water on ice-sheet dynamics over centennial to millennial timescales. However, until now, the resolution of the seismic-reflection data available in this region has not been high enough to resolve the delicate internal structures of tunnel valleys and to gain clues as to their impact on ice-sheet dynamics during periods of abundant surface meltwater production.

The HR3D seismic data examined in Chapter 5 represent a step-change in our ability to observe the detailed morphology of tunnel valleys and their internal structures. Although HR3D seismic data have been used to examine the morphology of glacial landforms in other regions (Bellwald et al., 2018; Tasianas et al., 2018; Bellwald et al., 2019; Bellwald et al., 2021), the results of Chapter 5 represent the first time that this technology has been applied to the study of tunnel valleys. Using this novel high-resolution data, the work presented in Chapter 5 shows that over 40 % of the tunnel valleys examined contain glacial landforms including eskers, crevasse-squeeze ridges, glacitectonic structures, kettle holes and braided channel structures buried within them (Kirkham et al., 2021).

The landforms reported in Chapter 5 represent the first time that many of these features have been observed inside tunnel valleys in either terrestrial or marine environments (Kehew et al., 2012; van der Vegt et al., 2012). Consequently, glacial landforms, both erosional and depositional in nature, are likely far more common inside tunnel valleys than previously recognised. The formation of many glacial landforms can be linked to the flow regime and behaviour of the ice sheets that formed them (Benn and Evans, 2010; Dowdeswell et al., 2016b). Accordingly, the landforms now resolvable within the North Sea tunnel valleys can be grouped into two classes based on their inferred relation to former ice-flow behaviour.

The first class of landforms are those which relate to fast ice-flow velocities. Braided channel structures, resolvable at the base of some tunnel valleys, are not decipherable in

conventional 3D seismic surveys (Kirkham et al., 2021; Kirkham et al., 2022). At 80 m wide and ~6 m deep on average, the dimensions of these smaller channel structures are similar, albeit slightly larger, than the canalised conduits theorised to exist beneath and contribute to the high flow velocities of some Antarctic ice streams (~50 m wide and <0.2 m deep) (Walder and Fowler, 1994; Engelhardt and Kamb, 1997; Murray et al., 2008). In addition, the braided channels are sometimes overlain by delicate crevasse-squeeze ridges which have been genetically related to surging ice-flow behaviour (Sharp, 1985; Solheim and Pfirman, 1985; Rea and Evans, 2011). Kettle holes are also observed within some tunnel valleys, which may form through the meltout of stagnant ice blocks stranded after a surge (Ottesen et al., 2017). The presence of these landform assemblages within tunnel valleys strongly implies that the hydrological conditions experienced during tunnel valley formation contribute to dynamic ice-flow behaviour, including surges of the ice margin (Kirkham et al., 2021).

In contrast, a second assemblage of landforms relate to slow-flowing ice. Landforms comprising this class mostly consist of eskers. Eskers are one of the most common glacial landforms observed within the buried tunnel valleys and are present far more frequently than recorded in previous studies. A small selection of other examples have been observed in unfilled tunnel valleys in North America (Shaw and Gilbert, 1990) and with low confidence in a small number of buried examples within Europe (Moscariello et al., 1998; Jørgensen and Sandersen, 2006). Traditionally, eskers and tunnel valleys are thought to coexist only rarely, with eskers theorised to form on bedrock substrates and tunnel valleys on sedimentary substrates (Clark and Walder, 1994). However, our results refute this hypothesis and support recent observational evidence that this association more likely reflects the poor preservation of eskers on soft sedimentary beds (Storrar et al., 2019). The high degree of lateral continuity of the eskers buried beneath the North Sea implies a gradual ice retreat from the tunnel valleys — potentially suggesting that the tunnel valleys promoted ice-sheet stabilisation and deceleration of ice flow during retreat. This conclusion has also been proposed from laboratory modelling experiments (Lelandais et al., 2016; Lelandais et al., 2018). However, an alternative interpretation for these features is that the eskers could have formed after a surge and may represent the remnants of the subglacial drainage system under relatively stagnant ice.

The novel HR3D seismic data presented in Chapter 5 provide unprecedented insights into the impact of tunnel valley formation on ice-sheet dynamics during deglaciation. Traditionally, tunnel valleys have largely been considered relatively non-dynamic features that simply reflect the export of water from beneath ice sheets with high meltwater availability (Kehew et al., 2012; van der Vegt et al., 2012; Lelandais et al.,

2018). The results of Chapter 5 challenge this perception and suggest that tunnel valleys may regulate and trigger dynamic ice-sheet behaviour, potentially in complex ways. As most of these landform assemblages had not previously been detected using conventional 3D seismic-reflection, borehole, or terrestrial surveying methods, the mechanisms that formed them are presently absent from models of tunnel valley genesis. Consequently, ice-sheet models currently lack sufficient complexity to incorporate the effects of tunnel valley formation on ice-sheet dynamics. This will skew projections of ice-sheet evolution in high-end climate warming scenarios characterised by abundant meltwater production.

8.3.2 Directions for future work

A major uncertainty for ice-sheet models is how increasing surface meltwater, once transported to the base of an ice sheet, will affect basal sliding and mass losses over the coming century (Nienow et al., 2017). One of the main origins for this uncertainty is that detailed satellite observations of ice-sheet dynamics date back only 2–3 decades, which is a very short period for the reference and evaluation of century-scale projections in numerical models (Hanna et al., 2020). These uncertainties could be addressed by combining insights into past subglacial drainage systems, such as those gleaned from HR3D seismic datasets, with new advances in ice-sheet modelling. These insights could then be used to predict how accelerating meltwater production in areas such as southwest Greenland will affect ice-sheet velocities when the subglacial hydrological system reorganises into a deglacial drainage configuration.

Although previous models can replicate seasonal accelerations in ice flow after summer melting (e.g., Bougamont et al., 2014; Koziol and Arnold, 2018), basal conditions such as thermal state and the evolution of sub-ice topography remain poorly constrained (Goelzer et al., 2017). Furthermore, even the most advanced models of these processes use relatively coarse resolutions (>1-km grid cells) and simplified parameterisations for basal water pressure, sediment movement and basal sliding, and are not extended to decadal-centennial timescales. As a result, these simulations tend to simplify subglacial hydrology by assuming that water flow is distributed across the ice-sheet bed; assumptions that are inconsistent with the abundant evidence of examples of meltwater drainage in channels in the palaeo record (e.g., Lewington et al., 2020; Livingstone et al., 2020; Dewald et al., 2022).

These shortcomings could be addressed by using high-resolution observations of past subglacial water flow, such as from HR3D seismic data in marine environments or optical stereo imagery in terrestrial environments (e.g., Porter et al., 2018), to initialize a high-resolution model of subglacial water flow under an idealised deglaciating ice sheet. Future

modelling work aiming to address these uncertainties could conduct sensitivity analyses of the range of parameters required to replicate the hydrological conditions needed to produce tunnel valleys and the landform assemblages observed within them. A high-resolution numerical model with a small domain (10 km \times 10 km) and a very fine mesh size (e.g., Gagliardini et al., 2013; Cook et al., 2020) could then be used to investigate the effect that the formation of a single tunnel valley would have on ice-sheet flow. These investigations would provide information about the influence of currently sub-grid scale hydrological processes on ice-sheet behaviour, and whether the next generation of ice-sheet models will need to develop mechanisms of representing these fine-scale processes to ensure accurate predictions of future ice-sheet response to climate warming.

Once established, these fine-scale preliminary model simulations could be used to assess how tunnel valley formation could affect specific regions of an ice sheet in the future. For example, a range of potential melt rates for the Greenland Ice Sheet has already been simulated for the next millennium (Aschwanden et al., 2019) under a range of potential Representative Concentration Pathways (Intergovernmental Panel on Climate Change, 2021). These data could be used as inputs to estimate at what timescales into the future tunnel valleys would be likely to switch on beneath contemporary ice sheets under different climate warming scenarios, providing important information to be incorporated into the next generation of ice-sheet models.

In addition to the use of the morphological findings of this thesis to drive new ice-sheet model development, there are significant opportunities to expand on the 3D seismic analyses conducted here. Although a wealth of information has been revealed from the HR3D seismic datasets investigated in this thesis, the tunnel valleys investigated only represent a small sample (23 tunnel valleys from 7 HR3D seismic datasets). Further investigation of additional datasets would help to expand knowledge of the true prevalence of subglacial landforms buried within tunnel valleys and their full range of examples and distribution.

Moreover, the HR3D seismic datasets contain abundant examples of other glacial landforms such as mega-scale glacial lineations, grounding-zone wedges and iceberg ploughmarks which can now be imaged in stunning detail. The incidence of iceberg ploughmarks represents one particularly interesting avenue for future research. This is because the HR3D seismic data used in this thesis have a high enough resolution to distinguish between different types of iceberg preserved beneath the seafloor, including multi-keeled iceberg ploughmarks which imply the presence of large tabular icebergs within the North Sea in the past (e.g., Figure 3.4). The type and orientation of iceberg

ploughmarks may provide information about palaeo-water depths, ocean-current directions, ice-shelf locations and the geometries of former ice sheets that can only be approximated presently using ice-sheet models constrained by palaeo-tidal information (Scourse et al., 2018; Clark et al., 2022b). Using these high-resolution geomorphological observations to better constrain numerical model reconstructions should thus be prioritised as a key target for future work.

8.4 Sedimentation patterns resulting from subglacial water flow and other processes during deglaciation

8.4.1 Advances made in this thesis

The third and final research objective of this thesis was to investigate the sedimentation patterns resulting from subglacial water flow and other glacier-influenced processes during deglaciation. Where Chapters 5 and 6 used HR3D datasets to examine a relatively small sample of tunnel valleys at a high level of detail, the third research objective required a broader spatial approach. Consequently, Chapter 7 used a much larger suite of datasets, including HR3D seismic data, ultra-high-resolution 2D seismic data, improved-resolution regional scale 3D seismic reflection data, and geotechnical information from industry-acquired boreholes to assess the deglacial sedimentary sequences captured within 321 tunnel valleys in the central North Sea.

The internal infill lithologies and sedimentary architectures of tunnel valleys are notoriously complex as they can reflect a range of sedimentary and erosional processes that occurred during both full-glacial and deglacial times (Kehew et al., 2012). Although efforts have been made previously to characterise the infill of the North Sea tunnel valleys (e.g., Huuse and Lykke-Andersen, 2000b; Kristensen and Huuse, 2012; Stewart et al., 2012), these investigations have been understandably handicapped by the resolution of the seismic data available. These previous seismic datasets have been sufficient to delineate the tunnel valley sides but not the delicate internal structures and the true number of infill packages contained within them. By tying together small areas of HR3D seismic data within a larger conventional 3D seismic survey, the methodological approach of Chapter 7 permits sedimentological signatures related to meltwater flow during ice-sheet retreat to be examined over a regional scale at a relatively high resolution.

The new HR3D seismic data utilised in Chapter 7 permit the morphological and sedimentological record of subglacial meltwater flow and incision in the North Sea to be re-examined. Previously, up to five cross-cutting generations of tunnel valleys were thought to exist in the eastern North Sea (Kristensen et al., 2007), and seven generations

had been mapped in the central North Sea (Stewart and Lonergan, 2011; Ottesen et al., 2020). The revised mappings of Chapter 7 reveal that ten cross-cutting generations of tunnel valleys are buried beneath the seafloor of the North Sea where only seven were visible previously. The presence of numerous generations of cross-cutting tunnel valleys in the North Sea adds weight to the growing body of evidence that the previous model of northwest Europe's glacial history is too simplistic and likely consists of more than three major glaciations over the last 460 kyr (Ehlers et al., 1984; Ehlers, 1990; Stewart and Lonergan, 2011).

Three additional tunnel valley generations are reported in Chapter 7 and compared to the most comprehensive mappings conducted previously (Stewart and Lonergan, 2011; Ottesen et al., 2020). These extra generations may represent either additional tunnel valley forming glaciations in the central North Sea that extend further back than the Elsterian Glaciation (MIS 12), or the formation, filling, and re-incision of tunnel valleys as part of minor retreats and readvances during a more dynamic glacial episode. The theoretical basis for the latter hypothesis was verified in Chapter 6, which demonstrated that tunnel valleys can form in just a few hundred years in the presence of abundant meltwater production during ice-sheet retreat (Kirkham et al., 2022). Alternatively, further cold periods in which tunnel valleys could have potentially formed occurred in MIS 14, 16, and 18, but more robust chronological dating constraints are required to test this hypothesis.

Chapter 7 also made progress towards understanding the broad-scale sedimentary infill patterns of the North Sea tunnel valleys. Whilst the infill architecture of these tunnel valleys remains complex, in accordance with previous studies (e.g., Cameron et al., 1987; Praeg, 1996; Huuse and Lykke-Andersen, 2000b; Kluiving et al., 2003; Praeg, 2003; Kristensen et al., 2007; Kristensen et al., 2008; Lutz et al., 2009; Stewart et al., 2012; van der Vegt et al., 2012), advances in the resolution of 3D seismic-reflection data permit some subtle patterns to be drawn out which were unresolvable in past investigations. The new HR3D seismic data show that the overall pattern of tunnel valley infill in the North Sea records decreasing ice sheet influence towards the top of the tunnel valleys and reflects the retreat of the ice-sheet margin away from the features after they are incised. At a more subtle level, the infill of earlier (older) tunnel valley generations reflects sedimentation during relatively gradual ice-sheet retreat with occasional episodes of overriding by re-advancing grounded ice. In contrast, tunnel valleys formed in more recent glaciations are characterised by greater variability in their sedimentation patterns which reflects dynamic fluctuations of the margins of these later ice sheets, including readvances and stagnation, during valley filling and ice retreat.

The systematic mapping of tunnel valley infill properties in Chapter 7 demonstrates that most tunnel valleys are characterised by a relatively simple infill architecture consisting of 1–2 seismic facies. However, notably more complex examples of tunnel valley fill exist (up to 5 seismic facies), especially in areas where HR3D seismic data coverage is available. Previously, investigations using conventional 3D seismic data had concluded that tunnel valleys exhibited simple bi- or tripartite infill patterns (e.g., Huuse and Lykke-Andersen, 2000b; Kluiving et al., 2003; Lonergan et al., 2006; Stewart et al., 2012), which contrasted with the more complex sedimentary sequences reported from borehole investigations (e.g., Hepp et al., 2012; up to 6 lithological units). The more complex infill patterns reported from the HR3D seismic data reconcile this difference between borehole and seismic observations — demonstrating that HR3D seismic data are capable of capturing fine-scale infill packages not visible in conventional 3D seismic data.

The additional detail provided by the HR3D seismic data permits relative retreat rates and the frequency of ice-margin readvances to be inferred from the geological record by exploring the thickness and patterns of tunnel valley sedimentation. The regional examination of tunnel valley infill reported in Chapter 7 suggests that the southern North Sea experienced greater ice-marginal retreat rates compared to the central North Sea. These inferences support recent numerical model simulations of rapid ice-sheet retreat in this region during the last deglaciation due to the collapse of the Norwegian Channel Ice Stream (Gandy et al., 2021; Clark et al., 2022b).

Whilst Chapter 5 first reported the incidence of subglacial landforms buried within the North Sea tunnel valleys, the distribution of these internal landforms over a broader spatial scale was examined in Chapter 7. This analysis reveals that the landforms are most commonly present within larger tunnel valleys (wider than ~400 m and deeper than ~75 m), particularly in the deepest ones, and typically occur within valleys characterised by more complex infill patterns. In addition, many of the landforms contain shallow gas accumulations. These gas accumulations generally occur within older tunnel valley generations, potentially indicating that the shallower sediments covering the younger tunnel valley generations might be an ineffective stratigraphic trap for shallow gas. Due to the extensive length (>14 km) and continuity of many of these landforms, they potentially represent a hazard for seafloor installations and may reduce the efficiency of carbon capture and storage efforts in areas where tunnel valleys are present.

8.4.2 Directions for future work

Although substantial progress has been made in this thesis by applying HR3D seismic data to the study of tunnel valleys in the North Sea, these advances remain hindered by the paucity of absolute dates for tunnel valley formation and infilling. Current models of tunnel valley chronology rely on their cross-cutting relationships (Lonergan et al., 2006; Kristensen et al., 2007; Stewart and Lonergan, 2011; Stewart et al., 2013) and their maximum age is estimated from palaeomagnetic evidence from a single borehole in the central North Sea (Stoker et al., 1983; Stewart and Lonergan, 2011). Improved chronological constraints may permit specific generations of tunnel valleys to be associated with particular glaciations. This information would help to clearly define former ice-marginal geometries and to further explore differences in the hydrological conditions experienced during the retreat of multiple ice sheets and their corresponding impact on ice-sheet dynamics.

Plans to target features like tunnel valleys in new shallow drilling proposals in the North Sea through efforts such as the International Ocean Discovery Program (e.g., CenoStore; <https://www.iodp.org/iodp/resources/>) provide exciting opportunities to place absolute timing constraints on tunnel valley formation and better determine the Quaternary history of the northwest Europe. However, obtaining records in this manner is rare, expensive, and subject to stringent time limits given the high demand for the drilling vessel in other locations. Another route through which similar data could be obtained is through retrieving and reanalysing borehole material originally gathered for geotechnical purposes at potential hydrocarbon drilling sites. The geotechnical information acquired from these boreholes during collection is already very useful alone, as demonstrated in Chapter 7. However, additional information could be gleaned from these data at relatively little cost if these samples, which are commonly put into permanent storage after preliminary analyses (Figure 8.3), were targeted with specific analyses designed to provide key information about subglacial hydrological processes active as the tunnel valleys are incised and infilled.

For example, micro-scale structures within the tunnel valley infill deposits could be analysed to infer palaeo-current speed estimates, flow conditions during tunnel valley infilling, and whether the infill material was recycled from local sources or supplied from a distal source before being deposited. X-rays or computed tomography scans of the infill material could be used to determine if any smaller depositional structures are present within the samples that may provide clues to their depositional conditions. Detailed measurements of grain size and shape could also be conducted on sub-samples from the boreholes to assess the degree of roundness and reconstruct variations in current velocity throughout the borehole sample. This analysis would provide indications of the erosion

and transport processes experienced by the infill material, and thus within tunnel valleys, during deposition.



Figure 8.3. Examples of borehole samples recovered from the North Sea by the hydrocarbon industry after triaxial geotechnical testing. Similar samples have been recovered from inside tunnel valleys in the North Sea. The sample number and references to the sample owner have been removed for confidentiality purposes. The yellow ruler is 0.12 m high for scale.

In addition, sediment provenance analyses such as clay mineralogy of the tunnel valley infill sediments could be conducted and compared to the sediment recovered in the surrounding boreholes. This would determine whether the detrital sediment infilling the tunnel valleys was locally recycled or transported from a greater distance away from the tunnel valleys, which to date has only been determined for the southern North Sea (Benvenuti et al., 2018). The abundance of samples from tunnel valleys currently held by hydrocarbon companies operating in the North Sea thus represents an opportunity to conduct valuable research into the sedimentary conditions experienced by deglaciating ice sheets for a relatively little outlay.

The association between tunnel valleys and features which host shallow gas accumulations, highlighted in Chapter 7, demonstrates the need to further investigate the role of tunnel valleys as obstacles for carbon capture and storage efforts. This need is especially urgent given that the North Sea is a major target for carbon sequestration in the coming decades (e.g., Haszeldine, 2009; Scott, 2013; Quirk et al., 2022). Present models of subsurface fluid flow that are used to investigate the potential of a site for carbon capture and storage (e.g., Yarushina et al., 2021) should incorporate data of a similar quality to the HR3D seismic data used in this thesis which is capable of resolving fine-scale subsurface structures that could act as preferential fluid flow pathways. Studies that combine high-resolution seismic-reflection data, sediment sampling, and multibeam-bathymetric data of seafloor fluid escape structures (Callow et al., 2021) offer a promising avenue for this research.

8.5 Thesis summary and conclusions

The Earth's cryosphere is undergoing a period of anthropogenically driven climate change that is unprecedented in millennia (Neukom et al., 2019). It is widely acknowledged that changes in meltwater production and the evolution of the subglacial hydrological system will play an increasingly important role in determining the fate and behaviour of contemporary ice sheets as the climate warms (Bell, 2008; Pattyn et al., 2018; Noble et al., 2020). Whilst spaceborne measurements permit these changes to be charted in never-before-seen levels of detail (Wingham et al., 2006; Fricker et al., 2007; Livingstone et al., 2019), the temporal timespan of these measurements is short in comparison to the timescales that ice-sheet processes operate over. Only the palaeo-record can provide context to modern-day changes and capture high-magnitude, low-frequency processes operating on centennial–millennial timescales; these observations are a prerequisite to accurate predictions of future ice-sheet evolution, sea-level rise, and coastal flooding. Technological advances in geophysical methods have led to a ‘geological Hubble’ moment in humankind’s ability to image the planet’s submerged and subsurface layers that are imprinted with records of the waxing and waning of Earth’s ice sheets over millions of years (Cartwright and Huuse, 2005). These methods are now ripe for deployment to understand some of the most inaccessible, yet rapidly changing, environments on Earth.

This thesis has made use of recent advances in marine surveying technology in formerly ice-covered regions to provide new insights into inaccessible subglacial processes. These processes will become increasingly relevant to predictions of ice-sheet evolution and sea-level rise as the Earth continues to warm. By examining landforms preserved on former ice-sheet beds, this thesis has quantified the routing and fluxes of subglacial meltwater beneath parts of the former West Antarctic and Eurasian ice sheets as they underwent retreat and deglaciation. The unprecedented detail provided by the novel geophysical data gathered from these formerly ice-covered settings has highlighted the linkages between subglacial hydrology and ice-sheet dynamics during deglaciation. These ancient records thus offer a window into the conditions that could be experienced by contemporary ice sheets in a future warmer World, and offer insights as to how they may evolve in response to increased meltwater transport beneath them. Future work should focus on understanding the specific mechanisms through which meltwater has influenced ice-sheet dynamics in the past, developing ways to detect when these processes will switch on beneath ice sheets in the present as melting increases, and identifying the locations on modern ice sheets where these processes will likely be most relevant in the future.

Bibliography

- Abdalati, W., and Steffen, K. (2001). Greenland Ice Sheet melt extent: 1979–1999. *Journal of Geophysical Research: Atmospheres*, 106, D24, 33983-33988.
- Adamczyk, A., Wysota, W., and Piotrowski, J. A. (2022). Inventory of glacial curvilineations (GCLs) at the southern periphery of the last Scandinavian Ice Sheet. *Geomorphology*, 400, 108094.
- Allen, M., Poggiali, D., Whitaker, K., et al. (2019). Raincloud plots: a multi-platform tool for robust data visualization. *Wellcome Open Research*, 4(63).
- Alley, R. B. (1989). Water pressure coupling of sliding and bed deformation: 1. water system. *Journal of Glaciology*, 35(119), 108-118.
- Alley, R. B. (1992). How can low pressure channels and deforming tills coexist subglacially? *Journal of Glaciology*, 38(128), 200-207.
- Alley, R. B., Anandakrishnan, S., Bentley, C. R., et al. (1994). A water-piracy hypothesis for the stagnation of Ice Stream C, Antarctica. *Annals of Glaciology*, 20, 187-194.
- Alley, R. B., Blankenship, D. D., Bentley, C. R., et al. (1986). Deformation of till beneath ice stream B, West Antarctica. *Nature*, 322(6074), 57-59.
- Alley, R. B., Cuffey, K. M., Evenson, E. B., et al. (1997). How glaciers entrain and transport basal sediment: Physical constraints. *Quaternary Science Reviews*, 16(9), 1017-1038.
- Alley, R. B., Lawson, D. E., Evenson, E. B., et al. (1998). Glaciohydraulic supercooling: a freeze-on mechanism to create stratified, debris-rich basal ice: II. Theory. *Journal of Glaciology*, 44(148), 563-569.
- Alley, R. B., Lawson, D. E., Evenson, E. B., et al. (2003). Sediment, glaciohydraulic supercooling, and fast glacier flow. *Annals of Glaciology*, 36, 135-141.
- Alley, R. B., Dupont, T. K., Parizek, B. R., et al. (2006). Outburst flooding and the initiation of ice-stream surges in response to climatic cooling: A hypothesis. *Geomorphology*, 75(1-2), 76-89.
- Alonso, B., Anderson, J. B., Díaz, J. I. et al. (1992). Pliocene-Pleistocene Seismic Stratigraphy of the Ross Sea: Evidence for Multiple Ice Sheet Grounding Episodes. *Contributions to Antarctic Research III*, 93-103.
- Anandakrishnan, S., Blankenship, D. D., Alley, R. B., et al. (1998). Influence of subglacial geology on the position of a West Antarctic ice stream from seismic observations. *Nature*, 394(6688), 62-65.
- Anderson, J. B., and Fretwell, L. O. (2008). Geomorphology of the onset area of a paleo-ice stream, Marguerite Bay, Antarctic Peninsula. *Earth Surface Processes and Landforms*, 33(4), 503-512.
- Andersen, K. K., Azuma, N., Barnola, J. M., et al. (2004). High-resolution record of Northern Hemisphere climate extending into the last interglacial period. *Nature*, 431(7005), 147-151.
- Andreassen, K., Nilssen, L. C., Rafaelsen, B., et al. (2004). Three-dimensional seismic data from the Barents Sea margin reveal evidence of past ice streams and their dynamics. *Geology*, 32(8), 729-732.
- Andrews, L. C., Catania, G. A., Hoffman, M. J., et al. (2014). Direct observations of evolving subglacial drainage beneath the Greenland Ice Sheet. *Nature*, 514(7520), 80-83.
- Anell, I., Thybo, H., and Rasmussen, E. (2012). A synthesis of Cenozoic sedimentation in the North Sea. *Basin Research*, 24(2), 154-179.
- Arias, P. A., Bellouin, N., Coppola, E., et al. (2021). Technical Summary. In: Masson-Delmotte, V., Zhai, P., Pirani, A., et al. (eds.), *Climate Change 2021: The Physical Science Basis. Contribution of Working Group I to the Sixth Assessment Report of the Intergovernmental Panel on Climate Change*: Cambridge, United Kingdom and New York, USA, Cambridge University Press, 33–144.
- Arndt, J. E., Schenke, H. W., Jakobsson, M., et al. (2013). The International Bathymetric Chart of the Southern Ocean (IBCSO) Version 1.0—A new bathymetric compilation covering circum-Antarctic waters. *Geophysical Research Letters*, 40(12), 3111-3117.

- Arndt, J. E., Larter, R. D., Friedl, P., et al. (2018). Bathymetric controls on calving processes at Pine Island Glacier. *The Cryosphere*, 12(6), 2039-2050.
- Arnold, N. (2010). A new approach for dealing with depressions in digital elevation models when calculating flow accumulation values. *Progress in Physical Geography: Earth and Environment*, 34(6), 781-809.
- Aschwanden, A., Fahnestock, M. A., Truffer, M., et al. (2019). Contribution of the Greenland Ice Sheet to sea level over the next millennium. *Science Advances*, 5(6), eaav9396.
- Ashmore, D. W., and Bingham, R. G. (2014). Antarctic subglacial hydrology: current knowledge and future challenges. *Antarctic Science*, 26(6), 758-773.
- Atkins, C., and Dickinson, W. (2007). Landscape modification by meltwater channels at margins of cold-based glaciers, Dry Valleys, Antarctica. *Boreas*, 36(1), 47-55.
- Atkinson, N., Andriashek, L. D., and Slattery, S. R. (2013). Morphological analysis and evolution of buried tunnel valleys in northeast Alberta, Canada. *Quaternary Science Reviews*, 65, 53-72.
- Augustin, L., Barbante, C., Barnes, P. R. F., et al. (2004). Eight glacial cycles from an Antarctic ice core. *Nature*, 429(6992), 623-628.
- Baker, C. A. (1977). Quaternary stratigraphy and environments in the Upper Cam Valley, North Essex. Unpublished PhD thesis, University of London.
- Bamber, J. L., Siegert, M. J., Griggs, J. A., et al. (2013). Paleofluvial mega-canyon beneath the central Greenland Ice Sheet. *Science*, 341(6149), 997-999.
- Bamber, J. L., Oppenheimer, M., Kopp, R. E., et al. (2019). Ice sheet contributions to future sea-level rise from structured expert judgment. *PNAS*, 116(23), 11195-11200.
- Banwell, A. F., Willis, I. C., and Arnold, N. S. (2013). Modeling subglacial water routing at Paakitsoq, W Greenland. *Journal of Geophysical Research: Earth Surface*, 118(3), 1282-1295.
- Banwell, A., Hewitt, I., Willis, I., et al. (2016). Moulin density controls drainage development beneath the Greenland ice sheet. *Journal of Geophysical Research: Earth Surface*, 121(12), 2248-2269.
- Barrand, N. E., Vaughan, D. G., Steiner, N., et al. (2013). Trends in Antarctic Peninsula surface melting conditions from observations and regional climate modeling. *Journal of Geophysical Research: Earth Surface*, 118(1), 315-330.
- Barth, A. M., Clark, P. U., Bill, N. S., et al. (2018). Climate evolution across the Mid-Brunhes Transition. *Climate of the Past*, 14(12), 2071-2087.
- Bartholomew, I., Nienow, P., Mair, D., et al. (2010). Seasonal evolution of subglacial drainage and acceleration in a Greenland outlet glacier. *Nature Geoscience*, 3(6), 408-411.
- Bartholomew, I., Nienow, P., Sole, A., et al. (2011a). Supraglacial forcing of subglacial drainage in the ablation zone of the Greenland ice sheet. *Geophysical Research Letters*, 38(8), L08502.
- Bartholomew, I. D., Nienow, P., Sole, A., et al. (2011b). Seasonal variations in Greenland Ice Sheet motion: Inland extent and behaviour at higher elevations. *Earth and Planetary Science Letters*, 307(3), 271-278.
- Batchelor, C. L., Dowdeswell, J. A., and Pietras, J. T. (2013). Seismic stratigraphy, sedimentary architecture and palaeo-glaciology of the Mackenzie Trough: evidence for two Quaternary ice advances and limited fan development on the western Canadian Beaufort Sea margin. *Quaternary Science Reviews*, 65, 73-87.
- Batchelor, C. L., Dowdeswell, J. A., and Rignot, E. (2018). Submarine landforms reveal varying rates and styles of deglaciation in North-West Greenland fjords. *Marine Geology*, 402, 60-80.
- Batchelor, C. L., Margold, M., Krapp, M., et al. (2019). The configuration of Northern Hemisphere ice sheets through the Quaternary. *Nature Communications*, 10(1), 3713.
- Batchelor, C. L., Montelli, A., Ottesen, D., et al. (2020). New insights into the formation of submarine glacial landforms from high-resolution Autonomous Underwater Vehicle data. *Geomorphology*, 370, 107396.
- Beaud, F., Flowers, G. E., and Venditti, J. G. (2016). Efficacy of bedrock erosion by subglacial water flow. *Earth Surface Dynamics*, 4(1), 125-145.

Bibliography

- Beaud, F., Flowers, G. E., and Venditti, J. G. (2018a). Modeling Sediment Transport in Ice-Walled Subglacial Channels and Its Implications for Esker Formation and Proglacial Sediment Yields. *Journal of Geophysical Research: Earth Surface*, 123(12), 3206-3227.
- Beaud, F., Venditti, J. G., Flowers, G. E., et al. (2018b). Excavation of subglacial bedrock channels by seasonal meltwater flow. *Earth Surface Processes and Landforms*, 43(9), 1960-1972.
- Bell, R. E. (2008). The role of subglacial water in ice-sheet mass balance. *Nature Geoscience*, 1, 297-304.
- Bell, R. E., Studinger, M., Shuman, C. A., et al. (2007). Large subglacial lakes in East Antarctica at the onset of fast-flowing ice streams. *Nature*, 445(7130), 904-907.
- Bell, R. E., Chu, W., Kingslake, J., et al. (2017). Antarctic ice shelf potentially stabilized by export of meltwater in surface river. *Nature*, 544(7650), 344-348.
- Bell, R. E., Banwell, A. F., Trusel, L. D., et al. (2018). Antarctic surface hydrology and impacts on ice-sheet mass balance. *Nature Climate Change*, 8(12), 1044-1052.
- Bellwald, B., Planke, S., Piasecka, E. D., et al. (2018). Ice-stream dynamics of the SW Barents Sea revealed by high-resolution 3D seismic imaging of glacial deposits in the Hoop area. *Marine Geology*, 402, 165-183.
- Bellwald, B., Planke, S., Lebedeva-Ivanova, N., et al. (2019). High-resolution landform assemblage along a buried glacio-erosive surface in the SW Barents Sea revealed by P-Cable 3D seismic data. *Geomorphology*, 332, 33-50.
- Bellwald, B., Planke, S., Polteau, S., et al. (2021). Characterization of a glacial paleo-outburst flood using high-resolution 3-D seismic data: Bjørnelva River Valley, SW Barents Sea. *Journal of Glaciology*, 1-17.
- Bellwald, B., Stokke, H., Winsborrow, M., et al. (2023). Structural and fluid-migration control on hill-hole pair formation: Evidence from high-resolution 3D seismic data from the SW Barents Sea. *Geomorphology*, 420, 108502.
- Benn, D. I., and Evans, D. J. A. (2010). *Glaciers & Glaciation*, Routledge.
- Benvenuti, A., and Moscariello, A. (2016). High-resolution seismic geomorphology and stratigraphy of a tunnel valley confined ice-margin fan (Elsterian glaciation, Southern North Sea). *Interpretation*, 4(4), T461-T483,
- Benvenuti, A., Šegvić, B., and Moscariello, A. (2018). Tunnel valley deposits from the southern North Sea - material provenance and depositional processes. *Boreas*, 47(2), 625-642.
- Beuf, S., Biju-Duval, B., De Charpal, O., et al. (1971). *Les Grés du Paléozoïque inférieur au Sahara*. Editions Technip, Paris.
- Bhattachan, A., Jurjonas, M. D., Moody, A. C., et al. (2018). Sea level rise impacts on rural coastal social-ecological systems and the implications for decision making. *Environmental Science & Policy*, 90, 122-134,
- Biasutti, M., Sobel, A. H., Camargo, S. J., et al. (2012). Projected changes in the physical climate of the Gulf Coast and Caribbean. *Climatic Change*, 112(3), 819-845.
- Bindschadler, R. (1983). The Importance of Pressurized Subglacial Water in Separation and Sliding at the Glacier Bed. *Journal of Glaciology*, 29(101), 3-19.
- Bingham, R. G., Vaughan, D. G., King, E. C., et al. (2017). Diverse landscapes beneath Pine Island Glacier influence ice flow. *Nature Communications*, 8(1), 1618.
- Bjarnadóttir, L. R., Winsborrow, M. C. M., and Andreassen, K. (2017). Large subglacial meltwater features in the central Barents Sea. *Geology*, 45(2), 159-162.
- Björnsson, H. (1992). Jokulhlaups in Iceland: prediction, characteristics and simulation. *Annals of Glaciology*, 16, 95-106.
- Björnsson, H. (1996). Scales and rates of glacial sediment removal: a 20 km long, 300 m deep trench created beneath Breiðamerkurjökull during the Little Ice Age. *Annals of Glaciology*, 22, 141-146.
- Björnsson, H. (2002). Subglacial lakes and jökulhlaups in Iceland. *Global and Planetary Change*, 35, 255-271.
- Blankenship, D. D., Bentley, C. R., Rooney, S. T., et al. (1986). Seismic measurements reveal a saturated porous layer beneath an active Antarctic ice stream. *Nature*, 322(6074), 54-57.

- Blankenship, D. D., Bentley, C. R., Rooney, S. T., et al. (1987). Till beneath ice stream B: 1. Properties derived from seismic travel times. *Journal of Geophysical Research*, 92, B9.
- Blankenship, D. D., Bell, R. E., Hodge, S. M., et al. (1993). Active volcanism beneath the West Antarctic ice sheet and implications for ice-sheet stability. *Nature*, 361(6412), 526-529.
- Bond, G., Broecker, W., Johnsen, S., et al. (1993). Correlations between climate records from North Atlantic sediments and Greenland ice. *Nature*, 365(6442), 143-147.
- Bougamont, M., Christoffersen, P., Hubbard, A. L., et al. (2014). Sensitive response of the Greenland Ice Sheet to surface melt drainage over a soft bed. *Nature Communications*, 5(1), 5052.
- Bougamont, M., Christoffersen, P., Nias, I., et al. (2019). Contrasting Hydrological Controls on Bed Properties During the Acceleration of Pine Island Glacier, West Antarctica. *Journal of Geophysical Research: Earth Surface*, 124(1), 80-96.
- Boulton, G. S., and Hindmarsh, R. C. A. (1987). Sediment deformation beneath glaciers: Rheology and geological consequences. *Journal of Geophysical Research*, 92, B9.
- Boulton, G. S., and Jones, A. S. (1979). Stability of Temperate Ice Caps and Ice Sheets Resting on Beds of Deformable Sediment. *Journal of Glaciology*, 24(90), 29-43.
- Boulton, G. S., Lunn, R., Vidstrand, P., et al. (2007). Subglacial drainage by groundwater-channel coupling, and the origin of esker systems: Part 1—glaciological observations. *Quaternary Science Reviews*, 26(7), 1067-1090.
- Boulton, G. S., Hagdorn, M., Maillot, P. B., et al. (2009). Drainage beneath ice sheets: groundwater-channel coupling, and the origin of esker systems from former ice sheets. *Quaternary Science Reviews*, 28(7-8), 621-638.
- Bowling, J. S., Livingstone, S. J., Sole, A. J., et al. (2019). Distribution and dynamics of Greenland subglacial lakes. *Nature Communications*, 10(1), 2810.
- Boyd, R., Scott, D. B., and Douma, M. (1988). Glacial tunnel valleys and Quaternary history of the outer Scotian shelf. *Nature*, 333(6168), 61-64.
- Bradley, S. L., Ely, J. C., Clark, C. D., et al. (2018). Glacial isostatic adjustment of the British Isles and north west Europe. *EGU General Assembly Conference Abstracts*, 20, 9701.
- Brennan, T. A., and Shaw, J. (1994). Tunnel channels and associated landforms south central Ontario their implications for ice sheet hydrology. *Canadian Journal of Earth Sciences*, 31(3), 505-522.
- Bretz, J. H. (1923). The Channeled Scablands of the Columbia Plateau. *The Journal of Geology*, 31(8), 617-649.
- Bretz, J. H. (1969). The Lake Missoula Floods and the Channeled Scabland. *The Journal of Geology*, 77(5), 505-543.
- Brookshire, J. B. N., Landers, F. P., and Stein, J. A. (2015). Applicability of ultra-high-resolution 3D seismic data for geohazard identification at mid-slope depths in the Gulf of Mexico: Initial results. *Underwater Technology: International Journal of the Society for Underwater*, 32(4), 271-278.
- Brown, A. R. (2011). *Interpretation of Three-Dimensional Seismic Data*. The American Association of Petroleum Geologists and the Society of Exploration Geophysicists. Tulsa, Oklahoma.
- Buckley, F. A. (2012). An Early Pleistocene grounded ice sheet in the Central North Sea. In: Huuse, M., Redfern, J., Le Heron, D. P., Dixon, R., Moscarillo, A., et al. (eds.). *Glaciogenic Reservoirs and Hydrocarbon Systems*, Volume 368, Geological Society, London, Special Publications, 185-209.
- Bulat, J. (2005). Some considerations on the interpretation of seabed images based on commercial 3D seismic in the Faroe-Shetland Channel. *Basin Research*, 17(1), 21-42.
- BurVal Working Group (2006). Groundwater resources in buried valleys: a challenge for geosciences, GGA-Institute.
- Callow, B., Bull, J. M., Provenzano, G., et al. (2021). Seismic chimney characterisation in the North Sea – Implications for pockmark formation and shallow gas migration. *Marine and Petroleum Geology*, 133, 105301.

Bibliography

- Cameron, T. D. J., Stoker, M. S., and Long, D. (1987). The history of Quaternary sedimentation in the UK sector of the North Sea Basin. *Journal of the Geological Society*, 144, 43-58.
- Caress, D. W., and Chayes, D. N. (1996). Improved processing of Hydrosweep DS multibeam data on the R/V Maurice Ewing. *Marine Geophysical Researches*, 18(6), 631-650.
- Caress, D. W., Chayes, D. N., and Ferreira, C. (2021). MB-System Seafloor Mapping Software, 2021.
- Carlson, A. E., LeGrande, A. N., Oppo, D. W., et al. (2008). Rapid early Holocene deglaciation of the Laurentide ice sheet. *Nature Geoscience*, 1(9), 620-624.
- Carter, S. P., Blankenship, D. D., Young, D. A., et al. (2009). Dynamic distributed drainage implied by the flow evolution of the 1996–1998 Adventure Trench subglacial lake discharge. *Earth and Planetary Science Letters*, 283(1-4), 24-37.
- Carter, S. P., Fricker, H. A., and Siegfried, M. R. (2017). Antarctic subglacial lakes drain through sediment-floored canals: theory and model testing on real and idealized domains. *The Cryosphere*, 11(1), 381-405.
- Cartwright, J., and Huuse, M. (2005). 3D seismic technology: the geological 'Hubble'. *Basin Research*, 17(1), 1-20.
- Cartwright, J. A. (2007). The impact of 3D seismic data on the understanding of compaction, fluid flow and diagenesis in sedimentary basins. *Journal of the Geological Society*, London, 164, 881-893.
- Catania, G., and Paola, C. (2001). Braiding under glass. *Geology*, 29(3), 259-262.
- Chandler, D. M., Wadham, J. L., Lis, G. P., et al. (2013). Evolution of the subglacial drainage system beneath the Greenland Ice Sheet revealed by tracers. *Nature Geoscience*, 6(3), 195-198.
- Christner, B. C., Priscu, J. C., Achberger, A. M., et al. (2014). A microbial ecosystem beneath the West Antarctic ice sheet. *Nature*, 512(7514), 310-313.
- Christoffersen, P., Bougamont, M., Carter, S. P., et al. (2014). Significant groundwater contribution to Antarctic ice streams hydrologic budget. *Geophysical Research Letters*, 41(6), 2003-2010.
- Chu, V. W. (2013). Greenland ice sheet hydrology: A review. *Progress in Physical Geography: Earth and Environment*, 38(1), 19-54.
- Chudley, T. R., Christoffersen, P., Doyle, S. H., et al. (2019). Supraglacial lake drainage at a fast-flowing Greenlandic outlet glacier. *PNAS*, 116(51), 25468-25477.
- Church, J. A., Clark, P. U., Cazenave, A., et al. (2013). Sea level change. In: Stocker, T. F., Qin, D., Plattner, G.-K., and al., e. (eds.). *Climate change 2013: The physical science basis*. Contribution of Working Group I to the Fifth Assessment Report of the Intergovernmental Panel on Climate Change, Cambridge University Press.
- Clague, J. J., and Mathews, W. H. (1973). The Magnitude of Jökulhlaups. *Journal of Glaciology*, 12(66), 501-504.
- Clark, C. D. (1993). Mega-scale glacial lineations and cross-cutting ice-flow landforms. *Earth Surface Processes and Landforms*, 18, 1-29.
- Clark, C. D., and Livingstone, S. J. (2018). Glacial curvilineations found along the southern sector of the Laurentide Ice sheet and a hypothesis of formation involving subglacial slope failure in tunnel valleys and subglacial lakes. *Earth Surface Processes and Landforms*, 43(7), 1518-1528.
- Clark, C. D., Ely, J. C., Greenwood, S. L., et al. (2018). BRITICE Glacial Map, version 2: a map and GIS database of glacial landforms of the last British-Irish Ice Sheet. *Boreas*, 47(1), 11-27.
- Clark, C. D., Chiverrell, R. C., Fabel, D., et al. (2021). Timing, pace and controls on ice sheet retreat: an introduction to the BRITICE-CHRONO transect reconstructions of the British–Irish Ice Sheet. *Journal of Quaternary Science*, 36(5), 673-680.
- Clark, C. D., Ely, J. C., Fabel, D., et al. (2022a). BRITICE-CHRONO maps and GIS data of the last British-Irish Ice Sheet 31 to 15 ka, including model reconstruction, geochronometric age spreadsheet, palaeotopographies and coastline positions, PANGAEA, <https://doi.org/10.1594/PANGAEA.945729>.
- Clark, C. D., Ely, J. C., Hindmarsh, R. C. A., et al. (2022b). Growth and retreat of the last British–Irish Ice Sheet, 31 000 to 15 000 years ago: the BRITICE-CHRONO reconstruction. *Boreas*, <https://doi.org/10.1111/bor.12594>.

- Clark, I. D., Douglas, M., Raven, K., et al. (2000). Recharge and Preservation of Laurentide Glacial Melt Water in the Canadian Shield. *Groundwater*, 38(5), 735-742.
- Clark, P. U., and Walder, J. S. (1994). Subglacial drainage, eskers, and deforming beds beneath the Laurentide and Eurasian ice sheets. *Geological Society of America Bulletin*, 106, 304-314.
- Clarke, G. K. C., Collins, S. G., and Thompson, D. E. (1984). Flow, thermal structure, and subglacial conditions of a surge-type glacier. *Canadian Journal of Earth Sciences*, 21(2), 232-240.
- Clayton, L., Attig, J. W., and Mickelson, D. M. (1999). Tunnel channels formed in Wisconsin during the last glaciations, in Mickelson, D. M., and Attig, J. W., eds., *Glacial Processes Past and Present: USA*, Geological Society of America Special Paper 337, p. 69-82.
- Clerc, S., Buoncristiani, J.-F., Guiraud, M., et al. (2013). Subglacial to proglacial depositional environments in an Ordovician glacial tunnel valley, Alnif, Morocco. *Palaeogeography, Palaeoclimatology, Palaeoecology*, 370, 127-144.
- Cleveland, C. J., and Morris, C. G. (2014). *Handbook of Energy: Chronologies, Top Ten Lists, and Word Clouds*. Elsevier, Amsterdam.
- Climate Change Committee (2021). Independent Assessment of UK Climate Risk: Advice to Government For The UK's Third Climate Change Risk Assessment (CCRA3).
- Cohen, K. M., and Gibbard, P. L. (2019). Global chronostratigraphical correlation table for the last 2.7 million years. Version 2019 QI-500. *Quaternary International*, 500, 20-31.
- Colgan, W., and Steffen, K. (2009). Modelling the spatial distribution of moulins near Jakobshavn, Greenland. *IOP Conference Series: Earth and Environmental Science*, 6(1).
- Cook, A. J., and Vaughan, D. G. (2010). Overview of areal changes of the ice shelves on the Antarctic Peninsula over the past 50 years. *The Cryosphere*, 4(1), 77-98.
- Cook, A. J., Holland, P. R., Meredith, M. P., et al. (2016). Ocean forcing of glacier retreat in the western Antarctic Peninsula. *Science*, 353(6296), 283-286.
- Cook, K. L., Turowski, J. M., and Hovius, N. (2013). A demonstration of the importance of bedload transport for fluvial bedrock erosion and knickpoint propagation. *Earth Surface Processes and Landforms*, 38(7), 683-695.
- Cook, S. J., Waller, R. I., and Knight, P. G. (2006). Glaciohydraulic supercooling: the process and its significance. *Progress in Physical Geography*, 30(5), 577-588.
- Cook, S. J., Christoffersen, P., Todd, J., et al. (2020). Coupled modelling of subglacial hydrology and calving-front melting at Store Glacier, West Greenland. *The Cryosphere*, 14(3), 905-924.
- Cooper, M. A., Michaelides, K., Siegert, M. J., et al. (2016). Paleofluvial landscape inheritance for Jakobshavn Isbrae catchment, Greenland. *Geophysical Research Letters*, 43(12), 6350-6357.
- Corr, H. F. J., and Vaughan, D. G. (2008). A recent volcanic eruption beneath the West Antarctic ice sheet. *Nature Geoscience*, 1(2), 122-125.
- Coughlan, M., Fleischer, M., Wheeler, A. J., et al. (2018). A revised stratigraphical framework for the Quaternary deposits of the German North Sea sector: a geological-geotechnical approach. *Boreas*, 47(1), 80-105.
- Cowton, T., Nienow, P., Bartholomew, I., et al. (2012). Rapid erosion beneath the Greenland ice sheet. *Geology*, 40(4), 343-346.
- Cowton, T., Nienow, P., Sole, A., et al. (2013). Evolution of drainage system morphology at a land-terminating Greenlandic outlet glacier. *Journal of Geophysical Research: Earth Surface*, 118(1), 29-41.
- Cox, D. R., Newton, A. M. W., and Huuse, M. (2020). An introduction to seismic reflection data: acquisition, processing and interpretation. *Regional Geology and Tectonics: Principles of Geologic Analysis*, 571-603.
- Creyts, T. T., and Schoof, C. G. (2009). Drainage through subglacial water sheets. *Journal of Geophysical Research*, 114, F4.
- Cronin, T. M. (1982). Rapid sea level and climate change: evidence from continental and island margins. *Quaternary Science Reviews*, 1(3), 177-214.

Bibliography

- Cuffey, K. M., and Paterson, W. S. B. (2010). *The Physics of Glaciers*. Academic Press.
- Cutler, P. M., Colgan, P. M., and Mickelson, D. M. (2002). Sedimentologic evidence for outburst floods from the Laurentide Ice Sheet margin in Wisconsin, USA: implications for tunnel channel formation. *Quaternary International*, 90, 23-40.
- Damsgaard, A., Suckale, J., Piotrowski, J. A., et al. (2017). Sediment behavior controls equilibrium width of subglacial channels. *Journal of Glaciology*, 63, 242, 1034-1048.
- Dansgaard, W., Johnsen, S. J., Clausen, H. B., et al. (1993). Evidence for general instability of past climate from a 250-kyr ice-core record. *Nature*, 364, 6434, 218-220.
- Das, S. B., Joughin, I., Behn, M. D., et al. (2008). Fracture propagation to the base of the Greenland Ice Sheet during supraglacial lake drainage. *Science*, 320(5877), 778-781.
- Dasgupta, S., Laplante, B., Meisner, C., et al. (2009). The impact of sea level rise on developing countries: a comparative analysis. *Climatic Change*, 93(3), 379-388.
- Davies, J. H. (2013). Global map of solid Earth surface heat flow. *Geochemistry, Geophysics, Geosystems*, 14(10), 4608-4622.
- Davison, B. J., Sole, A. J., Livingstone, S. J., et al. (2019). The Influence of Hydrology on the Dynamics of Land-Terminating Sectors of the Greenland Ice Sheet. *Frontiers in Earth Science*, 7.
- DeConto, R. M., and Pollard, D. (2003). A coupled climate-ice sheet modeling approach to the Early Cenozoic history of the Antarctic ice sheet. *Palaeogeography, Palaeoclimatology, Palaeoecology*, 198(1), 39-52.
- DeConto, R. M., and Pollard, D. (2016). Contribution of Antarctica to past and future sea-level rise. *Nature*, 531(7596), 591-597.
- DeConto, R. M., Pollard, D., Alley, R. B., et al. (2021). The Paris Climate Agreement and future sea-level rise from Antarctica. *Nature*, 593(7857), 83-89.
- Denis, M., Buoncristiani, J.-F., Konaté, M., et al. (2007). The origin and glaciodynamic significance of sandstone ridge networks from the Hirnantian glaciation of the Djado Basin (Niger). *Sedimentology*, 54(6), 1225-1243.
- Denton, G. H., and Sugden, D. (2005). Meltwater features that suggest Miocene ice sheet overriding of the Transantarctic Mountains in Victoria Land, Antarctica. *Geografiska Annaler A*, 87, 67-85.
- Denton, G. H., Prentice, M. L., Kellogg, D. E., et al. (1984). Late Tertiary history of the Antarctic ice sheet, evidence from the Dry Valleys. *Geology*, 12, 263-267.
- Denton, G. H., Sugden, D. E., Marchant, D. R., et al. (1993). East Antarctic Ice Sheet Sensitivity to Pliocene Climatic Change from a Dry Valleys Perspective. *Geografiska Annaler A*, 75(4), 155-204.
- Deschamps, P., Durand, N., Bard, E., et al. (2012). Ice-sheet collapse and sea-level rise at the Bølling warming 14,600 years ago. *Nature*, 483(7391), 559-564.
- Dewald, N., Livingstone, S. J., and Clark, C. D. (2022). Subglacial meltwater routes of the Fennoscandian Ice Sheet. *Journal of Maps*, 1-15.
- Domack, E., Amblàs, D., Gilbert, R., et al. (2006). Subglacial morphology and glacial evolution of the Palmer deep outlet system, Antarctic Peninsula. *Geomorphology*, 75(1-2), 125-142.
- Dorschel, B., Hehemann, L., Viquerat, S., et al. (2022). The International Bathymetric Chart of the Southern Ocean Version 2. *Scientific Data*, 9(1), 275.
- Douillet, G., Ghienne, J. F., Géraud, Y., et al. (2012). Late Ordovician tunnel valleys in southern Jordan. Geological Society, London, Special Publications, 368(1), 275-292.
- Dove, D., Evans, D. J. A., Lee, J. R., et al. (2017). Phased occupation and retreat of the last British-Irish Ice Sheet in the southern North Sea; geomorphic and seismostratigraphic evidence of a dynamic ice lobe. *Quaternary Science Reviews*, 163, 114-134.
- Dow, C. F., Kulesa, B., Rutt, I. C., et al. (2015). Modeling of subglacial hydrological development following rapid supraglacial lake drainage. *Journal of Geophysical Research: Earth Surface*, 120(6), 1127-1147.
- Dow, C. F., Lee, W. S., Greenbaum, J. S., et al. (2018a). Basal channels drive active surface hydrology and transverse ice shelf fracture. *Science Advances*, 4(6), eaao7212.

- Dow, C. F., Werder, M. A., Babonis, G., et al. (2018b). Dynamics of Active Subglacial Lakes in Recovery Ice Stream. *Journal of Geophysical Research: Earth Surface*, 123(4), 837-850.
- Dowdeswell, J. A., and Siegert, M. J. (1999). The dimensions and topographic setting of Antarctic subglacial lakes and implications for large scale water storage beneath continental ice sheets. *Geological Society of America Bulletin*, 111(2), 254-263.
- Dowdeswell, J. A., Ottesen, D., Rise, L., et al. (2007). Identification and preservation of landforms diagnostic of past ice-sheet activity on continental shelves from three-dimensional seismic evidence. *Geology*, 35(4), 359-362.
- Dowdeswell, J. A., Evans, J., Mugford, R., et al. (2008). Autonomous underwater vehicles (AUVs) and investigations of the ice-ocean interface in Antarctic and Arctic waters. *Journal of Glaciology*, 54(187), 661-672.
- Dowdeswell, J. A., Evans, J., and Ó Cofaigh, C. (2010). Submarine landforms and shallow acoustic stratigraphy of a 400 km-long fjord-shelf-slope transect, Kangerlussuaq margin, East Greenland. *Quaternary Science Reviews*, 29(25-26), 3359-3369.
- Dowdeswell, J. A., and Ottesen, D. (2013). Buried iceberg ploughmarks in the early Quaternary sediments of the central North Sea: A two-million year record of glacial influence from 3D seismic data. *Marine Geology*, 344, 1-9.
- Dowdeswell, J. A., Hogan, K. A., Arnold, N. S., et al. (2015). Sediment-rich meltwater plumes and ice-proximal fans at the margins of modern and ancient tidewater glaciers: Observations and modelling. *Sedimentology*, 62(6), 1665-1692.
- Dowdeswell, J. A., Canals, M., Jakobsson, M., et al. (2016a). The variety and distribution of submarine glacial landforms and implications for ice-sheet reconstruction. In Dowdeswell, J. A., Canals, M., Jakobsson, M., Todd, B. J., Dowdeswell, E. K., et al. (eds.). *Atlas of Submarine Glacial Landforms: Modern, Quaternary and Ancient*. Geological Society, London, Memoirs, 519-552.
- Dowdeswell, J. A., Canals, M., Jakobsson, M., et al. (2016b). Introduction: an Atlas of Submarine Glacial Landforms. In: Dowdeswell, J. A., Canals, M., Jakobsson, M., Todd, B. J., Dowdeswell, E. K., et al., (eds.). *Atlas of Submarine Glacial Landforms: Modern, Quaternary and Ancient*, 46, Geological Society, London, Memoirs, 3-14.
- Dowdeswell, J. A., Batchelor, C. L., Montelli, A., et al. (2020). Delicate seafloor landforms reveal past Antarctic grounding-line retreat of kilometers per year. *Science*, 368(6494), 1020-1024.
- Dowsett, H. J. (2007). The PRISM palaeoclimate reconstruction and Pliocene sea-surface temperature, in Williams, M., Haywood, A. M., Gregory, F. J., and Schmidt, D. N. (eds.). *Deep-Time Perspectives on Climate Change: Marrying the Signal from Computer Models and Biological Proxies*, Volume 2, Geological Society of London.
- Doyle, S. H., Hubbard, A., van de Wal, R. S. W., et al. (2015). Amplified melt and flow of the Greenland ice sheet driven by late-summer cyclonic rainfall. *Nature Geoscience*, 8(8), 647-653.
- Dutrieux, P., Rydt, J. D., Jenkins, A., et al. (2014). Strong Sensitivity of Pine Island Ice-Shelf Melting to Climatic Variability. *Science*, 343(6167), 174-178.
- Dutton, A., Carlson, A. E., Long, A. J., et al. (2015). Sea-level rise due to polar ice-sheet mass loss during past warm periods. *Science*, 349(6244), aaa4019.
- Ehlers, J. (1990). Reconstructing the dynamics of the north-west European Pleistocene ice sheets. *Quaternary Science Reviews*, 9, 71-83.
- Ehlers, J., and Gibbard, P. L. (2007). The extent and chronology of Cenozoic Global Glaciation. *Quaternary International*, 164-165, 6-20.
- Ehlers, J., and Linke, G. (1989). The origin of deep buried channels of Elsterian age in Northwest Germany. *Journal of Quaternary Science*, 4(3), 255-265.
- Ehlers, J., Meyer, K. D., and Stephan, H. J. (1984). The pre-Weichselian glaciations of north-west Europe. *Quaternary Science Reviews*, 3(1), 1-40.

Bibliography

- Ehlers, J., and Wingfield, R. (1991). The extension of the Late Weichselian/Late Devensian ice sheets in the North Sea Basin. *Journal of Quaternary Science*, 6(4), 313-326.
- Ekholm, S., Keller, K., Bamber, J. L., et al. (1998). Unusual surface morphology from digital elevation models of the Greenland Ice Sheet. *Geophysical Research Letters*, 25(19), 3623-3626.
- Ellison, J. C., and Stoddart, D. R. (1991). Mangrove Ecosystem Collapse during Predicted Sea-Level Rise: Holocene Analogues and Implications. *Journal of Coastal Research*, 7(1), 151-165.
- Elsworth, C. W., and Suckale, J. (2016). Rapid ice flow rearrangement induced by subglacial drainage in West Antarctica. *Geophysical Research Letters*, 43(22), 11697-11707.
- Ely, J. C., Clark, C. D., Spagnolo, M., et al. (2016). Do subglacial bedforms comprise a size and shape continuum? *Geomorphology*, 257, 108-119.
- EMODnet Bathymetry Consortium (2018). EMODnet Digital Bathymetry DTM.
- Engelhardt, H., Humphrey, N., Kamb, B., et al. (1990). Physical Conditions at the Base of a Fast Moving Antarctic Ice Stream. *Science*, 248(4951), 57-59.
- Engelhardt, H., and Kamb, B. (1997). Basal hydraulic system of a West Antarctic ice stream: constraints from borehole observations. *Journal of Glaciology*, 43(144), 207-230.
- Eriksson, B., Kirchner, N., Nitsche, F. O., et al. (2021). High-resolution bathymetry data from expedition OSO, Southern Ocean, 2010. Dataset version 1.0.
- Eschard, R., Abdallah, H., Braik, F., et al. (2005). The Lower Paleozoic succession in the Tassili outcrops, Algeria: sedimentology and sequence stratigraphy. *First Break*, 23, 10.
- Escutia, C., Bárcena, M. A., Lucchi, R. G., et al. (2009). Circum-Antarctic warming events between 4 and 3.5Ma recorded in marine sediments from the Prydz Bay (ODP Leg 188) and the Antarctic Peninsula (ODP Leg 178) margins. *Global and Planetary Change*, 69(3), 170-184.
- Evans, D. J. A., Storrar, R. D., and Rea, B. R. (2016). Crevasse-squeeze ridge corridors: Diagnostic features of late-stage palaeo-ice stream activity. *Geomorphology*, 258, 40-50.
- Evatt, G. W., Fowler, A. C., Clark, C. D., et al. (2006). Subglacial floods beneath ice sheets. *Philosophical Transactions of the Royal Society A*, 364(1844), 1769-1794.
- Eyles, N., and de Broekert, P. (2001). Glacial tunnel valleys in the Eastern Goldfields of Western Australia cut below the Late Paleozoic Pilbara ice sheet. *Palaeogeography, Palaeoclimatology, Palaeoecology*, 171, 29-40.
- Fader, G. B. J. (1997). The Effects of Shallow Gas on Seismic Reflection Profiles. In: Davies, T. A., Bell, T., Cooper, A. K., Josenhans, H., Polyak, L., et al. (eds.). *Glaciated Continental Margins: An Atlas of Acoustic Images*. Dordrecht, Springer Netherlands, 29-30.
- Fairbanks, R. G. (1989). A 17,000-year glacio-eustatic sea level record: influence of glacial melting rates on the Younger Dryas event and deep-ocean circulation. *Nature*, 342(6250), 637-642.
- Feldmann, J., and Levermann, A. (2015). Collapse of the West Antarctic Ice Sheet after local destabilization of the Amundsen Basin. *PNAS*, 112(46), 14191-14196.
- Fernandez, R., Gulick, S., Domack, E., et al. (2018). Past ice stream and ice sheet changes on the continental shelf off the Sabrina Coast, East Antarctica. *Geomorphology*, 317, 10-22.
- Flament, T., Berthier, E., and Rémy, F. (2014). Cascading water underneath Wilkes Land, East Antarctic ice sheet, observed using altimetry and digital elevation models. *The Cryosphere*, 8(2), 673-687.
- Flowers, G. E. (2015). Modelling water flow under glaciers and ice sheets. *Proceedings of the Royal Society A: Mathematical, Physical and Engineering Sciences*, 471(2176), 20140907.
- Fogwill, C. J., Turney, C. S. M., Meissner, K. J., et al. (2014). Testing the sensitivity of the East Antarctic Ice Sheet to Southern Ocean dynamics: past changes and future implications. *Journal of Quaternary Science*, 29(1), 91-98.
- Fountain, A. G., and Walder, J. S. (1998). Water flow through temperate glaciers. *Reviews of Geophysics*, 36(3), 299-328.
- Fowler, A. C. (2009). Dynamics of subglacial floods. *Proceedings of the Royal Society A: Mathematical, Physical and Engineering Sciences*, 465(2106), 1809-1828.

- Frahm, L., Hübscher, C., Warwel, A., et al. (2020). Misinterpretation of velocity pull-ups caused by high-velocity infill of tunnel valleys in the southern Baltic Sea. *Near Surface Geophysics*, 18, 643-657.
- Fransner, O., Noormets, R., Flink, A. E., et al. (2016). Crag-and-tail landforms in outer Rijpfjorden, Nordaustlandet, Svalbard. In: Dowdeswell, J. A., Canals, M., Jakobsson, M., Todd, B. J., Dowdeswell, E. K., et al. (eds.). *Atlas of Submarine Glacial Landforms: Modern, Quaternary and Ancient*. Volume 46, The Geological Society of London, 57-58.
- Fretwell, P., Pritchard, H. D., Vaughan, D. G., et al. (2013). Bedmap2: improved ice bed, surface and thickness datasets for Antarctica. *The Cryosphere*, 7(1), 375-393.
- Fricker, H. A., and Scambos, T. A. (2009). Connected subglacial lake activity on lower Mercer and Whillan Ice Streams, West Antarctica, 2003-2008. *Journal of Glaciology*, 55(190), 303-315.
- Fricker, H. A., Scambos, T. A., Bindschadler, R., et al. (2007). An Active Subglacial Water System in West Antarctica Mapped from Space. *Science*, 315, 1544-1548.
- Fricker, H. A., Carter, S. P., Bell, R. E., et al. (2014). Active lakes of Recovery Ice Stream, East Antarctica: a bedrock-controlled subglacial hydrological system. *Journal of Glaciology*, 60(223), 1015-1030.
- Fricker, H. A., Siegfried, M. R., Carter, S. P., et al. (2016). A decade of progress in observing and modelling Antarctic subglacial water systems. *Philosophical Transactions of the Royal Society A*, 374, 2059.
- Fyfe, J., Gregersen, U., Jordt, H., et al. (2003). Oligocene to Holocene. *The Millennium Atlas: Petroleum Geology of the Central and Northern North Sea*. Geological Society, London, 279.
- Gagliardini, O., Zwinger, T., Gillet-Chaulet, F., et al. (2013). Capabilities and performance of Elmer/Ice, a new-generation ice sheet model. *Geoscientific Model Development*, 6(4), 1299-1318.
- Gales, J. A., Larter, R. D., Mitchell, N. C., et al. (2013). Geomorphic signature of Antarctic submarine gullies: Implications for continental slope processes. *Marine Geology*, 337, 112-124.
- Games, K. P. (2012). Shallow gas detection - why HRS, why 3D, why not HRS 3D? *First Break*, 30, 25-33.
- Games, K. P., and Wakefield, N. D. (2014). The successful design, development and acquisition of a UHRS 3D seismic dataset, Near Surface Geoscience: Athens, Greece.
- Games, K. P., and Self, E. (2017). HRS 3D data — a fundamental change in site survey geohazard interpretation. *First Break*, 35(2152).
- Gandy, N., Gregoire, L. J., Ely, J. C., et al. (2019). Exploring the ingredients required to successfully model the placement, generation, and evolution of ice streams in the British-Irish Ice Sheet. *Quaternary Science Reviews*, 223, 105915.
- Gandy, N., Gregoire, L. J., Ely, J. C., et al. (2021). Collapse of the Last Eurasian Ice Sheet in the North Sea Modulated by Combined Processes of Ice Flow, Surface Melt, and Marine Ice Sheet Instabilities. *Journal of Geophysical Research: Earth Surface*, 126(4), e2020JF005755.
- Ghienne, J. F., and Deynoux, M. (1998). Large scale channel fill structures in Late Ordovician glacial deposits in Mauritania, western Sahara. *Sedimentary Geology*, 119(1-2), 141-159.
- Ghienne, J. F., Le Heron, D. P., Moreau, J., et al. (2007). The Late Ordovician glacial sedimentary system of the North Gondwana platform. In: Hambrey, M. J., Christoffersen, P., Glasser, N. F., and Hubbard, B. (eds.). *Glacial Sedimentary Processes and Products*, Wiley, 295-319.
- Giglio, C., Benetti, S., Sacchetti, F., et al. (2021). A Late Pleistocene channelized subglacial meltwater system on the Atlantic continental shelf south of Ireland. *Boreas*, 51, 118-135.
- Gilbert, A., Vincent, C., Wagnon, P., et al. (2012). The influence of snow cover thickness on the thermal regime of Tête Rousse Glacier (Mont Blanc range, 3200 m a.s.l.): Consequences for outburst flood hazards and glacier response to climate change. *Journal of Geophysical Research: Earth Surface*, 117, F4.
- Girard, F., Ghienne, J.-F., Rubino, J.-L., et al. (2012). Channelized sandstone bodies ('cordons') in the Tassili N'Ajjer (Algeria & Libya): snapshots of a Late Ordovician proglacial outwash plain. *Glaciogenic Reservoirs and Hydrocarbon Systems*, Volume 368, Geological Society of London.
- Gledhill, L. A., and Williamson, A. G. (2017). Inland advance of supraglacial lakes in north-west Greenland under recent climatic warming. *Annals of Glaciology*, 59, 66-82.

Bibliography

- Goelzer, H., Robinson, A., Seroussi, H., et al. (2017). Recent Progress in Greenland Ice Sheet Modelling. *Current Climate Change Reports*, 3(4), 291-302.
- Goelzer, H., Nowicki, S., Payne, A., et al. (2020). The future sea-level contribution of the Greenland ice sheet: a multi-model ensemble study of ISMIP6. *The Cryosphere*, 14(9), 3071-3096.
- Gohl, K. (2012). Basement control on past ice sheet dynamics in the Amundsen Sea Embayment, West Antarctica. *Palaeogeography, Palaeoclimatology, Palaeoecology*, 335-336, 35-41.
- Gohl, K., Denk, A., Eagles, G., et al. (2013). Deciphering tectonic phases of the Amundsen Sea Embayment shelf, West Antarctica, from a magnetic anomaly grid. *Tectonophysics*, 585, 113-123.
- Golledge, N. R., Fogwill, C. J., Mackintosh, A. N., et al. (2012). Dynamics of the last glacial maximum Antarctic ice-sheet and its response to ocean forcing. *PNAS*, 109(40), 16052-16056.
- Golledge, N. R., Levy, R. H., McKay, R. M., et al. (2013). Glaciology and geological signature of the Last Glacial Maximum Antarctic ice sheet. *Quaternary Science Reviews*, 78, 225-247.
- Golledge, N. R., Menviel, L., Carter, L., et al. (2014). Antarctic contribution to meltwater pulse 1A from reduced Southern Ocean overturning. *Nature Communications*, 5, 5107.
- Gooch, B. T., Young, D. A., and Blankenship, D. D. (2016). Potential groundwater and heterogeneous heat source contributions to ice sheet dynamics in critical submarine basins of East Antarctica. *Geochemistry, Geophysics, Geosystems*, 17(2), 395-409.
- Gowan, E. J., Zhang, X., Khosravi, S., et al. (2021). A new global ice sheet reconstruction for the past 80 000 years. *Nature Communications*, 12(1), 1199.
- Graham, A. G. C., Lonergan, L., and Stoker, M. S. (2007). Evidence for Late Pleistocene ice stream activity in the Witch Ground Basin, central North Sea, from 3D seismic reflection data. *Quaternary Science Reviews*, 26(5), 627-643.
- Graham, A. G. C., Larter, R. D., Gohl, K., et al. (2009a). Bedform signature of a West Antarctic palaeo-ice stream reveals a multi-temporal record of flow and substrate control. *Quaternary Science Reviews*, 28(25), 2774-2793.
- Graham, A. G. C., Lonergan, L., and Stoker, M. S. (2009b). Seafloor glacial features reveal the extent and decay of the last British Ice Sheet, east of Scotland. *Journal of Quaternary Science*, 24(2), 117-138.
- Graham, A. G. C., Larter, R. D., Gohl, K., et al. (2010a). Flow and retreat of the Late Quaternary Pine Island-Thwaites palaeo-ice stream, West Antarctica. *Journal of Geophysical Research*, 115, F3.
- Graham, A. G. C., Lonergan, L., and Stoker, M. S. (2010b). Depositional environments and chronology of Late Weichselian glaciation and deglaciation in the central North Sea. *Boreas*, 39, 471-491.
- Graham, A. G. C., Dutrieux, P., Vaughan, D. G., et al. (2013). Seabed corrugations beneath an Antarctic ice shelf revealed by autonomous underwater vehicle survey: Origin and implications for the history of Pine Island Glacier. *Journal of Geophysical Research: Earth Surface*, 118(3), 1356-1366.
- Graham, A. G. C., Wåhlin, A., Hogan, K. A., et al. (2022). Rapid retreat of Thwaites Glacier in the pre-satellite era. *Nature Geoscience*, 15, 706-713.
- Grasby, S., Osadetz, K., Betcher, R., et al. (2000). Reversal of the regional-scale flow system of the Williston basin in response to Pleistocene glaciation. *Geology*, 28(7), 635-638.
- Gray, L., Joughin, I., Tulaczyk, S. M., et al. (2005). Evidence for subglacial water transport in the West Antarctic Ice Sheet through three-dimensional satellite radar interferometry. *Geophysical Research Letters*, 32(3), L03501.
- Greenbaum, J. S., Blankenship, D. D., Young, D. A., et al. (2015). Ocean access to a cavity beneath Totten Glacier in East Antarctica. *Nature Geoscience*, 8(4), 294-298.
- Greenwood, S. L., Clason, C. C., and Jakobsson, M. (2016). Ice-flow and meltwater landform assemblages in the Gulf of Bothnia. In: Dowdeswell, J. A., Canals, M., Jakobsson, M., Todd, B. J., Dowdeswell, E. K., et al. (eds.). *Atlas of Submarine Glacial Landforms: Modern, Quaternary and Ancient*, Volume 46, Geological Society, London, Memoirs, 321-324.
- Greenwood, S. L., Clason, C. C., Nyberg, J., et al. (2017). The Bothnian Sea ice stream: early Holocene retreat dynamics of the south-central Fennoscandian Ice Sheet. *Boreas*, 46(2), 346-362.

- Gudmundsson, G. H., Paolo, F. S., Adusumilli, S., et al. (2019). Instantaneous Antarctic ice sheet mass loss driven by thinning ice shelves. *Geophysical Research Letters*, 46(23), 13903-13909.
- Gudmundsson, M. T., Björnsson, H., and Pálsson, F. (1995). Changes in jökulhlaup sizes in Grímsvötn, Vatnajökull, Iceland, 1934-91, deduced from in-situ measurements of subglacial lake volume. *Journal of Glaciology*, 41(138), 263-272.
- Gulick, S. P. S., Shevenell, A. E., Montelli, A., et al. (2017). Initiation and long-term instability of the East Antarctic Ice Sheet. *Nature*, 552(7684), 225-229.
- Gupta, S., Collier, J. S., Palmer-Felgate, A., et al. (2007). Catastrophic flooding origin of shelf valley systems in the English Channel. *Nature*, 448(7151), 342-345.
- Gustafson, C. D., Key, K., Siegfried, M. R., et al. (2022). A dynamic saline groundwater system mapped beneath an Antarctic ice stream. *Science*, 376(6593), 640-644.
- Hager, A. O., Hoffman, M. J., Price, S. F. et al. (2022). Persistent, extensive channelized drainage modeled beneath Thwaites Glacier, West Antarctica. *The Cryosphere*, 16(9), 3575-3599.
- Hanna, E., Huybrechts, P., Steffen, K., et al. (2008). Increased Runoff from Melt from the Greenland Ice Sheet: A Response to Global Warming. *Journal of Climate*, 21(2), 331-341.
- Hanna, E., Pattyn, F., Navarro, F., et al. (2020). Mass balance of the ice sheets and glaciers – Progress since AR5 and challenges. *Earth-Science Reviews*, 201, 102976.
- Haszeldine, R. S. (2009). Carbon Capture and Storage: How Green Can Black Be? *Science*, 325(5948), 1647-1652.
- Hepp, D. A., Hebbeln, D., Kreiter, S., et al. (2012). An east-west-trending Quaternary tunnel valley in the south-eastern North Sea and its seismic-sedimentological interpretation. *Journal of Quaternary Science*, 27(8), 844-853.
- Hewitt, I. J. (2013). Seasonal changes in ice sheet motion due to melt water lubrication. *Earth and Planetary Science Letters*, 371-372, 16-25.
- Hintze, J. L., and Nelson, R. D. (1998). Violin Plots: A Box Plot-Density Trace Synergism. *The American Statistician*, 52(2), 181-184.
- Hirst, J. P. P., Benbakir, A., Payne, D. F., et al. (2002). Tunnel valleys and density flow processes in the upper Ordovician glacial succession, Illizi Basin, Algeria: Influence on reservoir quality. *Journal of Petroleum Geology*, 25(3), 297-324.
- Hirst, J. P. P., Huuse, M., Redfern, J., et al. (2012). Ordovician proglacial sediments in Algeria: insights into the controls on hydrocarbon reservoirs in the In Amenas field, Illizi Basin. *Glaciogenic Reservoirs and Hydrocarbon Systems*, Volume 368, Geological Society of London, 319-353.
- Hoffman, A. O., Christianson, K., Holschuh, N., et al. (2022). The impact of basal roughness on inland Thwaites Glacier sliding. *Geophysical Research Letters*, 49, e2021GL096564.
- Hoffman, M., and Price, S. (2014). Feedbacks between coupled subglacial hydrology and glacier dynamics. *Journal of Geophysical Research: Earth Surface*, 119(3), 414-436.
- Hoffman, M. J., Andrews, L. C., Price, S. F., et al. (2016). Greenland subglacial drainage evolution regulated by weakly connected regions of the bed. *Nature Communications*, 7(1), 13903.
- Hogan, K. A., Larter, R. D., Graham, A. G. C., et al. (2020). Revealing the former bed of Thwaites Glacier using sea-floor bathymetry: implications for warm-water routing and bed controls on ice flow and buttressing. *The Cryosphere*, 14(9), 2883-2908.
- Hogan, K. A., Arnold, N. S., Larter, R. D., et al. (2022). Subglacial Water Flow Over an Antarctic Palaeo-Ice Stream Bed. *Journal of Geophysical Research: Earth Surface*, 127, e2021JF006442.
- Holland, P. R., Bracegirdle, T. J., Dutrieux, P., et al. (2019). West Antarctic ice loss influenced by internal climate variability and anthropogenic forcing. *Nature Geoscience*, 12(9), 718-724.
- Holtedahl, H. (1967). Notes on the Formation of Fjords and Fjord-Valleys. *Geografiska Annaler: Series A*, 49(2-4), 188-203.
- Hooke, R. L. (1989). Englacial and Subglacial Hydrology: A Qualitative Review. *Arctic and Alpine Research*, 21(3), 221-233.

Bibliography

- Hooke, R. L., and Jennings, C. E. (2006). On the formation of the tunnel valleys of the southern Laurentide ice sheet. *Quaternary Science Reviews*, 25(11-12), 1364-1372.
- Hooke, R. L., Laumann, T., and Kohler, J. (1990). Subglacial Water Pressures and the Shape of Subglacial Conduits. *Journal of Glaciology*, 36(122), 67-71.
- Hubbard, B. P., Sharp, M. J., Willis, I. C., et al. (1995). Borehole water-level variations and the structure of the subglacial hydrological system of Haut Glacier d'Arolla, Valais, Switzerland. *Journal of Glaciology*, 41(139), 572-583.
- Huber, C., Leuenberger, M., Spahni, R., et al. (2006). Isotope calibrated Greenland temperature record over Marine Isotope Stage 3 and its relation to CH₄. *Earth and Planetary Science Letters*, 243(3), 504-519.
- Hughes, A. L. C., Gyllencreutz, R., Lohne, Ø. S., et al. (2016). The last Eurasian ice sheets – a chronological database and time-slice reconstruction, DATED-1. *Boreas*, 45(1), 1-45.
- Hulbe, C. (2017). Is ice sheet collapse in West Antarctica unstoppable? *Science*, 356(6341), 910-911.
- Humbert, A., Steinhage, D., Helm, V., et al. (2018). Missing evidence of widespread subglacial lakes at Recovery Glacier, Antarctica. *Journal of Geophysical Research: Earth Surface*, 123, 2802-2826.
- Huuse, M., and Lykke-Andersen, H. (2000a). Large-scale glaciogenic thrust structures in the eastern Danish North Sea. Geological Society, London, Special Publications, 176(1), 293-305.
- Huuse, M., and Lykke-Andersen, H. (2000b). Overdeepened Quaternary valleys in the eastern Danish North Sea morphology and origin. *Quaternary Science Reviews*, 19, 1233-1253.
- Huuse, M., Le Heron, D. P., Dixon, R., et al. (2012). Glaciogenic reservoirs and hydrocarbon systems: an introduction. In: Huuse, M., Redfern, J., Le Heron, D. P., Dixon, R. J., Moscariello, A., et al. (eds.). *Glaciogenic Reservoirs and Hydrocarbon Systems*, Volume 368: London, Geological Society, Special Publications, 1-28.
- Iken, A. (1981). The Effect of the Subglacial Water Pressure on the Sliding Velocity of a Glacier in an Idealized Numerical Model. *Journal of Glaciology*, 27(97), 407-421.
- IMBIE (2018). Mass balance of the Antarctic Ice Sheet from 1992 to 2017. *Nature*, 558(7709), 219-222.
- Intergovernmental Panel on Climate Change (2021). *Climate Change 2021: The Physical Science Basis*. Contribution of Working Group I to the Sixth Assessment Report of the Intergovernmental Panel on Climate Change, Cambridge, United Kingdom and New York, NY, USA, Cambridge University Press.
- Iverson, N., Hooyer, T. S., and Baker, R. W. (1998). Ring-shear studies of till deformation: Coulomb-plastic behaviour and distributed strain in glacier beds. *Journal of Glaciology*, 44(148), 634-642.
- Iverson, N., Hooyer, T. S., Fischer, U. H., et al. (2007). Soft-bed experiments beneath Engabreen, Norway: regelation infiltration, basal slip and bed deformation. *Journal of Glaciology*, 53(182), 323-340.
- Iverson, N., and Person, M. (2012). Glacier-bed geomorphic processes and hydrologic conditions relevant to nuclear waste disposal. *Geofluids*, 12(1), 38-57.
- Ives, J. (1958). Glacial Drainage Channels as Indicators of Late-glacial Conditions in Labrador-Ungava: a Discussion. *Cahiers de géographie du Québec*, 3(5), 57-72.
- Jacobel, R. W., Scambos, T. A., Nereson, N. A., et al. (2000). Changes in the margin of Ice Stream C, Antarctica. *Journal of Glaciology*, 46(152), 102-110.
- Jakobsson, M., Anderson, J. B., Nitsche, F. O., et al. (2011). Geological record of ice shelf break-up and grounding line retreat, Pine Island Bay, West Antarctica. *Geology*, 39(7), 691-694.
- Jakobsson, M., Gyllencreutz, R., Mayer, L. A., et al. (2016). Mapping submarine glacial landforms using acoustic methods. In: Dowdeswell, J. A., Canals, M., Jakobsson, M., Todd, B. J., Dowdeswell, E. K., et al. (eds.). *Atlas of Submarine Glacial Landforms: Modern, Quaternary and Ancient*, Volume 46: London, Geological Society Memoirs, 17-40.
- Jansen, J. D., Codilean, A. T., Stroeven, A. P., et al. (2014). Inner gorges cut by subglacial meltwater during Fennoscandian ice sheet decay. *Nature Communications*, 5, 3815.
- Janszen, A., Moreau, J., Moscariello, A., et al. (2012a). Time-transgressive tunnel-valley infill revealed by a three-dimensional sedimentary model, Hamburg, north-west Germany. *Sedimentology*, 60(3), 693-719.

- Janszen, A., Spaak, M., and Moscariello, A. (2012b). Effects of the substratum on the formation of glacial tunnel valleys: an example from the Middle Pleistocene of the southern North Sea Basin. *Boreas*, 41(4), 629-643.
- Jentzsch, A. (1884). Über die Bildung der preussischen Seen. *Zeitschrift der deutschen geologischen Gesellschaft für Erdkunde*, 10, 699-702.
- Jordan, T. A., Ferraccioli, F., Corr, H., et al. (2010). Hypothesis for mega-outburst flooding from a palaeo-subglacial lake beneath the East Antarctic Ice Sheet. *Terra Nova*, 283-289.
- Jørgensen, F., and Sandersen, P. B. E. (2006). Buried and open tunnel valleys in Denmark—erosion beneath multiple ice sheets. *Quaternary Science Reviews*, 25(11-12), 1339-1363.
- Joughin, I., Tulaczyk, S., Bindschadler, R., et al. (2002). Changes in west Antarctic ice stream velocities: Observation and analysis. *Journal of Geophysical Research: Solid Earth*, 107, B11, 2289.
- Joughin, I., Das, S. B., King, M. A., et al. (2008). Seasonal Speedup Along the Western Flank of the Greenland Ice Sheet. *Science*, 320(5877), 781-783.
- Joughin, I., Tulaczyk, S. M., Bamber, J. L., et al. (2009). Basal conditions for Pine Island and Thwaites Glaciers, West Antarctica, determined using satellite and airborne data. *Journal of Glaciology*, 55(190), 245-257.
- Joughin, I., Smith, B. E., and Medley, B. (2014). Marine ice sheet collapse potentially under way for the Thwaites Glacier basin, West Antarctica. *Science*, 344(6185), 735-738.
- Jouzel, J., Masson-Delmotte, V., Cattani, O., et al. (2007). Orbital and Millennial Antarctic Climate Variability over the Past 800,000 Years. *Science*, 317(5839), 793-796.
- Kallweit, R. S., and Wood, L. C. (1982). The limits of resolution of zero-phase wavelets. *GEOPHYSICS*, 47(7), 1035-1046.
- Kamb, B. (1987). Glacier surge mechanism based on linked cavity configuration of the basal water conduit system. *Journal of Geophysical Research*, 92, B9, 9083-9100.
- Kamb, B. (2001). Basal Zone of the West Antarctic Ice Streams and its Role in Lubrication of Their Rapid Motion. In: Alley, R.B. and Bindschadler, R.A. (eds.) *The West Antarctic Ice Sheet: Behavior and Environment*, 157-199.
- Karl, D. M., Bird, D. F., Björkman, K., et al. (1999). Microorganisms in the Accreted Ice of Lake Vostok, Antarctica. *Science*, 286(5447), 2144-2147.
- Karlsson, N. B., Solgaard, A. M., Mankoff, K. D., et al. (2021). A first constraint on basal melt-water production of the Greenland ice sheet. *Nature Communications*, 12(1), 3461.
- Kehew, A. E., and Kozłowski, A. L. (2007). Tunnel channels of the Saginaw lobe, Michigan, USA. Applied Quaternary research in the central part of glaciated terrain. Geological Survey of Finland, Special Paper, 46, 69-78.
- Kehew, A. E., Piotrowski, J. A., and Jørgensen, F. (2012). Tunnel valleys: Concepts and controversies — A review. *Earth-Science Reviews*, 113(1-2), 33-58.
- Keisling, B. A., Nielsen, L. T., Hvidberg, C. S., et al. (2020). Pliocene–Pleistocene megafloods as a mechanism for Greenlandic megacanyon formation. *Geology*, 48(7), 737-741.
- Kindler, P., Guillevic, M., Baumgartner, M., et al. (2014). Temperature reconstruction from 10 to 120 kyr b2k from the NGRIP ice core. *Climate of the Past*, 10(2), 887-902.
- King, E. C. (2020). The precision of radar-derived subglacial bed topography: a case study from Pine Island Glacier, Antarctica. *Annals of Glaciology*, 61(81), 154-161.
- King, E. C., Hindmarsh, R. C. A., and Stokes, C. R. (2009). Formation of mega-scale glacial lineations observed beneath a West Antarctic ice stream. *Nature Geoscience*, 2(8), 585-588.
- King, J. C., and Turner, J. (2007). *Antarctic meteorology and climatology*, Cambridge University Press, UK.
- Kingslake, J., Ely, J. C., Das, I., et al. (2017). Widespread movement of meltwater onto and across Antarctic ice shelves. *Nature*, 544(7650), 349-352.
- Kipf, A., Mortimer, N., Werner, R., et al. (2012). Granitoids and dykes of the Pine Island Bay region, West Antarctica. *Antarctic Science*, 24(5), 473-484.

Bibliography

- Kirkham, J. D. (2017). Constraining the pathways and fluxes of subglacial meltwater beneath the palaeo-Antarctic Ice Sheet. Unpublished M.Phil thesis. University of Cambridge, 143 p.
- Kirkham, J. D., Hogan, K. A., Larter, R. D., et al. (2019). Past water flow beneath Pine Island and Thwaites glaciers, West Antarctica. *The Cryosphere*, 13(7), 1959-1981.
- Kirkham, J. D., Hogan, K. A., Larter, R. D., et al. (2020). Morphometry of bedrock meltwater channels on Antarctic inner continental shelves: Implications for channel development and subglacial hydrology. *Geomorphology*, 370, 107369.
- Kirkham, J. D., Hogan, K. A., Larter, R. D., et al. (2021). Tunnel valley infill and genesis revealed by high-resolution 3-D seismic data. *Geology*, 49(12), 1516-1520.
- Kirkham, J. D., Hogan, K., Larter, R. D., et al. (2022). Tunnel valley formation beneath deglaciating mid-latitude ice sheets: Observations and modelling. *Quaternary Science Reviews*.
- Kirshner, A. E., Anderson, J. B., Jakobsson, M., et al. (2012). Post-LGM deglaciation in Pine Island Bay, West Antarctica. *Quaternary Science Reviews*, 38, 11-26.
- Kluiwing, S. J., Bosch, J. A., Ebbing, J. H., et al. (2003). Onshore and offshore seismic and lithostratigraphic analysis of a deeply incised Quaternary buried valley system in the Northern Netherlands. *Journal of Applied Geophysics*, 53(4), 249-271.
- Konrad, H., Shepherd, A., Gilbert, L., et al. (2018). Net retreat of Antarctic glacier grounding lines. *Nature Geoscience*, 11(4), 258-262.
- Kor, P. S. G., Shaw, J., and Sharpe, D. R. (1991). Erosion of bedrock by subglacial meltwater, Georgian Bay, Ontario: a regional view. *Canadian Journal of Earth Sciences*, 28(4), 623-642.
- Koziol, C., Arnold, N., Pope, A., et al. (2017). Quantifying supraglacial meltwater pathways in the Paakitsoq region, West Greenland. *Journal of Glaciology*, 63(239), 464-476.
- Koziol, C. P., and Arnold, N. (2018). Modelling seasonal meltwater forcing of the velocity of land-terminating margins of the Greenland Ice Sheet. *The Cryosphere*, 12(3), 971-991.
- Kristensen, T. B., and Huuse, M. (2012). Multistage erosion and infill of buried Pleistocene tunnel valleys and associated seismic velocity effects. Geological Society London, Special Publications, 368(1), 159-172.
- Kristensen, T. B., Huuse, M., Piotrowski, J. A., et al. (2007). A morphometric analysis of tunnel valleys in the eastern North Sea based on 3D seismic data. *Journal of Quaternary Science*, 22(8), 801-815.
- Kristensen, T. B., Piotrowski, J. A., Huuse, M., et al. (2008). Time-transgressive tunnel valley formation indicated by infill sediment structure, North Sea – the role of glaciohydraulic supercooling. *Earth Surface Processes and Landforms*, 33(4), 546-559.
- Krüger, J. (1989). Gletscheren og landskabet – i nutid og istid, Nordisk Forlag, Copenhagen, Gyldendal, Geografiske temahæfter.
- Kuhn, G., Hillenbrand, C. D., Kasten, S., et al. (2017). Evidence for a palaeo-subglacial lake on the Antarctic continental shelf. *Nature Communications*, 8, 15591.
- Kurjanski, B., Rea, B. R., Spagnolo, M., et al. (2019). Morphological evidence for marine ice stream shutdown, central Barents Sea. *Marine Geology*, 414, 64-76.
- Laban, C. (1995). The Pleistocene glaciations in the Dutch sector of the North Sea. Unpublished PhD thesis: University of Amsterdam.
- Lamb, M. P., and Fonstad, M. A. (2010). Rapid formation of a modern bedrock canyon by a single flood event. *Nature Geoscience*, 3(7), 477-481.
- Lamb, R. M., Harding, R., Huuse, M., et al. (2018). The early Quaternary North Sea Basin. *Journal of the Geological Society*, 175(2), 275-290.
- Lang, J., Winsemann, J., Steinmetz, D., et al. (2012). The Pleistocene of Schöningen, Germany: a complex tunnel valley fill revealed from 3D subsurface modelling and shear wave seismics. *Quaternary Science Reviews*, 39, 86-105.
- Lanoil, B., Skidmore, M., Priscu, J. C., et al. (2009). Bacteria beneath the West Antarctic Ice Sheet. *Environmental Microbiology*, 11(3), 609-615.

- Larsen, I. J., and Lamb, M. P. (2016). Progressive incision of the Channeled Scablands by outburst floods. *Nature*, 538(7624), 229-232.
- Larsen, N. K., Piotrowski, J. A., and Kronborg, C. (2004). A multiproxy study of a basal till: a time-transgressive accretion and deformation hypothesis. *Journal of Quaternary Science*, 19(1), 9-21.
- Larter, R. D., Graham, A. G. C., Gohl, K., et al. (2009). Subglacial bedforms reveal complex basal regime in a zone of paleo-ice stream convergence, Amundsen Sea embayment, West Antarctica. *Geology*, 37(5), 411-414.
- Larter, R. D., Hogan, K. A., Hillenbrand, C.-D., et al. (2019). Subglacial hydrological control on flow of an Antarctic Peninsula palaeo-ice stream. *The Cryosphere*, 13(6), 1583-1596.
- Lawson, D. E., Strasser, J. C., Evenson, E. B., et al. (1998). Glaciohydraulic supercooling: a freeze-on mechanism to create stratified, debris-rich basal ice: I. Field evidence. *Journal of Glaciology*, 44(148), 547-562.
- Le Brocq, A. M., Ross, N., Griggs, J. A., et al. (2013). Evidence from ice shelves for channelized meltwater flow beneath the Antarctic Ice Sheet. *Nature Geoscience*, 6(11), 945-948.
- Le Heron, D. P., and Craig, J. (2008). First-order reconstructions of a Late Ordovician Saharan ice sheet. *Journal of the Geological Society*, 165(1), 19-29.
- Le Heron, D. P., Sutcliffe, O., Bourqig, K., et al. (2004). Sedimentary architecture of Upper Ordovician tunnel valleys, Gargaf Arch, Libya: Implications for the genesis of a hydrocarbon reservoir. *GeoArabia*, 9(2), 137-160.
- Le Heron, D. P., Sutcliffe, O. E., Whittington, R. J., et al. (2005). The origins of glacially related soft-sediment deformation structures in Upper Ordovician glaciogenic rocks: implication for ice-sheet dynamics. *Palaeogeography, Palaeoclimatology, Palaeoecology*, 218(1-2), 75-103.
- Lebedeva-Ivanova, N., Polteau, S., Bellwald, B., et al. (2018). Toward one-meter resolution in 3D seismic. *The Leading Edge*, 37(11), 818-828.
- Lee, J. R., Busschers, F. S., and Sejrup, H. P. (2012). Pre-Weichselian Quaternary glaciations of the British Isles, The Netherlands, Norway and adjacent marine areas south of 68°N: implications for long-term ice sheet development in northern Europe. *Quaternary Science Reviews*, 44, 213-228.
- Leeson, A. A., Shepherd, A., Briggs, K., et al. (2015). Supraglacial lakes on the Greenland ice sheet advance inland under warming climate. *Nature Climate Change*, 5(1), 51-55.
- Lelandais, T., Mourgues, R., Ravier, É., et al. (2016). Experimental modeling of pressurized subglacial water flow: Implications for tunnel valley formation. *Journal of Geophysical Research: Earth Surface*, 121(11), 2022-2041.
- Lelandais, T., Ravier, É., Pochat, S., et al. (2018). Modelled subglacial floods and tunnel valleys control the life cycle of transitory ice streams. *The Cryosphere*, 12(8), 2759-2772.
- LeMasurier, W. (2013). Shield volcanoes of Marie Byrd Land, West Antarctic rift: oceanic island similarities, continental signature, and tectonic controls. *Bulletin of Volcanology*, 75(6), 726.
- Lemieux, J.-M., Sudicky, E. A., Peltier, W. R., et al. (2008). Dynamics of groundwater recharge and seepage over the Canadian landscape during the Wisconsinian glaciation. *Journal of Geophysical Research: Earth Surface*, 113, F1.
- Lenaerts, J. T. M., Lhermitte, S., Drews, R., et al. (2016). Meltwater produced by wind-albedo interaction stored in an East Antarctic ice shelf. *Nature Climate Change*, 7(1), 58-62.
- Lendemer, J. C., and Allen, J. L. (2014). Lichen Biodiversity under Threat from Sea-Level Rise in the Atlantic Coastal Plain. *BioScience*, 64(10), 923-931.
- Lenton, T. M., Rockström, J., Gaffney, O., et al. (2019). Climate tipping points—too risky to bet against. *Nature*, 575, 592-595.
- Lepp, A. P., Simkins, L. M., Anderson, J. B., et al. (2022). Sedimentary Signatures of Persistent Subglacial Meltwater Drainage From Thwaites Glacier, Antarctica. *Frontiers in Earth Science*, 10.

Bibliography

- Lesemann, J.-E., Alsop, G. I., and Piotrowski, J. A. (2010a). Incremental subglacial meltwater sediment deposition and deformation associated with repeated ice-bed decoupling: a case study from the Island of Funen, Denmark. *Quaternary Science Reviews*, 29(23), 3212-3229.
- Lesemann, J.-E., Piotrowski, J. A., and Wysota, W. (2010b). “Glacial curvilineations”: New glacial landforms produced by longitudinal vortices in subglacial meltwater flows. *Geomorphology*, 120(3-4), 153-161.
- Lesemann, J.-E., Piotrowski, J. A., and Wysota, W. (2014). Genesis of the ‘glacial curvilinear’ landscape by meltwater processes under the former Scandinavian Ice Sheet, Poland. *Sedimentary Geology*, 312, 1-18.
- Lewington, E. L. M., Livingstone, S. J., Clark, C. D., et al. (2020). A model for interaction between conduits and surrounding hydraulically connected distributed drainage based on geomorphological evidence from Keewatin, Canada. *The Cryosphere*, 14(9), 2949-2976.
- Lewis, A. R., Marchant, D. R., Kowalewski, D. E., et al. (2006). The age and origin of the Labyrinth, western Dry Valleys, Antarctica: Evidence for extensive middle Miocene subglacial floods and freshwater discharge to the Southern Ocean. *Geology*, 34(7), 513-516.
- Lewis, A. R., Marchant, D. R., Ashworth, A. C., et al. (2007). Major middle Miocene global climate change evidence from East Antarctica and the Transantarctic Mountains. *Geological Society of America Bulletin*, 119(11/12), 1449-1461.
- Lewis, A. R., Marchant, D. R., Ashworth, A. C., et al. (2008). Mid Miocene cooling and the extinction of tundra in continental Antarctica. *PNAS*, 105(31), 10676-10680.
- Li, L., Aitken, A. R. A., Lindsay, M. D., et al. (2022). Sedimentary basins reduce stability of Antarctic ice streams through groundwater feedbacks. *Nature Geoscience*, 15, 645-650.
- Liljedahl, L. C., Meierbachtol, T., Harper, J., et al. (2021). Rapid and sensitive response of Greenland’s groundwater system to ice sheet change. *Nature Geoscience*, 14(10), 751-755.
- Lin, Y., Hibbert, F. D., Whitehouse, P. L., et al. (2021). A reconciled solution of Meltwater Pulse 1A sources using sea-level fingerprinting. *Nature Communications*, 12(1), 2015.
- Lindbäck, K., Pettersson, R., Hubbard, A. L., et al. (2015). Subglacial water drainage, storage, and piracy beneath the Greenland ice sheet. *Geophysical Research Letters*, 42(18), 7606-7614.
- Lindow, J., Kamp, P. J. J., Mukasa, S. B., et al. (2016). Exhumation history along the eastern Amundsen Sea coast, West Antarctica, revealed by low-temperature thermochronology. *Tectonics*, 35(10), 2239-2257.
- Livingstone, S. J., and Clark, C. D. (2016). Morphological properties of tunnel valleys of the southern sector of the Laurentide Ice Sheet and implications for their formation. *Earth Surface Dynamics*, 4(3), 567-589.
- Livingstone, S. J., Cofaigh, C. Ó., Stokes, C. R., et al. (2013a). Glacial geomorphology of Marguerite Bay Palaeo-Ice stream, western Antarctic Peninsula. *Journal of Maps*, 9(4), 558-572.
- Livingstone, S. J., Clark, C. D., Woodward, J., et al. (2013b). Potential subglacial lake locations and meltwater drainage pathways beneath the Antarctic and Greenland ice sheets. *The Cryosphere*, 7(6), 1721-1740.
- Livingstone, S. J., Utting, D. J., Ruffell, A., et al. (2016). Discovery of relict subglacial lakes and their geometry and mechanism of drainage. *Nature Communications*, 7, 11767.
- Livingstone, S. J., Chu, W., Ely, J. C., et al. (2017). Paleofluvial and subglacial channel networks beneath Humboldt Glacier, Greenland. *Geology*, 45(6), 551-554.
- Livingstone, S. J., Sole, A. J., Storrar, R. D., et al. (2019). Brief communication: Subglacial lake drainage beneath Isunguata Sermia, West Greenland: geomorphic and ice dynamic effects. *The Cryosphere*, 13(10), 2789-2796.
- Livingstone, S. J., Lewington, E. L. M., Clark, C. D., et al. (2020). A quasi-annual record of time-transgressive esker formation: implications for ice-sheet reconstruction and subglacial hydrology. *The Cryosphere*, 14(6), 1989-2004.

- Livingstone, S. J., Li, Y., Rutishauser, A., et al. (2022). Subglacial lakes and their changing role in a warming climate. *Nature Reviews Earth & Environment*, 3, 106-124.
- Lliboutry, L. (1968). General Theory of Subglacial Cavitation and Sliding of Temperate Glaciers. *Journal of Glaciology*, 7(49), 21-58.
- Lohrberg, A., Schwarzer, K., Unverricht, D., et al. (2020). Architecture of tunnel valleys in the southeastern North Sea: new insights from high-resolution seismic imaging. *Journal of Quaternary Science*, 35(7), 892-906.
- Loncarevic, B. D., Courtney, R. C., Fader, G. B. J., et al. (1994). Sonography of a glaciated continental shelf. *Geology*, 22(8), 747-750.
- Lonergan, L., Maidment, S. C. R., and Collier, J. S. (2006). Pleistocene subglacial tunnel valleys in the central North Sea basin: 3-D morphology and evolution. *Journal of Quaternary Science*, 21(8), 891-903.
- Loose, B., Naveira Garabato, A. C., Schlosser, P., et al. (2018). Evidence of an active volcanic heat source beneath the Pine Island Glacier. *Nature Communications*, 9(1), 2431.
- Lowe, A. L., and Anderson, J. B. (2002). Reconstruction of the West Antarctic ice sheet in Pine Island Bay during the Last Glacial Maximum and its subsequent retreat history. *Quaternary Science Reviews*, 21, 1879-1897.
- Lowe, A. L., and Anderson, J. B. (2003). Evidence for abundant subglacial meltwater beneath the paleo ice sheet in Pine Island Bay, Antarctica. *Journal of Glaciology*, 49(164), 125-138.
- Lüthi, D., Le Floch, M., Bereiter, B., et al. (2008). High-resolution carbon dioxide concentration record 650,000–800,000 years before present. *Nature*, 453(7193), 379-382.
- Lutz, R. K., Gaedicke, C., Reinhardt, L., et al. (2009). Pleistocene tunnel valleys in the German North Sea: spatial distribution and morphology. *Zeitschrift der Deutschen Gesellschaft für Geowissenschaften*, 160(3), 225-235.
- MacGregor, J. A., Fahnstock, M. A., Catania, G. A., et al. (2016). A synthesis of the basal thermal state of the Greenland Ice Sheet. *Journal of Geophysical Research: Earth Surface*, 121(7), 1328-1350.
- MacKie, E. J., Schroeder, D. M., Caers, J., et al. (2020). Antarctic Topographic Realizations and Geostatistical Modeling Used to Map Subglacial Lakes. *Journal of Geophysical Research: Earth Surface*, 125(3), e2019JF005420.
- MacRae, R. A., and Christians, A. R. (2013). A reexamination of Pleistocene tunnel valley distribution on the central Scotian Shelf. *Canadian Journal of Earth Sciences*, 50(5), 535-544.
- Maier, N., Gimbert, F., and Gillet-Chaulet, F. (2022). Threshold response to melt drives large-scale bed weakening in Greenland. *Nature*, 607(7920), 714-720.
- Mäkinen, J., Kajuutti, K., Palmu, J. P., et al. (2017). Triangular-shaped landforms reveal subglacial drainage routes in SW Finland. *Quaternary Science Reviews*, 164, 37-53.
- Mannerfelt, C. M. s. (1945). Några Glacialmorfologiska Formelement. *Geografiska Annaler*, 27(1-2), 3-5.
- Marchant, D. R., and Denton, G. H. (1996). Miocene and Pliocene palaeoclimate of the Dry Valleys region, Southern Victoria land a geomorphological approach. *Marine Micropaleontology*, 27, 253-271.
- Marchant, D. R., Denton, G. H., Sugden, D. E., et al. (1993). Miocene Glacial Stratigraphy and Landscape Evolution of the Western Asgard Range, Antarctica. *Geografiska Annaler: Series A*, 75(4), 303-330.
- Marchant, D. R., Jamieson, S. S. R., and Sugden, D. (2011). The geomorphic signature of massive subglacial floods in Victoria Land, Antarctica. In: Siegert, M. J., and Kennicutt, M. C. (eds.). *Antarctic Subglacial Aquatic Environments*, Volume 192, American Geophysical Union, p. 111-127.
- Marczinek, S., and Piotrowski, J. A. (2006). Groundwater Flow Under the Margin of the Last Scandinavian Ice Sheet Around the Eckernförde Bay, Northwest Germany. In: Knight, P. G., ed., *Glacier Science and Environmental Change*, 60-62.
- Marshall, S. J., Tarasov, L., Clarke, G. K. C., et al. (2000). Glaciological reconstruction of the Laurentide Ice Sheet: physical processes and modelling challenges. *Canadian Journal of Earth Sciences*, 37(5), 769-793.

Bibliography

- Martos, Y. M., Catalán, M., Jordan, T. A., et al. (2017). Heat Flux Distribution of Antarctica Unveiled. *Geophysical Research Letters*, 44(22), 11417-11426.
- Maschinski, J., Ross, M. S., Liu, H., et al. (2011). Sinking ships: conservation options for endemic taxa threatened by sea level rise. *Climatic Change*, 107(1), 147-167.
- Maule, C. F., Purucker, M. E., Olsen, N., et al. (2005). Heat Flux Anomalies in Antarctica Revealed by Satellite Magnetic Data. *Science*, 309(5733), 464-467.
- Mayer, L. A., Paton, M., Gee, L., et al. (2000). Interactive 3-D visualization: a tool for seafloor navigation, exploration and engineering. Proceedings OCEANS 2000 MTS/IEEE Conference and Exhibition. 11-14 September 2000. Volume 2, 913-919.
- Mayer, L. A., Jakobsson, M., Allen, G., et al. (2018). The Nippon Foundation—GEBCO Seabed 2030 Project: The Quest to See the World's Oceans Completely Mapped by 2030. *Geosciences*, 8(2), 63.
- McEwen, T., and Marsily, G. D. (1991). The potential significance of permafrost to the behaviour of a deep radioactive waste repository. Swedish Nuclear Power Inspectorate, Stockholm (Sweden).
- McMillan, M., Corr, H., Shepherd, A., et al. (2013). Three-dimensional mapping by CryoSat-2 of subglacial lake volume changes. *Geophysical Research Letters*, 40(16), 4321-4327.
- Mejía, J. Z., Gulley, J. D., Trunz, C., et al. (2021). Isolated cavities dominate Greenland Ice Sheet dynamic response to lake drainage. *Geophysical Research Letters*, 48, e2021GL094762.
- Mercer, J. H. (1978). West Antarctic ice sheet and CO₂ greenhouse effect: a threat of disaster. *Nature*, 271(5643), 321-325.
- Meyer, C. R., Fernandes, M. C., Creyts, T. T., et al. (2016). Effects of ice deformation on Røthlisberger channels and implications for transitions in subglacial hydrology. *Journal of Glaciology*, 62(234), 750-762.
- Mikucki, J. A., and Priscu, J. C. (2007). Bacterial Diversity Associated with Blood Falls, a Subglacial Outflow from the Taylor Glacier, Antarctica. *Applied and Environmental Microbiology*, 73(12), 4029-4039.
- Millan, R., Rignot, E., Bernier, V., et al. (2017). Bathymetry of the Amundsen Sea Embayment sector of West Antarctica from Operation IceBridge gravity and other data. *Geophysical Research Letters*, 44(3), 1360-1368.
- Millan, R., Mouginot, J., Rabatel, A., et al. (2022). Ice velocity and thickness of the world's glaciers. *Nature Geoscience*, 15(2), 124-129.
- Miller, K. G., Wright, J. D., Browning, J. V., et al. (2012). High tide of the warm Pliocene: Implications of global sea level for Antarctic deglaciation. *Geology*, 40(5), 407-410.
- Montelli, A., Dowdeswell, J. A., Ottesen, D., et al. (2017). Ice-sheet dynamics through the Quaternary on the mid-Norwegian continental margin inferred from 3D seismic data. *Marine and Petroleum Geology*, 80, 228-242.
- Montelli, A., Gulick, S. P. S., Fernandez, R., et al. (2019). Seismic stratigraphy of the Sabrina Coast shelf, East Antarctica: Early history of dynamic meltwater-rich glaciations. *GSA Bulletin*, 132(3-4), 545-561.
- Montelli, A., Dowdeswell, J. A., Pirogova, A., et al. (2020). Deep and extensive meltwater system beneath the former Eurasian Ice Sheet in the Kara Sea. *Geology*, 48, 179-183.
- Mooers, H. D. (1989). On the formation of the tunnel valleys of the Superior Lobe Central Minnesota. *Quaternary Research*, 32, 24-35.
- Moreau, J., and Huuse, M. (2014). Infill of tunnel valleys associated with landward-flowing ice sheets: The missing Middle Pleistocene record of the NW European rivers? *Geochemistry, Geophysics, Geosystems*, 15(1), 1-9.
- Morley, C. K., Maczak, A., Rungprom, T., et al. (2017). New style of honeycomb structures revealed on 3D seismic data indicate widespread diagenesis offshore Great South Basin, New Zealand. *Marine and Petroleum Geology*, 86, 140-154.

- Morlighem, M., Williams, C. N., Rignot, E., et al. (2017). BedMachine v3: Complete Bed Topography and Ocean Bathymetry Mapping of Greenland From Multibeam Echo Sounding Combined With Mass Conservation. *Geophysical Research Letters*, 44(21), 11051-11061.
- Morlighem, M., Rignot, E., Binder, T., et al. (2019). Deep glacial troughs and stabilizing ridges unveiled beneath the margins of the Antarctic ice sheet. *Nature Geoscience*, 13(2), 132-137.
- Moscariello, A., Pugin, A., Wildi, W., et al. (1998). Déglaciation wurmienne dans des conditions lacustres à la terminaison occidentale du bassin lémanique (Suisse occidentale et France). *Eclogae Geologicae Helvetiae*, 91, 185-201.
- Mosher, D., Bigg, S., and Lapierre, A. (2006). 3D seismic versus multibeam sonar seafloor surface renderings for geohazard assessment: Case examples from the central Scotian Slope. *The Leading Edge*, 25(12), 1484-1494.
- Mouginot, J., Rignot, E., Bjork, A. A., et al. (2019). Forty-six years of Greenland Ice Sheet mass balance from 1972 to 2018. *PNAS*, 116(19), 9239-9244.
- Mugford, R. I., and Dowdeswell, J. A. (2011). Modeling glacial meltwater plume dynamics and sedimentation in high-latitude fjords. *Journal of Geophysical Research: Earth Surface*, 116, F1.
- Mullins, H. T., and Hinchey, E. J. (1989). Erosion and infill of New York Finger Lakes implications for Laurentide ice sheet deglaciation. *Geology*, 17, 622-625.
- Murray, T., Corr, H., Forieri, A., et al. (2008). Contrasts in hydrology between regions of basal deformation and sliding beneath Rutford Ice Stream, West Antarctica, mapped using radar and seismic data. *Geophysical Research Letters*, 35, 12.
- Müther, D., Back, S., Reuning, L., et al. (2012). Middle Pleistocene landforms in the Danish Sector of the southern North Sea imaged on 3D seismic data. In: Huuse, M., Redfern, J., Le Heron, D. P., Dixon, R. J., Moscariello, A., et al. (eds.). *Glaciogenic Reservoirs and Hydrocarbon Systems*, Volume 368: London, Geological Society, Special Publications, 111-127.
- Nakayama, Y., Cai, C., and Seroussi, H. (2021). Impact of Subglacial Freshwater Discharge on Pine Island Ice Shelf. *Geophysical Research Letters*, 48(18), e2021GL093923.
- Naughten, K. A., Holland, P. R., Dutrioux, P., et al. (2022). Simulated Twentieth-Century Ocean Warming in the Amundsen Sea, West Antarctica. *Geophysical Research Letters*, 49(5), e2021GL094566.
- Nechay, W. (1927). Utwory lodowcowe Ziemi Dobrzyńskiej. Sprawozdania Państwowego Instytutu Geologicznego, 4(1-2), 61-144.
- Neukom, R., Steiger, N., Gómez-Navarro, J. J., et al. (2019). No evidence for globally coherent warm and cold periods over the preindustrial Common Era. *Nature*, 571(7766), 550-554.
- Neumann, B., Vafeidis, A. T., Zimmermann, J., et al. (2015). Future Coastal Population Growth and Exposure to Sea-Level Rise and Coastal Flooding - A Global Assessment. *PLOS ONE*, 10(3), e0118571.
- Newton, A. M., Huuse, M., and Brocklehurst, S. H. (2016). Buried iceberg scours reveal reduced North Atlantic Current during the stage 12 deglacial. *Nature Communications*, 7, 10927.
- Newton, A. M. W., and Huuse, M. (2017). Late Cenozoic environmental changes along the Norwegian margin. *Marine Geology*, 393, 216-244.
- Ng, F. S. L. (2000). Canals under sediment-based ice sheets. *Annals of Glaciology*, 30, 146-152.
- Nicholls, R. J., Hoozemans, F. M. J., and Marchand, M. (1999). Increasing flood risk and wetland losses due to global sea-level rise: regional and global analyses. *Global Environmental Change*, 9, S69-S87.
- Nienow, P. W., Sole, A. J., Slater, D. A., et al. (2017). Recent Advances in Our Understanding of the Role of Meltwater in the Greenland Ice Sheet System. *Current Climate Change Reports*, 3(4), 330-344.
- Nitsche, F. O., and Correia, R. (2019). East Antarctic ice flow dynamic based on subglacial landforms near Dibble Glacier. *Marine Geology*, 417, 106007.
- Nitsche, F. O., Jacobs, S. S., Larter, R. D., et al. (2007). Bathymetry of the Amundsen Sea continental shelf: Implications for geology, oceanography, and glaciology. *Geochemistry, Geophysics, Geosystems*, 8, Q10009.

Bibliography

- Nitsche, F. O., Gohl, K., Larter, R. D., et al. (2013). Paleo ice flow and subglacial meltwater dynamics in Pine Island Bay, West Antarctica. *The Cryosphere*, 7(1), 249-262.
- Niu, L. U., Lohmann, G., Hinck, S., et al. (2019). The sensitivity of Northern Hemisphere ice sheets to atmospheric forcing during the last glacial cycle using PMIP3 models. *Journal of Glaciology*, 65(252), 645-661.
- Noble, T. L., Rohling, E. J., Aitken, A. R. A., et al. (2020). The Sensitivity of the Antarctic Ice Sheet to a Changing Climate: Past, Present, and Future. *Reviews of Geophysics*, 58(4), e2019RG000663.
- Noël, B., Berg, W. J. v. d., Lhermitte, S., et al. (2019). Rapid ablation zone expansion amplifies north Greenland mass loss. *Science Advances*, 5(9), eaaw0123.
- Noormets, R., Dowdeswell, J. A., Larter, R. D., et al. (2009). Morphology of the upper continental slope in the Bellingshausen and Amundsen Seas – Implications for sedimentary processes at the shelf edge of West Antarctica. *Marine Geology*, 258(1), 100-114.
- Nordmann, V. (1958). Beskrivelse til Geologisk kort over Danmark. Kortbladet Fredericia. A: Kvartære aflejringer. Geological Survey of Denmark (Series I), v. 22-A, 1-125.
- Nye, J. F. (1976). Water Flow in Glaciers: Jökulhlaups, Tunnels and Veins. *Journal of Glaciology*, 17(76), 181-207.
- O'Connor, J. E., and Baker, V. R. (1992). Magnitudes and implications of peak discharges from glacial Lake Missoula. *GSA Bulletin*, 104(3), 267-279.
- O'Connor, J. E., and Costa, J. E. (2004). The world's largest floods, past and present - Their causes and magnitudes. U.S. Geological Survey Circular 1254, 13p.
- Ó Cofaigh, C. (1996). Tunnel valley genesis. *Progress in Physical Geography*, 20(1), 1-19.
- Ó Cofaigh, C., Pudsey, C. J., Dowdeswell, J. A., et al. (2002). Evolution of subglacial bedforms along a paleo-ice stream, Antarctic Peninsula continental shelf. *Geophysical Research Letters*, 29(8), 1199.
- Ó Cofaigh, C., Dowdeswell, J. A., Evans, J., et al. (2004). Timing and significance of glacially influenced mass-wasting in the submarine channels of the Greenland Basin. *Marine Geology*, 207(1-4), 39-54.
- Ó Cofaigh, C., Dowdeswell, J. A., Allen, C. S., et al. (2005). Flow dynamics and till genesis associated with a marine-based Antarctic palaeo-ice stream. *Quaternary Science Reviews*, 24(5-6), 709-740.
- O'Leary, M. J., Hearty, P. J., Thompson, W. G., et al. (2013). Ice sheet collapse following a prolonged period of stable sea level during the last interglacial. *Nature Geoscience*, 6(9), 796-800.
- Oerlemans, J. (1994). Quantifying Global Warming from the Retreat of Glaciers. *Science*, 264(5156), 243-245.
- Ojala, A. E. K., Peterson, G., Mäkinen, J., et al. (2019). Ice-sheet scale distribution and morphometry of triangular-shaped hummocks (murtoos): a subglacial landform produced during rapid retreat of the Scandinavian Ice Sheet. *Annals of Glaciology*, 60(80), 115-126.
- Oppenheimer, M., Glavovic, B., Hinkel, J., et al. (2019). Sea level rise and implications for low lying islands, coasts and communities. In: Pörtner, H.-O., Roberts, D. C., Masson-Delmotte, V., Zhai, P., Tignor, M., et al., (eds.), *IPCC Special Report on the Ocean and Cryosphere in a Changing Climate*: Cambridge University Press, Cambridge, UK, 321-445.
- Oswald, G. K. A., and Robin, G. D. Q. (1973). Lakes Beneath the Antarctic Ice Sheet. *Nature*, 245(5423), 251-254.
- Ottesen, D., and Dowdeswell, J. A. (2006). Assemblages of submarine landforms produced by tidewater glaciers in Svalbard. *Journal of Geophysical Research*, 111, F1, F01016.
- Ottesen, D., and Dowdeswell, J. A. (2009). An inter-ice-stream glaciated margin: Submarine landforms and a geomorphic model based on marine-geophysical data from Svalbard. *GSA Bulletin*, 121(11-12), 1647-1665.
- Ottesen, D., Dowdeswell, J. A., Bellec, V. K., et al. (2017). The geomorphic imprint of glacier surges into open marine waters: Examples from eastern Svalbard. *Marine Geology*, 392, 1-29.
- Ottesen, D., Batchelor, C. L., Dowdeswell, J. A., et al. (2018). Morphology and pattern of Quaternary sedimentation in the North Sea Basin (52–62°N). *Marine and Petroleum Geology*, 98, 836-859.

- Ottesen, D., Stewart, M., Brønner, M., et al. (2020). Tunnel valleys of the central and northern North Sea (56°N to 62°N): Distribution and characteristics. *Marine Geology*, 425, 106199.
- Palmer, S., Shepherd, A., Nienow, P., et al. (2011). Seasonal speedup of the Greenland Ice Sheet linked to routing of surface water. *Earth and Planetary Science Letters*, 302(3), 423-428.
- Palmer, S. J., Dowdeswell, J. A., Christoffersen, P., et al. (2013). Greenland subglacial lakes detected by radar. *Geophysical Research Letters*, 40(23), 6154-6159.
- Pankhurst, R. J., Millar, I. L., Grunow, A. M., et al. (1993). The Pre-Cenozoic magmatic history of the Thurston Island Crustal Block, west Antarctica. *Journal of Geophysical Research: Solid Earth*, 98(B7), 11835-11849.
- Paolo, F. S., Fricker, H. A., and Padman, L. (2015). Volume loss from Antarctic ice shelves is accelerating. *Science*, 348(6232), 327-331.
- Passchier, S., Laban, C., Mesdag, C. S., et al. (2010). Subglacial bed conditions during Late Pleistocene glaciations and their impact on ice dynamics in the southern North Sea. *Boreas*, 39, 633-647.
- Patterson, C. J. (1997). Southern Laurentide ice lobes were created by ice streams: Des Moines Lobe in Minnesota, USA. *Sedimentary Geology*, 111, 249-261.
- Patton, H., Hubbard, A., Andreassen, K., et al. (2016). The build-up, configuration, and dynamical sensitivity of the Eurasian ice-sheet complex to Late Weichselian climatic and oceanic forcing. *Quaternary Science Reviews*, 153, 97-121.
- Pattyn, F. (2008). Investigating the stability of subglacial lakes with a full Stokes ice sheet model. *Journal of Glaciology*, 54(185), 353-361.
- Pattyn, F., and Van Huele, W. (1998). Power law or power flow? *Earth Surface Processes and Landforms*, 23(8), 761-767.
- Pattyn, F., Ritz, C., Hanna, E., et al. (2018). The Greenland and Antarctic ice sheets under 1.5 °C global warming. *Nature Climate Change*, 8(12), 1053-1061.
- Pérez, L. F., McKay, R. M., De Santis, L., et al. (2022). Early to middle Miocene ice sheet dynamics in the westernmost Ross Sea (Antarctica): Regional correlations. *Global and Planetary Change*, 216, 103891.
- Perol, T., Rice, J. R., Platt, J. D., et al. (2015). Subglacial hydrology and ice stream margin locations. *Journal of Geophysical Research: Earth Surface*, 120(7), 1352-1368.
- Person, M., McIntosh, J., Bense, V., et al. (2007). Pleistocene hydrology of North America: The role of ice sheets in reorganizing groundwater flow systems. *Reviews of Geophysics*, 45(3), RG3007.
- Peters, L. E., Anandakrishnan, S., Alley, R. B., et al. (2006). Subglacial sediments as a control on the onset and location of two Siple Coast ice streams, West Antarctica. *Journal of Geophysical Research*, 111(B1), B01302.
- Peters, N. J., Willis, I. C., and Arnold, N. (2009). Numerical analysis of rapid water transfer beneath Antarctica. *Journal of Glaciology*, 55(192), 640-650.
- Petersen, C. J., Büinz, S., Hustoft, S., et al. (2010). High-resolution P-Cable 3D seismic imaging of gas chimney structures in gas hydrated sediments of an Arctic sediment drift. *Marine and Petroleum Geology*, 27(9), 1981-1994.
- Peterson, G., Johnson, M. D., Dahlgren, S., et al. (2018). Genesis of hummocks found in tunnel valleys: an example from Hörda, southern Sweden. *GFF*, 140(2), 189-201.
- PGS (2017). Technote: Towed Streamer EM - Survey Design and Acquisition.
- PGS (2020). CNS MegaSurveyPlus, 2020 version, <https://doi.org/https://www.pgs.com/data-library/europe/nw-europe/north-sea/cns/>.
- Piotrowski, J. A. (1994). Tunnel valley formation in northwest Germany - geology mechanisms of formation and subglacial bed conditions for the Bornhöved tunnel valley. *Sedimentary Geology*, 89, 107-141.
- Piotrowski, J. A. (1997a). Subglacial groundwater flow during the last glaciation in northwestern Germany. *Sedimentary Geology*, 111, 217-224.
- Piotrowski, J. A. (1997b). Subglacial hydrology in north-western Germany during the last glaciation: groundwater flow, tunnel valleys and hydrological cycles. *Quaternary Science Reviews*, 16, 169-185.

Bibliography

- Piotrowski, J. A. (1999). Channelized subglacial drainage under soft-bedded ice sheets: evidence from small N-channels in Central European Lowland. *Geological Quarterly*, 43(2), 153-162.
- Piotrowski, J. A., Geletneky, J., and Vater, R. (1999). Soft-bedded subglacial meltwater channel from the Welzow-Süd opencast lignite mine, Lower Lusatia, eastern Germany. *Boreas*, 28(3), 363-374.
- Piotrowski, J. A., Hermanowski, P., and Piechota, A. M. (2009). Meltwater discharge through the subglacial bed and its land-forming consequences from numerical experiments in the Polish lowland during the last glaciation. *Earth Surface Processes and Landforms*, 34(4), 481-492.
- Plaza-Faverola, A., Büinz, S., and Mienert, J. (2011). Repeated fluid expulsion through sub-seabed chimneys offshore Norway in response to glacial cycles. *Earth and Planetary Science Letters*, 305(3-4), 297-308.
- Pollard, D., and DeConto, R. M. (2009). Modelling West Antarctic ice sheet growth and collapse through the past five million years. *Nature*, 458(7236), 329-332.
- Porter, C., Morin, P., Howat, I., et al. (2018). ArcticDEM, Version 3, Harvard Dataverse, <https://doi.org/doi:10.7910/DVN/OHHUKH>.
- Posamentier, H. W., Davies, R. J., Cartwright, J. A., et al. (2007). Seismic geomorphology - an overview. In: Davies, R. J., Posamentier, H. W., Wood, L. J., and Cartwright, J. A. (eds.). *Seismic Geomorphology: Applications to Hydrocarbon Exploration and Production*, Volume 277: London, Geological Society Special Publications, 1-14.
- Power, H. E., and Clarke, S. L. (2019). 3D seismic-derived bathymetry: a quantitative comparison with multibeam data. *Geo-Marine Letters*, 39(6), 447-467.
- Praeg, D. (1996). Morphology, stratigraphy and genesis of buried Mid-Pleistocene tunnel valleys in the southern North Sea Basin. Unpublished PhD thesis: University of Edinburgh.
- Praeg, D. (2003). Seismic imaging of mid-Pleistocene tunnel-valleys in the North Sea Basin—high resolution from low frequencies. *Journal of Applied Geophysics*, 53(4), 273-298.
- Prins, L. T., Andresen, K. J., Clausen, O. R., et al. (2020). Formation and widening of a North Sea tunnel valley - the impact of slope processes on valley morphology. *Geomorphology*, 368, 107347.
- Priscu, J. C., Adams, E. E., Lyons, W. B., et al. (1999). Geomicrobiology of Subglacial Ice Above Lake Vostok, Antarctica. *Science*, 286(5447), 2141-2144.
- Pritchard, H. D., Ligtenberg, S. R. M., Fricker, H. A., et al. (2012). Antarctic ice-sheet loss driven by basal melting of ice shelves. *Nature*, 484(7395), 502-505.
- Prothro, L. O., Simkins, L. M., Majewski, W., et al. (2018). Glacial retreat patterns and processes determined from integrated sedimentology and geomorphology records. *Marine Geology*, 395, 104-119.
- Pugin, A. J. M., Oldenborger, G. A., Cummings, D. I., et al. (2014). Architecture of buried valleys in glaciated Canadian Prairie regions based on high resolution geophysical data. *Quaternary Science Reviews*, 86, 13-23.
- Quirk, D. G., Underhill, J. R., Gluyas, J. G., et al. (2022). A low-carbon future for The North Sea Basin. Geological Society, London, Special Publications, 494(1), 197-213.
- Raper, S. C. B., and Braithwaite, R. J. (2006). Low sea level rise projections from mountain glaciers and icecaps under global warming. *Nature*, 439(7074), 311-313.
- Ravier, E., Buoncristiani, J.-F., Guiraud, M., et al. (2014). Porewater pressure control on subglacial soft sediment remobilization and tunnel valley formation: A case study from the Alnif tunnel valley (Morocco). *Sedimentary Geology*, 304, 71-95.
- Ravier, E., Buoncristiani, J.-F., Menzies, J., et al. (2015). Does porewater or meltwater control tunnel valley genesis? Case studies from the Hirnantian of Morocco. *Palaeogeography, Palaeoclimatology, Palaeoecology*, 418, 359-376.
- Raymo, M. E., Lisiecki, L. E., and Nisancioglu, K. H. (2006). Plio-Pleistocene Ice Volume, Antarctic Climate, and the Global $\delta^{18}\text{O}$ Record. *Science*, 313(5786), 492-495.
- Rea, B. R., and Evans, D. J. A. (2011). An assessment of surge-induced crevassing and the formation of crevasse squeeze ridges. *Journal of Geophysical Research*, 116, F4.

- Rea, B. R., Newton, A. M. W., Lamb, R. M., et al. (2018). Extensive marine terminating ice sheets in Europe from 2.5 million years ago. *Science Advances*, 4(6), eaar8327.
- Reyes, A. V., Carlson, A. E., Beard, B. L., et al. (2014). South Greenland ice-sheet collapse during Marine Isotope Stage 11. *Nature*, 510(7506), 525-528.
- Rignot, E., Casassa, G., Gogineni, P., et al. (2004). Accelerated ice discharge from the Antarctic Peninsula following the collapse of Larsen B ice shelf. *Geophysical Research Letters*, 31(18), L18401.
- Rignot, E., Bamber, J. L., van den Broeke, M. R., et al. (2008). Recent Antarctic ice mass loss from radar interferometry and regional climate modelling. *Nature Geoscience*, 1(2), 106-110.
- Rignot, E., Mouginot, J., and Scheuchl, B. (2011). Antarctic grounding line mapping from differential satellite radar interferometry. *Geophysical Research Letters*, 38(10), L10504.
- Rignot, E., Mouginot, J., Morlighem, M., et al. (2014). Widespread, rapid grounding line retreat of Pine Island, Thwaites, Smith, and Kohler glaciers, West Antarctica, from 1992 to 2011. *Geophysical Research Letters*, 41(10), 3502-3509.
- Rignot, E., Mouginot, J., Scheuchl, B., et al. (2019). Four decades of Antarctic Ice Sheet mass balance from 1979-2017. *PNAS*, 116(4), 1095-1103.
- Ritz, C., Edwards, T. L., Durand, G., et al. (2015). Potential sea-level rise from Antarctic ice-sheet instability constrained by observations. *Nature*, 528(7580), 115-118.
- Roberts, M. J. (2005). Jökulhlaups: A reassessment of floodwater flow through glaciers. *Reviews of Geophysics*, 43(1), RG1002.
- Robin, G. d. Q., Swithinbank, C. W. M., and Smith, B. M. E. (1970). Radio exploration of the Antarctic Ice Sheet. International symposium on Antarctic glaciological exploration (ISAGE), Hanover, New Hampshire, USA, 3-7 September 1970.
- Rose, K. C., Ross, N., Bingham, R. G., et al. (2014). A temperate former West Antarctic ice sheet suggested by an extensive zone of subglacial meltwater channels. *Geology*, 42(11), 971-974.
- Rose, P., Byerley, G., Vaughan, O., et al. (2018). Aviat: a Lower Pleistocene shallow gas hazard developed as a fuel gas supply for the Forties Field. Geological Society, London, Petroleum Geology Conference series, 8(1), 485-505.
- Rosier, S. H. R., Hofstede, C., Brisbourne, A. M., et al. (2018). A New Bathymetry for the Southeastern Filchner-Ronne Ice Shelf: Implications for Modern Oceanographic Processes and Glacial History. *Journal of Geophysical Research: Oceans*, 123(7), 4610-4623.
- Roskosch, J., Winsemann, J., Polom, U., et al. (2015). Luminescence dating of ice-marginal deposits in northern Germany: evidence for repeated glaciations during the Middle Pleistocene (MIS 12 to MIS 6). *Boreas*, 44(1), 103-126.
- Röthlisberger, H. (1972). Water pressure in intra- and subglacial channels. *Journal of Glaciology*, 11(62), 177-203.
- Rott, H., Skvarca, P., and Nagler, T. (1996). Rapid Collapse of Northern Larsen Ice Shelf, Antarctica. *Science*, 271(5250), 788-792.
- Russell, A. J. (2007). Tunnel channel formation during the November 1996 jökulhlaup, Skeiðarárjökull, Iceland. *Annals of Glaciology*, 45, 95-103.
- Russell, H. A. J., Arnott, R. W. C., and Sharpe, D. R. (2003). Evidence for rapid sedimentation in a tunnel channel, Oak Ridges Moraine, southern Ontario, Canada. *Sedimentary Geology*, 160(1), 33-55.
- Rutishauser, A., Blankenship, D. D., Sharp, M., et al. (2018). Discovery of a hypersaline subglacial lake complex beneath Devon Ice Cap, Canadian Arctic. *Science Advances*, 4(4), eaar4353.
- Sandersen, P. B. E., Jørgensen, F., Larsen, N. K., et al. (2009). Rapid tunnel-valley formation beneath the receding Late Weichselian ice sheet in Vendsyssel, Denmark. *Boreas*, 38(4), 834-851.
- Sasgen, I., van den Broeke, M., Bamber, J. L., et al. (2012). Timing and origin of recent regional ice-mass loss in Greenland. *Earth and Planetary Science Letters*, 333, 293-303.
- Sasgen, I., Wouters, B., Gardner, A. S., et al. (2020). Return to rapid ice loss in Greenland and record loss in 2019 detected by the GRACE-FO satellites. *Communications Earth & Environment*, 1(1), 8.

Bibliography

- Sawagaki, T., and Hirakawa, K. (1997). Erosion of bedrock by subglacial meltwater, soya coast, east antarctica. *Geografiska Annaler: Series A*, 79(4), 223-238.
- Scambos, T. A., Hulbe, C., Fahnestock, M. A., et al. (2000). The link between climate warming and break-up of ice shelves in the Antarctic Peninsula. *Journal of Glaciology*, 46, 516-530.
- Scambos, T. A., Bohlander, J. A., Shuman, C. A., et al. (2004). Glacier acceleration and thinning after ice shelf collapse in the Larsen B embayment, Antarctica. *Geophysical Research Letters*, 31(18), L18402.
- Scambos, T. A., Bell, R. E., Alley, R. B., et al. (2017). How much, how fast?: A science review and outlook for research on the instability of Antarctica's Thwaites Glacier in the 21st century. *Global and Planetary Change*, 153, 16-34.
- Schenk, T., Csatho, B., Ahn, Y., et al. (2004). DEM generation from the Antarctic LIDAR data: Site report, US Geological Survey.
- Scherer, R. P., Aldahan, A., Tulaczyk, S., et al. (1998). Pleistocene Collapse of the West Antarctic Ice Sheet. *Science*, 281(5373), 82-85.
- Schoof, C. (2010). Ice-sheet acceleration driven by melt supply variability. *Nature*, 468(7325), 803-806.
- Schroeder, D. M., Blankenship, D. D., and Young, D. A. (2013). Evidence for a water system transition beneath Thwaites Glacier, West Antarctica. *PNAS*, 110(30), 12225-12228.
- Scott, V. (2013). What can we expect from Europe's carbon capture and storage demonstrations? *Energy Policy*, 54, 66-71.
- Scourse, J. D., Ward, S. L., Wainwright, A., et al. (2018). The role of megatides and relative sea level in controlling the deglaciation of the British-Irish and Fennoscandian ice sheets. *Journal of Quaternary Science*, 33(2), 139-149.
- Selby, M. J., and Wilson, A. T. (1971). The origin of the Labyrinth, Wright Valley, Antarctica. *Geological Society of America Bulletin*, 82(2), 471-476.
- Selmes, N., Murray, T., and James, T. D. (2011). Fast draining lakes on the Greenland Ice Sheet. *Geophysical Research Letters*, 38(15), L15501.
- Seppälä, M. V. J. (2016). Lidar-Based Detection and Interpretation of Glaciotectonic Features of the Morainic Topography of Finland. *Journal of Geological Research*, 2016, 4292806.
- Sergienko, O. V., and Hulbe, C. L. (2011). 'Sticky spots' and subglacial lakes under ice streams of the Siple Coast, Antarctica. *Annals of Glaciology*, 52(58), 18-22.
- Serov, P., Vadakkepuliambatta, S., Mienert, J., et al. (2017). Postglacial response of Arctic Ocean gas hydrates to climatic amelioration. *PNAS*, 114(24), 6215-6220.
- Severinghaus, J. P., and Brook, E. J. (1999). Abrupt Climate Change at the End of the Last Glacial Period Inferred from Trapped Air in Polar Ice. *Science*, 286(5441), 930-934.
- Shackleton, C., Patton, H., Hubbard, A., et al. (2018). Subglacial water storage and drainage beneath the Fennoscandian and Barents Sea ice sheets. *Quaternary Science Reviews*, 201, 13-28.
- Sharp, M. (1985). Sedimentation and Stratigraphy at Eyjabakkajökull—An Icelandic Surging Glacier. *Quaternary Research*, 24(3), 268-284.
- Sharp, M., Richards, K., Willis, I., et al. (1993). Geometry, bed topography and drainage system structure of the haut glacier d'Arolla, Switzerland. *Earth Surface Processes and Landforms*, 18(6), 557-571.
- Sharpe, D., Dyke, L., Hinton, M., et al. (1996). Groundwater prospects in the Oak Ridges Moraine area, southern Ontario: application of regional geological models. *Current research*, 1996, 181-190.
- Shaw, J., and Gilbert, R. (1990). Evidence for large scale subglacial meltwater flood events in southern Ontario and northern New York State. *Geology*, 18, 1169-1172.
- Shepard, C. C., Agostini, V. N., Gilmer, B., et al. (2012). Assessing future risk: quantifying the effects of sea level rise on storm surge risk for the southern shores of Long Island, New York. *Natural Hazards*, 60(2), 727-745.
- Shepherd, A., Hubbard, A., Nienow, P., et al. (2009). Greenland ice sheet motion coupled with daily melting in late summer. *Geophysical Research Letters*, 36(1), L01501.

- Shepherd, A., Fricker, H. A., and Farrell, S. L. (2018). Trends and connections across the Antarctic cryosphere. *Nature*, 558(7709), 223-232.
- Shepherd, A., Ivins, E., Rignot, E., et al. (2020). Mass balance of the Greenland Ice Sheet from 1992 to 2018. *Nature*, 579(7798), 233-239.
- Shoemaker, E. M. (1986). Subglacial hydrology for an ice sheet resting on a deformable aquifer. *Journal of Glaciology*, 32, 20-30.
- Shreve, R. L. (1972). Movement of water in glaciers. *Journal of Glaciology*, 11(62), 205-214.
- Shreve, R. L. (1985). Late Wisconsin ice surface profile calculated from esker paths and types Katahdin esker system Maine. *Quaternary Research*, 23(1), 27-37.
- Siegert, M. J. (2000). Antarctic subglacial lakes. *Earth-Science Reviews*, 50(1-2), 29-50.
- Siegert, M. J., and Bamber, J. L. (2000). Subglacial water at the heads of Antarctic ice-stream tributaries. *Journal of Glaciology*, 46(155), 702-703.
- Siegert, M. J., Dowdeswell, J. A., Gorman, M. R., et al. (1996). An inventory of Antarctic sub-glacial lakes. *Antarctic Science*, 8(3), 281-286.
- Siegert, M. J., Ellis-Evans, J. C., Tranter, M., et al. (2001). Physical, chemical and biological processes in Lake Vostok and other Antarctic subglacial lakes. *Nature*, 414(6864), 603-609.
- Siegert, M. J., Tranter, M., Ellis-Evans, J. C., et al. (2003). The hydrochemistry of Lake Vostok and the potential for life in Antarctic subglacial lakes. *Hydrological Processes*, 17(4), 795-814.
- Siegert, M. J., Hindmarsh, R., Corr, H., et al. (2004). Subglacial Lake Ellsworth: A candidate for in situ exploration in West Antarctica. *Geophysical Research Letters*, 31(23), L23403.
- Siegert, M. J., Carter, S., Tabacco, I., et al. (2005). A revised inventory of Antarctic subglacial lakes. *Antarctic Science*, 17(3), 453-460.
- Siegert, M. J., Ross, N., and Le Brocq, A. M. (2016). Recent advances in understanding Antarctic subglacial lakes and hydrology. *Philosophical Transactions of the Royal Society A*, 374(2059), 20140306.
- Siegert, M. J., Kulesa, B., Bougamont, M., et al. (2018). Antarctic subglacial groundwater: a concept paper on its measurement and potential influence on ice flow. In: Siegert, M. J., Jamieson, S. S. R., and White, D. A. (eds.). *Exploration of Subsurface Antarctica: Uncovering Past Changes and Modern Processes*, Volume 461: London, Geological Society, Special Publications, 197-213.
- Siegfried, M. R., Fricker, H. A., Carter, S. P., et al. (2016). Episodic ice velocity fluctuations triggered by a subglacial flood in West Antarctica. *Geophysical Research Letters*, 43(6), 2640-2648.
- Simkins, L. M., Anderson, J. B., Greenwood, S. L., et al. (2017). Anatomy of a meltwater drainage system beneath the ancestral East Antarctic ice sheet. *Nature Geoscience*, 10(9), 691-697.
- Simkins, L. M., Greenwood, S. L., Munevar Garcia, S., et al. (2021). Topographic Controls on Channelized Meltwater in the Subglacial Environment. *Geophysical Research Letters*, 48(20), e2021GL094678.
- Sissons, J. B. (1958). Supposed Ice-Dammed Lakes in Britain with Particular Reference to the Eddleston Valley, Southern Scotland. *Geografiska Annaler*, 40(3-4), 159-187.
- Smed, P. (1962). Studier over den fynske øgruppens glacielle landskabsformer. *Meddelelser fra Dansk Geologisk Forening*, 15, 1-74.
- Smed, P. (1998). Die Entstehung der dänischen und norddeutschen Rinnentäler (Tunneltäler) -Glaziologische Gesichtspunkte. *E&G Quaternary Science Journal*, 48, 1-18.
- Smith, A. M., Woodward, J., Ross, N., et al. (2018). Evidence for the long-term sedimentary environment in an Antarctic subglacial lake. *Earth and Planetary Science Letters*, 504, 139-151.
- Smith, B. E., Fricker, H. A., Joughin, I., et al. (2009a). An inventory of active subglacial lakes in Antarctica detected by ICESat (2003-2008). *Journal of Glaciology*, 55(192), 573-595.
- Smith, J. A., Hillenbrand, C.-D., Larter, R. D., et al. (2009b). The sediment infill of subglacial meltwater channels on the West Antarctic continental shelf. *Quaternary Research*, 71(2), 190-200.
- Smith, B. E., Gourmelen, N., Huth, A., et al. (2017). Connected subglacial lake drainage beneath Thwaites Glacier, West Antarctica. *The Cryosphere*, 11(1), 451-467.

Bibliography

- Smith, L. C., Chu, V. W., Yang, K., et al. (2015). Efficient meltwater drainage through supraglacial streams and rivers on the southwest Greenland ice sheet. *PNAS*, 112(4), 1001-1006.
- Solheim, A., and Pfirman, S. L. (1985). Sea-floor morphology outside a grounded, surging glacier; Bråsvellbreen, Svalbard. *Marine Geology*, 65, 127-143.
- Stackebrandt, W. (2009). Subglacial channels of Northern Germany—a brief review. *Zeitschrift der deutschen Gesellschaft für Geowissenschaften*, 160(3), 203-210.
- Stearns, L. A., Smith, B. E., and Hamilton, G. S. (2008). Increased flow speed on a large East Antarctic outlet glacier caused by subglacial floods. *Nature Geoscience*, 1(12), 827-831.
- Stevens, L. A., Behn, M. D., Das, S. B., et al. (2016). Greenland Ice Sheet flow response to runoff variability. *Geophysical Research Letters*, 43(21), 11295-11303.
- Stewart, M. A. (2009). 3D Seismic Analysis of Pleistocene Tunnel Valleys in the Central North Sea. Unpublished PhD Thesis: Imperial College London, 317 p.
- Stewart, M. A. (2016). Assemblage of buried and seabed tunnel valleys in the central North Sea: from morphology to ice-sheet dynamics. In: Dowdeswell, J. A., Canals, M., Jakobsson, M., Todd, B. J., Dowdeswell, E. K., et al. (eds.). *Atlas of Submarine Glacial Landforms: Modern, Quaternary and Ancient*, Volume 46: Geological Society, London, 317-320.
- Stewart, M. A., and Lonergan, L. (2011). Seven glacial cycles in the middle-late Pleistocene of northwest Europe: Geomorphic evidence from buried tunnel valleys. *Geology*, 39(3), 283-286.
- Stewart, M. A., Lonergan, L., and Hampson, G. (2013). 3D seismic analysis of buried tunnel valleys in the central North Sea: morphology, cross-cutting generations and glacial history. *Quaternary Science Reviews*, 72, 1-17.
- Stewart, M., Lonergan, L., and Hampson, G. (2012). 3D seismic analysis of buried tunnel valleys in the Central North Sea: tunnel valley fill sedimentary architecture. In: Huuse, M., Redfern, J., Le Heron, D. P., Dixon, R., Moscariello, A., et al. (eds.). *Glaciogenic Reservoirs and Hydrocarbon systems*, Volume 368, Geological Society, London, Special Publications, 173-184.
- Stoker, M. S., Balson, P. S., Long, D., et al. (2011). An overview of the lithostratigraphical framework for the Quaternary deposits on the United Kingdom continental shelf. British Geological Survey, 40 pp.
- Stoker, M. S., Long, D., and Fyfe, J. A. (1985). A revised Quaternary stratigraphy for the central North Sea. British Geological Survey.
- Stoker, M. S., Skinner, A. C., Fyfe, J. A., et al. (1983). Palaeomagnetic evidence for early Pleistocene in the central and northern North Sea. *Nature*, 304, 332-334.
- Stoker, M. S., Pheasant, J. B., and Josenhans, H. (1997). Seismic methods and interpretation. In: Davies, T. A., Bell, T., and Cooper, A. K., (eds.). *Glaciated Continental Margins. An Atlas of Acoustic Images*. Chapman and Hall, London, 9-26.
- Stokes, C. R., and Clark, C. D. (2002). Are long subglacial bedforms indicative of fast ice flow? *Boreas*, 31, 239-249.
- Storrar, R. D., Stokes, C. R., and Evans, D. J. A. (2014). Morphometry and pattern of a large sample (>20,000) of Canadian eskers and implications for subglacial drainage beneath ice sheets. *Quaternary Science Reviews*, 105, 1-25.
- Storrar, R. D., Ewertowski, M., Tomczyk, A. M., et al. (2019). Equifinality and preservation potential of complex eskers. *Boreas*, 49, 211-231.
- Studinger, M., Bell, R. E., and Tikku, A. A. (2004). Estimating the depth and shape of subglacial Lake Vostok's water cavity from aerogravity data. *Geophysical Research Letters*, 31(12), L12401.
- Sugden, D., and Denton, G. (2004). Cenozoic landscape evolution of the Convoy Range to Mackay Glacier area, Transantarctic Mountains: Onshore to offshore synthesis. *GSA Bulletin*, 116(7-8), 840-857.
- Sugden, D., Denton, G. H., and Marchant, D. R. (1991). Subglacial meltwater channel systems and ice sheet overriding, Asgard Range, Antarctica. *Geografiska Annaler: Series A*, 73(2), 109-121.

- Sugden, D. E., Summerfield, M. A., Denton, G. H., et al. (1999). Landscape development in the Royal Society Range, southern Victoria Land, Antarctica: stability since the mid-Miocene. *Geomorphology*, 28(3), 181-200.
- Sundal, A. V., Shepherd, A., Nienow, P., et al. (2011). Melt-induced speed-up of Greenland ice sheet offset by efficient subglacial drainage. *Nature*, 469(7331), 521-524.
- Svendsen, J. I., Alexanderson, H., Astakhov, V. I., et al. (2004). Late Quaternary ice sheet history of northern Eurasia. *Quaternary Science Reviews*, 23(11), 1229-1271.
- Syvitski, J. P. M. (1989). On the deposition of sediment within glacier-influenced fjords: Oceanographic controls. *Marine Geology*, 85(2), 301-329.
- Talbot, C. J. (1999). Ice ages and nuclear waste isolation. *Engineering Geology*, 52(3), 177-192.
- Tarasov, L., and Peltier, W. R. (2004). A geophysically constrained large ensemble analysis of the deglacial history of the North American ice-sheet complex. *Quaternary Science Reviews*, 23(3), 359-388.
- Tasianas, A., Büinz, S., Bellwald, B., et al. (2018). High-resolution 3D seismic study of pockmarks and shallow fluid flow systems at the Snøhvit hydrocarbon field in the SW Barents Sea. *Marine Geology*, 403, 247-261.
- Tedesco, M. (2009). Assessment and development of snowmelt retrieval algorithms over Antarctica from K-band spaceborne brightness temperature (1979–2008). *Remote Sensing of Environment*, 113(5), 979-997.
- Tedesco, M., and Monaghan, A. J. (2009). An updated Antarctic melt record through 2009 and its linkages to high-latitude and tropical climate variability. *Geophysical Research Letters*, 36(18), L18502.
- Tedesco, M., Willis, I., Hoffman, M. J., et al. (2013). Ice dynamic response to two modes of surface lake drainage on the Greenland ice sheet. *Environmental Research Letters*, 8, 034007.
- Tedstone, A. J., Nienow, P. W., Gourmelen, N., et al. (2015). Decadal slowdown of a land-terminating sector of the Greenland Ice Sheet despite warming. *Nature*, 526(7575), 692-695.
- Thoma, M., Jenkins, A., Holland, D. et al. (2008). Modelling Circumpolar Deep Water intrusions on the Amundsen Sea continental shelf, Antarctica. *Geophysical Research Letters*, 35(18), L18602.
- Todd, B. J., Lewis, C. F. M., and Ryall, P. J. C. (1988). Comparison of trends of iceberg scour marks with iceberg trajectories and evidence of paleocurrent trends on Saglek Bank, northern Labrador Shelf. *Canadian Journal of Earth Sciences*, 25(9), 1374-1383.
- Trusel, L. D., Frey, K. E., Das, S. B., et al. (2013). Satellite-based estimates of Antarctic surface meltwater fluxes. *Geophysical Research Letters*, 40(23), 6148-6153.
- Trusel, L. D., Frey, K. E., Das, S. B., et al. (2015). Divergent trajectories of Antarctic surface melt under two twenty-first-century climate scenarios. *Nature Geoscience*, 8(12), 927-932.
- Tulaczyk, S., Kamb, B., and Engelhardt, H. F. (2001). Estimates of effective stress beneath a modern West Antarctic ice stream from till preconsolidation and void ratio. *Boreas*, 30(2), 101-114.
- Tulaczyk, S., Kamb, W. B., and Engelhardt, H. F. (2000a). Basal mechanics of Ice Stream B, west Antarctica: 1. Till mechanics. *Journal of Geophysical Research: Solid Earth*, 105, B1, 463-481.
- Tulaczyk, S., Kamb, W. B., and Engelhardt, H. F. (2000b). Basal mechanics of Ice Stream B, west Antarctica: 2. Undrained plastic bed model. *Journal of Geophysical Research: Solid Earth*, 105, 483-494.
- U.S. Geological Survey (2007). Landsat Image Mosaic of Antarctica (LIMA). U.S. Geological Survey Fact Sheet 2007-3116. 4 pp.
- Ussing, N. V. (1903). Om Jyllands hedesletter og teorierne for deres dannelse. *Oversigt over Det Kongelige danske Videnskabernes Selskabs Forhandlinger*, 2, 99-152.
- Ussing, N. V. (1907). Om floddale og randmoræner i Jylland. *Oversigt over Det Kongelige danske Videnskabernes Selskabs Forhandlinger*, 4, 161-213.
- van den Broeke, M. R., Enderlin, E. M., Howat, I. M., et al. (2016). On the recent contribution of the Greenland ice sheet to sea level change. *The Cryosphere*, 10(5), 1933-1946.

Bibliography

- van der Vegt, P., Janszen, A., and Moscariello, A. (2012). Tunnel valleys: current knowledge and future perspectives. In: Huuse, M., Redfern, J., Le Heron, D. P., Dixon, R., Moscariello, A., et al., (eds.). *Glaciogenic Reservoirs and Hydrocarbon Systems*, Volume 368: London, Geological Society, Special Publications, 75-97.
- van Wyk de Vries, M., Bingham, R. G., and Hein, A. S. (2018). A new volcanic province: an inventory of subglacial volcanoes in West Antarctica. In: Siegert, M. J., Jamieson, S. S. R., and White, D. A., (eds.). *Exploration of Subsurface Antarctica: Uncovering Past Changes and Modern Processes*, Volume 461: London, Geological Society, Special Publications, 231-248.
- Vaslet, D. (1990). Upper Ordovician glacial deposits in Saudi Arabia. *Episodes*, 13(3), 147-161.
- Vaughan, D. G., and Doake, C. S. M. (1996). Recent atmospheric warming and retreat of ice shelves on the Antarctic Peninsula. *Nature*, 379(6563), 328-331.
- Vaughan, D., Comiso, J. C., Allison, I., et al. (2013). Observations: Cryosphere. In: Stocker, T. F., Qin, D., Plattner, G.-K., Tignor, M., Allen, S. K., et al., (eds.). *Climate Change 2013: The Physical Science Basis. Contribution of Working Group I to the Fifth Assessment Report on the Intergovernmental Panel on Climate Change*: Cambridge, United Kingdom and New York, NY, USA, Cambridge University Press, 317-382.
- Vesely, F. F., Assine, M. L., França, A. B., et al. (2021). Tunnel-valley fills in the Paraná Basin and their implications for the extent of late Paleozoic glaciation in SW Gondwana. *Journal of South American Earth Sciences*, 106, 102969.
- Waite, W. F., Santamarina, J. C., Cortes, D. D., et al. (2009). Physical properties of hydrate-bearing sediments. *Reviews of Geophysics*, 47(4), RG4003.
- Waite, R. B., JR. (1985). Case for periodic, colossal jökulhlaups from Pleistocene glacial Lake Missoula. *GSA Bulletin*, 96(10), 1271-1286.
- Walder, J., and Hallet, B. (1979). Geometry of Former Subglacial Water Channels and Cavities. *Journal of Glaciology*, 23(89), 335-346.
- Walder, J. S. (1982). Stability of sheet flow of water beneath temperate glaciers and implications for glacier surging. *Journal of Glaciology*, 28(99), 273-293.
- Walder, J. S. (1986). Hydraulics of subglacial cavities. *Journal of Glaciology*, 32(112), 439-445.
- Walder, J. S., and Costa, J. E. (1996). Outburst floods from glacier-dammed lakes: The effect of mode of lake drainage on flood magnitude. *Earth Surface Processes and Landforms*, 21(8), 701-723.
- Walder, J. S., and Fowler, A. C. (1994). Channelized subglacial drainage over a deformable bed. *Journal of Glaciology*, 40(134), 3-15.
- WCRP Global Sea Level Budget Group (2018). Global sea-level budget 1993–present. *Earth System Science Data*, 10(3), 1551-1590.
- Weertman, J. (1957). On the Sliding of Glaciers. *Journal of Glaciology*, 3(21), 33-38.
- Weertman, J. (1972). General theory of water flow at the base of a glacier or ice sheet. *Reviews of Geophysics and Space Physics*, 10(1), 287-333.
- Weertman, J. (1974). Stability of the Junction of an Ice Sheet and an Ice Shelf. *Journal of Glaciology*, 13(67), 3-11.
- Wei, W., Blankenship, D. D., Greenbaum, J. S., et al. (2020). Getz Ice Shelf melt enhanced by freshwater discharge from beneath the West Antarctic Ice Sheet. *The Cryosphere*, 14(4), 1399-1408.
- Wellner, J. S., Heroy, D. C., and Anderson, J. B. (2006). The death mask of the antarctic ice sheet: Comparison of glacial geomorphic features across the continental shelf. *Geomorphology*, 75(1), 157-171.
- Wellner, J. S., Lowe, A. L., Shipp, S. S., et al. (2001). Distribution of glacial geomorphic features on the Antarctic continental shelf and correlation with substrate implications for ice behavior. *Journal of Glaciology*, 47(158), 397-411.
- Werder, M. A., Hewitt, I. J., Schoof, C. G., et al. (2013). Modeling channelized and distributed subglacial drainage in two dimensions. *Journal of Geophysical Research: Earth Surface*, 118(4), 2140-2158.

- Wilch, T. I., McIntosh, W. C., and Dunbar, N. W. (1999). Late Quaternary volcanic activity in Marie Byrd Land: Potential $^{40}\text{Ar}/^{39}\text{Ar}$ -dated time horizons in West Antarctic ice and marine cores. *GSA Bulletin*, 111(10), 1563-1580.
- Williams, G. P. (1989). Sediment concentration versus water discharge during single hydrologic events in rivers. *Journal of Hydrology*, 111, 89-106.
- Willis, I., Richards, K., and Sharp, M. (1996). Links between proglacial stream suspended sediment dynamics, glacier hydrology and glacier motion at Midtdalsbreen, Norway. *Hydrological Processes*, 10(4), 629-648.
- Willis, I. C., Fitzsimmons, C. D., Melvold, K. et al. (2012). Structure, morphology and water flux of a subglacial drainage system, Midtdalsbreen, Norway. *Hydrological Processes*, 26(25), 3810-3829.
- Willis, M. J., Herried, B. G., Bevis, M. G., et al. (2015). Recharge of a subglacial lake by surface meltwater in northeast Greenland. *Nature*, 518(7538), 223-227.
- Willis, I. C., Pope, E. L., Leysinger Vieli, G. J. M. C., et al. (2016). Drainage networks, lakes and water fluxes beneath the Antarctic ice sheet. *Annals of Glaciology*, 57(72), 96-108.
- Wingfield, R. (1989). Glacial incisions indicating Middle and Upper Pleistocene ice limits off Britain. *Terra Nova*, 1, 538-548.
- Wingfield, R. (1990). The origin of major incisions within the Pleistocene deposits of the North Sea. *Marine Geology*, 91(1-2), 31-52.
- Wingham, D. J., Siegert, M. J., Shepherd, A., et al. (2006). Rapid discharge connects Antarctic subglacial lakes. *Nature*, 440(7087), 1033-1036.
- Winkelmann, R., Martin, M. A., Haseloff, M., et al. (2011). The Potsdam Parallel Ice Sheet Model (PISM-PIK) – Part 1: Model description. *The Cryosphere*, 5(3), 715-726.
- Winsborrow, M., Andreassen, K., Hubbard, A., et al. (2016). Regulation of ice stream flow through subglacial formation of gas hydrates. *Nature Geoscience*, 9(5), 370-374.
- Winters, W. J., Pecher, I. A., Waite, W. F., et al. (2004). Physical properties and rock physics models of sediment containing natural and laboratory-formed methane gas hydrate. *American Mineralogist*, 89(8-9), 1221-1227.
- Wise, M. G., Dowdeswell, J. A., Jakobsson, M., et al. (2017). Evidence of marine ice-cliff instability in Pine Island Bay from iceberg-keel plough marks. *Nature*, 550(7677), 506-510.
- Witus, A. E., Branecky, C. M., Anderson, J. B., et al. (2014). Meltwater intensive glacial retreat in polar environments and investigation of associated sediments: example from Pine Island Bay, West Antarctica. *Quaternary Science Reviews*, 85, 99-118.
- Wöfl, A.-C., Snaith, H., Amirebrahimi, S., et al. (2019). Seafloor Mapping – The Challenge of a Truly Global Ocean Bathymetry. *Frontiers in Marine Science*, 6, 283.
- Wood, M., Rignot, E., Fenty, I., et al. (2018). Ocean-Induced Melt Triggers Glacier Retreat in Northwest Greenland. *Geophysical Research Letters*, 45(16), 8334-8342.
- Woodland, A. W. (1970). The buried tunnel-valleys of East Anglia. *Proceedings of the Yorkshire Geological Society*, 37, 521-578.
- World Meteorological Organization (2022). State of the Global Climate. WMO Report Number 1290.
- Wright, A., and Siegert, M. (2012). A fourth inventory of Antarctic subglacial lakes. *Antarctic Science*, 24(6), 659-664.
- Wright, H. E. (1973). Tunnel valleys, glacial surges and subglacial hydrology of the Superior Lobe, Minnesota. In: Black, R. F., Goldthwait, R. P., and Willman, H. B. (eds.). *The Wisconsinan Stage*. Geological Society of America, 251-276.
- Yarushina, V. M., Wang, L. H., Connolly, D., et al. (2021). Focused fluid-flow structures potentially caused by solitary porosity waves. *Geology*, 50(2), 179-183.
- Young, T. J., Christoffersen, P., Bougamont, M., et al. (2022). Rapid basal melting of the Greenland Ice Sheet from surface meltwater drainage. *PNAS*, 119(10), e2116036119.

Bibliography

- Yu, H., Rignot, E., Seroussi, H., et al. (2018). Retreat of Thwaites Glacier, West Antarctica, over the next 100 years using various ice flow models, ice shelf melt scenarios and basal friction laws. *The Cryosphere*, 12(12), 3861-3876.
- Zemp, M., Huss, M., Thibert, E., et al. (2019). Global glacier mass changes and their contributions to sea-level rise from 1961 to 2016. *Nature*, 568(7752), 382-386.
- Ziegler, P. A. (1990). *Geological Atlas of Western and Central Europe*. Geological Society, London.
- Ziegler, P. A. (1992). North Sea rift system. *Tectonophysics*, 208, 55-75.
- Zoet, L. K., and Iverson, N. (2020). A slip law for glaciers on deformable beds. *Science*, 368(6486), 76-78.
- Zoet, L. K., Muto, A., Rawling, J. E., et al. (2019). The effects of tunnel channel formation on the Green Bay Lobe, Wisconsin, USA. *Geomorphology*, 324, 36-47.
- Zwally, H. J., Abdalati, W., Herring, T., et al. (2002). Surface Melt-Induced Acceleration of Greenland Ice-Sheet Flow. *Science*, 297(5579), 218-222.
- Zweck, C., and Huybrechts, P. (2005). Modeling of the northern hemisphere ice sheets during the last glacial cycle and glaciological sensitivity. *Journal of Geophysical Research: Atmospheres*, 110, D7.